Distributed Wireless Body-Centric Networks: Optimisation via Predictive Analytics and Cross-Layer Designs

Samiya M. Shimly

March 2019

A thesis submitted for the degree of Doctor of Philosophy
of The Australian National University

Research School of Electrical, Energy, and Materials Engineering
College of Engineering and Computer Science
The Australian National University

To my beloved parents, Kamal and Hasina,
and my loving husband, Fahim.

Declaration

The contents of this thesis are the results of original research and have not been submitted for a higher degree to any other university or institution. Much of this work has either been published as journal/conference papers or submitted for publications as journal papers. Following is a list of these papers:

Journal Articles

- **Samiya M. Shimly**, David B. Smith, and Samaneh Movassaghi: 'Experimental Analysis of Cross-layer Optimization for Distributed Wireless Body-to-Body Networks', *IEEE Sensors Journal*, p. 1-16, August, 2019, DOI: 10.1109/JSEN.2019.2937356.

- **Samiya M. Shimly**, Samaneh Movassaghi, and David B. Smith: 'Cooperative communications for sleep monitoring in wireless body area networks', *IET Electronics Letters*, p. 594-596, February, 2016.

- **Samiya M. Shimly** and David B. Smith: 'Multi-Objective Markov Decision Process for Adaptive Scheduling in Wireless Body-to-Body Networks', under review, *IEEE Internet of Things Journal*, March, 2019.

- **Samiya M. Shimly**, David B. Smith, Samaneh Movassaghi, and Leif W. Hanlen: 'An Empirical Study of Stationarity and Long-Range Dependence of Wireless Body-centric Channels', under review, *ACM Transactions on Sensor Networks*, September, 2019.

Conference Proceedings

- **Samiya M. Shimly**, David B. Smith, and Samaneh Movassaghi: 'Cross-Layer Designs for Body-to-Body Networks: Adaptive CSMA/CA with Distributed Routing', in *IEEE International Conference on Communications (ICC'*18*)*, pp. 1-6, Kansas, USA, May, 2018.

- **Samiya M. Shimly**, David B. Smith, and Samaneh Movassaghi: 'Wide-Sense-Stationarity of Everyday Wireless Channels for Body-to-Body Networks', in 2018 *IEEE International Conference on Communications (ICC'*18*)*, pp. 1-6, Kansas, USA, May, 2018.

- **Samiya Shimly**, David B. Smith, and Samaneh Movassaghi: 'Cross-layer optimized routing with low duty cycle TDMA across multiple wireless body area networks', in *IEEE International Conference on Communications (ICC'*17*)*, pp. 1-6, Paris, France, May, 2017.

The following articles/posters are also results from my Ph.D. study:

- **Samiya Shimly**, 'everybody working together', *featured interview by Electronics Letters, IET*, p-570, Apr, 2016.

- 'Towards Smart Wireless Body-centric Networks', *poster presentation at joint 7th* N^2 *WOMEN-WICE Workshop (ICC)*, May, 2018.

- 'Cross-layer optimized routing across multiple wireless body area networks', *poster presentation at Australian Communications Theory Workshop (AusCTW)*, Jan, 2017.

The research work presented in this thesis is my own original work, unless indicated otherwise.

Samiya Shimly
Research School of Electrical, Energy, and Materials Engineering
The Australian National University
Canberra ACT 2600
March 2019

Acknowledgments

I would like to take this opportunity to acknowledge and thank each of the following people, who helped me scientifically and emotionally throughout this study:

Firstly, I would like to express my deepest appreciation and sincere gratitude to my Ph.D. supervisor, Dr. David Smith, who tremendously helped and encouraged me at each stage of the process. I am grateful for his unconditional support, patience, scholarly inputs, and invaluable guidance throughout my Ph.D. study. Without his advice, direction, and persistent help, this dissertation would not have been possible. I consider it as a great opportunity to pursue my Ph.D. under his supervision and to learn from his research expertise.

Also, I would especially like to thank my Ph.D. co-supervisors, Prof. Thushara Abhayapala and Dr. Leif Hanlen for their helpful advice and support from time to time.

The Australian National University (ANU) and CSIRO (Commonwealth Scientific and Industrial Research Organisation) Data61 for the Ph.D. scholarships and the Vice Chancellor's travel grant.

Prof. Jan Rabaey, for generously welcoming me to visit his research group at the University of California, Berkeley, and providing valuable feedback on my work.

The HDR members of ANU for their timely support and making the administrative works effortless.

My peers — Samaneh, Nicole, and Yizhou for their help, friendship, and encouragement throughout this time.

I owe a special thanks to my parents and family. I will forever be grateful to my parents for their eternal love and support, for having faith in me, for their sacrifice and patience, and providing me with the opportunity to be where I am today. Also, my lovely brother, Sakib, and gorgeous sisters, Kanak and Raka, my amazing in-laws, and all my dearest friends who were greatly supportive and understanding during this period.

Finally, I do not know how to begin with saying thank you to my wonderful husband and best friend, Fahim, for understanding me, for being there through all ups and downs, for the true love, patience, and enormous support and encouragement throughout the whole Ph.D. journey. It was Fahim who motivated me to keep going whenever I felt like giving up, and always lent a helping hand, a listening ear, and a shoulder to lean on. Thank you for always being there!

Abstract

In this thesis, methods for optimisation are designed and developed for wireless body-centric channels in order to best enable intelligent, self-organised, and distributed human-centered networks. Due to human-body shadowing and mobility, body-centric channels change dramatically over time — with intermittent periods of longer stability — often causing unnecessary delay and energy consumption under significant radio channel attenuation. Hence, robust and efficient communications across these networks require adaptive, optimised mechanisms. Thus, we propose, and investigate the performance of various cross-layer and predictive optimisation techniques for real-life body-centric channels. Our analysis employs real-life experimental datasets collected from different numbers of co-located wireless body area networks (BANs), over many hours in 'everyday' scenarios.

We first investigate cooperative receive diversity for a BAN used to monitor a sleeping person, and we find that cooperative combining improves packet delivery ratio (PDR) and latency for these atypical slowly-varying radio channels. Then, we propose two cross-layer optimised techniques for multiple coexisting BANs, forming wireless body-to-body networks (BBNs). These techniques are shortest path routing (SPR) and cooperative multi-path routing (CMR), where CMR incorporates cooperative selection combining. In CMR and SPR, the best route is periodically selected at the network layer according to channel state information from the physical layer. We show that CMR reduces retransmissions and increases PDR due to an available alternate path, reducing end-to-end delay and energy consumption with respect to state-of-the-art protocols. We then add MAC layer interference mitigation using low duty cycle TDMA, for which CMR gains up to 14 dB improvement over SPR at 10% outage probability. Moreover, we also apply CMR incorporating novel MAC layer CSMA/CA with adaptive carrier sensing, giving improvement over TDMA for both throughput and spectral efficiency.

Next, we explore the feasibility of applying predictive optimisation over wire-

less body-centric channels (i.e., body-to-body, on-body), by studying wide-sense-stationarity (WSS) and long-range dependence (LRD) characteristics, which are crucial to predictive analysis. The results of different stationarity tests show that unlike on-body channels (which are considered non-stationary), body-to-body channels possess WSS characteristics for a range of window lengths between 0.5 s and 15 s (typically $5-8$ s) depending upon on-body sensor locations and shadowing. Moreover, the Hurst exponent of body-centric channels is very high (around 0.9) and temporal auto-correlation decreases very slowly (a power-like decay), indicating LRD (i.e., long-memory) characteristics are maintained.

Then, based on the results for WSS and LRD, we apply multi-objective optimisation for adaptive scheduling in BBNs, by using a multi-objective Markov decision process (MOMDP) to jointly optimise three separate metrics: throughput, latency, and energy consumption. The adaptive scheduling combines both TDMA and CSMA/CA schemes. From performance analysis, employing real-life channel measurements, we find an MOMDP outcome that is Pareto optimal, providing a desirable trade-off between the three objectives of maximising throughput, and minimising continuous latency and energy consumption. It is also observed that WSS characteristics of the body-to-body channels have a significant effect on the outcome of such analytics.

The outcomes here help the development of pervasive real-world applications with large-scale and highly-connected systems, comprising many closely-located BANs.

List of Abbreviations

AAL	ambient assisted living
ACF	auto-correlation function
ACK	acknowledgement
ANOVA	analysis of variance
AODV	adhoc on-demand distance vector
ARFIMA	auto-regressive fractionally integrated moving average
ARMA	auto-regressive moving average
B2B	body-to-body
BANs	wireless body area networks
BBNs	wireless body-to-body networks
B–F	Brown-Forsythe
BLE	bluetooth low energy
CAP	contention access period
CDC	cooperative diversity combining
CDF	cumulative distribution function
CFP	contention free period
CICADA	cascading information retrieval by controlling access with distributed slot assignment
CL-RRS	cross-layer reliable retransmission scheme

C/M	control and management
CMDP	constrained Markov decision process
CMR	cooperative multi-path routing
CNC	cooperative network coding
COD	continuous outage duration
COMR	cross-layer opportunistic MAC/routing protocol
CSMA/CA	carrier sense multiple access with collision avoidance
CTP	collection tree protocol
DL	direct link
DODAG	destination oriented directed acyclic graph
DTMDP	discrete-time Markov decision process
DQBAN	distributed queuing body area network
EAP	exclusive access phase
EC	energy consumption
EDC	expected duty cycle
EDR	enhanced data rate
EFC	electric field coupling
ETSI	European telecommunications standards institute
ETX	expected transmission count
FM	frequency-modulated
GEV	generalised extreme value
HIT	hybrid indirect transmissions
HS	high speed
IEEE	institute of electrical and electronics engineers

IMD	implantable medical device
IoH	internet of humans
IR	impulse-radio
ISM	industrial, scientific, and medical
K–S	Kolmogorov-Smirnov
LANs	local area networks
LH	left-hip
LLNs	low power lossy networks
LLV	log-likelihood value
LRD	long-range dependence
LW	left-wrist
MAC	media access control
MANETs	mobile ad hoc networks
MAP	managed access phase
MCA	multi-use channel access
MDP	Markov decision process
MIMO	multiple-input-multiple-output
MLE	maximum likelihood estimation
MOMDP	multi-objective Markov decision process
MPCS	aximum-interference-power carrier-sensing
NaN	not a number
NB	narrowband
NET	network
OP	outage probability

OR	opportunistic relaying
ORPL	opportunistic routing protocol
OSI	open systems interconnection
OSPF	open shortest path first
PAL	protocol adaptation layer
PANs	personal area networks
PAR	packet arrival rate
PER	packet error rate
PHY	physical
PDR	packet delivery ratio
PDF	probability density function
POMDP	partially observable Markov decision process
PRR	packet reception rate
PSD	power spectral density
QoS	quality of service
RA	right-upper-arm
RAP	random access phase
RF	radio-frequency
RH	right-hip
RHT	route hold time
RS	receive sensitivity
RSSI	receive signal strength indicator
Rx	receiver
SC	selection combining

SINR	signal-to-interference-plus-noise ratio
SMDP	semi-Markov decision process
SOR	simple opportunistic routing
SPR	shortest path routing
SSE	sum of squared errors
STFT	short time Fourier transform
SwC	switch-and-examine combining
TC	technical committee
TP	transmit power
TDMA	time division multiple access
TICOSS	timezone coordinated sleep scheduling
Tx	transmitter
UWB	ultra-wideband
WASP	wireless autonomous spanning tree
WLANs	wireless local area networks
WPANs	wireless personal area networks
WSNs	wireless sensor networks
WSS	wide-sense-stationarity

Notations and Symbols

The following mathematical notations and symbols are consistent throughout the thesis:

$\Gamma(\cdot)$	gamma function
$I_o(\cdot)$	modified Bessel function of the first kind with order zero
Φ	CDF of the standard normal distribution
$\mathbb{E}(\cdot)$	expectation operator
$Cov(\cdot)$	covariance
$\sum$	summation
$\lvert \cdot \rvert$	absolute value operator
lim	limit
$(\cdot\cdot)$	range operator
H_0	null hypothesis
H_1	alternative hypothesis
h_E	Hurst exponent
Δ	total time
$\setminus$	set difference
$\cap$	intersection
$\approx$	approximation

$\emptyset$	empty set
$\wedge$	AND
$\vee$	OR
h	channel gain
τ	time instant
$\widehat{(\cdot)}^{\xi}$	eigenspectrum
min	minimum
max	maximum
$\overline{(\cdot)}$	mean
$\widetilde{(\cdot)}$	median
exp	exponential
log	logarithm
ln	natural logarithm
$\sim$	asymptotically equal

Contents

List of Figures

List of Tables

Chapter 1

Introduction

1.1 Background, Motivation, and Scope

The advent of wearable technology has led to the communication of data from, and across sensors, worn by people in independent networks. According to a study in [4], the number of connected wearable devices worldwide is expected to jump from an estimate of 526 million in 2016 to 1.1 billion in 2022 (Fig. 1.1). This

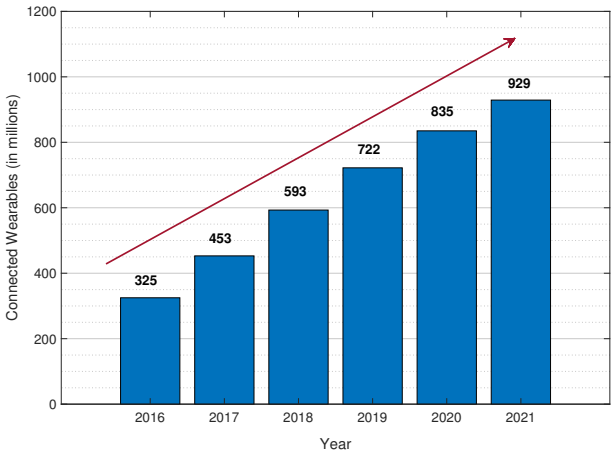

Figure 1.1: The growth of connected wearable devices worldwide

demonstrates the need for ongoing research and development of body-centric communications, in particular the design of body-centric networks that can function

independently. Body-centric wireless communications is now accepted as an important part of 4G and 5G mobile communications systems as well as a variety of personal area networks (PANs), which can take the form of human-to-human networking incorporating wearable sensors [5–7].

Wireless body-centric networks are created from the communications between different sensors placed on, in, around, and/or near the human body. Based on the placement of the wearable sensors, body-centric communications can be classified into the following types:

On-body communications: The communications between sensors that are placed on the body (on surface of the body) or inside the body (implanted node). The end-points of these channels are on/inside the body.

Off-body communications: The communications between sensors that are placed on the body and near the body (not on-body). One of the end point of these channels is placed on the body.

Body-to-body (B2B) communications: The communications between sensors that are placed on different peoples' body. The end points of these channels are located on the body of two different subjects.

The body-centric communications described above, can particularly form two types of body-centric networks:

1.1.1 Wireless Body Area Networks (BANs)

Wireless Body Area Networks (BANs) are the latest generations of PANs where low power, short-range micro and nano technology sensors/actuators are placed on, in, around or/and near the human body, typically to monitor, or enable physiological functions (Fig. 1.2). The BAN paradigm offers a vast range of applications such as, ubiquitous healthcare, military, sports, entertainment and many other areas [2], but advanced healthcare is a unique motivator for such networks, specifically in medical rehabilitation, diagnosis and monitoring of patients.

Vitally, patients can be continuously, and effectively, monitored at home or community healthcare, rather than being confined to a hospital or other primary

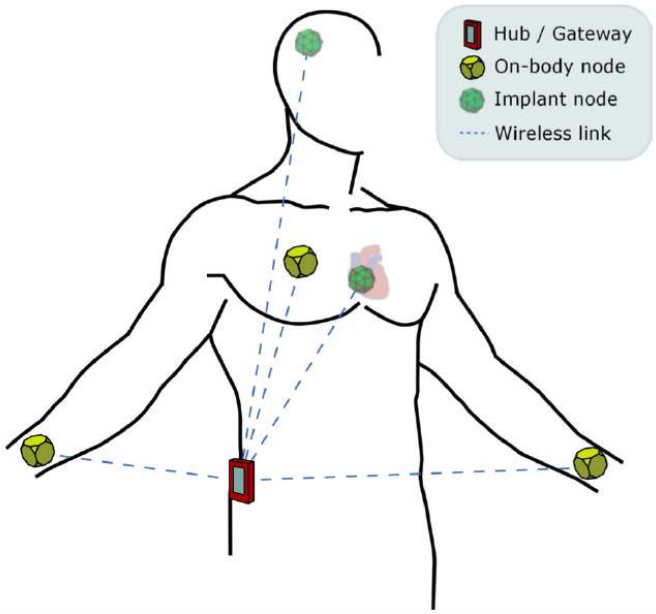

Figure 1.2: A BAN demonstrating wireless on-body and in-body links with on-body and implanted sensors/hub

healthcare facilities. In this context, the sensors incorporated in BANs may monitor numerous biometric parameters such as: body temperature; heart rate; respiration; blood pressure; and electrical parameters from the heart, muscles and brain. Moreover, BANs can enable early medical detection and intervention, which can save lives and improve quality of life. In this context, as BANs provide very long contiguous data from a patient's everyday environment, doctors can get a clearer picture of the patient's condition [8]. Some further examples of very promising applications of BANs in healthcare are for rehabilitation including stroke rehabilitation, physical rehabilitation after hip or knee surgeries, myocardial infarction rehabilitation and traumatic brain injury rehabilitation. Miniature, wireless, wearable technology offers a tremendous opportunity to enable and assess rehabilitation.

A BAN can also be used to help people with disabilities via actuation. For example, retina prosthesis chips can be implanted in the human eye to see adequately [9, 10]. Non-medical applications of BANs include data file transfer, gaming, secure authentication, assessing soldier fatigue and battle readiness, body gesture recognition/motion capture, personal item tracking, iris/facial recognition,

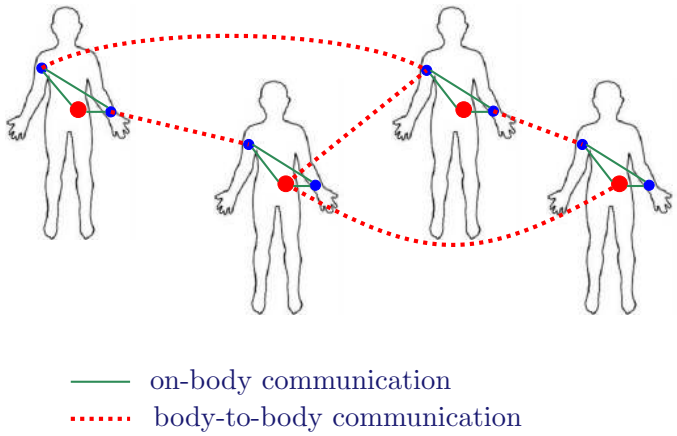

Figure 1.3: A BBN demonstrating body-to-body communications between on-body hubs and sensors

emotion detection and social networking applications [2, 11]. However, the underlying technology is still at an early stage of deployment and typically based on very specific wireless communications technologies. Some well-known international standards for BANs are — IEEE 802.15.6 Standard [12]; Bluetooth Low Energy (BLE) [13]; ETSI SmartBAN [14]; which support low-power, short-range communications with star or multi-hop topology, to serve a variety of medical and non-medical applications. BANs may interact with the Internet and other existing wireless technologies like ZigBee [15], WSNs [16], Bluetooth [17], Wireless Local Area Networks (WLAN) [18], Wireless Personal Area Networks (WPAN) [19], video surveillance systems [20] and cellular networks [21].

1.1.2 Wireless Body-to-Body Networks (BBNs)

When multiple closely-located BANs coexist, the potential inter-network communications and cooperation across BANs leads to a significant extension of the concept of wireless body area networks (BANs) [22] – known as wireless body-to-body networks (BBNs) [23] or, more broadly, the Internet of Humans (IoH) [24] (Fig. 1.3). The main motivations behind BBNs are:

- to make use of body-to-body (B2B) communications to overcome the problems of coexistence and general performance degradation for closely located BANs;

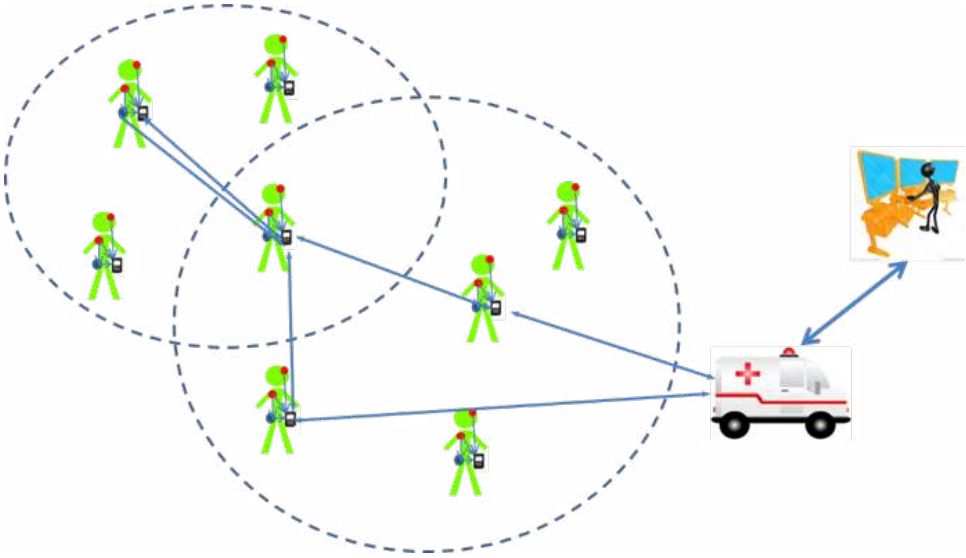

Figure 1.4: BBN providing outdoor medical service

- to provide connectivity as independent or subsidiary networks when traditional network connectivity is unavailable or limited, e.g., in emergency situations and densely populated areas.

Importantly BBNs can provide greater radio coverage and connectivity than BANs while maintaining all the advantages of BANs. BBNs are more dynamic and potentially larger-scale than individual BANs, such that any BAN member can join or leave the network seamlessly, without the need for any centralised infrastructure. The concept of BBNs is to send collected data, i.e., physiological information across closely located BANs via wearable sensors, to reach the intended destination in case of unavailable or out-of-range network infrastructure, e.g., in emergency indoor/outdoor scenarios. For instance, in a disaster where many people are injured and the cellular and fixed-line networks are damaged, BBNs can help in the triaging and monitoring of patients by relaying information from body to body up to the access point of the on-site medical service provider (Fig. 1.4), providing timely intervention and treatment.

BBNs have a wide range of potential applications besides remote population monitoring, such as group rehabilitation and therapy; avoiding outages (due to body shadowing) in individual BANs, through cooperative body-to-body commu-

nications; facilitating rescue/medical teams in a disaster area, and ambient assisted living (AAL) [25]. Further applications beyond health-care include: battlefield communications; precision monitoring of athletes; augmented reality [26]; performing synchronised activities, e.g., interactive dancing [27]; interactive gaming [28], and better enabling communications in densely populated areas, e.g., city centres, concerts and sports venues, where the primary network service is not sufficient.

1.2 Problem Statement and Proposed Solution

As BANs are continuing to become more pervasive, their coexistence is a major concern. And, as a major application of body-centric networks is for healthcare and emergencies, reliable communications is of utmost importance. The requirement for better coexistence and reliable communications leads to the need for body to body networks (BBNs). BBNs operate in a dynamic environment consisting of highly mobile individual BANs moving in and out of each others range, such that global coordination is typically not possible. In BBNs, radio channels experience significant shadowing due to obstructions and power absorption by nearby human bodies and body-parts due to frequent, different, movements. A simple postural change can block communications for a long period of time, resulting in decreased reliability, increased latency and increased energy consumption. In this context, body-centric channels have long coherence times, which can cause longer performance degradation when there is significant channel attenuation. Moreover, due to resource constraints of these low-power networks, providing best communications efficiency is vital in their optimisation.

Hence, in this thesis, we aim to address the following problem:

How to improve communications reliability and optimise connectivity amongst many co-located BANs or, more broadly, BBNs in order to facilitate self-organised, efficient, and distributed body-centric networks?

To this end, we develop and analyse cross-layer optimised routing techniques to disseminate information among distributed coexisting BANs (or BBN) by utilising body-to-body (B2B) channels with cooperative communications. The cross-layer optimisation is performed between different OSI layers, i.e., physical, MAC, and

network layers, to improve packet delivery ratio and latency along with accelerated reaction/response time within the network. We implement adaptive mechanisms based on time-varying channel condition estimated with longer coherence time of body-centric channels. We also investigate the predictive characteristics, i.e., wide sense stationarity and long-range dependence, of body-centric channels in order to build intelligent network, which can learn and self-organise. Based on the body-centric channels' predictive characteristics, we apply multi-objective decision-making with adaptive scheduling to jointly optimise throughput, latency, and energy consumption of body-to-body channels. It is demonstrated with experimental analysis that the proposed methods provide the following benefits, in key performance metrics, for BBNs:

- **Increased packet delivery ratio;** In distributed BBNs, making use of alternative/cooperative paths available through nearby BANs, enables greater network reliability. It is shown that negligible (almost 0%) packet error rate is achieved with the proposed cross-layer optimised routing techniques in a practical scenario with 10 coexisting BANs.

- **Reduced latency;** Longer outages can be avoided with alternative paths through available sensors within the range of the nodes-of-interest. Also, adaptive techniques applied over such networks enable real-time delivery of critical/non-critical information. With the cross-layer methods, an acceptable amount of latency (according to the IEEE 802.15.6 BAN standard guideline [29]) is achieved for both medical (< 125 ms) and non-medical (< 250 ms) applications.

- **Increased throughput;** It is shown that with the increased packet delivery ratio, throughput in terms of successfully received packets per second, also increases after applying the proposed methods, specifically with adaptive carrier sensing mechanism with CSMA/CA and multi-objective decision-making.

- **Reduced Energy Consumption;** The cross-layer optimisation used in this thesis, avoids the redundant use of resources, which decreases energy consumption. It is observed that with cooperative communications, although

there is extra energy consumption for the alternative path, the overall energy consumption is reduced due to decreased packet failure rate. Also, the applied multi-objective optimisation provides a suitable trade-off between throughput, latency, and energy consumption of the channels.

In summary, the proposed solution provides improved reliability, together with optimised and efficient connectivity, amongst many closely-located BANs (or BBNs) for large-scale and highly connected distributed real-world applications. Very importantly, this is validated in this thesis using many hours of empirical everyday on-body, and body-to-body, radio channel data.

1.3 Thesis Overview and Outline

This thesis provides design and analysis for optimisation of narrowband body-centric communications near the 2.4 GHz ISM band. Cross-layer and predictive techniques are applied over large-scale real-life experimental channel measurements collected from groups of mobile subjects wearing sensor radios on their body performing 'everyday' mixed activities (e.g., walking, sitting, standing, turning, talking) in indoor/outdoor environments (e.g., building, office space, street, cafe/pub), for a significant amount of time — which provides a normalised outcome from many typical BBN scenarios. Throughout the thesis, we mainly focus on the performance analysis and optimisation of narrowband body-to-body channels between coexisting BANs, but also provide some accompanying study of the performance of narrowband on-body and off-body channels. The experimental analysis performed with extensive real-life body-centric channels in this thesis, answers the following:

- How much improvement does cooperative communications provide for direct link body-centric communications under significant shadowing?
- How can the available channels (body-to-body) between coexisting BANs be efficiently utilised, for improving the reliability of BBNs, with cooperative multi-path routing?
- How can the slowly-varying, frequency non-selective, radio channels be exploited with adaptive mechanisms, to improve the performance of BBNs?

- Does cross-layer optimisation between non-adjacent layers (physical-network layers), without radio interference mitigation, provide acceptable latency and packet delivery ratio for closely located BANs?
- Are wireless body-to-body channels wide-sense-stationary (WSS) or second-order stationary?
- Do wireless body-centric channels have long-range dependence (LRD) or long-memory?
- What is an appropriate model to characterise the shadow fading of body-to-body channels for coexisting BANs?
- Do the predictive characteristics , i.e., WSS and LRD, of B2B channels vary for different sensor radio placements?
- How to utilise the predictive characteristics of B2B channels for multi-objective optimisation over BBNs?

The technical contributions of this thesis are detailed in four chapters (as demonstrated in Fig. 1.5), which address the questions outlined above. Chapters 3 and 4 describe cross-layer optimisation for BBNs, and chapters 5 and 6 analyse the predictive behaviour of body-centric channels and apply multi-objective optimisation suited to this behaviour over body-centric channels.

The contributions of each chapter of this thesis can be summarised as:

Chapter 2: An up-to-date literature review of existing work relevant to this thesisis provided, along with key research gaps addressed in this thesis. For body-centric networks, the general architecture and communications technologies are described, along with the typical challenges associated with practical deployment of these networks.

Chapter 3: Cooperative combining mechanisms, and cross-layer optimisation over real-life body-centric channels, are investigated. First, we investigate the performance of cooperative receive diversity for BANs used for monitoring sleeping people, where we show that cooperative combining over two-hop channels provides

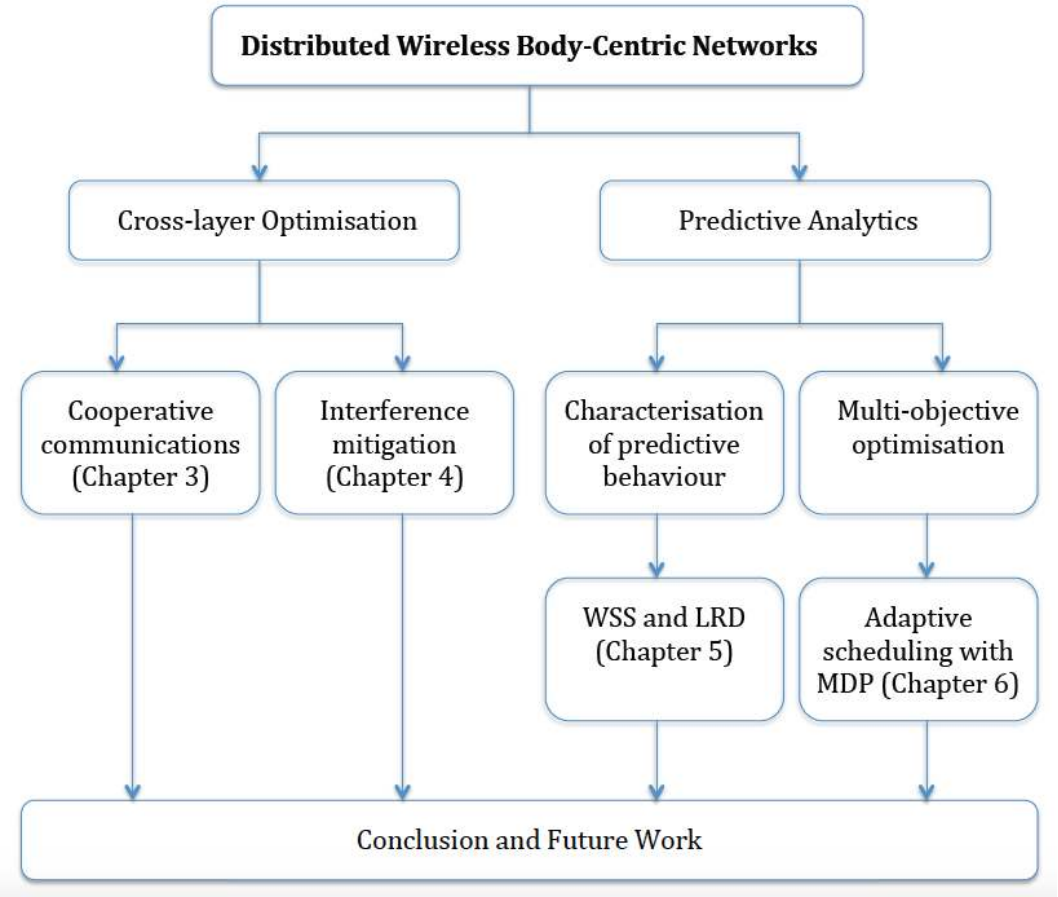

Figure 1.5: Thesis Flowchart

very large improvements over the direct link communications of a star topology for monitoring a sleeping subject. Then we propose two different cross-layer optimised routing techniques – shortest path routing (SPR) and cooperative multi-path routing (CMR) — that incorporate 3-branch cooperative selection combining, without central coordination across multiple coexisting BANs. The best route is selected at the network layer according to channel state information from the physical layer The key findings from this chapter are:

- For BANs used to monitor sleeping subjects, cooperative combining techniques (i.e., selection combining and switch-and-examine combining) with two-hop communications provide up to 7 dB and 20% improvement over direct link communications, with respect to outage probability and continuous

outage duration, respectively.

- The proposed CMR provides up to 8 dB improvement over state-of-the-art routing protocols at 10% outage probability.
- CMR outperforms other protocols in case of throughput (packets/second) by providing 95% successful packet delivery.
- CMR produces the lowest amount of average end-to-end delay with respect to other protocols, when estimated with lower receive sensitivity, i.e., −90 dBm and −86 dBm.
- With less receive sensitivity, i.e., −90 dBm and −86 dBm, the energy consumption of CMR remains relatively constant, while the energy consumption of other protocols increases significantly due to an increase in packet failure rate and retransmissions.

Chapter 4 This chapter analyses the performance of the SPR and CMR techniques (proposed in Chapter 3) across distributed BBNs with interference mitigation schemes, by associating the PHY-Network cross-layer optimisation with different MAC layer schemes, i.e., time division multiple access (TDMA) and novel carrier sense multiple access with collision avoidance (CSMA/CA). The key outcomes of this analysis with experimental measurements are as follows:

- CMR provides up to 14 dB improvement with 8.3% TDMA duty cycle over SPR at 10% outage probability, and up to 9 dB improvement over SPR, at 90% packet delivery ratio.
- The proposed adaptive carrier sensing mechanism provides 20% and 6% improvement, over a coordinated TDMA approach with higher duty cycle, for throughput and spectral efficiency, respectively, and provides acceptable packet delivery ratio and outage probability with respect to SINR.

Chapter 5 In order to apply predictive optimisation over body-centric channels, it is important to investigate the feasibility of applying predictive schemes over

body-centric channels. Hence, in this chapter, we investigate the predictive characteristics, i.e., wide-sense-stationarity (WSS) and long-range dependence (LRD, long-memory), of on-body and body-to-body channels. We employ different hypothesis tests for evaluating mean and variance stationarity, along with evaluating distribution consistency of several body-centric channels. We also examine the pattern of the decaying auto-correlation function and estimate the Hurst exponent for investigating the LRD characteristics. We show that

- Unlike on-body channels, which are non-stationary, body-to-body channels can possess WSS characteristics for a range of window lengths between 0.5 s to 15 s (typically 5–8 s), depending on on-body sensor locations and the amount of shadowing in the corresponding channel.
- The Hurst exponent is very high (around 0.9) for body-centric channels and the auto-correlation between data points of the channels decreases very slowly (power-like decay), which both indicate retaining LRD or long-memory characteristics.

Chapter 6 Influenced by the existence of WSS and LRD characteristics (presented in Chapter 5) of body-to-body channels, we apply multi-objective optimisation with adaptive scheduling over BBNs, by following a discrete time Markov decision process (MDP) that utilises the predictive characteristics (i.e., WSS and LRD) of B2B channels. For adaptive scheduling, time division multiple access (TDMA) and carrier sense multiple access with collision avoidance (CSMA/CA) — are combined, to utilise the advantages of both TDMA and CSMA/CA. The outcome is Pareto optimal that provides a desired trade-off between three objectives — maximising throughput, and minimising continuous latency and energy consumption of the B2B communications, between any two BANs (direct link) in the presence of other coexisting (interfering) BANs. We compare the Pareto optimum (obtained from adaptive scheduling with MDP), with the results of TDMA and CSMA/CA applied separately. From the experimental results, we find that

- The Pareto optimum outcome (f^*) can provide up to 3.4 times better throughput than TDMA (with a 10% duty cycle), but also can consume up to 3.2 times more energy (because of the increased active period) than TDMA (as

TDMA schemes have fixed duty cycles). Then again, f^* produces a slightly (around 5%) higher amount of continuous latency than TDMA schemes for smaller intervals, and similar amount of continuous latency as TDMA for longer intervals (≥ 4 s).

- CSMA/CA with -70 dBm carrier sense threshold (cs_{th}) consumes around 2.3 times more energy, and has much higher continuous latency, than the Pareto optimum f^*, although it provides almost twice as much throughput than the Pareto optimum (f^*). For instance, CSMA/CA with $cs_{th} = -70$ dBm has a continuous latency of greater than or equal to 250 ms for around 46% of the total time, whereas f^* produces the same amount of latency for less than 30% of the total time.

- The Pareto optimum has the highest packet delivery ratio (PDR $> 80\%$), than all other individual actions.

Chapter 7 Finally, this chapter provides a summary of the results drawn from this thesis including possible directions for future research.

Chapter 2

Literature Review

In wireless body-to-body networks (BBNs), communication takes place among sensors and hubs worn by multiple human subjects, where each subject can have an operating wireless body area network (BAN). Hence, the general architecture and technology of BANs can also be applied within BBNs. In this chapter, first we provide a description of the communication architecture and technology for body-centric networks, along with associated challenges. Then we discuss the current state-of-art for optimising body-centric communications in detail. Following these discussions we highlight research gaps. Although the main focus of our research is BBNs, which have not been investigated to nearly as a large extent as BANs, here we discuss both BAN and BBN communications research, as BAN operations provide context to BBNs.

2.1 Communications Architecture and Technology of Body-centric Networks

2.1.1 Communications Architecture

Communications architecture in body-centric networks generally follows a multi-tier architecture, where the communications occurs in multiple hierarchical tiers:

- **Tier-**1 **(intra-BAN communications)** Intra-body communications [30–32] in tier-1 includes in-body, on-body, and off-body communications that

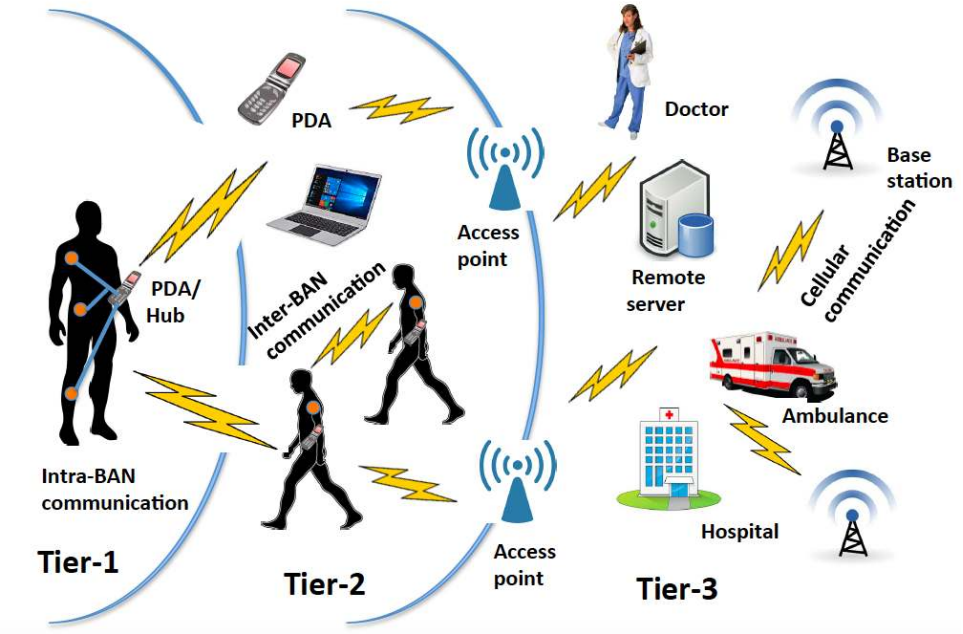

Figure 2.1: Multi-tier architecture for body-centric communications.

occurs in/on or around an individual BAN. In this tier, the wearable sensors send physiological information to the hub or personal device of a BAN and actuators can receive control information from the hub.

- **Tier-2 (inter-BAN communications)** In this tier, communications occurs between personal devices or hubs of different BANs (i.e., body-to-body communications or inter-BAN communications [23, 33, 34]) and possible access points (e.g., routers) [35, 36] or gateways (e.g., smartphones) [37, 38]. The hub or personal devices in tier-2 can relay the information between hubs to the nearby access point to send to tier-3 entities (e.g., servers).

- **Tier-3 (beyond-BAN communications)** Tier-3 communications is beyond BANs/BBNs, which helps to enhance the coverage area for applications of body-centric networks, e.g, remote patient monitoring [39, 40], e-health care [41], emergency medical services [42, 43], enabling authorised health care personnel (doctor/nurse) through the Internet or a cellular network.

The communications strategy in different tiers can be further divided in to the

following categories:

Centralised:

The use of a centralised architecture [44–47] is the most common communications strategy in a BAN where a central hub/gateway device (placed on/in/around the body) coordinates the sensor/actuator nodes placed on different parts of the body — collects data/information from the sensor nodes and sends control information to actuators. This type of communications particularly occurs in tier-1 at small-scale (typically within a single BAN). A number of BANs in tier-1 can also be coordinated with a coordinator BAN (e.g., cluster-head) or a central access point in tier-2.

Cluster-based:

In a cluster-based architecture [48, 49], multiple clusters or groups are formed between coexisting BANs, where in each cluster there are multiple BANs (tier-1 communications). Each cluster has a cluster head or coordinator/gateway, e.g., a BAN node/hub, which further communicates with other cluster heads for inter-cluster communications and data transfer (tier-2 communications). The cluster head controls the cluster, and the coverage of the cluster is usually one or two hops from the cluster head. This type of architecture is useful for dense networks, and when separate groups of BANs are performing different tasks [50–53].

Distributed:

In a distributed architecture [54,55], information is disseminated from one node to another adjacent node, until it reaches the intended destination (i.e., coordinator, hub, personal device, access point). A distributed architecture provides scalability and resilience to the network where the nodes can enter or leave the network at any time, without interrupting the communications as all the nodes are connected through various alternate paths. The distributed architecture can be applied in both tiers (tiers 1 and 2) for body-centric communications, such as, intra-BAN

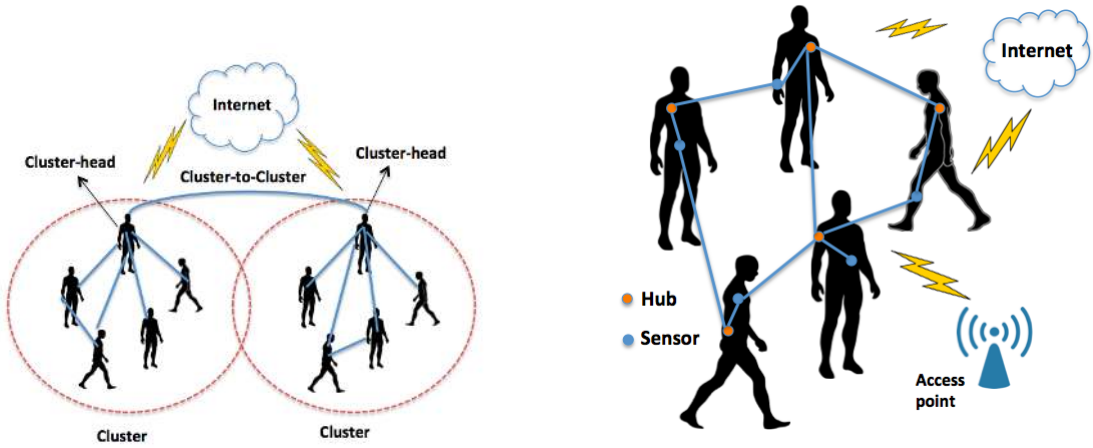

(a) (b)

Figure 2.2: (a) Cluster-based and (b) Distributed architecture of coexisting BANs.

communications to reach the coordinator/hub in tier-1, and inter-BAN communications to reach the intended access point in tier-2. Also the communications between a BAN sensor (in tier-1) and the intended access point (in tier-2) can also be performed in a distributed manner by combining tier-1 and tier-2 communications. A distributed architecture helps to establish communications in the case of multiple BANs coexistence without external coordination.

2.1.2 Radio Technology

Body-centric networks are radio-frequency (RF) based wireless networks that require low-power, low-complexity radio technology for practical deployment at a large-scale. Most of the literature in BANs is focused on RF techniques classified according to the frequency bands in which they operate [30, 56–60]. The IEEE 802.15 Task Group 6 provided an overview of the frequency band regulation for BANs in [61] (shown in Fig. 2.3). Some of the popular radio technology standards used in BAN communications are – IEEE 802.15.4/ZigBee [15], IEEE 802.15.6 [12], and Bluetooth Low Energy [13]. Other technologies that can also be used in body-centric communications, such as BANs/BBNs, include WLAN [18, 62], Bluetooth [17], ultra-wideband (UWB) [63], cellular [21], and 3G/4G/5G [64].

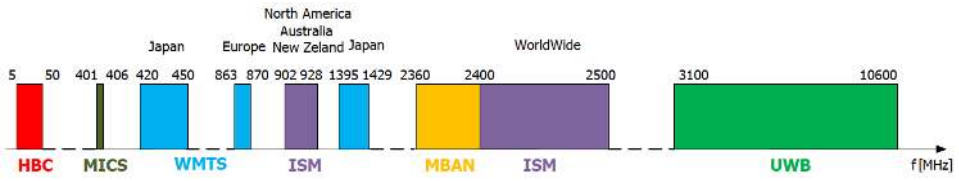

Figure 2.3: Some of the available bands for BAN based on RF technology [1].

Unlike the BAN standard (IEEE 802.15.6), there is no specific standard designed for BBNs. More recently, an European standard (ETSI TC SmartBAN) [14] has been developed, which can support coexistence of BANs in an IoT environment to bridge between devices operating in different radio standards. The choice of a suitable technology for BBNs depends on their particular applications, as no single industrial standard has all the required specifications for large-scale BBN (due to different data rates, power consumption, coverage, and topology). Some proprietary wireless technologies have been developed for low power WSNs and healthcare applications, e.g., ANT/ANT+ [65], Sensium [66], Zarlink (now acquired by Microsemi) [67], Insteon [68], Z-Wave [69]. However, the radio technologies used in BANs can be applied for BBNs as the nodes/sensors in BBN are placed on different bodies in a close proximity. The specifications of different technologies used in body-centric networks are provided in Table 2.1 and the description of some technologies from literature [1–3, 70] is as follows:

IEEE 802.15.4 Standard

IEEE 802.15.4 technology (ZigBee) [15] is a widely used radio standard in BANs [71,72], which was typically intended for wireless personal area networks (WPANs) and wireless sensor networks (WSNs) applications [73,74]. The key features of this technology are: low power, short-range (up to 100 m), low bit rate, low cost and low complexity. The IEEE 802.15.4 specifies the two bottom layers of the ISO/OSI protocol stack – physical and MAC layers for low rate WPANs (LowPAN). For a definition of upper layers, there are two options – ZigBee protocols (specified by the industrial consortia ZigBee Alliance) and 6LowPAN [75]. IEEE 802.15.4/ZigBee can operate in three ISM (Industrial, Scientific, and Medical) bands (i.e., 868/915/2400 MHz) with a data rate of $20 - 250$ kbps [76]. It supports star, cluster, and mesh

topology and provides the advantage of network coverage by providing multi-hop routing in both cluster and mesh topology [77].

The 802.15.4 MAC layer supports two operational modes: beacon enabled and non-beacon enabled mode. In beacon enabled mode, the coordinator initiates the channel access with a beacon packet and a superframe structure is used that is divided into an active and an inactive period. The active period consists of a contention access period (CAP) and a contention free period (CFP). During the CAP, the channels follow a slotted CSMA/CA mechanism, whereas the CFP contains guaranteed time slots (without contention), supporting TDMA. The inactive period allows nodes to go into sleep mode or low power mode according to the specific application. In the non-beacon enabled mode, the channels only use an unslotted CSMA/CA mechanism [15].

ZigBee suffers from interference from WLAN transmissions [78] and low data rate (only up to 250 kbps) that is not adequate for large-scale deployment of connected BANs [70], rather ZigBee is more suitable for home automation [79] and industrial automation and control [80].

IEEE 802.15.6 Standard

The IEEE 802.15 Task Group 6 developed a standard specifically designed for BANs – namely IEEE 802.15.6 [12], which is one of the latest and well-known international standard for BANs. The aim of the IEEE 8012.5.6 standard was to describe the PHY and MAC layers so as to provide a certain quality level for low power devices in communications surrounding the human body [81]. The PHY layer defines three different communications bands:

- **Narrowband (NB) PHY:** The frequency bands supported in NB PHY are as follows: $402 - 405$ MHz, $420 - 450$ MHz, $863 - 870$ MHz, $902 - 928$ MHz, $950 - 958$ MHz, $2360 - 2400$ MHz and $2400 - 2483.5$ MHz. Among the three communication bands, NB PHY is best suited to a greater number of healthcare applications [82], due to its lower carrier frequency (results in less attenuation) and smaller bandwidth (1 MHz or less), hence reducing multi-path propagation and inter-symbol interference [83].
- **Ultra-wideband (UWB) PHY:** The frequency bands supported in UWB

are divided in to a low ($3.25 - 4.75$ GHz) and a high ($6.6 - 10.25$ GHz) band for supporting high quality, low complexity and ultra low power operations [1]. Also, UWB PHY considers two types of UWB technology: frequency-modulated FM-UWB and impulse-radio IR-UWB. As stated in [82], IR-UWB is best suited for BANs due to lower power consumption and efficient implementation of non-coherent receivers [84]. Also UWB offers higher throughput with a large bandwidth – each UWB channel has a bandwidth of 499 MHz in IEEE 802.15.6 [12].

- **Human-body communications (HBC) PHY:** This band supports the frequency band from $5 - 50$ MHz and uses the human body as a communication medium. HBC is the first technology to use electric field coupling (EFC) – capacitive and galvanic coupling where the transmission is over the medium of human skin by an electrode, rather than by an antenna [82].

The 802.15.6 MAC layer divides the channel into beacon periods or superframes of equal length, and provides three access modes coordinated by the hub:

- **Beacon mode with superframe boundaries:** In this mode, the coordinator sets the time for superframes by sending a beacon packet to indicate the beginning of an active superframe period. The superframe is again divided into different access phases: exclusive access phase (EAP), random Access phase (RAP), contention access period (CAP), and managed access phase (MAP). The EAP is used for transmission of emergency data, both the RAP and CAP use CSMA/CA or slotted ALOHA methods. In MAP, the coordinator may schedule intervals, or poll nodes [12].

- **Non-beacon mode with superframe boundaries:** In this mode, beacons are not sent at the beginning of the transmission, but the superframe period and phases (possibly in MAP) are defined and unscheduled frames are transmitted by the coordinator.

- **Non-beacon mode without superframe boundaries:** This mode also does not need a beacon to be sent, and the superframe period and slot allocation are also not defined. The coordinator supplies unscheduled frames of

type 2 and as a portion of EAP or RAP to employ CSMA/CA based random access schemes.

Bluetooth Low Energy

Bluetooth wireless technology [17] is a short-range, low-power, and low-cost standard designed for replacing the cables connecting portable or fixed electronic devices in a WPAN or piconets [85, 86]. Bluetooth devices operate in the 2.4 GHz ISM band with coverage ranging from $1-100$ meter, and supports only star topology and a maximum data rate of 3 Mbps (with Enhanced Data Rate or EDR). Bluetooth low energy (BLE) [13] is a configuration of Bluetooth technology that includes lower power consumption and complexity with lower cost than EDR with a data rate of up to 1 Mbps, and operates with a simpler protocol stack than other Bluetooth technology and star-configured networks, which makes it suitable for some BAN applications, e.g., consumer applications [87] and regular (less critical) health parameters monitoring [88]. However, it is not suitable for critical and high data rate healthcare applications due to the low data rate short-range communication that requires line-of-sight connection for reliable operation [89]. Also, BLE is not appropriate for BBNs as it does not support multi-hop communications (only supports on-body communications with star topology), and has limited scalability, QoS, and interoperability [56].

SmartBAN

A new standard has been developed for BANs recently by the ETSI TC (European Telecommunication Standards Institute Technical Committee) – namely SmartBAN [14], which specifies low-power, low-complexity PHY and MAC layers with lighter data presentation formats compared to IEEE 802.15.6. SmartBAN seeks to provide a robust strategy for coexistence of an individual BAN co-located with devices/entities operating according to different radio standards. It supports a star topology with variable data rates and can be interfaced with Bluetooth, BLE, and other existing radio standards. The SmartBAN PHY utilises two different channels: a control channel where control beacons are broadcast by hubs; and a data channel where data and control transmissions take place. This two channel concept

provides fast channel acquisition and easy hub-to-hub communication. In SmartBAN MAC, the data channel is divided into inter-beacon intervals that consist of three parts: contention free scheduled access period (uses TDMA), control and management (C/M) period (uses slotted-Aloha), and an inactive period. Additionally, a multi-use channel access (MCA) mode is defined that utilises scheduled, but unused, time slots for increasing channel utilisation.

Other Technology

Some other technologies used in body-centric networks are: ultra-wideband (UWB) [63], Bluetooth High Speed (HS) [90], WLAN [18,62]. Bluetooth HS supports data rate from $3 - 24$ Mbps and includes 802.11 protocol adaptation layer (PAL) into the protocol stack [3]. Also, some commercial and proprietary technologies are used in body-centric networks, e.g., ANT/ANT+ [65], RuBee [91], Sensium [66], Zarlink (now acquired by Microsemi) [67], Insteon [68], Z-Wave [69], RFID [92], BodyLAN [93]. ANT features simpler protocol stack and lower power consumption, which has been embedded in Nike shoes and can be interfaced with iPod products [3]. Insteon and Z-Wave are used for home automation with mesh networking technologies [94,95]. RuBee and RFID are complimentary to each other in terms of frequency bands, and both are used for asset management and tracking [3]. Sensium features ultra-low power transceiver platform that is custom designed for healthcare and lifestyle management applications [56]. The communications architecture is centralised with single-hop connection. Zarlink developed an ultra-low power RF transceiver that is configured as an implantable medical device (IMD), and supports extremely low power consumption [56].

2.2 Challenges of Wireless Body-centric Communications

Even though body-centric networks can provide major enhancements in human life style through the use of ubiquitous networking, several challenges remain that hinder practical deployment of these networks.

Table 2.1: Specifications of different wireless technologies used in body-centric networks [2, 3].

Technology	Frequency	Data Rate	Coverage	Topology
Bluetooth	2.4 GHz ISM	780 Kbps	10 – 150 m (on-body)	star
Bluetooth (EDR)	2.4 GHz ISM	3 Mbps	10 – 100 m (on-body)	star
Bluetooth (HS)	2.4 GHz ISM 5 GHz	3 – 24 Mbps	10 m (on-body)	star
Bluetooth (LE)	2.4 GHz ISM	1 Mbps	10 m (on-body)	star
IEEE 802.15.4 (ZigBee)	2.4 GHz ISM 868 MHz 915 MHz	20 – 250 Kbps	10 – 100 m (on-body)	star, multi-hop mesh, cluster
IEEE 802.15.6	2.4 GHz ISM 401 – 406 MHz 902 – 928 MHz	1 Kbps to 10 Mbps	2 – 5 m up to 10 m	star, two-hop
Ultra-wideband (UWB)	3.1 – 10.6 GHz	110 – 480 Mbps	5 – 10 m (on-body)	star
RFID (ISO/IEC 18000 – 6)	860 – 960 MHz	10 – 100 Kbps	1 – 100 m	peer-to-peer
SmartBAN	2.4 GHz ISM	(variable) 75 Kbps to 15 Mbps	< 2 m	star hub-to-hub
ANT	2.4 GHz ISM	1 Mbps	30 m on-body	star, mesh peer-to-peer
IEEE 1902.1 (RuBee)	131 KHz	9.6 Kbps	30 m	peer-to-peer
Zarlink (ZL70101)	402 – 405 MHz 433 – 434 MHz	200 to 800 Kbps	2 m (in-body)	peer-to-peer
Insteon	131.65 KHz 902 – 924 MHz	13 Kbps	Home area	mesh
Z-Wave	900 MHz ISM	9.6 Kbps	30 m	mesh
Sensium	868 KHz 915 MHz	50 Kbps	1 – 5 m (on-body)	star

2.2.1 Mobility

Since the human body is constantly moving, sensor nodes on the body have mobility features. Due to the postural body movements affecting BANs/BBNs as well as their mobility, the use of networks incorporating infrastructure such as backbone routers would generally be very costly and unfeasible. Even for indoor BANs coexistence with mobile people, while deploying a backbone router is possible to some extent, the connection between a BAN hub and the router can be blocked/shadowed by any obstacle or may go out of range because of the movement, e.g., postural changes or mobility [96]. Importantly, people having mobility issues can incur life-threatening risks, as these type of outages can be for a longer period of time with only a simple postural change.

2.2.2 Time-varying dynamic topology

Unlike wireless sensor networks, the communication channels in BANs are heavily attenuated from shadowing by the human body. Due to this shadowing and postural body movements, the path loss between sensor nodes in a BAN will be non-stationary and constantly changing [97–99]. BAN radio propagation typically encounters significant path loss with deep fades that can last for a long time, of the order of seconds [82]. This will cause serious topological partition problems and time-varying channel conditions where links between nodes are broken, and built, frequently. Additionally, when multiple BANs coexist in a very close proximity for any special indoor/outdoor activity, or in any emergency indoor/outdoor situation, the interfering radio communications and shadowing from different bodies or BANs (including the body parts of the BAN-of-interest) make it very difficult for the BAN-of-interest to transfer the collected information to the intended access point [96].

2.2.3 Routing challenges

Due to limited resources, unstable links, interference and network lifetime, selection of routing protocols and routing metrics play a critical role in order to find out the efficient route to the destination in wireless body-centric networks. Both periodic

and real-time data transfer are required for BANs/BBNs. As stated in [100], even though the general characteristics of BANs are somewhat similar to mobile ad hoc networks (MANETs) [101] and wireless sensor networks (WSNs) [102], the stringent requirements of BANs/BBNs impose certain constraints on the design of their networking protocols that leads to novel challenges, which can not be met through typical WSN/MANET routing protocols.

For example, the frequent topological changes in highly mobile coexisting BANs particularly occur with group-based movement, rather than node-based movement in MANETs, which suggests that all nodes in BANs move with keeping their position with respect to one another, while in MANET each node moves independently from other nodes in the network [103]. In fact, the on-body sensor nodes used in BANs move relative to the coordinator node of the corresponding BAN which is used as their reference point [104]. As the user moves, the whole network moves and then may move into (and out of) the range of other networks frequently, which results in network collision [105]. It is different to the interference events of cellular/sensor networks where only one or two nodes interfere, and base stations rarely interfere [96]. The random nature of BAN movement means that network collisions in BBN can be very short (e.g., people passing on the street) or very long (e.g., family members/hospital patients may remain close for hours) [105].

2.2.4 Power Constraints

The management of scarce resources, such as, low-power battery, and low transmit power considering human body reaction to electromagnetic radiation is one of the major issues to deal with in these types of networks. BANs have more strict energy constraints in terms of transmit power when compared to traditional sensor and ad hoc networks as frequent node replacements can be quite unfeasible, and might require surgery in some scenarios, for implant nodes [2].

2.2.5 QoS consideration and Context-awareness

Body-centric networks exhibit specific QoS requirements at every single layer: data reliability, traffic segmentation, data resolution, bandwidth, path latency, routing maintenance, congestion management, path cost, connectivity robustness, com-

munication range, throughput and transmission reliability [106, 107]. Moreover, context-aware and adaptive strategies need to be developed where the network adapt to topological, channel state, and environmental changes in a timely manner.

2.2.6 Network Scalability and Interoperability

The number of people using wireless sensor devices for healthcare and other purposes is rising at an alarming rate [4,108,109]. When the number of nodes increases in the neighbourhood, scalability issues arise, which affect throughput, latency and resource allocation of dense networks. Moreover, neighbouring BANs operating in the same frequency bands are likely to interfere with each other. For instance, as each member of a BBN can join or leave the network seamlessly, a variable number of BANs need to be supported by the BBNs to increase the capacity and spectral efficiency of the network with reduced latency.

2.2.7 Security and Privacy Issues

A number of security and privacy risks [110–113] arises from the advancement of body-centric communications, specifically in health related applications. For instance, unauthorised access, message disclosure, message modification, denial of service, compromised node, routing attacks, eavesdropping, and malicious activities [111]. The networks associated with the user's health data are prone to potential risks of internal and external intrusions during data storage, access, and wireless data transmission, which can lead to life-threatening and serious health consequences. Furthermore, the stringent resource constraints, design, and usability of these miniaturised sensor devices derive challenges to implement lightweight security and authentication protocols with minimal complexity.

As the main focus of this thesis is in reliability and optimised connectivity, we discuss existing works related to these specific matters in the following sections.

2.3 Existing Research for Optimising Body-centric Communications

2.3.1 Research on Cooperative Communications

Cooperative communications is widely used for improving and optimising reliability and efficiency in body-centric communications. In [114], Chen *et al.* analysed cooperative diversity schemes in an ultra-wideband (UWB) BAN (in a sitting posture) with a two-stage single-hop transmission model to statistically characterised the channel parameters of a single-hop cooperative network. Huang *et al.* [115] investigated three transmission schemes in a BAN, i.e., direct transmission, single-relay cooperation, and multi-relay cooperation and studied optimal power allocation with and without posture state information. They showed that power allocation making use of posture information can reduce energy consumption. The authors in [116] investigated an incremental relay based cooperative communication scheme where they demonstrated that the cooperative schemes improve energy efficiency significantly when compared to direct communication. In [117], Arrobo *et al.* proposed a cooperative network coding technique for improving throughput and network reliability in multiple-input-multiple-output (MIMO) BANs. In [118], the authors proposed a cooperative BAN environment that supports multi-hop transmission through cooperation involving both environmental sensors and BAN nodes. Their solution extends the cooperation at the MAC layer to a cross-layered gradient based routing solution that allows interaction between a BAN and environmental sensors in order to ensure data delivery from BANs to a distant gateway. Arrobo *et al.* [119] compared two different approaches – cooperative network coding (CNC) and cooperative diversity combining (CDC) for BANs — where they found that CDC provides higher throughput than CNC with lower complexity.

In [120], Dong. *et al.* showed that cooperative selection combining with two dual-hop relayed links in an individual BAN provides significantly better co-channel interference mitigation than single-link star topology BAN communications in case of distributed multi-BANs coexistence. Dong. *et al.* [121] also proposed an opportunistic relaying scheme together with cooperative two-hop communication scheme

for mitigating interference in a single BAN in case of multiple BANs coexistence. In [122], the authors presented two-hop relay-assisted cooperative communications, integrated with transmit power control, based on simple channel prediction for a single BAN, where they demonstrated that relay assisted power control can reduce circuit power consumption by approximately 60% from that of constant transmission at 0 dBm, without much loss in reliability. Wang *et al.* [123] proposed a distributed cooperative scheduling scheme for increasing the packet reception rate (PRR) of intra-BAN communications by reducing the inter-BAN interference for coexisting BANs.

2.3.2 Research on Cross-layer Optimisation

In the past decade, several cluster-based and cross-layer routing protocols have been proposed for BANs along with other routing protocols [100]. Some of the cluster-based routing protocols (e.g. ANYBODY [124], HIT [125]) that have been designed for BANs aim to minimise the number of direct transmissions from sensors to the base station. WASP [126], CICADA [127], TICOSS [128] and BIOCOMM [129] are some cross-layer protocols between Network and MAC layers for BANs. Amongst these protocols, TICOSS and CICADA consume less energy, whereas the WASP scheme outperforms others in terms of efficient packet delivery ratio (PDR) [130]. Also, CICADA performs well among the other protocols in terms of reducing packet delivery delay [130]. Otal et al. proposed an energy-saving MAC protocol, DQBAN (Distributed Queuing Body Area Network) for BANs in [131], as an alternative to the 802.15.4 MAC protocol, which suffers from low scalability, low reliability and limited QoS in real-time environments. The proposed DQBAN is a combination of a cross-layer fuzzy-logic scheduler and energy-aware radio-activation policies [132]. The fuzzy-logic scheduling algorithm is shown to optimise QoS and energy-consumption by considering cross-layer parameters such as residual battery lifetime, physical layer quality and system wait time [132].

A number of interference-aware coexistence schemes for multiple BANs have been proposed in [104,121]. In [121], a cooperative two-hop communication scheme together with opportunistic relaying (OR) is applied on a single BAN (amongst coexisting BANs), which improves the outage probability and level crossing rate of on-

body channels with respect to suitable SINR threshold values. The authors in [104] proposed an energy efficient and interference-aware channel allocation scheme that also incorporates an intra-BAN and inter-BAN mobility model for BAN coexistence. A Cross-layer Opportunistic MAC/Routing protocol (COMR) [133] has also been proposed for improving reliability in BAN, where the authors have used a timer-based approach with combined metrics of residual energy and receive signal strength indicator (RSSI) as their relay selection mechanism in a single BAN, and compared it with Simple Opportunistic Routing (SOR) [134]. In [135], the authors have proposed an efficient cross-layer reliable retransmission scheme (CL-RRS) without additional control overheads between physical (PHY) and MAC layers, which significantly improves frame loss rate and average transmission time as well as reduces power consumption.

Some WSN routing protocols for low power lossy networks (LLNs) are proposed in literature. For example, RPL [136] uses a DODAG/rooted topology based on expected transmission count (ETX) metric which is similar to the collection tree protocol (CTP) proposed in [137] for WSNs, where the sink node collects data from different sensors with datapath validation and adaptive beaconing. In RPL, any-to-any routing is performed with a non-storing mode through the root node. To improve the performance of RPL, opportunistic routing protocol (ORPL) is proposed in [138], which combines opportunistic routing with a rooted topology, where any-to-any routing is supported through the common ancestors along with the root node based on EDC (Expected Duty Cycle) metric. In [139], the authors proposed a reactive distance-vector routing protocol named LOADng, which inherits the basic properties and operation of AODV (Adhoc On-demand Distance Vector routing) [140], yet aims to reduce the per packet overhead for route discovery by a smart route request [141] and expanding ring search [142]. Cooperative multi-path routing [143] yields better performance than single-path routing by providing simultaneous parallel transmissions with load balancing over available resources. We proposed a new CMR scheme in [22] for coordinated BANs, that uses two different paths (incorporating shortest path routing) which are combined at the destination. Also, it uses TDMA with low duty cycling to save energy consumption and avoid interference from surrounding non-coordinated BANs.

2.3.3 Research on Predictive Characteristics

In literature, there has not been much investigation into characterising predictive properties, i.e., wide-sense-stationarity (WSS), long-range dependence (LRD) of body-centric channels. To determine the WSS length/duration of wireless channels, a parametric approach (Rao test) is proposed in [144] to detect non-stationarity based on the time-variant auto-regressive (TVAR) model. A parametric unit-root test is proposed in [145] to parameterise a predetermined structure. Willink found non-stationarity in multiple-input multiple-output (MIMO) wireless channels in [146] by investigating the first and second moment with parametric one-way ANOVA (analysis of variance) and non-parametric time-dependent evolutionary spectrum analysis, respectively. In [147], the authors investigated WSS for vehicular communications with co-linearity of the local scattering function, where they found the channels to be strongly non-WSS. Other non-parametric approaches to identify the stationarity intervals include run-test described in [148], comparison of the delay power spectral density (PSD) estimated at different time instances [149] and evaluation of the variation of time-localised PSD estimate [150]. In [99], the authors used different parametric and non-parametric approaches for testing WSS of on-body channels and showed that on-body channels have non-stationary characteristics.

The concept of long-range dependence was introduced by Hurst in [151] with rescaled range analysis for studying the flow of water in the Nile river, which was further evaluated by Mandelbrot et al. in [152]. LRD characteristics are vastly investigated in spatial and time series analysis of econometrics and statistical measurements. However, several works have found LRD characteristics to exist in different empirical local area, wide area and ad-hoc networks [153–156]. The authors in [157] investigated the LRD property for bit, symbol and packet level error process of IEEE 802.15.4 networks, where they found existence of memory in bit and symbol level error process.

2.3.4 Research on Predictive Optimisation

Body-centric networks are resource-constrained networks that operate in dynamic environments where global coordination is not possible and the channels experience

interference and shadowing due to human-body movements, e.g., ambulatory and postural movements, obstruction by body-parts. Therefore, these networks need to be self-organised and perform dynamic optimisation for efficient resource utilisation [158,159]. One of the widely used powerful optimisation tools for such dynamic systems is a Markov decision process (MDP) [160,161]. The MDP framework [160,161] is a widely used powerful optimisation model for decision-making in stochastic and dynamic environments under uncertainty where the outcome partially depends on the decision made at each decision epoch. In wireless networks, MDPs are generally used to solve optimisation problem for obtaining desired objectives where the channels are unstable and resource constrained such as wireless sensor networks (WSNs). In [162], the authors performed an extensive survey of MDP models that are proposed for various design, optimisation and resource management issues in WSNs. To state a few, Lin *et al.* suggested a distributed algorithm for delay-sensitive WSN in [163] based on an MDP framework to autonomously enable routing and select transmission strategies to maximise the network utility. Similarly in [164], Hao *et al.* proposed an adaptive routing protocol for WSNs where they studied the energy consumption and delay trade-off based on an MDP framework. In [165], the authors presented distributed and centralised channel access models with hybid CSMA/CA-TDMA based on MDP, to access both contention period and contention-free period of the IEEE 802.15.4 based single-hop wireless personal area networks. Some further applications of MDP in WSNs include opportunistic transmission policy [166], transmit power control [167], relay selection for cooperative communications [168, 169], energy harvesting [170, 171]. Also, a detailed survey of MDPs in communications networks can be found in [172].

While MDP solutions have been rigorously investigated for WSNs, they have not been widely studied for deployment in wireless body area networks (BANs), or broadly BBNs (wireless Body-to-Body Networks), which falls within a specific part of WSNs. BANs/BBNs possess more stringent requirements than WSNs or MANETs as the body-centric networks are highly mobile due to the postural movements and shadowing by body parts of the closely located BANs, and experience sporadic periods (sometimes very long) of stability over time. The random nature of BAN movement means that network collisions in BBNs can be very short (e.g., people passing on the street) or very long (e.g., family members/hospital patients

may remain close for hours) [105]. Body-centric networks have strict power constraints as opposed to other standard wireless networks due to the management of scarce resources, such as, low-power battery and low transmit power considering human body reaction to electromagnetic radiation. Also, as stated in [100], the frequent topological changes in highly mobile coexisting BANs particularly occur with group-based movement, rather than node-based movement in MANETs and the interference events are also quite different to those of cellular/sensor networks [96, 105]. The above mentioned factors differentiating BANs/BBNs from WSNs/MANETs motivate the need for distinct study of MDPs in the field of body-centric networks. In [173], the authors use an MDP in order to tune a MAC-frame payload of BANs with a priority-based mechanism to optimize energy consumption of each sensor node. In [174], the authors use a simple Markov model to optimise the retransmission strategies of BAN under variable TDMA scheduling based on the trade-off between energy consumption and packet delivery ratio. In [175], the authors proposed a partially observable MDP (POMDP) to optimise physical activity detection in a BAN based on the energy budget of the sensor nodes. Chaganti *et. al* [97] presented a semi-Markov model for on-body fading channels where they showed that the on-body channels are better modelled via a semi-Markov approach than a pure finite state Markov (FSM) process.

In [176], the authors use a multi-objective genetic algorithm formulation with POMDP to maximise the spectrum sensing in cognitive radio while keeping the sensing overhead within a target value. The authors in [177] presented a comprehensive survey on the basics, metrics and relevant algorithms conceived for multi-objective optimisation in WSNs, where they discussed on optimisation with trade-offs between different performance metrics. Some other works in literature formulates the multi-objective optimisation by using constrained MDP (CMDP) [178] where each objective is optimised with constraints on others based on liner programming method. The authors in [179] used constrained multi-objective reinforcement learning for routing decisions in cognitive radio networks to minimise average transmission delay with acceptable packet loss rate. In case of body-centric networks, a fair weights scheduling scheme that makes use of IEEE 802.15.6 standard TDMA and a constrained MDP (CMDP) model to balance the network lifetime and fairness of a BAN is proposed in [180]. The proposed scheme obtains optimal

lifetime utilising an optimal policy under different degrees of constraints.

2.4 Research Gaps

Although extensive research has been conducted for optimising body-centric communications in terms of improving reliability and efficiency, some important aspects have not yet been studied or investigated in terms of enabling BANs coexistence (or BBNs) as follows:

- Most of the works regarding BAN coexistence in literature focused on improving the communication performance, e.g., reducing interference [121,181, 182], increasing reliability [183], reducing latency and outage [120, 184, 185] due to shadowing of an individual BAN when multiple BANs come in to the vicinity of a BAN-of-interest. However, the inter-BAN communications or body-to-body (B2B) communications has not been properly investigated and analysed for improving the connectivity among BANs when building an independent network connection of BAN entities, which can serve as a proxy network in different scenarios. Although inter-BAN or B2B communications is a part of the existing communication architecture of body-centric networks, this specific type of body-centric communications needs further attention and in-depth research for enabling BAN coexistence at a large-scale for highly connected systems.

- Very few works, e.g., [122, 186–188] for BAN coexistence consider real-life channel measurements for investigating the performance of BANs. Most works, e.g., [189–192] analyse the performance of simulated channels produced by simple traditional channel models, without taking into account the spatial and temporal variation of the radio channels, as well as mobility conditions of body-centric networks. Moreover, most of the channel models developed for BANs are activity-oriented (i.e., standing, sitting, walking, running, sleeping) [31, 193–196] or from anechoic chambers (hence avoiding realistic scenarios) [197–199], which is not appropriate for practical BAN/BBN scenarios where the subjects are performing various mixed activities in different indoor/outdoor scenarios.

Specifically, in BBNs, the body-to-body communications experience a higher amount of shadowing from surrounding human body and body-parts for continuous postural and ambulatory movements that blocks the communication path time to time. Also, almost all of the experimental works have considered a single or small number of channels (e.g., on-body channels of a single subject, inter-body channels between only two coexisting subjects) for characterising and investigating the performance of body-centric communications [23, 200, 201]. Therefore, it is very important to characterise the body-to-body channels from an adequate amount of real-life data collected from practical scenarios for multiple BANs coexistence, and employ actual real-life measurements for investigating performance of designed body-centric networks optimisation.

- In traditional stack layered communication models, e.g., the OSI model [202], the independent protocol layers only communicate directly with upper and lower layers. Hence, layers are not jointly optimised and waste resources, which is inadequate for resource-constrained networks like BANs, especially in the case of vital healthcare deployment at large-scale. To remedy this situation, cross-layer design averts the layered hierarchy by allowing protocols from different layers to exchange information and relevant parameters. However, most of the cross-layer protocols designed for BANs consider adjacent layer optimisation, e.g., physical-MAC, MAC-network layers [203–207]. To improve the network reaction performance (for networks which experience frequent changes, e.g., BBNs), non-adjacent cross-layer protocols (e.g., physical-network layer) are an important option to consider where the upward/downward exchange of information are performed by creation of new interfaces between non-adjacent layers.

- BBNs are envisioned to be self-organised networks, which require systematic prediction of channel characteristics. For better modelling and prediction of channels with higher accuracy, it is very important to characterise predictive behaviour of the channels, i.e., can the channels be predicted? Some important predictive characteristics of wireless channels are stationarity, in particular, wide-sense-stationarity (WSS) or second-order stationarity, and

statistical dependence, i.e., long-range dependence (LRD, or long-memory) of the channel. In predictive analysis of wireless channels, in literature it is generally assumed that the time-varying channels are wide-sense-stationary (i.e., first and second moments of the channels are time-invariant) [208–212] and memoryless (i.e., negligible correlation between samples) [210, 211]. However, in real-life the channels are not always wide-sense-stationary, such as for narrowband on-body channels [99]. Furthermore, the very slowly-varying nature of body-centric channels indicates possible dependence and significant correlation between samples. Therefore, it is very important to investigate and characterise the predictive behaviour of wireless body-centric channels, particularly B2B channels, to avoid potential errors and deficient implementation by using standard memoryless models that assume a WSS property, and also for accurate characterisation and modelling (e.g., shadow fading, correlation, path-loss) of body-centric channels.

- In resource-constrained body-centric networks, it is often not possible to improve network performance by optimising or improving a single objective or performance metric. For example, increasing throughput will cause an increase in energy consumption due to a higher active period and transmission overhead. On the other hand, for reducing power consumption, the active period needs to be decreased with lower transmit power, which will cause increased delay and packet failure rate. In existing literature, most of the works related to body-centric networks concentrate on improving a single performance metric without considering the effect on other performance metrics of the channel, e.g., [117, 213, 214]. Hence, multi-objective optimisation is required for jointly optimising different performance metric with suitable trade-offs for effective use of the scarce resources.

2.5 Summary

In this chapter, we have discussed existing research, studies, and developments relevant to the scope of this thesis. We also presented the communication structure and technology used for body-centric networks, along with some major challenges

for BAN coexistence or BBNs. At the end, we discussed the research gaps found in the literature directly related to the stated thesis problem of effective optimisation of body-centric networks, and particularly body-to-body networks. These research gaps are addressed well in the following four chapters.

Chapter 3

Experimentally-based Two-layer Optimisation for Distributed BBNs

3.1 Introduction

Wireless body-centric channels are slowly-varying, which means the channel condition changes very slowly and remains similar for a longer time period, e.g., hundreds of milliseconds. As a result, when the channel is in outage, it can remain in outage for a very long time that significantly degrades the reliability of the channel. To avoid this situation, a cooperative path through nearby node/sensor (acting as relay) can be utilised to reach the destination. For the same reason, cooperative paths are also practical in routing information within a wireless body-to-body network (BBN) through nearby BANs. Also, due to the resource constraints of BANs/BBNs, optimised communications is required to avoid unnecessary delay and outages. In this chapter, we investigate the cross-layer optimisation between physical and network layers, with cooperative communications in a distributed BBN, to extend end-to-end network connectivity across co-located BANs without central coordination, and validate the outcomes with experimental analysis. First, we investigate cooperative receive diversity with on-body sensors and off-body relays/hubs for sleeping subjects (with a star topology), where we find that

cooperative combining significantly improves the outage probability and continuous latency with two-hop communications for on-body/off-body channels of a BAN used for monitoring a sleeping person. Then, we introduce two different cross-layer optimised routing techniques across a BBN — shortest path routing (SPR) and cooperative multi-path routing (CMR) that incorporates cooperative selection combining, which improves reliability, latency, and energy efficiency of B2B channels. The methods are applied to an experimental radio measurement dataset[1] recorded from 'everyday' mixed-activities and a range of measurement scenarios with people wearing radios. In this chapter, we aim to address the following issues:

- *How to improve the reliability of real-life body-centric communications under significant shadowing with cooperative communications?*
- *How can the available channels (body-to-body) between coexisting BANs be efficiently utilised, for improving the reliability of real-life BBNs?*

In the following sections, we describe cooperative receive diversity for deployment in real-life BAN channels for monitoring sleeping people; and the proposed cross-layer PHY/NET schemes in detail, and discuss the experimental outcomes obtained from applying those schemes over real-life experimental channel measurements.

3.2 Cooperative Communications for monitoring a sleeping person

Because of its relatively slow varying and non-stationary or quasi-stationary (not mobile, nor static) nature [216], the BAN radio channel for monitoring a sleeping person is a difficult channel to communicate over. Due to shadowing by body parts and simple postural movements, transmission links may be completely blocked for very long periods of time (as people move relatively little during sleeping) [82], which is critical as many patients can incur life-threatening risks during their sleep. Hence, to improve the reliability of this atypical body-centric channel, we use cooperatively combined relayed links, e.g., on-body, off-body with two hop

[1] available in http://doi.org/10.4225/08/5947409d34552 [215]

communications. We analyse the performance from real-life experimental channels collected from adult sleeping subjects and we find that

- The cooperative combining with two-hop communications provides up to 7 dB improvement over single/direct link communications, at 10% outage probability.
- In best-case scenario (at -100 dBm receive sensitivity), the outage probability for cooperative communications is much lower (up to 8% less) than the direct link outage probability.
- 3-branch selection combining (SC) provides a slight improvement in diversity gain over 3-branch switch-and-examine combining (SwC), in terms of outage probability.
- With cooperative combining, up to 20% less continuous outage duration (greater than $>$ 125 ms) is achieved over a star topology communications, with a receive sensitivity of -86 dBm.

The experimental setup, cooperative schemes, and the performance analysis are provided in the following subsections.

3.2.1 Experimental Setup for monitoring a sleeping person

Extensive on-body and off-body channel gain data taken over at least 2 hours per measurement set from eight adult sleeping subjects are used for testing the relayed cooperative schemes. Each measurement set contains 7 small wearable radios operating at 2.36 GHz, of which three are transceivers (T_x/R_x) and four are receivers (R_x). Radios were placed on different body-parts of the sleeping subject in bed, some of them were also placed around the bed (illustrated in Fig. 3.1). The radio locations described in our experiment were chosen as likely communications locations that spanned the human body by plausible one-hop (star topology) and two-hop links. The gateway/hub of a BAN is expected to be located on the places central to the human body where a subject can comfortably wear a device that is typically larger than the sensor nodes, for example, near the torso, at the hips or on the chest. The on-body and off-body sensor locations are given in Table

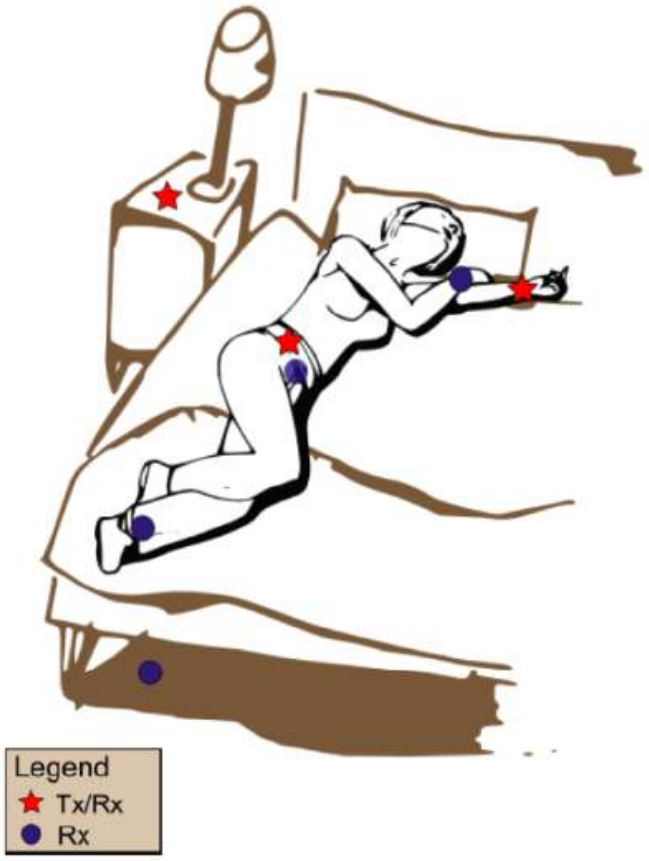

Figure 3.1: An illustration of a sleeping person wearing transceivers and receivers

Table 3.1: On-body and off-body sensor locations. NTB_h: Next To Bed (head), L_w: Left wrist, H_f: Hip front, R_w: Right wrist, H_b: Hip back, L_a: Left ankle, NTB_f: Next To Bed (foot); T_x/R_x implies to Transceiver and R_x implies to Receiver

Sensor Locations	NTB_h	L_w	H_f	R_w	H_b	L_a	NTB_f
Transceiver/Receiver	T_x/R_x	T_x/R_x	T_x/R_x	R_x	R_x	R_x	R_x

3.1. The wearable radios are described in [217] and the experimental datasets are available for download in [215]. Each transmitter was broadcasting for 5 ms in round-robin fashion. Hence, the received signal strength indicator (RSSI), in dBm, was captured from any given transmitter every 15 ms (3 transceivers were transmitting). With a T_x power of 0 dBm, each RSSI measurement provides an equivalent channel gain (magnitude) in dB for each T_x to R_x packet transmission.

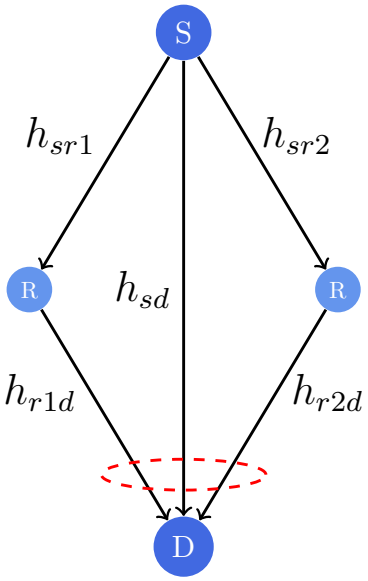

Figure 3.2: Three-branch cooperative combining: one of the branches is a direct link (h_{sd}) and the other two are cooperative relay links (with two hops).

3.2.2 System Model

BAN channels are suitable for investigating cooperative receive diversity using relays because of their stability and reciprocity. The channels are considered to be stable, since 15 ms is significantly less than the channel coherence time for a BAN, e.g., typically 500 ms, even in a highly dynamic scenario [218]. Also, due to the reciprocity property, the channel from any T_x at position a to R_x at position b is similar for T_x at b to R_x at a [217]. Effectively, simultaneous measurements based on channel coherence describe the channel gains for relayed packets from T_x-$R_{x_{relay}}$-R_x, where a direct link and two relayed links are accounted for. We investigate two different types of cooperative combining: three-branch cooperative selection combining (SC) and cooperative switch-and-examine combining (SwC), and compare those with non-cooperative direct link. The three-branch cooperative combining (one of the branches is a direct link and the other two are cooperative relay links) is illustrated in Fig. 3.2. The RSSI-based narrowband channel gain (used as a negative measure of the channel attenuation) statistics are used for result estimation. For two-hop communications, where every packet at a relay is transmitted to the destination, the channel gain for one diversity branch can be described as h_{sr_nd}

$= \min\{h_{sr_n}, h_{r_nd}\}$, for any given relay r_n where s indicates source (sensor) and d indicates destination. h_{sr_n} and h_{r_nd} are the channel gains from source to n^{th} relay and n^{th} relay to destination, respectively.

Cooperative Selection Combining For three-branch cooperative selection combining, three branches (one of the branches is a direct link) are combined at the destination, where the best branch is selected as the output gain. The equivalent channel gain at the output of the selection combining (h_{sc}) at time instant τ can be calculated as follows:

$$h_{sc}(\tau) = \max\Big\{h_{sd}(\tau), h_{sr_1d}(\tau), h_{sr_2d}(\tau)\Big\}, \tag{3.1}$$

where h_{sd} is the channel gain from source-to-destination (direct branch), h_{sr_1d} and h_{sr_2d} are the channel gain of first and second diversity branch, respectively.

Cooperative Switch-and-Examine Combining In three-branch switch-and-examine combining, a switch to another branch occurs when the channel gain on the current branch goes below a given threshold, h_T at time instant τ [218]. However, if the channel gain on this alternate branch is also less than h_T, then another switch occurs to the last branch and, whether or not the channel gain of this branch is above or below h_T, it becomes the chosen branch. Choosing the switching threshold is important for the relative performance of switch-and-examine combining. In this work, an optimum threshold of -86 dB is used for three-branch switch-and-examine combining according to [219], due to optimal switching rate achieved at this threshold. The equivalent channel gain from the output of switch-and-examine

combining $(h_{sw}(\tau))$ at time instant τ can be estimated as follows:

$$h_{sw}(\tau) = \begin{cases} h_{sd}(\tau), \iff & (h_{sd}(\tau) \geq h_T) \wedge \\ & \left\{ \begin{array}{l} (h_{sw}(\tau-1) = h_{sd}(\tau-1)) \\ \vee (h_{sr_2d}(\tau) < h_T) \end{array} \right\} \\ h_{sr_1d}(\tau), \iff & (h_{sr_1d}(\tau) \geq h_T) \wedge \\ & \left\{ \begin{array}{l} (h_{sw}(\tau-1) = h_{sr_1d}(\tau-1)) \\ \vee (h_{sd}(\tau) < h_T) \end{array} \right\} \\ h_{sr_2d}(\tau), \iff & \left[\begin{array}{l} (h_{sr_2d}(\tau) \geq h_T) \wedge \\ \left\{ \begin{array}{l} (h_{sr_1d}(\tau) < h_T) \vee \\ (h_{sw}(\tau-1) = h_{sr_2d}(\tau-1)) \end{array} \right\} \end{array} \right] \\ & \vee \left\{ \begin{array}{l} (h_{sd}(\tau) < h_T) \wedge \\ (h_{sr_1d}(\tau) < h_T) \end{array} \right\} \end{cases} \tag{3.2}$$

3.2.3 Performance Analysis

We consider outage probability and continuous outage duration as the two main performance measures for the very slowly time-varying channels of a BAN monitoring a sleeping person [193]. We investigate the performance of the cooperative schemes from agglomerated data (from 8 sleeping subjects) between an on-body transceiver (located at the hip front) and all other possible nodes from the set-up (described above). We also examine the same performance measures between an off-body transceiver (located next to bed-head) and other possible nodes. For proper estimation of outages, the effect of non-recorded measurements are referred as incorrectly decoded packets and set to a value less than the radio's receive sensitivity (≈ -100 dBm).

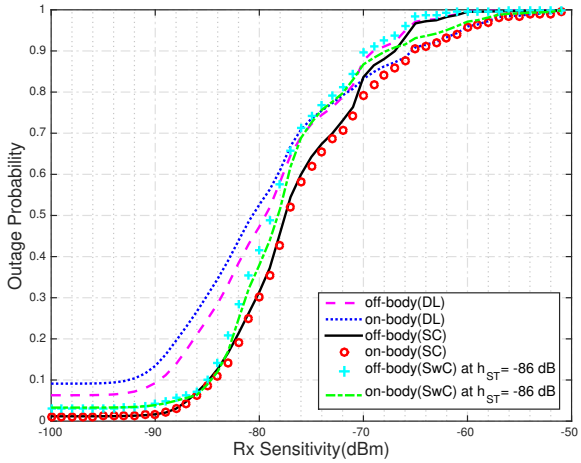

Figure 3.3: Outage probability as a function of receive sensitivity with T_x power of 0 dBm, for direct link (DL), selection combining (SC), and switch-and-examine combining (SwC), with on-body and off-body transceivers.

Outage Probability

The outage probability is estimated according to the mode of operation described in equation (3.1) for cooperative selection combining and equation (3.2) for cooperative switch-and-examine combining. The empirical outage probability for direct link (DL) and cooperative combining (with SC & SwC), for on-body and off-body channels are shown in Fig. 3.3. At 10% outage probability, there is 3 dB and 7 dB performance improvement of cooperative combining over direct link for off-body and on-body channels, respectively. Also, the best-case outage probabilities (for both on-body and off-body channels) are almost 3% and 1.2% for cooperative switch-and-examine combining and cooperative selection combining, respectively. This implies better improvement over the best-case outage probability of direct link for on-body (9.1%) and off-body (6.3%) channels. Additionally, this indicates better diversity gain for 3-branch SC over 3-branch SwC, although switch-and-examine combining has significantly lower switching rate and reduced complexity than that of selection combining [219].

Table 3.2: Empirical result analysis for direct link (DL) and cooperatively combined links (with SwC/SC); RS, OP, and COD imply receive sensitivity, outage probability, and continuous outage duration, respectively

	DL(on-body)	SwC(on-body)	SC(on-body)	DL(off-body)	SwC(off-body)	SC(off-body)
Best case OP	9.1%	3.3%	1.15%	6.3%	3%	1.17%
COD $>$ 10s at RS of -86 dBm	16.3%	2%	2%	11.5%	1.8%	1.8%
COD $>$ 125ms at RS of -86 dBm	24%	4%	4%	17%	4%	4%

Continuous Outage Duration

Continuous outage duration provides an estimate of continuous latency, hence is of significant importance for body-centric channels. Figs. 3.4 and 3.5 illustrate the percentage of time that continuous outages larger than x seconds (on horizontal axis) occur with direct link and cooperatively combined links for on-body and off-body channels, correspondingly. As can be seen in Fig. 3.4, an on-body receiver (with a receive sensitivity of -86 dBm) will experience outages of larger than 10 seconds for more than 16% of the time in case of direct link; whereas, the occurrence has reduced to 2% for cooperatively combined links. As per Fig. 3.5, an off-body receiver (with a receive sensitivity of -86 dBm) will experience outages of larger than 10 seconds for more than 11% of the time for direct link, while for cooperatively combined links, outages of larger than 10 seconds will occur less than 2% of the total measured time. In addition, outages of larger than a typical latency requirement of 125 ms [220, 221] occur almost 24% (Fig. 3.4) and 17% (Fig. 3.5) of the time for on-body and off-body direct links, respectively; while it has been considerably reduced to 4% for both on-body (Fig. 3.4) and off-body (Fig. 3.5) cooperatively combined links. The empirical results are shown in Table 3.2, as per results obtained from Figs. 3.3 to 3.5.

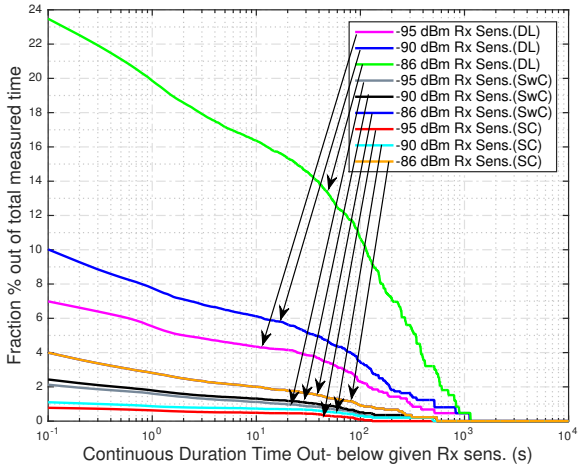

Figure 3.4: Percentage of continuous outage duration (at x-axis), below a given R_x sensitivity with T_x power of 0 dBm, from agglomerate data for on-body transceiver; with direct link (DL), switch-and-examine combining (SwC), and selection combining (SC)

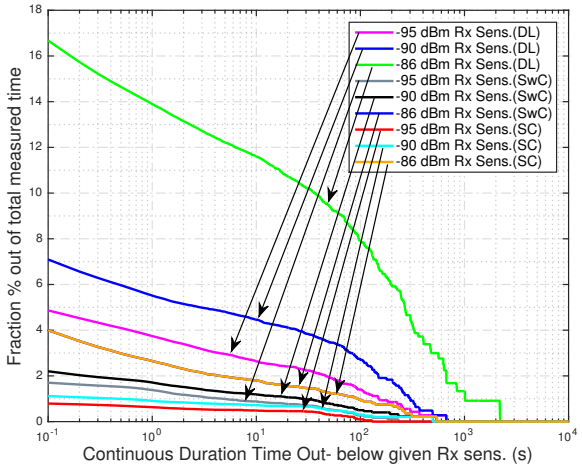

Figure 3.5: Percentage of continuous outage duration (at x-axis), below a given R_x sensitivity with T_x power of 0 dBm, from agglomerate data for off-body transceiver; with direct link (DL), switch-and-examine combining (SwC), and selection combining (SC)

3.3 Cross-layer optimised routing across multiple BANs

We now investigate cross-layer optimisation to route information across distributed wireless body-to-body networks, to analyse the general performance of closely located BANs while utilising body-to-body communications. We perform and analyse the cross-layer optimisation techniques (i.e., SPR and CMR) across the physical and network layers for two-tiered communications, with on-body BANs at the lower tier and a BBN at the upper tier to enable real-time, reliable human monitoring and communications across narrowband BANs. The methods are applied to the experimental radio measurement dataset[2] with 10 co-located BANs (people wearing radios) performing 'everyday' mixed-activities. We compare the results of cooperative multi-path routing (CMR) with shortest path routing (SPR) and other state-of-the-art WSN protocols (i.e., ORPL [138], LOADng [139]). The key findings, based on empirical results derived from real-life measurements [215], are as follows:

- Negligible (almost 0%) packet error rate (less than 10%, thus fulfilling the requirement of the IEEE 802.15.6 Standard [222]) is achieved with reasonably sensitive receivers for both shortest path routing (SPR) and cooperative multi-path routing (CMR) in a dynamic environment associated with mobile subjects, using the available nodes/hubs as relays.

- CMR provides up to 8 dB, 7 dB, and 6 dB performance improvement over ORPL[3], SPR, and LOADng[3], respectively, at 10% outage probability.

- ETX (Expected Transmission Count) or hop count metric (used in SPR, CMR, and LOADng in a mesh) can perform better than EDC (Expected Duty Cycles) metric (used in ORPL with DODAG[4] topology) in case of any-to-any routing among BANs.

[2]available in http://doi.org/10.4225/08/5947409d34552 [215]

[3]We have implemented these protocols (i.e., ORPL, LOADng) in MATLAB and applied on the same measurement dataset (used in this chapter) to compare with SPR and CMR.

[4]Destination Oriented Directed Acyclic Graph [137, 223].

- CMR outperforms other protocols in case of throughput (packets/second) by providing 95% successful packet delivery (19 packets/s at a packet transmission rate of 20 Hz).
- The maximum amount of end-to-end delay is the lowest for CMR (135 ms) with respect to other protocols and also below the IEEE 802.15.6 latency requirement ($<$ 250 ms) for non-medical applications [29]. Also, the average end-to-end delay for CMR (47.5 ms) is an acceptable amount ($<$ 125 ms) for BAN medical applications [29].
- CMR consumes more energy on average than other techniques due to the cooperative combining at route-hops, although the maximum energy consumption with CMR is much lower than other protocols (except SPR with hop restriction).
- CMR produces the lowest amount of average end-to-end delay with respect to other protocols, when estimated with lower receive sensitivity, e.g., -90 dBm, -86 dBm.
- With less receive sensitivity, e.g., -90 dBm, -86 dBm, the energy consumption of CMR remains relatively similar, while the energy consumption of other protocols increases significantly due to an increase in packet failure rate and retransmissions.
- The empirical received signal amplitude through SPR has a gamma distribution while the empirical received signal amplitude through CMR has a Rician distribution.

In the following sections, we provide the system model and discuss the experimentally-based results in detail.

3.3.1 System model

We assume a two-tiered network architecture formed from 10 co-located mobile BANs (people with fitted wearable radios) deployed for experimental measurements, where the hubs of the BANs are in tier-2 in a mesh (inter-BAN/ BBN

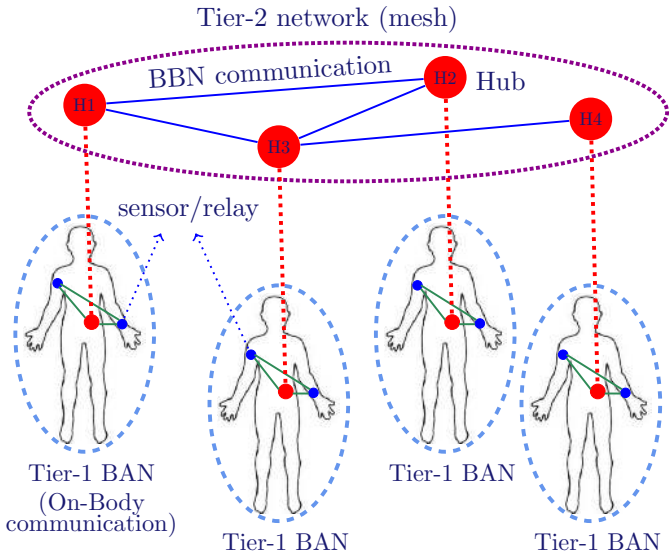

Figure 3.6: Two tiered architecture with 4 coexisting BANs (intra-BAN communications at the lower tier and inter-BAN communications at the upper tier); Hub on the left-hip and two sensors/relays on the left-wrist and right-upper-arm, respectively.

communications) and the on-body sensors of the corresponding BANs are in tier-1 (intra-BAN communications). An abstraction of the architecture is given in Fig. 3.6, with four co-located BANs. It can be portrayed as a hybrid mesh architecture where BANs (hubs/gateways) are performing as both clients and routers/relays, which will enable flexible and fast deployment of BANs to provide greater radio coverage, scalability and mobility. When a node/BAN hub is unable to send information directly to the intended destination node/hub, it tries to relay the information through the nearby BAN hubs. A given node, when acting as relay, follows the decode-and-forward relaying scheme for which it decodes the signal and then retransmits it. Any-to-any routing is performed in a cross-layered approach, with two different routing techniques, i.e., shortest path routing (SPR) and cooperative multi-path routing (CMR), that utilise and interact with the physical layer. Therefore, changes in channel states (i.e., expected transmission counts, hop counts) are directly sent from the physical layer to the network layer, so that the routes with the most favourable channel conditions are chosen (illustrated in Fig. 3.7). The cross-layer approach across the PHY–Network layer can be implemented by the

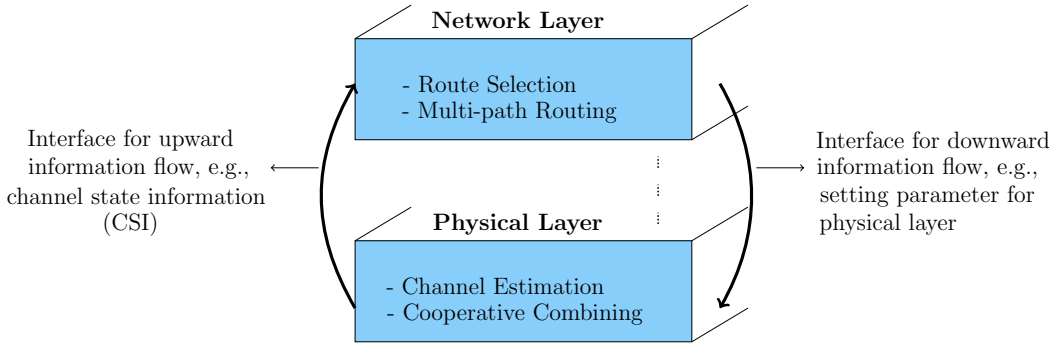

Figure 3.7: Cross-layer optimisation between Physical and Network layers.

creation of new interfaces for upward/downward information flow [224]. In this chapter, we investigate the performance of SPR and CMR without any multiple access scheme or interference mitigation among the co-located BANs.In the next chapter, we demonstrate the performance of these routing techniques including some appropriate MAC layer schemes.

For real-time dynamic estimation, we time-stamp[5] the samples of any given link continuously with a reasonable time-stamp period of 500 ms, given the longer coherence times of 500 ms (up to 1 s) for 'everyday' activities of narrowband on-body BAN channels [82], and 900 ms (calculated in [225]) for narrowband body-to-body channels used here. Therefore, the routing table for a given time-stamp is updated based on the estimated channel condition from the previous time-stamp. We consider 10 mobile people (with intra-body and inter-body interactions) for BAN coexistence experimentation, to adequately capture the dramatic impact caused by the slowly-varying human-body dynamics and shadowing by body-parts, both for the on-body and inter-body channels [226–228]. This also meets the guideline for the number of closely-located BANs to be supported at the physical layer according to the IEEE 802.15.6 Standard [222]. We use MATLAB for analysing and investigating the performance of coexisting BANs according to the experimental dataset. The parameters applied for estimating the performance metrics are listed in Table 3.3. The experimental scenario for the co-located BANs and the routing techniques (i.e., SPR, CMR) are described in detail in the following sections.

[5]The whole channel is divided into time-stamps of a given period and the routing table updates after each time-stamp. The samples are taken periodically over the time-stamp period.

Table 3.3: Applied Parameters

Parameter	Value
Carrier Frequency	2.36 GHz
Data rate	486 kbps
Packet size	273 bits
Sampling rate	20 Hz
Packet transmission time (T_{packet})	0.6 ms
Transmission period (T_{active})	5 ms
Sampling period	50 ms
Tx/Rx mode power consumption: on-body hub (P_{TX_h}/P_{RX_h})	6 mW
Tx/Rx mode power consumption: on-body sensor (P_{TX_s}/P_{RX_s})	5 mW
Idle mode power consumption (P_{idle})	1 mW
Transmit power	0 dBm
Timestamp period	500 ms
Total time	45 mins

Experimental Scenario for co-located mobile BANs

A group of experimental radio measurement datasets[6] consisting of large-scale measurements[7] were captured from a range of measurement scenarios with various numbers of co-located mobile people (wearing body-worn sensors/radios developed in NICTA[8]) at different times. The closely located mobile subjects were performing 'everyday' mixed activities, e.g., walking, sitting, standing in indoor/outdoor environments, e.g., building, office space, street, cafe/pub, hence capturing measurement data from typical dynamic real-life scenarios for standard BBN framework. The team walked along a corridor, into a lift, out into a 3-storey foyer, and then walked along a street towards a cafe and also a pub where they sat around a table, after a while they walked back to the office building. The walking segments were 'natural' in the sense that people clumped together, moved near and away from

[6]available in http://doi.org/10.4225/08/5947409d34552 [215].

[7]intra-BAN (on-body) and inter-BAN (body-to-body) channel gain data (RSSI values) of around one hour per link.

[8]National Information and Communications Technology Australia (NICTA) has been incorporated into Data61 of CSIRO.

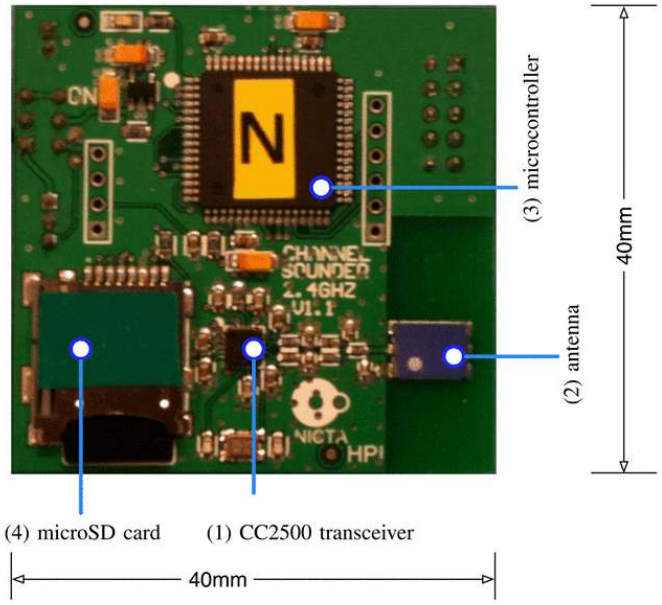

Figure 3.8: The radio-frequency testbed with major components highlighted. Battery (disconnected) is on reverse side

others (relatively at 1 meter distance), and generally moved as a group – chatting and walking (not in formation).

The wearable radios (XBee/ZigBee devices) in each dataset were transmitting in a sequential order at 0 dBm transmit power (along with −100 dBm receive sensitivity) with 5 ms separation between each other. A range of different carrier frequencies (near 400, 900 and 2400 MHz) and communication bandwidths were used during the measurements [229]. In the works throughout the thesis, 2.36 GHz narrow-band is used per link, as it is close to the 2.4 GHz ISM band and also is free of ISM interference. A detailed description of the testbed used in the measurements (shown in Fig. 3.8) along with the wearable radios and the hardware platform can be found in [217]. As described in [217], the testbed used in the measurement is a programmable radio transceiver with non-volatile data storage, designed to be worn by test subjects for several hours. The testbed is comprised of – radio transceiver (Texas Instruments CC2500) which communicates digital data in the form of packets with the micro controller, Bluetooth surface-mount ceramic multi-layer 'chip' antenna (YAGEO CAN4311111002451K), micro controller (Atmel ATmega1281),

microSD card socket and rechargeable battery (Energiser CP18NM). The microSD card is used to store gain measurements, which is transferred to a computer using an off-the-shelf card reader. Each transmitter sends packets with a transmit ID attached. When a channel sounder device receives a packet from another device it logs the packet ID and RSSI (receive signal strength indicator): the ID provides the link identification and the RSSI provides the instantaneous signal strength for that link [96].

The open-access dataset [215] stated here, consists of continuous extensive intra-BAN (on-body) and inter-BAN (body-to-body) channel gain data[9] incorporating mixed 'everyday' activities including different ambulatory and postural movements, e.g., walking, sitting, chatting, turning, standing at indoor/outdoor environments. We analyse the performance of the protocols upon a suitable portion of the dataset (can be downloaded from [215]) of around 45 minutes, captured from 10 closely located mobile subjects (adult male and female). We consider 10 mobile people (with intra-body and inter-body interactions) as a reasonable amount for BAN coexistence experimentation, due to the dramatic impact caused by the slowly-varying human-body dynamics and shadowing by body-parts, both on the on-body and inter-body channels [226–228]. The experimented subjects were walking together to a hotel bar, sitting there for a while and then walking back to the office. Each subject wore 1 transceiver on the left-hip and 2 receivers on the left-wrist and right-upper-arm, respectively (shown in Fig. 3.6).

For real-time dynamic estimation, we time-stamp the samples of a given link periodically with a continuous time-stamp period of 600 ms, given the longer coherence times of up to 1 s for the 'everyday' mixed activities for narrowband body-centric channels [82, 225]. Each transceiver is broadcasting in every 50 ms with a transmission time of 5 ms to every 9 other subject's receivers as well as their own receivers (all small body-worn radios/hubs/sensors), along with capturing the RSSI values in dBm, which gives a total of 300 channel measurements (including both on-body and body-to-body links) in real-time over the whole network during the measurement period. Due to the reciprocity property, the channel from any T_x (transmitter) at position a to R_x (receiver) at position b, is similar for T_x at b to

[9] estimated from measured RSSI values with 0 dBm transmit power, with a receive sensitivity of -100 dBm and a noise floor at (≈ -101) dBm.

R_x at a [217], thus transmitters and receivers can be considered interchangeably to model multiple synchronous networks [96].

Shortest Path Routing (SPR)

We perform dynamic shortest path routing (SPR) [230] based on an Open Shortest Path First (OSPF) protocol, which uses link-state algorithm, e.g., Dijkstra's algorithm, where any source node intends to find route with a minimum cost (based on routing metrics) to any destination and updates the routing table dynamically to adapt variable channel conditions and topological changes. Routing metric predicts the cost of the route calculated from the use of a certain routing protocol, which plays a critical role in finding out the efficient route to the destination in a network. For investigating the performance of the dynamic routing, we use a combination of different routing metrics (e.g. ETX, hop count etc.). Although some well-known WSN protocols, e.g., CTP [137], RPL [136] make use of the ETX metric, the calculation of ETX in our work differs with respect to the gradient descent technique followed by those protocols to calculate ETX.

As these protocols (i.e., CTP, RPL) use a rooted topology (for collecting information), each node maintains an estimation of its route cost to a collection point/specific sink node, where the collection point exhibits a cost of zero, which leads to a convergence towards the root node, as a node only selects forwarding nodes that provide strictly more progress than itself with a lower ETX. By contrast, in our work, we simply find routes between two nodes (from any source to any destination) which have minimum cost (sum of the ETX values of the links in a route), without any back propagation to a root node. Furthermore, in RPL, if a source node wants to communicate with any node (other than root or sink node), the route has to go first upwards (towards the root node) and then downwards (towards the destination), as RPL uses only one common ancestor node instead of a full mesh (similar as CTP) [138]. This increases the number of hops in a route as well as the delay and energy consumption. In our work, we have restricted the routes to a maximum of two hops, which saves energy and latency while providing acceptable packet delivery ratio (demonstrated in following sections).

Algorithm 1: Finding shortest path route (ETX + max. two hops count)

input : Source node (S), destination node (D), and set of intermediate nodes (N).
output: Shortest path from S to D.

$P_{etx} \leftarrow$ Set of ETX values for every possible paths from S to D;
$[i, j] \leftarrow$ [1,`length(`P_{etx}`)`];
while $i \neq j$ **do**
    $etx_{min} \leftarrow$ `minimum(`P_{etx}`)`;
    if `PathHopCount(`etx_{min}`)` $= 2$ **then**
        $Output_{SPR} \leftarrow$ `Path(`etx_{min}`)`;
    else
        $P_{etx} \leftarrow P_{etx} - etx_{min}$;
        $etx_{min} \leftarrow$ `minimum(`P_{etx}`)`;
        $j \leftarrow j - 1$;
    end
    $i \leftarrow i + 1$;
end
if `isempty(`$Output_{SPR}$`)` **then**
    $Output_{SPR} \leftarrow$ direct path;
end

ETX The Expected Transmission Count (ETX) path metric is a simple, proven routing path metric that favours high capacity and reliable links. This metric estimates the number of retransmissions required to send unicast packets by measuring the loss rate of broadcasted packets between pairs of neighbouring nodes [231], which can be calculated as follows:

$$ETX = \frac{1}{1 - O_p}, \tag{3.3}$$

where O_p is the outage probability with respect to the receiver sensitivity, e.g., -100 dBm. ETX adds more reasonable behaviour under real life conditions, since this metric is based on packet loss and thus the number of packets sent.

Hop count Hop count identifies the route which has minimal number of hops. The primary advantage of this metric is its simplicity. Once the network topology is known, it is easy to compute and minimise the hop count between a source and

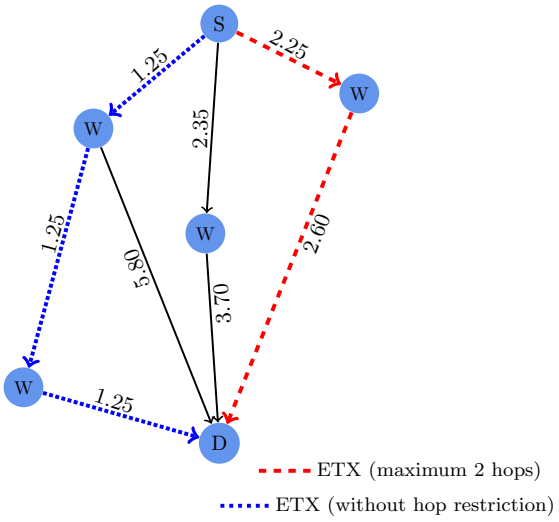

Figure 3.9: Shortest path routing (SPR), with and without hop restriction. The path taken without hop restriction can be a longer path with the lowest cost.

its destination. However, the primary disadvantage of this metric is that it doesn't take packet loss, bandwidth, power consumption or any other characteristic of a link into account [231].

Here, an optimal path is selected by combining these two metrics (ETX + Hop count), restricting the hop count to two hops. A pseudo-code for this process is given in Algorithm 1. The ETX of a given link is estimated from EQ. (3.3) with the RSSI values of the previous time-stamp (500 ms) to be applied in the next time-stamp of 500 ms. As the router performs periodic updates, when there is no route from source to destination (ETX = ∞), the router chooses the direct link for the given time-stamp period to possibly avoid longer delay. In SPR, the combined channel gains at the destination can be measured as follows:

$$spr_{comb} = min\big(h_1, ..., h_k\big), \tag{3.4}$$

where k is the number of hops in the route; $k = 2$ when two hop restriction is applied on SPR. In Fig. 3.9, an illustration of shortest path routing (SPR) is presented, where the difference between using the ETX metric with and without hop restriction is demonstrated. The path taken without hop restriction can be a longer path with the lowest cost. However, the path associated with combined

metric (ETX + maximum two hops) is an optimal path, having the lowest cost possible with a maximum of two hops.

Cooperative Multi-path Routing (CMR)

Multi-path routing yields better performance than single-path routing by providing simultaneous parallel transmissions with load balancing over available resources. Hence, cooperative multi-path routing (CMR) has been considered in [143]. We propose a new CMR scheme that employs 3-branch selection combining (SC) within individual route paths, incorporating shortest path routing (SPR) and improving the performance of SPR.

In dynamic cooperative multi-path routing, we use cooperative paths from source to destination with combined channels in each route-hop. Here, route-hop refers to each hop of a path/route in CMR from source hub to destination hub through an intermediate BAN hub (acting as a mesh router/relay). In each route-hop, 3-branch cooperative selection combining is used, where one of the branches is the direct link and the other two branches (cooperative relayed links) have two link-hops. Link-hop refers to each hop of the branch from a BAN hub through on-body relays of the corresponding BAN. A decode-and-forward protocol is applied at each on-body relay. The equivalent channel gain at the output of selection combining can be estimated as follows:

$$h_{sc}(\tau) = \max\Big\{h_{sd}(\tau), h_{sr_1d}(\tau), h_{sr_2d}(\tau)\Big\}, \tag{3.5}$$

where $h_{sc}(\tau)$ is the equivalent channel gain at the output of the selection combining, at time instant τ. h_{sd} is the channel gain from source-to-destination (direct link), $h_{sr_id} = \min\{h_{sr_i}, h_{r_id}\}$ are the channel gains of the first and second cooperative relayed links (with two link-hops, s to r_i, and r_i to d), $i = [1, 2]$, respectively.

For multi-path routing here, two different paths are used (if more than one path is available) from source hub to destination hub, where both paths can have maximum of two route-hops. The shortest path is chosen according to an SPR calculation, hence the two paths go through the two nearest BAN hubs from the source. The nearest BANs from any given source can be found from the source hub-to-connected hub channel gains, approximated from the RSSI at the connected

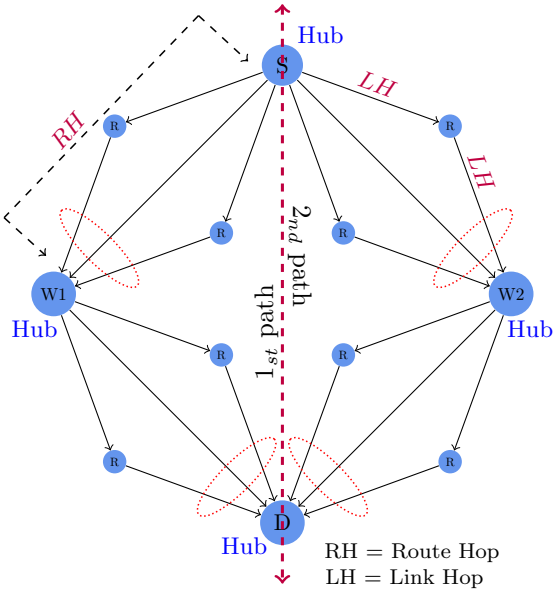

Figure 3.10: Cooperative multi-path routing (CMR) with 3-branch selection combining in each route hop.

BAN hubs. In CMR, the combined channel gains at the destination for a given path/route is measured as follows:

$$cmr_{comb} = min\{h_{RH_1}, h_{RH_2}\}, \tag{3.6}$$

where h_{RH_j} are the cooperatively combined (with selection combining) channel gains at route hop $j = [1, 2]$ of the route. h_{RH_j} can be calculated from Eq. (3.5).

The destination process the data/information once it receives the packet/data through any of the paths. Also, for body-centric channels (specially for B2B channels), retransmissions of failed packets are often impractical (except for critical applications) [232] due to the longer coherence times. For instance, retransmitting a failed packet multiple times (with a retransmission timeout period) will increase the delay and energy consumption, with lower probability of successful delivery as the channel condition remains similar for hundreds of milliseconds. One of the main objective of cooperative multi-path routing is to reduce such retransmissions in order to avoid unnecessary delay. Here, retransmission is only permitted in CMR when the shortest path has a single route-hop and no alternate path is possible.

Algorithm 2: Estimating Output of CMR

input : Source node (S), destination node (D), and set of intermediate nodes (N).
output: Result of CMR at destination node.

```
1  P1 ← FindShortestPathWithHopRestriction(S, D, N);
2  P2 ← FindShortestPathWithHopRestriction(S, D, N) ≠ P1;
3  if isempty(P2) ≠ 1 then
4      for i ← 1 to 2 do
5          for j ← 1 to length(P_i) do
6              Pi_{RH_j} ← SelectionCombining(Route_Hop_j);
7          end
8      end
9      if length(P_1) > 2 then
10         Comb_{P1} ← minimum(P1_{RH_1}, P1_{RH_2});
11     else
12         Comb_{P1} ← P1_{RH_1};
13     end
14     Comb_{P2} ← Repeat steps 9 to 13 for P2;
15     if Comb_{P1} is successful then
16         Output_{CMR} ← Comb_{P1};
17     else
18         Output_{CMR} ← Comb_{P2};
19     end
20 else
21     Repeat steps 4 to 14;
22     if Comb_{P1} is successful then
23         Output_{CMR} ← Comb_{P1};
24     else
25         Retransmit through P1;
26     end
27 end
```

However, in CMR, the use of an alternate path and the cooperative combining in each route-hop of a path increases the chance of successful packet delivery despite avoiding retransmissions (as shown in the following section). The process for CMR is illustrated in Fig. 3.10 and described with a pseudo-code in Algorithm 2.

3.3.2 Experimentally-based Results

In this section, we analyse the performance of the cross-layer approach and compare the results with different WSN protocols, i.e., ORPL [138], LOADng [139] for low-power and lossy networks (LLNs) that support any-to-any routing. We implement ORPL and LOADng in MATLAB, and applied those protocols on the same measurement dataset [215] for a fair comparison with SPR and CMR. When implementing ORPL and LOADng, two nodes are considered as neighbours if the link RSSI is greater than or equal to the receiver sensitivity (i.e., -100 dBm).

ORPL ORPL uses a combination of a rooted/DODAG (Destination Oriented Directed Acyclic Graph) topology with opportunistic routing based on the EDC (Expected Duty Cycles) metric [233]. As described in [233], the EDC_i of node i for a given subset S_i of neighbours with link quality p_{ij} and EDC_j ($j \in Si$) is as follows:

$$EDC_i(S_i) = \frac{1}{\sum_{j \in S_i} p_{ij}} + \frac{\sum_{j \in S_i} p_{ij} EDC_j}{\sum_{j \in S_i} p_{ij}} + \omega, \tag{3.7}$$

where the first term is the single hop EDC, which denotes how many units of time it requires on average to transmit a packet to one of the neighbouring nodes in S_i. The second term describes the routing progress that the neighbouring nodes in S_i offer, weighted by their link qualities p_{ij} (estimated from Packet Reception Rate (PRR)). The third term, ω, adds a weight to reflect the cost of forwarding.

With a DODAG topology, the root node has an EDC of 0. We select node 6 from the experimental measurement used in our work as the root node because of its suitable position (with better proximity) and communication with all other nodes, hence $EDC_{node6} = 0$. The forwarding cost ω is chosen to be 0.1 according to [233] as a good balance between energy efficiency, delay and reliability. EDC selects the forwarder sets (the nodes that can forward/relay the data) for each node from the neighbours. According to ORPL, node a will only forward to a receiver

node b, if and only if it has the destination on its routing set and,

$$(EDC_b + \omega < EDC_a) \ \cap \ (p_{ab} > 50\%)$$
(when routing upwards towards root)

$$(EDC_a < EDC_b + \omega) \ \cap \ (p_{ab} > 50\%)$$
(when routing downwards towards destination)

If there are multiple successful forwarders the node will select the forwarder with the best EDC or, link quality. ORPL uses randomised periodic broadcast for updating the routing information with a Trickle timer (based on Trickle algorithm [234,235]). Here, for the wake-up interval of the trickle timer, the lower bound is set to be 400 ms and the upper bound is set to be 1000 ms. We analysed the performance of ORPL with different redundancy constants, e.g., $k = 2, 3, 4$ of the trickle timer and we obtained nearly identical results. We chose the redundancy constant as $k = 4$ according to [138, 236], where $k = 3$ to 5 is investigated as an optimal redundancy constant in deployments.

LOADng We implement LOADng based on a distance-based routing followed from traditional AODV protocol [140]. Here, the RSSI values from the measurements are used for anticipating the distance between particular nodes and estimating the hop count to reach from source to destination. However, BAN radio propagation is dominated by local variations and not by distance-based path losses [96]. As a reactive protocol, LOADng routes are updated whenever a packet is lost due to a broken link condition. Besides being a reactive protocol, LOADng also uses a Route Hold Time (RHT) [237] to specify the lifetime of a route. After the RHT expires, the router updates the route to ensure the selection of a shortest path. Here, we have used a RHT of 500 ms.

We consider outage probability, throughput (successful packets/s), average end-to-end delay and average energy consumption (per packet) as the performance metrics for evaluating the experimentally-based optimisation techniques in this chapter. Furthermore, we demonstrate the percentage of hop count induced from different protocols. Additionally, the statistical distribution fits for SPR and CMR

are investigated.

Outage Probability

An estimation of packet error rate and packet delivery ratio, and hence general performance can be made from outage probability, since it is the cumulative distribution function of channel gains. The average outage probability for a network of 10 co-located mobile BANs with SPR and CMR, is presented in Fig. 3.11 and can be expressed as follows:

$$P_{out_x} = Prob\big(x_{comb} < rs_{th}\big), \tag{3.8}$$

where P_{out_x} is the probability of combined channel gain x_{comb} across routing technique x, being less than a given receive sensitivity threshold, rs_{th}. The outage probabilities are taken from the overall network at assuming different receive sensitivities at a transmit power of 0 dBm. For estimating the outages properly, the effect of non-recorded measurements (NaN) due to incorrectly decoded packets were replaced with a value of -101 dBm, just below the receiver sensitivity of -100 dBm. In Fig. 3.11, it can be seen that SPR, LOADng and ORPL techniques have approximately similar results, where SPR (without hop restriction) has only marginally better packet delivery ratio than the SPR method with hop restriction, as it takes the path with lowest cost (where most of the routes consist of one or two hops) but can consume more energy and network lifetime due to the length of some routes (up to eight hops).

LOADng provides slightly better packet delivery ratio than SPR because of the immediate route repair technique, however it can also take lengthy routes without hop count restriction. In that case, the routes chosen by SPR with respect to the combined metric (ETX + maximum two hops) provide a good trade-off between throughput and energy consumption (as shown in following subsections), as it is restricted to two hops. On the other hand, CMR (which uses a similar hop count restriction) provides up to 8 dB, 7 dB, and 6 dB improvement over ORPL, SPR with hop restriction, and LOADng (as well as SPR without hop restriction), respectively, at 10% outage probability. It is shown that in the best-case scenario (at -100 dBm receive sensitivity), there is 0% outage probability for 10 hubs

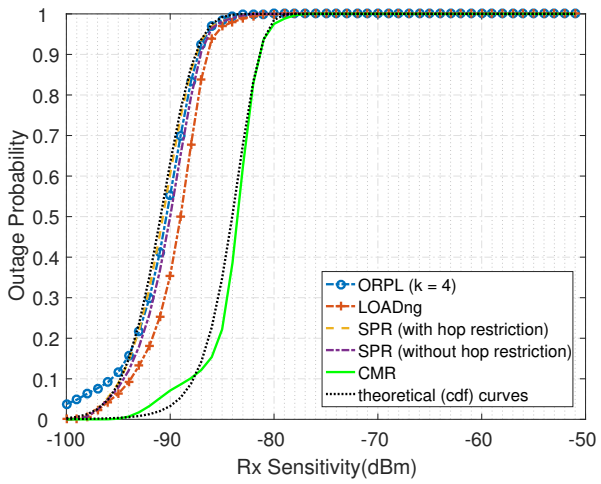

Figure 3.11: Outage probability of the averaged gains (over the network with 10 BANs) found from ORPL (routing metric: EDC, k = 4), LOADng (routing metric: hop count), SPR and CMR (routing metric: ETX, hop count); transmit power 0 dBm. Black dotted curves represent the theoretical cdf (cumulative distribution function) of the corresponding outage probability and are well aligned.

with all the protocols (with ORPL, that is 0.4%), which indicates a packet error rate close to 0% ($< 10\%$), thus achieving the requirement of the IEEE 802.15.6 Standard. Importantly, SPR (along with LOADng) and CMR techniques achieve less than 10% outage probability at -95 dBm and -88 dBm receive sensitivity, respectively.

The same process is repeated for SPR and CMR with transmit power 10 dBm (at hubs) and 5 dBm (at relays) in Fig. 3.12. The minimum receive sensitivity is considered to be -90 dBm, owing to the increased transmit power, which causes the lower limit of measured channel gains to be at -100 dB. For the same reason, the actual receiver sensitivity of the sensors is considered to be -86 dBm for calculating ETX values. By comparing Figs. 3.11 and 3.12, it can be seen that the curves in Fig. 3.12 shift right with the change of transmit power and receive sensitivity, which implies that with increased transmit power of on-body nodes, excellent reliability is obtained with less sensitive receivers. In this case, the average outage probability for 10 hubs is also less than 10% for both SPR and CMR, for receive sensitivities of ≤ -84 dBm and ≤ -80 dBm, respectively.

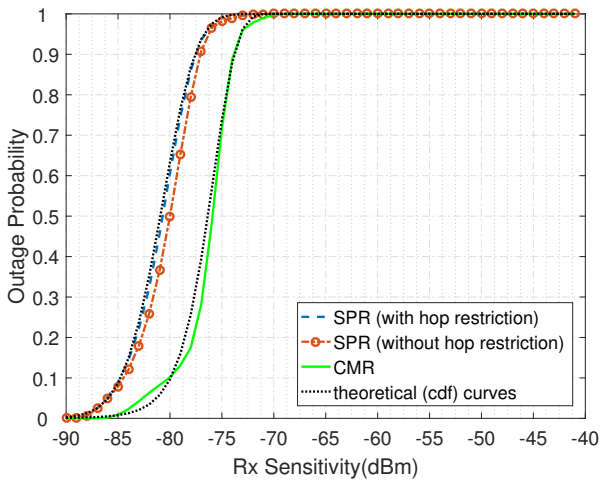

Figure 3.12: Outage probability of the averaged gains (over the network with 10 BANs) found from SPR and CMR (routing metric: ETX, hop count); transmit power 10 dBm (at hubs) and 5 dBm (at relays). Black dotted curves represent the theoretical cdf (cumulative distribution function) of the corresponding outage probability and are well aligned.

Throughput (successful packets/s)

Throughput provides an assumption of how much information can be transferred per unit time (with a given transmission rate). The throughput (in packets/s) is analysed considering that in each transmission period (or active period) the node will transmit at least one packet, however given the transmission period and packet transmission time (Table 3.3), more than one packet can be transmitted during the transmission period. We then estimate the throughput, Θ_x (number of successful packets per second) based on the received signal strength at the destination for different protocols as follows:

$$\Theta_x = \frac{\sum \left(x_{comb} \geq rs_{th}\right)}{Total\_time\ (s)}, \tag{3.9}$$

where Θ_x is the total number of successful packets (estimated from the combined channel gain x_{comb} across routing technique x, with respect to the given receive sensitivity threshold, rs_{th}) per unit time (second). The number of successful packets is averaged over the whole network at continuous times. The average throughput

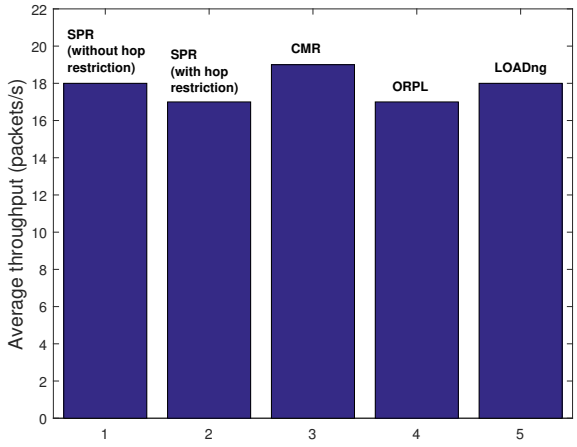

Figure 3.13: Average throughput (packets/s) for SPR, CMR, ORPL, and LOADng; at −100 dBm receive sensitivity with transmit power 0 dBm.

over the network with 10 BANs with different protocols is shown in Fig. 3.13. It can be seen that CMR outperforms the other protocols in terms of throughput by providing 95% successful packet delivery (19 packets/s at a packet transmission rate of 20 Hz), which indicates increased successful transmissions with multi-path routing incorporating cooperative combining. Also, SPR (with hop restriction) and ORPL has lower throughput with respect to other protocols.

Delay

Delay is an important design and performance characteristic of network. The term delay used throughout this chapter is referred to as the end-to-end delay, which specifies how long it takes for a data packet to travel across the entire network path from source to destination. End-to-end delay can be roughly estimated as follows:

$$D_{end\_end} = D_{trans} + D_{queue} + D_{proc} + D_{prop}, \tag{3.10}$$

where D_{trans}, D_{queue}, D_{proc}, and D_{prop} are the transmission, queuing, processing, and propagation delays, respectively. As the processing and propagation delays are negligible in the scenario described in this chapter, we have calculated transmission and queuing delays to evaluate the end-to-end delay. The transmission

delay (D_{trans}) is the delay for packet transmission (T_{packet}). The queuing delay is referred to as the waiting delay that occurs at intermediate nodes (hubs/relays) during a packet delivery. As each node is transmitting every 50 ms without central coordination, we consider the highest possible amount of waiting period (e.g., 49 ms, excluding the packet transmission time of around 1 ms) when estimating the waiting/queuing delay at intermediate BANs/relays.

In case of retransmission due to the failure of delivering a packet, the amount of D_{end_end} is doubled. In CMR, the on-body sensors/relays (in each route-hop) are operating in a different tier and coordinated by their hub with a sequential transmission. Again, we consider the highest amount of waiting delay for the intermediate BAN/relay node in CMR, e.g., 59 ms considering the extra waiting time for the packet transmission of the cooperative relayed links at the route-hop. It should be noted that in practical situations the end-to-end delay may be less than the estimated delay here, e.g., the waiting period at an intermediate node can be lower than the maximum amount, as the packet can arrive at any time during the transmission period and the intermediate BAN hub can transmit at any time during the sampling period.

The average end-to-end delays at continuous times with different protocols over the whole network consisting of 10 co-located BANs are presented in Fig. 3.14. According to the IEEE 802.15.6 Standard guideline [29], latency should be less than 125 ms in medical applications and less than 250 ms in non-medical applications. The average and maximum end-to-end delay over the whole period of the BBN with different protocols are shown in Fig. 3.15, where all of them are producing an acceptable amount of delay (on average) according to the IEEE 802.15.6 BAN Standard for medical and non-medical applications. As the average delay is estimated for the specific dataset with a finite amount of channel measurements, the knowledge of the maximum amount of delay (with the dataset) is beneficial in the long run to get an assumption of the upper limit of the delay that can be caused by the protocols.

Although CMR generates slightly increased delay (still acceptable) on average than SPR (with hop restriction) and LOADng due to the selection combining at route-hops, the maximum delay caused by CMR is lower then all other protocols owing to the reduced retransmissions (yet producing the highest throughput). The

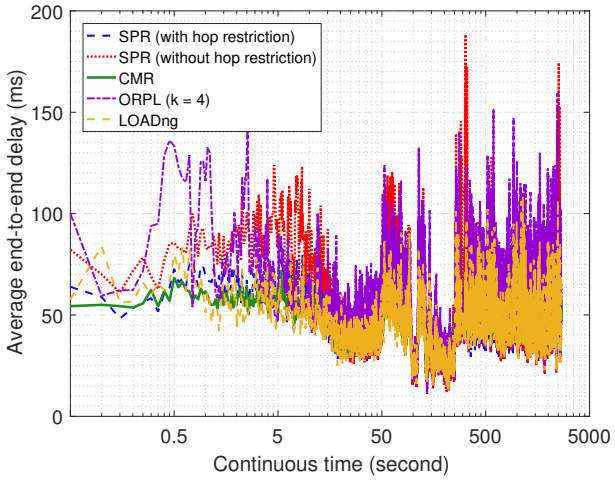

Figure 3.14: Average end-to-end delay at continuous times for SPR, CMR, ORPL, and LOADng; at −100 dBm receive sensitivity with transmit power 0 dBm.

maximum amount of delay of CMR and SPR (with hop restriction) is less than 250 ms, which is an acceptable amount of latency for BAN non-medical applications. The maximum delay generated by other protocols are very high, specially for ORPL, which produces the highest amount of delay (61 ms on average, can go up to 605 ms), as the delay increases when there is no possible forwarding node in the forwarding set. In all of the cases, the transmit power and receive sensitivity are 0 dBm and −100 dBm, respectively, across all nodes (hubs/relays).

We also estimate the average end-to-end delays with differing receive sensitivities, e.g., −90 dBm, −86 dBm for different protocols (results are shown in Table 3.4). It can be seen from Table 3.4 that with respect to CMR, the average delays for other protocols, e.g., SPR, ORPL, LOADng increase significantly, due to the added retransmission delays for increased packet failure rate and longer paths taken for reliable packet delivery with less receive sensitivity. More importantly, with less receive sensitivity, e.g., −90 dBm, −86 dBm at the same transmit power, i.e., 0 dBm, the average amount of delay for CMR remains lower than all other protocols.

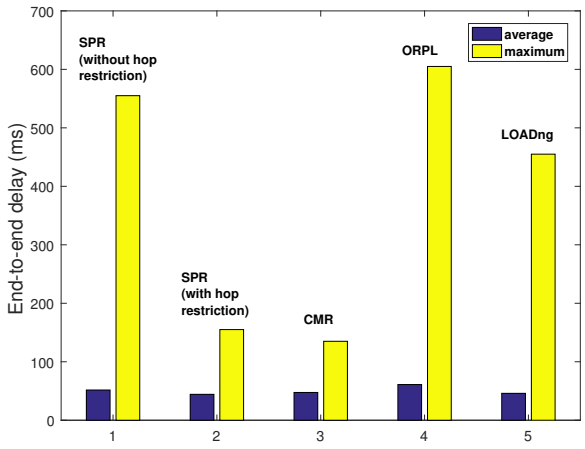

Figure 3.15: Average and maximum end-to-end delay over the whole period for SPR, CMR, ORPL, and LOADng with the network consisting of 10 BANs; with transmit power 0 dBm at −100 dBm receive sensitivity.

Energy Consumption

Energy consumption is one of the main performance metrics for resource-constrained networks like BANs. The energy consumption for each transmitted packet is calculated as follows:

$$E_p = \sum_{i=1}^{h} E_{packet_i} + \sum_{j=1}^{n} E_{idle_j}, \tag{3.11}$$

where E_{packet_i} is the energy consumption for packet transmission in i^{th} hop and E_{idle_j} is the energy consumed by the j^{th} transceiver in idle period during packet transmission. h and n are the number of hops and intermediate nodes/relays of a given route from source to destination, respectively.

E_{packet} and E_{idle} for each hop are calculated as follows:

$$E_{packet} = \begin{cases} T_{packet} \times (P_{TX_h} + P_{RX_h}), & \text{for hub-to-hub.} \\ T_{packet} \times (P_{TX_h} + P_{RX_s}), & \text{for hub-to-sensor.} \\ T_{packet} \times (P_{TX_s} + P_{RX_h}), & \text{for sensor-to-hub.} \end{cases} \tag{3.12}$$

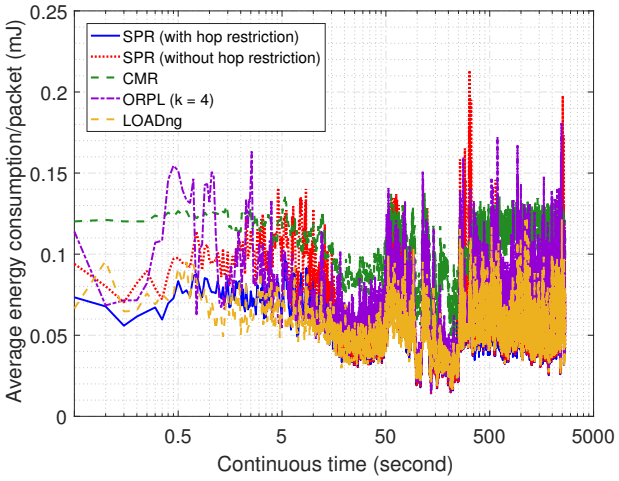

Figure 3.16: Average energy consumption (per packet delivery) at continuous times for SPR, CMR, ORPL, and LOADng; at −100 dBm receive sensitivity with transmit power 0 dBm.

$$E_{idle} = T_{idle} \times P_{idle}, \tag{3.13}$$

where T_{packet} is the packet transmission time, T_{idle} is the idle period of the transceiver during a packet transmission, P_{TX_h}/P_{RX_h} are the power consumption of the on-body hubs during TX/RX mode, P_{TX_s}/P_{RX_s} are the power consumption of the on-body sensors during TX/RX mode and P_{idle} is the power consumption in idle mode. The applied parameters for the energy consumption estimation are given in Table 3.3.

The average energy consumption (per packet delivery) at continuous times over the whole network with different protocols is shown in Fig. 3.16. Also, the average and maximum energy consumption of the network over the whole measurement period is shown in Fig. 3.17. From Fig. 3.17, reasonably, the average energy consumption over the total time for CMR (0.1 mJ) is more than the other protocols because of the extra energy consumption of the on-body sensors in each route hop. But CMR consumes less energy (0.2 mJ) with respect to other protocols (except SPR with hop restriction) in terms of maximum energy consumption, e.g., ORPL can consume up to 0.7 mJ energy per packet delivery. Although LOADng consumes lower energy on average (0.05 mJ) because of its highly reactive characteristic,

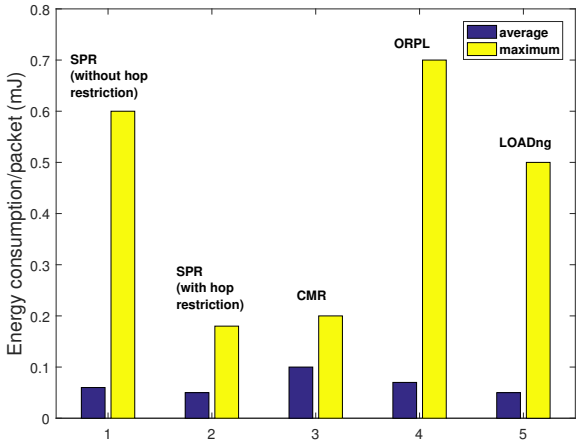

Figure 3.17: Average and maximum energy consumption (per packet delivery) over the whole period for SPR, CMR, ORPL, and LOADng with the network consisting of 10 BANs; with transmit power 0 dBm at −100 dBm receive sensitivity.

the energy consumption can rise 10 times higher (0.5 mJ) when considering the maximum energy consumption, which can further increase in high-density networks with larger hop counts [237]. Also, it can be seen from Fig. 3.16 that in some cases, the other protocols, e.g., SPR without hop restriction, ORPL, LOADng consume more energy than CMR, owing to the extra energy consumption of an increased number of hops and from retransmission of packets in case of failure. Interestingly, from Table 3.4, when lowering the receive sensitivity, e.g., −90 dBm, −86 dBm with the same transmit power, the average energy consumption increases for all the protocols except CMR. In this case, CMR in fact helps to improve energy consumption by reducing the packet failure rate and retransmissions with a cooperative path, having a possible route (up to two hops) with a lower idle period.

However, it is plausible to further reduce the energy consumption by optimising the overhearing and broadcasting transmissions of nodes, reducing the overhead of frequent periodic updates of the routing table (updating when necessary) and opportunistic relaying in route hops of CMR. Besides that, if the hub can be carried by the BAN, e.g., as a smart phone or any other device rather than worn as an on-body sensor, then the energy consumption will cause limited overhead for hub-to-hub communications.

Percentage of Hop Count

The hop count percentage of routes taken by a given protocol indicates how much overhead, e.g., delay, energy consumption is caused by that protocol. We have investigated the percentage of different number of hop counts with different protocols (with -100 dBm receiver sensitivity), as shown in Fig. 3.18. It can be seen in Fig. 3.18 that a major portion of the time for all protocols is occupied by routes that consist of one hop (around 45% on average) or two hops (around 38% on average). On the other hand, the ORPL protocol takes more than two hops (up to nine hops) for a significant amount of time (26% of the total period) because of the DODAG topology, which increases the overall delay and energy consumption due to extra overhead, e.g., finding forwarding node which has the destination on its routing set. Additionally, it is found that with the EDC metric (which partially depends on the quality of the links connected to the root node), there is no possible route for up to 13% of the time with ORPL, as ORPL only takes the forwarder nodes which has PRR greater than 50%. Hence, the restriction to a maximum of two hops (in conjunction with the ETX metric) is a suitable choice to jointly optimise energy consumption and reliability, while incorporating less overhead. However, with a maximum two hop restriction, SPR and CMR choose direct (one hop) links more than 50% of the time, as it chooses the best path (with one or two hops) that has a smaller transmission/retransmission count. Furthermore, as shown in this section, we have gained an acceptable outage probability and delay performance (compliant with the IEEE 802.15.6 Standard guideline [29]) by the use of the combined metric (ETX + maximum two hops).

The empirical results found from Figs. 3.11 to 3.17, are summarised in Table 3.4.

Probability Density Functions

We investigate distribution fits, using typical statistical distributions, for the combined channel gains, acquired after SPR and CMR techniques are applied on the experimentally measured channel gain data. In Figs. 3.19 and 3.20, it is shown that the probability density function of the combined channel gains across dynamic SPR and dynamic CMR provide gamma (Fig. 3.19) and Rician (Fig. 3.20)

Table 3.4: Empirical result analysis for different protocols; OP, RS, TP, and EC imply outage probability, receive sensitivity, transmit power, and energy consumption, respectively

	SPR (without hop restriction)	SPR (with hop restriction)	CMR	ORPL (k = 4)	LOADng (RHT = 500 ms)
Best-case OP; RS: −100 dBm; TP: 0 dBm	0%	0%	0%	0.4%	0%
At 10% OP, CMR gain w.r.t. others; TP: 0 dBm	6 dB	7 dB	-	8 dB	6 dB
Avg. throughput RS: −100 dBm	18	17	19	17	18
Avg. latency RS: −100 dBm	51.7 ms	44.3 ms	47.5 ms	61 ms	45.9 ms
Max. latency RS: −100 dBm	555 ms	155 ms	135 ms	605 ms	455 ms
Avg. latency RS: −90 dBm	61.9 ms	53.3 ms	50.5 ms	72.2 ms	57 ms
Avg. latency RS: −86 dBm	84.5 ms	72.3 ms	60 ms	97.1 ms	81.4 ms
Avg. EC RS: −100 dBm	0.06 mJ	0.05 mJ	0.1 mJ	0.07 mJ	0.05 mJ
Max. EC RS: −100 dBm	0.6 mJ	0.17 mJ	0.2 mJ	0.7 mJ	0.5 mJ
Avg. EC RS: −90 dBm	0.07 mJ	0.06 mJ	0.1 mJ	0.08 mJ	0.07 mJ
Avg. EC RS: −86 dBm	0.1 mJ	0.08 mJ	0.12 mJ	0.11 mJ	0.09 mJ

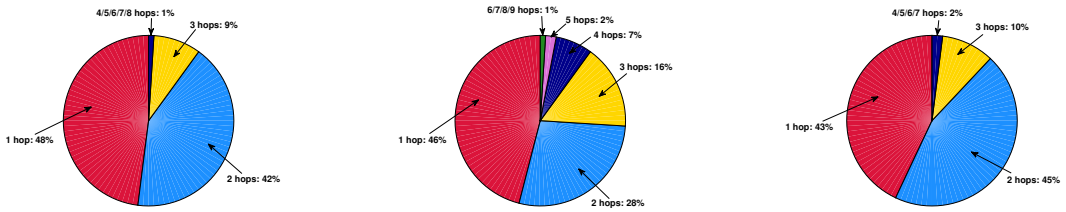

(a) SPR (without hop restriction)

(b) ORPL (k = 4)

(c) LOADng (RHT = 500 ms)

Figure 3.18: Percentage of hop count of routes with different protocols (SPR, ORPL, LOADng), at −100 dBm receiver sensitivity.

distribution fits, respectively. The maximum likelihood estimation (MLE) parameter [238] is used to select the best fit. Channel gains are taken over 5329 continuous time-stamps, each of which is for 500 ms.

The probability distribution for the combined channel after applying shortest path routing (SPR) over coexisting BANs is gamma, which can be calculated from

$$f(x \mid \kappa, \theta) = \frac{1}{\theta^{\kappa}\Gamma(\kappa)} x^{\kappa-1} \exp\left(\frac{-x}{\theta}\right), \quad x > 0, \tag{3.14}$$

where $\kappa = 9.58$ and $\theta = 0.00000334$ are the shape and scale parameter, respectively, for this channel gain fit after SPR is performed.

A Rice or Rician distribution (also known as a Nakagami-n distribution) models Rician fading, in which signal cancellations affect radio propagation [239]. Rician fading occurs when the signal arrives at the receiver by several different paths and one of the paths (typically a line-of-sight path) is stronger than the others. Here, the probability distribution for the combined channel gains from cooperative multipath routing (CMR) with coexisting BANs can be approximated from the Rician probability distribution as follows:

$$f(x \mid \nu, \sigma) = \frac{x}{\sigma^2} \exp\left(\frac{-(x^2+\nu^2)}{2\sigma^2}\right) I_o\left(\frac{x\nu}{\sigma^2}\right), \tag{3.15}$$

where $I_o(z)$ is the modified Bessel function of the first kind with order zero, and $\nu = 0.0000626$ and $\sigma = 0.0000185$ are the two shape parameters, for the combined

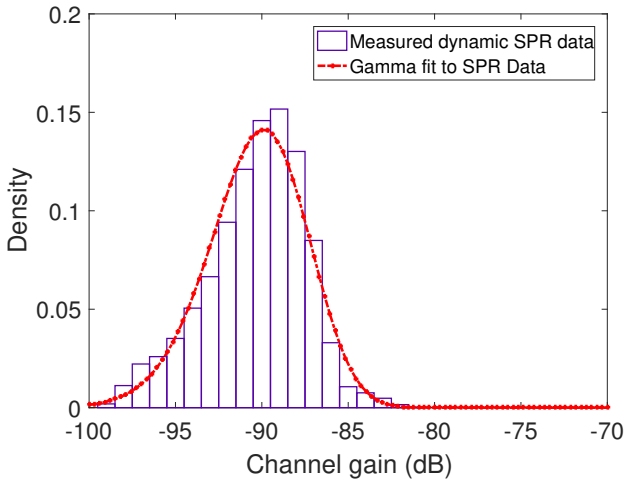

Figure 3.19: The empirical probability density of combined channel gain data from SPR with a gamma distribution fit, where $\kappa = 9.58$ and $\theta = 0.00000334$ are the shape and scale parameter, respectively.

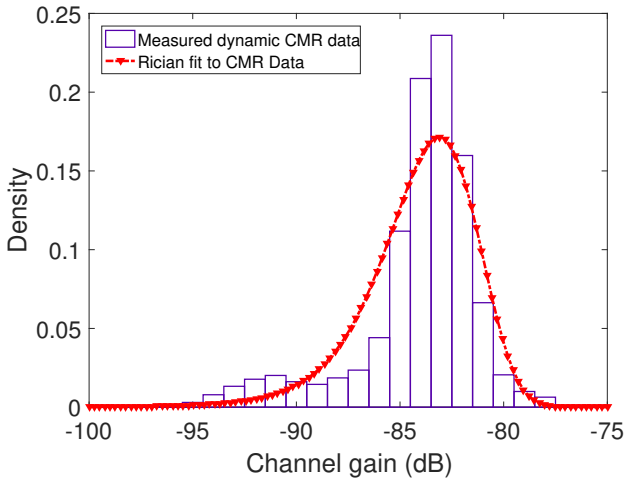

Figure 3.20: The empirical probability density of combined channel gain data from CMR with a Rician distribution fit, where $\nu = 0.0000626$ and $\sigma = 0.0000185$ are the two shape parameters.

channel gain fit after CMR is performed.

3.4 Summary

In this chapter, we have investigated the performance of cooperative communications for a BAN for monitoring a sleeping person, where we have demonstrated that up to 7 dB and 20% performance improvement can be achieved with cooperative communications (with two-hop links), for outage probability and outage duration, respectively. We have also proposed and analysed cross-layer methods, i.e., shortest path routing (SPR) and cooperative multi-path routing (CMR) with experimental measurements, to optimise radio communications across distributed wireless body-to-body networks (BBNs), by utilising distinct features at the physical and network layers. Physical layer information, e.g., ETX, hop count was dynamically fed into the network layer for determining real-time and reliable routes among BAN hubs. We have compared the performance of SPR and CMR with some state-of-the-art WSN protocols, e.g., ORPL, LOADng that support any-to-any routing. From our analysis, it is evident that the ETX or the hop count metric with mesh topology can perform better than the EDC metric (with DODAG topology) in case of any-to-any routing, as ORPL performance (which makes use of the EDC metric) falls behind the other protocols. This also implies that SPR and CMR provides improvement over the CTP and RPL protocols (other state-of-the-art WSN protocols) as ORPL outperforms those protocols.

We have shown that in the best-case scenario (at -100 dBm receive sensitivity), shortest path routing (SPR) and cooperative multi-path routing (CMR) along with other protocols provide negligible packet error rate and an acceptable amount of end-to-end delay (on average) according to the IEEE 802.15.6 BAN Standard. At 10% outage probability, CMR gives significantly better performance than other protocols by contributing up to 8 dB, 7 dB, and 6 dB improvement over ORPL, SPR, and LOADng, respectively, occurring at practical receive sensitivities. The maximum amount of end-to-end delay with CMR (135 ms) is lowest amongst all protocols (e.g., ORPL generates a maximum end-to-end delay of 605 ms) due to the reduced retransmissions and hop count restrictions. Notably, CMR outperforms other protocols in terms of throughput (successful packets/s) while providing an acceptable amount (for medical/non-medical applications) of average end-to-end delay (47.5 ms), at -100 dBm receive sensitivity. Also, CMR provides

the lowest amount of average end-to-end delay with respect to other protocols for reduced receive sensitivity, e.g., −86 dBm, −90 dBm. Our analysis has shown that CMR consumes more energy (on average) than other protocols because of the power consumption in the cooperative relayed links at route-hops. However, the maximum energy consumption with CMR is much lower than other protocols (excepting SPR with hop restriction). Also, in some cases, CMR in fact reduces the energy consumption by increasing packet delivery ratio with less retransmissions. For instance, with less receive sensitivity, e.g., −86 dBm, −90 dBm, the average energy consumption for other protocols, e.g., SPR, ORPL, LOADng increases while the average energy consumption of CMR remains approximately the same.

Furthermore, it has been demonstrated that most of the routes for all of the protocols consist of one or two hops, thus validating the applicability of two hop restriction using the ETX metric to optimise the performance of BBN communications in real-life scenarios. We have also observed that the combined channel gains across a complete SPR route with narrowband communications possess a gamma distribution, whereas the complete combined channel gains from CMR have a Rician distribution. This work has provided a feasible method for the deployment of many closely-located BANs in decentralised real-world applications with large-scale and highly-connected medical/non-medical systems. In the next chapter, we analyse the performance of the routing techniques (proposed here) with different, suitable, MAC layer schemes, i.e., time division multiple access (TDMA) and carrier sense multiple access with collision avoidance (CSMA/CA).

3.5 Related Publication

- **Samiya M. Shimly**, Samaneh Movassaghi, and David B. Smith: 'Cooperative communications for sleep monitoring in wireless body area networks', *IET Electronics Letters*, p. 594-596, February, 2016.
- **Samiya M. Shimly**, David B. Smith, and Samaneh Movassaghi: 'Experimental Analysis of Cross-layer Optimization for Distributed Wireless Body-to-Body Networks', *IEEE Sensors Journal*, p. 1-16, August, 2019, DOI: 10.1109/JSEN.2019.2937356.

Chapter 4

Experimentally-based Three-layer Optimisation for Distributed BBNs

4.1 Introduction

When multiple co-located BANs form a network, i.e., a wireless body-to-body network (BBN) with local coordination between them, some other mobile BANs can enter in their proximity, which can cause interference and performance degradation of the coordinated BBN. Here, we investigate such real-life scenarios where some mobile BANs (people wearing sensors) are coming into the vicinity of coordinated BANs, hence causing interference. This chapter is an extension of the previous chapter, where now we perform cross-layer optimisation across three layers: the physical, MAC, and network layers; to route information across the BBN. At the network layer, the best route is selected according to channel state information directly fed from the physical layer, associated with different suitable MAC layer interference mitigation schemes, i.e., low duty cycle TDMA (time division multiple access), and a novel adaptive CSMA/CA (carrier sense multiple access with collision avoidance). Among these two top foremost popular medium access techniques used in BANs, TDMA has maximum bandwidth utilisation and lower power consumption compared to CSMA/CA [240], whereas CSMA/CA improves the overall

throughput by avoiding a fixed waiting period. The routing techniques proposed in Chapter 3 – i.e., shortest path routing (SPR) and cooperative multi-path routing (CMR) incorporating three branch selection combining, are applied over real-life channel measurements to analyse the performance. In this chapter we aim to address the following issues:

- *How to improve reliability with interference mitigation amongst real-life co-existing BANs?*

- *How to utilise the slowly varying channel conditions to apply adaptive mechanisms over real-life body-centric channels?*

In the following sections, we demonstrate the outcomes of cross-layer optimisation across PHY-MAC-NET layers, validated with experimental analysis, for distributed co-located BANs.

4.2 Cross-layer optimised routing with low duty cycle TDMA across BBNs

We study the performance of cross-layer optimisation across the physical, MAC and network layers, with radio interference mitigation for two-tiered communications across multiple coexisting wireless body area networks (BANs), based on real-life measurements. Time division multiple access (TDMA) is used as the MAC layer protocol with low duty cycling for improving co-channel interference. The routing techniques (i.e., shortest path routing (SPR), and cooperative multi-path routing (CMR) incorporating 3-branch selection combining) perform real-time and reliable data transfer across co-located BANs operating near the 2.4 GHz ISM band. Our key findings according to empirical analysis are as follows:

- CMR obtains up to 14 dB and 10 dB improvement over SPR with higher (8.3%) and lower (0.2%) duty cycles, respectively, at 10% outage probability with respect to an acceptable SINR in a dynamic environment associated with mobile subjects.

- With 90% packet delivery ratio (PDR), CMR provides up to 9 dB (with 8.3% duty cycle) and 8 dB (with 0.2% duty cycle) performance improvement over SPR, at −89 dBm receive sensitivity.
- In the best-case scenario (at −100 dBm receive sensitivity), both SPR and CMR achieve almost 100% PDR (equivalent to negligible packet error rate).
- CMR has better spectral efficiency than SPR with a spectral efficiency of up to 0.15 bits/s/Hz at −95 dBm receive sensitivity.
- The empirical received SINR through SPR has an inverse Gaussian or, log-normal distribution while the empirical received SINR through CMR has a Burr (type XII) distribution.

4.2.1 System Model

In this work, 10 co-located mobile BANs (people with fitted wearable radios) are deployed for experimental measurements (the experimental scenario is described in Chapter 3) where we consider 4 BANs as coordinated and 6 other BANs causing interference by coming in the range of the transmissions. We follow the same two-tiered network architecture (described in Chapter 3) formed from the coordinated BANs, where the hubs of the BANs are in tier-2 in a mesh (inter-BAN/ BBN communications) and the on-body sensors of the corresponding BANs are in tier-1 (intra-BAN communications), illustrated in Fig. 4.1 with four coordinated BANs. Each subject wore 1 transceiver (hub) on the left-hip and 2 receivers (sensors/ relays) on the left-wrist and right-upper-arm, respectively. As the transceivers are broadcasting in a sequential order, with 4 coordinated BANs (a total of 12 nodes), each transmitter is transmitting every 60 ms (5 ms $\times$12) to every 3 other subject's receivers as well as their own receivers (all small body-worn radios/hubs/sensors), along with capturing the RSSI (Receive Signal Strength Indicator) values in dBm.

An abstraction of the PHY-MAC-Network cross-layer optimisation is provided in Fig. 4.2. Dynamic routing is performed at the network layer according to the changes directed from physical layer, and TDMA is employed as the co-channel access scheme across all BANs to enable co-channel interference mitigation. As

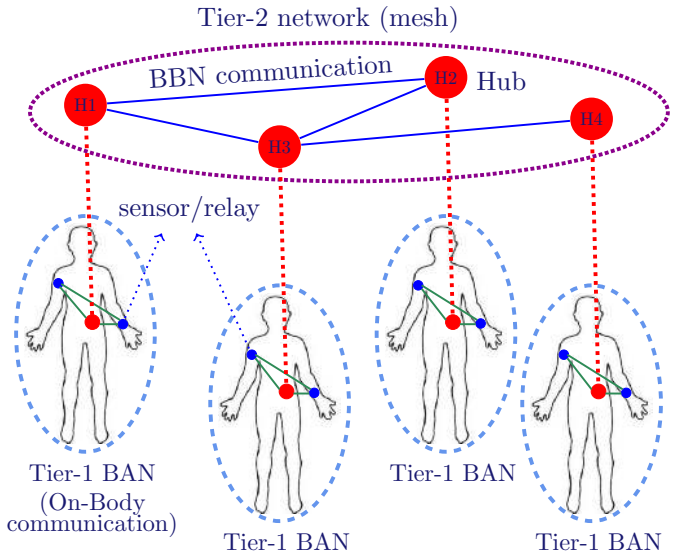

Figure 4.1: Two-tiered architecture of 4 coordinated BANs

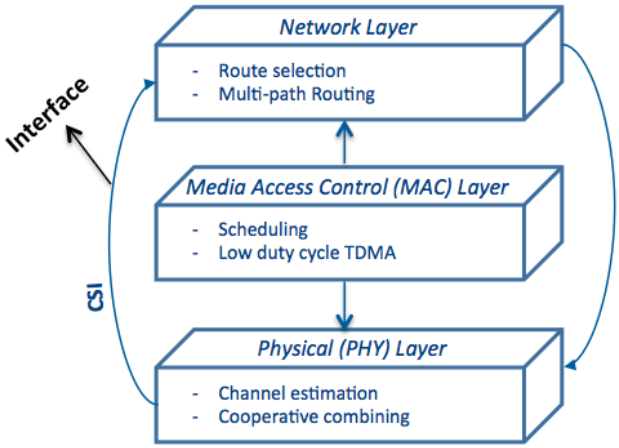

Figure 4.2: Cross-layer optimisation across physical-MAC-network layers

global coordination is not feasible across coexisting BANs [121], the starting time of each coordinated node is randomly selected from an uniform distribution between 0 ms and the idle period ($[0, T_{idle}]$). The idle period of the coordinated nodes, T_{idle} is calculated as $T_{idle} = (n_d - 1)(P_{trans} \times t)$, where n_d is the total number of nodes (hubs + relays/sensors) of the coordinated BANs, P_{trans} is the number of packets

transmitted per node and t is the packet transmission time. The duty cycle, D_c of a given node is measured as follows:

$$D_c = \Big(\frac{P_{trans} \times t}{\Delta}\Big) \times 100\%, \tag{4.1}$$

where $(P_{trans} \times t)$ is the active period of the node in a given time period Δ.

To substantially decrease the interference level, the duty cycles are lowered by increasing the idle period of the nodes, hence decreasing the active period. The time-stamp[1] is set to be 10 times the sampling period of the coordinated BANs for considering different ranges of duty cycles.

Cross-layer Optimised Routing

We perform dynamic shortest path routing (SPR) [230] and cooperative multi-path routing (CMR) that incorporates SPR. The routing techniques are based on Open Shortest Path First (OSPF) protocol that uses link-state algorithm (i.e., Dijkstra's algorithm), where the source nodes intend to find routes with a minimum cost (based on routing metrics, i.e., expected transmission count and hop count) to their destinations for periodically updating the routing table. In CMR, two paths are used from source hub to destination hub, where both paths have two route-hops [22]. In each route-hop, 3-branch selection combining is performed. The detailed description of SPR and CMR can be found in Chapter 3. Here, for CMR, we combine the two different paths at the end destination as follows:

$$Out_{comb(cmr)} = max\big(Out_{P_1}, Out_{P_2}\big), \tag{4.2}$$

where $Out_{P_i} = min\big(Out_{RH_1}, Out_{RH_2}\big); [i = 1, 2]$ is the combined output of path i with two route hops. $Out_{RH_j}; [j = 1, 2]$ is the combined output of the 3-branch selection combining in route hop j. The process for CMR incorporating SPR described with a pseudo-code in Algorithm 3.

[1]The routing table updates after each time-stamp and the samples are taken periodically over the time-stamp period.

Algorithm 3: Estimating output of CMR, incorporating SPR (with ETX + max. 2 hops count)

input : Source node (S), destination node (D), and set of intermediate nodes (N).
output: Result of CMR at destination node.

1 $P_{etx} \leftarrow$ Set of ETX values for every possible paths from S to D;
2 $[i, j] \leftarrow$ [1,`length(`P_{etx}`)`];
3 **while** $i \neq j$ **do**
4 $\quad etx_{min} \leftarrow$ `minimum(`P_{etx}`)`;
5 $\quad$ **if** `PathHopCount(`etx_{min}`)` $= 2$ **then**
6 $\quad\quad Output_{SPR} \leftarrow$ `Path(`etx_{min}`)`;
7 $\quad$ **else**
8 $\quad\quad P_{etx} \leftarrow P_{etx} - etx_{min}$;
9 $\quad\quad etx_{min} \leftarrow$ `minimum(`P_{etx}`)`;
10 $\quad\quad j \leftarrow j - 1$;
11 $\quad$ **end**
12 $\quad i \leftarrow i + 1$;
13 **end**
14 **if** `isempty(`$Output_{SPR}$`)` **then**
15 $\quad Output_{SPR} \leftarrow$ direct path;
16 **end**
17 $P1 \leftarrow Output_{SPR}$;
18 $P_{etx} \leftarrow P_{etx} \setminus P1$;
19 $P2 \leftarrow$ Repeat steps 2 to 16;
20 **for** $i \leftarrow 1$ **to** 2 **do**
21 $\quad$ **for** $j \leftarrow 1$ **to** `length(`P_i`)` **do**
22 $\quad\quad Pi_{RH_j} \leftarrow$ `SelectionCombining(`$Route\_Hop_j$`)`;
23 $\quad$ **end**
24 **end**
25 **if** `length(`P_1`)` > 2 **then**
26 $\quad Comb_{P1} \leftarrow$ `minimum(`$P1_{RH_1}, P1_{RH_2}$`)`;
27 **else**
28 $\quad Comb_{P1} \leftarrow P1_{RH_1}$;
29 **end**
30 $Comb_{P2} \leftarrow$ Repeat steps 20 to 29 for $P2$;
31 $Output_{CMR} \leftarrow$ `maximum(`$Comb_{P1}, Comb_{P2}$`)`;

Table 4.1: Applied Parameters

Parameter	Value
Bandwidth (B)	1 MHz
Carrier Frequency	2.36 GHz
Data rate	486 kbps
Packet size (ℓ)	273 bits
Packet transmission time (t)	0.6 ms
Transmit power (p_{tx})	0 dBm
Total Time (T)	45 mins
T_{SIFS}	50 μs
T_{ACK}	0.2 ms

4.2.2 Performance Analysis with Experimental Results

In this subsection, we discuss and compare the results found from SPR and CMR techniques with the experimental measurements. The results are averaged from 1000 trials for obtaining comprehensive outcomes. We consider outage probability with respect to SINR as a performance metric for the optimisation techniques applied on the coordinated network in case of interference mitigation. For estimating the outages properly, the effect of non-recorded measurements (NaN) due to incorrectly decoded packets were replaced with a value of -101 dBm, just below the receiver sensitivity of -100 dBm. We also estimate the packet delivery ratio and spectral efficiency of the network with respect to different receive sensitivities when applying those routing techniques on the experimental measurements. Furthermore, we investigate the theoretical results of SINR distributions produced from simulated channels (modelled with a lognormal distribution with distribution parameters found from the measured channels) and compare them with the experimental results. The applied parameters for the performance analysis are listed in Table 4.1.

Outage Probability with respect to SINR

The outage probability with respect to SINR threshold can be expressed as,

$$P_{out} = Prob\big(\gamma_s < \gamma_{th}\big), \tag{4.3}$$

where P_{out} is the probability of received SINR (γ_s) being less than a given threshold value, γ_{th}. The signal-to-interference-plus-noise ratio (SINR) for any given link/branch is measured as follows:

$$\gamma_s(\tau) = \frac{p_{tx}\left|h_{s,d}(\tau)\right|^2}{\sum_{i=1}^{n}\left(p_{tx}\left|h_{int_i,d}(\tau)\right|^2\right) + \left|\nu(\tau)\right|^2}, \tag{4.4}$$

where $\gamma_s(\tau)$ is the measured SINR value of a signal s at time instant τ, p_{tx} is the transmit power, n is the number of interfering nodes, $|h_{s,d}|$ and $|h_{int_i,d}|$ are the average channel gains across the time instant of the signal-of-interest and the i^{th} interfering signal, respectively. $|\nu|$ represents the instantaneous noise level at the destination node. The received noise power is set at -100 dBm. In SPR, the combined SINR at the destination node is measured as follows:

$$\gamma_{comb(spr)} = min\big(\gamma_{H_1}, \gamma_{H_2}\big), \tag{4.5}$$

where γ_{H_1} and γ_{H_2} are the SINR of the first and second hops of the shortest path from source to destination, respectively. In CMR, the completely combined SINR at the destination is measured as follows:

$$\gamma_{comb(cmr)} = max\big(\gamma_{P_1}, \gamma_{P_2}\big), \tag{4.6}$$

where $\gamma_{P_i} = min\big(\gamma_{RH_1}, \gamma_{RH_2}\big); [i = 1, 2]$ is the combined SINR of path i with two route hops. $\gamma_{RH_j}; [j = 1, 2]$ is the combined SINR of the 3-branch selection combining (by following equation (3.5) for SINR values instead of channel gains) in route hop j. The averaged outage probability with respect to SINR for SPR and CMR with different duty cycles is presented in Fig. 4.3. As can be seen, CMR provides up to 14 dB performance improvement over SPR at 10% outage probability with respect to a SINR of 5 dB with 8.3% duty cycle. Also, with a lower duty cycle of 0.2%, CMR obtains up to 10 dB performance improvement over SPR at the same outage probability with respect to a SINR of 10 dB. Also, the best fits for the SINR distributions are validated according to their cumulative distribution functions (black dotted curve with each outage probability curve) where the

theoretical cumulative distribution functions (cdfs) show a good match with the empirical results.

The distribution parameters found from the best fit of the SINR values (obtained from experimental measurements) from SPR and CMR with different duty cycles are given in Table 4.2. According to Table 4.2, the SINR values obtained from SPR provide a good fit for an inverse Gaussian distribution with higher duty cycles and for a lognormal distribution with lower duty cycles. An inverse Gaussian distribution with shape parameter $\lambda \to \infty$ becomes more like a normal (Gaussian) distribution. SINR values obtained from CMR posses a three-parameter Burr (burr type XII) or generalised log-logistic distribution. In reliability applications, the use of the log-logistic is often proposed as an alternative to the lognormal. Thus, the Burr offers an even more flexible alternative to the lognormal with all of the advantages of the log-logistic (as the log-logistic distribution is a special case of the Burr) [241]. The cdf of the inverse Gaussian distribution is:

$$\begin{aligned} F(x \mid \mu, \lambda) = \exp^{2\mu/\lambda} \Phi\Big\{ -\sqrt{(\lambda/\mu)}(1 + x/\mu)\Big\} + \\ \Phi\Big\{\sqrt{(\lambda x)}(x\mu - 1)\Big\}, \quad x > 0, \end{aligned} \tag{4.7}$$

where Φ is the cdf of the standard normal distribution, $\mu(> 0)$ and $\lambda(> 0)$ are the mean and shape parameters of the inverse Gaussian distribution, respectively.

The cdf of the Burr (type XII) distribution is:

$$F(x \mid \alpha, c, k) = 1 - \Big(1 + (x/a)^c\Big)^{-k}, \quad x > 0, \tag{4.8}$$

where $\alpha(> 0)$ is the scale parameter and $c(> 0)$ and $k(> 0)$ are the shape parameters of the Burr distribution. The density of the distribution is unimodal (having one clear peak) if $c > 1$ and L-shaped if $c \leq 1$.

And, the cdf of lognormal distribution is:

$$F(x \mid \mu, \sigma) = \frac{1}{x\sigma\sqrt{2\pi}} \exp\left(\frac{-(\ln(x) - \mu)^2}{2\sigma^2}\right), \quad x > 0, \tag{4.9}$$

where μ and σ are the measured log-mean and log-standard deviation, respectively. The distributional relationship on x can be expressed as $x = \exp(z)$, where x is

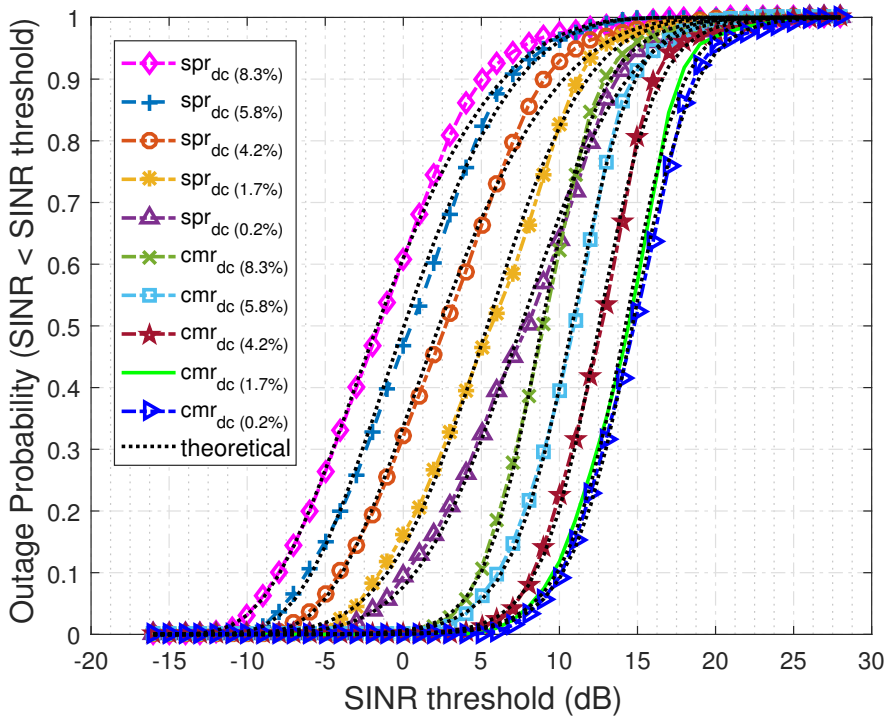

Figure 4.3: Average outage probability with respect to SINR threshold for SPR and CMR, with different duty cycles (dc) per node for the 4 coordinated BANs. Receiver sensitivity −100 dBm, transmit power 0 dBm; black dotted curves represent the theoretical cdf of SINR with corresponding duty cycles

the log-normally distributed random variable and $z \sim Normal(\mu, \sigma)$.

Packet Delivery Ratio (PDR)

The packet delivery ratio (PDR) with respect to different receive sensitivities is given in Fig. 4.4. It is shown that the packet delivery ratio, which is the ratio of the successfully delivered packets (P_{succ}) to the transmitted packets (P_{trans}) at a given time, remains stable (slightly improved) as the duty cycle is lowered. With a packet delivery ratio of 90% (or, packet error rate (PER) of 10%, as $PER = 1 - PDR$), the CMR provides up to 9 dB and 8 dB performance improvement over SPR with a higher duty cycle of 8.3% and a lower duty cycle of 0.2%, respectively, at −89 dBm receive sensitivity. Also, the best-case (at −100 dBm receive sensitivity) PDR for SPR and CMR are almost 100%, which is equivalent to a negligible PER (thus

Table 4.2: Distribution parameters of SINR values; $\{\mu,\lambda\}$ are the mean and shape parameter of the inverse Gaussian distribution; $\{\mu,\sigma\}$ are the log-mean and log-standard deviation of the lognormal distribution; $\{\alpha,\ c,\ k\}$ are the scale and two shape parameters of the burr distribution; exp. and sim. imply experimental and simulated data, respectively

Routing method	Duty cycle	Distribution fit	Parameters
SPR (exp.)	8.3%	Inv. Gaussian	$\mu = 1.799,\ \lambda = 0.511$
	5.8%	Inv. Gaussian	$\mu = 2.27,\ \lambda = 0.856$
	4.2%	Inv. Gaussian	$\mu = 4.39,\ \lambda = 1.29$
	1.7%	Lognormal	$\mu = 1.24,\ \sigma = 1.15$
	0.2%	Lognormal	$\mu = 1.74,\ \sigma = 1.22$
SPR (sim.)	8.3%	Inv. Gaussian	$\mu = 1.65,\ \lambda = 0.593$
	5.8%	Inv. Gaussian	$\mu = 2.0012,\ \lambda = 0.989$
	4.2%	Inv. Gaussian	$\mu = 4.1002,\ \lambda = 1.45$
	1.7%	Lognormal	$\mu = 1.304,\ \sigma = 1.11$
	0.2%	Lognormal	$\mu = 1.702,\ \sigma = 1.22$
CMR (exp.)	8.3%	Burr	$\alpha = 6.56,\ c = 2.58,\ k = 0.752$
	5.8%	Burr	$\alpha = 14.4,\ c = 2.056,\ k = 1.32$
	4.2%	Burr	$\alpha = 18.1,\ c = 2.35,\ k = 1.019$
	1.7%	Burr	$\alpha = 33.6,\ c = 2.086,\ k = 1.46$
	0.2%	Burr	$\alpha = 32.1,\ c = 2.105,\ k = 1.15$
CMR (sim.)	8.3%	Burr	$\alpha = 8.302,\ c = 2.99,\ k = 0.632$
	5.8%	Burr	$\alpha = 13.8,\ c = 2.49,\ k = 0.817$
	4.2%	Burr	$\alpha = 19.9,\ c = 2.71,\ k = 0.799$
	1.7%	Burr	$\alpha = 36.02,\ c = 2.26,\ k = 1.13$
	0.2%	Burr	$\alpha = 32.2,\ c = 2.13,\ k = 1.14$

fulfilling the IEEE 802.15.6 BAN Standard requirement of PER being less than 10%).

Spectral Efficiency

The spectral efficiency (ζ) of the network with coordinated BANs is estimated as follows:

$$\zeta = \frac{\Theta \times \omega}{B}, \tag{4.10}$$

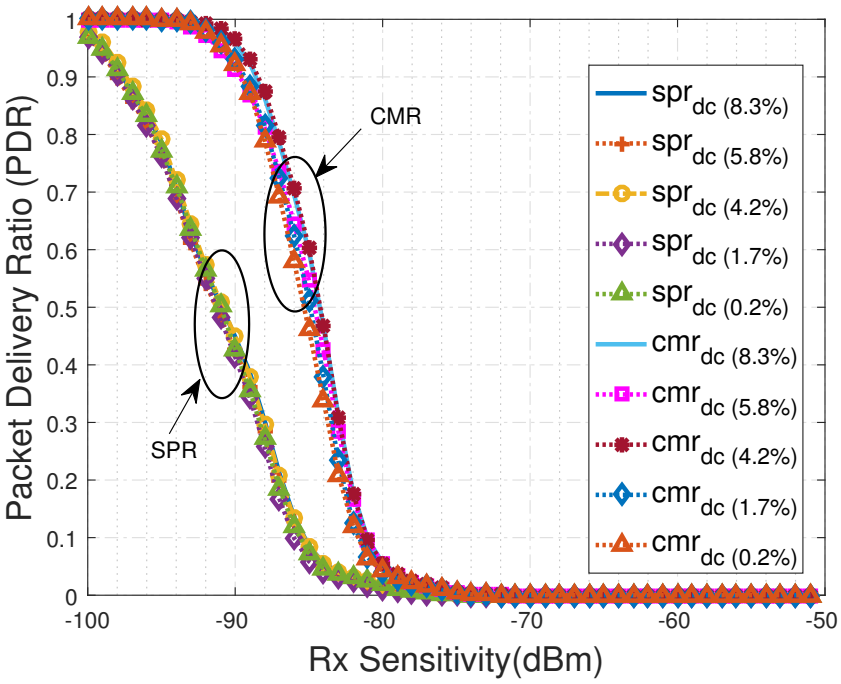

Figure 4.4: Average packet delivery ratio (PDR) in terms of different receive sensitivities for SPR and CMR, with different duty cycles (dc) per node for the 4 coordinated BANs, at 0 dBm transmit power

where ω is the number of coordinated BANs and B is the bandwidth. The aggregated throughput of the network can be defined as $(\Theta \times \omega)$, where the throughput Θ can be measured as follows:

$$\Theta = \frac{P_{succ} \times \ell}{T}, \tag{4.11}$$

where P_{succ} is the number of successfully delivered packets over the total time T and ℓ is the length of the packet. The bandwidth and packet size can be found from Table 4.1, which are chosen in accordance with the IEEE 802.15.6 Standard for narrowband communications [222]. The average spectral efficiency with respect to different receive sensitivities (e.g. -95 dBm, -88 dBm) with different number of coordinated BANs (e.g. 4,5,6 coBANs) and corresponding different duty cycles are presented in Figs. 4.5 and 4.6. In Figs. 4.5 and 4.6, duty cycles $(dc1, dc2, dc3, dc4, dc5)$ refer to $(8.3\%, 5.8\%, 4.2\%, 1.7\%, 0.2\%)$ for 4

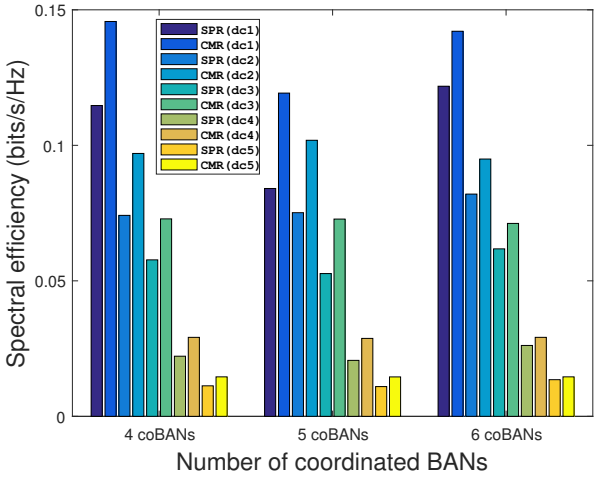

Figure 4.5: Average spectral efficiency with respect to −95 dBm receive sensitivity for SPR and CMR, with different duty cycles (dc) of 4, 5 and 6 co-ordinated BANs (coBANs)

coordinated BANs, $(6.7\%, 4.7\%, 3.3\%, 1.3\%, 0.1\%)$ for 5 coordinated BANs and $(5.6\%, 3.9\%, 1.7\%, 1.1\%, 0.1\%)$ for 6 coordinated BANs. It is shown in Fig. 4.5 that, CMR provides up to 0.15 bits/s/Hz spectral efficiency with 8.3% duty cycle at −95 dBm receive sensitivity. Also, with a lower duty cycle (e.g. $0.2\%, 0.1\%$), the spectral efficiency is greater than or equal to 0.01 bits/s/Hz for SPR and CMR at −95 dBm receive sensitivity. Furthermore, Fig. 4.6 shows CMR provides better spectral efficiency than SPR (with 0.2% or, 0.1% duty cycle, the spectral efficiency for CMR is greater than or equal to 0.01 bits/s/Hz at −88 dBm receive sensitivity).

Distributions from Simulated SINR

For investigation purposes, we model the measured on-body and inter-body links using a lognormal distribution (as lognormal is the typical distribution for single-link narrowband small-scale fading channels [82]). We simulate the dynamic on-body and inter-body channels according to the appropriate log-mean and log-standard deviation parameters found from the measured channels. The best fit parameters for the SINR distributions (averaged from 1000 trials) with different duty cycles after applying SPR and CMR on the lognormally modelled channels

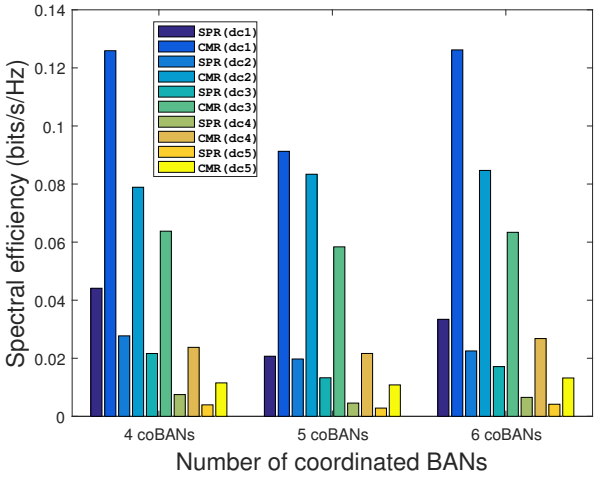

Figure 4.6: Average spectral efficiency with respect to −88 dBm receive sensitivity for SPR and CMR, with different duty cycles (dc) of 4, 5 and 6 co-ordinated BANs (coBANs)

are given in Table 4.2. It can be seen that, the distribution results found from simulated channels match well with the results obtained from experimental data.

4.3 Cross-layer optimised routing with adaptive CSMA/CA across BBNs

In this section, we propose an adaptive carrier sensing mechanism with CSMA/CA as the MAC layer scheme for interference mitigation across a distributed BBN, to obtain a suitable trade-off between the amount of interference, throughput, latency and energy consumption of CSMA/CA channels. The channel state information from the physical layer is passed on to the network layer using an adaptive cross-layer carrier sensing mechanism between the physical and MAC layer, which adjusts the carrier sense threshold, e.g., RSSI periodically based on the slowly-varying channel conditions with an adequate periodic time-stamping for routing updates. From the implementation of the proposed adaptive CSMA/CA with the experimental measurements used here, we demonstrate the following:

- With the proposed adaptive carrier sensing, the percentage of longer (greater

than 3 s) continuous back-off duration is trivial (0%), whereas with static threshold, e.g., −95 dBm, the channel can remain continuously in back-off for very long period (more than 1000 s) with 6% of the total time.

- The average continuous back-off duration of the CSMA/CA channels with the proposed adaptive carrier sensing mechanism is 237 ms, whereas it can goes up to 11 s on average with a static carrier sensing threshold of −95 dBm.
- The proposed adaptive mechanism can provide more than 50% improvement over static carrier sensing, in terms of throughput (successful packets/s) and packet arrival rate.
- Even though static carrier sensing provides better outage probability with respect to signal-to-interference-plus-noise-ratio (SINR) as it is strict towards avoiding larger interference levels, it suffers from decreased throughput and increased latency.
- Adaptive CSMA/CA provides up to 20% and 30% improvement over TDMA (with a higher duty cycle of 8.3%), in terms of average throughput (successful packets/s) and packet arrival rate, respectively.
- For spectral efficiency, adaptive CSMA/CA provides up to 6% improvement over TDMA with 8.3% duty cycle.

4.3.1 System Model

We use the same two-tiered network architecture (Fig. 4.1) used for the TDMA approach in the previous section. Here, all 10 BANs form a distributed BBN (with decentralised coordination between them) on which we apply the same routing techniques: SPR and CMR. Hence, the experimental scenario is also same for this work. As all the co-located BANs are used, each transmitter is transmitting in every 50 ms (with a sampling rate of 20 Hz) to all 9 other subject's receivers as well as their own receivers (all small body-worn radios/hubs/sensors), along with capturing the RSSI (Receive Signal Strength Indicator) values in dBm[2], which

[2]Any received signal strength below −100 dBm, resulting in incorrectly decoded packets in experiment, is set at −101 dBm in analysis

gives a total of 300 channel measurements (including both on-body and body-to-body links) in real-time over the whole network during the measurement period. For effective dynamic estimation of the channel, continuous time-stamping is used every 600 ms which is reasonable, given the longer coherence times of 500 ms (up to 1 s) for 'everyday' activities of narrowband on-body BAN channels [82], and for body-to-body channels used here where we have calculated the coherence time to be 900 ms (with auto-correlation coefficient of 0.7).

Proposed Adaptive carrier sensing mechanism

Adaptive CSMA/CA with maximum-interference-power carrier-sensing (MPCS) is employed as the co-channel access scheme across (inter-BAN/coordinator level) and within (intra-BAN/sensor level) all BANs to enable co-channel interference mitigation without global coordination. Whenever a node is ready to transmit data, it checks the availability of the channel by measuring the maximum interference power from the potential interference caused by the surrounding nodes that are trying to access the channel at the same time. For a given time instant τ of i^{th} time-stamp (τ_i), the transmission of a given link (signal-of-interest from source to destination) is permitted by the simple carrier sensing mechanism with collision avoidance by MPCS, if

$$\begin{aligned} &\max(\boldsymbol{\eta}) < cs_{th_i} \\ &\text{where } \boldsymbol{\eta} = \left(p_{tx} \left|h_{int_k,d}(\tau_i)\right|^2\right),\ k = 1, \ldots, n \end{aligned} \tag{4.12}$$

where p_{tx} is the transmit power, $|h_{int_k,d}(\tau_i)|$ is the interfering channel gain from the k^{th} interfering BAN to the destination d at time instant τ of i^{th} time-stamp, n is the number of interfering BANs and cs_{th_i} is the adaptive carrier sense threshold, e.g., RSSI in i^{th} time-stamp. If the condition in (4.12) is not fulfilled, the node defers its transmission for a back-off period (still sensing the medium) until it finds the channel available for transmission. When the channel is found available by the node, it waits for a short inter-frame space period (T_{SIFS}) and then transmits the data. If an acknowledgement (ACK) is not received by the node, it implies a failure has occurred and the node tries to retransmit the data with the same procedure.

We apply adaptive carrier sensing to reduce the longer back-off period, hence

improving throughput and end-to-end delay of the overall network. The channel conditions, e.g., back-off percentage, ill-conditioned periods of incorrectly decoded packets of each time-stamp are used as an approximation of the channel conditions of the next time-stamp:

$$X_{i+1} \approx X_i, \quad i \geq 1, \tag{4.13}$$

where for time-stamp i, the channel condition of the next time-stamp X_{i+1} can be estimated from the current channel condition X_i. This estimation is a systematic approach for dynamic prediction of the inter-BAN channels given the longer coherence time of around 900 ms and the time-stamp period (600 ms) used in this work. In our proposed method, if the probability of back-off period is higher than 50%, the carrier-sense threshold is adjusted to permit more transmissions, despite the amount of interference, to reduce continuous latency. Additionally, if the probability of transmitting incorrectly decoded packets is higher than 50% even though having a lower back-off duration, the threshold is adjusted to decrease the amount of interference to reduce packet failure rate. This way there is a suitable trade-off between the latency, throughput and amount of interference of the CSMA/CA channels. The RSSI threshold for the first time-stamp is predicted to be -90 dBm from an estimated median of typical on-body and inter-body RSSI measurements. The routes for the first time-stamp are estimated with a randomly selected value (≥ 1 and $< \infty$) for each link, based on the defined routing metric, i.e., ETX. The dynamic setting of the carrier-sense threshold is described in Algorithm 4.

4.3.2 Performance Analysis

In this section, we discuss and compare the results found from adaptive CSMA/CA applied on SPR and CMR techniques with the experimental measurements. We compare the performance of applying static and adaptive carrier sensing thresholds for CSMA/CA in case of continuous back-off duration and throughput (successful packets/s) vs. packet arrival rate and outage probability with respect to SINR. We also provide a performance comparison between adaptive CSMA/CA and coordinated TDMA in terms of throughput vs. packet arrival rate, packet delivery ratio and spectral efficiency. The applied parameters for the performance analysis are listed in Table 4.1.

Algorithm 4: Estimating Adaptive Carrier Sense Threshold

input : The current time-stamp (i) and the carrier sense threshold for the current time-stamp (CS_{th_i}).
output: The carrier sense threshold for the next time-stamp ($CS_{th_{i+1}}$).

$TS_i \leftarrow$ outcome of CSMA/CA for the i^{th} time-stamp;
$BOP_i \leftarrow$ estimate back-off percentage of TS_i;
$ICP_i \leftarrow$ estimate the percentage of ill-conditioned period of TS_i;
if $BOP_i \geq 50\%$ **then**
    $CS_{th_{i+1}} \leftarrow CS_{th_i} + 1$;
else
    if $BOP_i < 50\%$ *&* $ICP_i > 50\%$ **then**
        $CS_{th_{i+1}} \leftarrow CS_{th_i} - 1$;
    else
        $CS_{th_{i+1}} \leftarrow CS_{th_i}$;
    end
end

Continuous Back-off Duration

Since the continuous back-off duration is a key contributor to latency, this duration is an important performance metric for CSMA/CA channels. The continuous back-off duration of the CSMA/CA channels for body-to-body communications with different static carrier sense thresholds and an adaptive threshold, applied according to Algorithm 4, are shown in Fig. 4.7. It is demonstrated that apart from having a higher percentage of shorter continuous back-off duration, using an adaptive carrier sense threshold yields a negligible (0%) occurrence of longer (greater than 3 s) back-off duration, whereas there is a higher percentage of longer continuous back-off duration with static carrier sense thresholds. According to the IEEE 802.15.6 BAN Standard guidelines [29], latency should be less than 125 ms in medical applications and less than 250 ms in non-medical applications. With the adaptive technique, the estimated average continuous back-off duration over the total time is 237 ms ($<$ 250 ms). Also, the highest percentage (more than 7% of the measured time) in Fig. 4.7 is for continuous back-off duration of 100 ms ($<$ 125 ms) with this approach. On the other hand, with a static threshold of -95 dBm, channels can remain continuously in back-off over more than 1000 s, almost 6% of the time, and

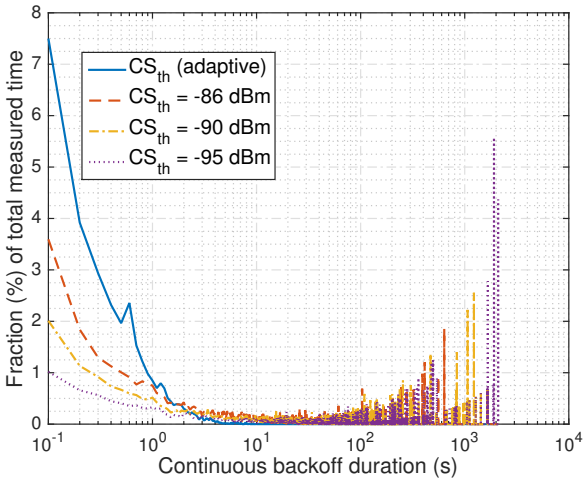

Figure 4.7: Percentage of continuous back-off duration of CSMA/CA links with an adaptive carrier sense threshold (CS_{th}) and different static carrier sense thresholds (CS_{th}), at transmit power 0 dBm, with 10 coexisting BANs.

more importantly, the average continuous back-off duration within this threshold is up to 11 s, which is very large for delay-constrained networks like BANs.

Throughput (Successful Packets/s) vs. Packet Arrival Rate

The average throughput (in terms of successful packets per-second) vs. the average packet arrival rate is shown in Fig. 4.8. It can be seen that the proposed adaptive CSMA/CA achieves the best result in terms of both throughput and packet arrival rate. Notably, with a higher static carrier sense threshold of -86 dBm the throughput is significantly lower with respect to packet arrival rate which indicates that, although more packets can be transmitted with a higher threshold (as it permits a higher interference level), the overall performance will degrade because of possibly lower SINR of the signal-of-interest. In Fig. 4.8, we also compare the CSMA/CA approach with a coordinated TDMA approach from [22], where the same setup is used with 4 coordinated BANs receiving interference from 6 non-coordinated nearby BANs. It is shown that adaptive CSMA/CA provides up to 20% and 30% improvement over TDMA (with a higher duty cycle of 8.3%), in terms of average throughput and packet arrival rate, respectively.

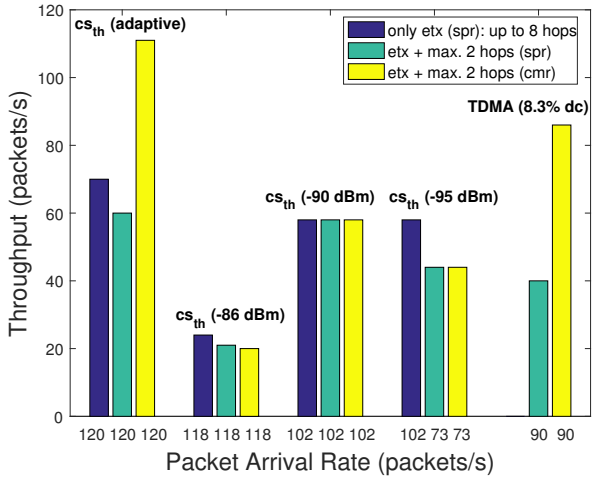

Figure 4.8: Average throughput (successful packets/s) vs. packet arrival rate over 10 coexisting BANs for SPR and CMR (associated with CSMA/CA), with adaptive/static carrier sense thresholds (CS_{th}) and TDMA with 8.3% duty cycle (dc). Transmit power 0 dBm and receiver sensitivity -90 dBm

Outage Probability with respect to SINR

The outage probability with respect to SINR threshold can be expressed as,

$$P_{out} = Prob\big(\gamma_s < \gamma_{th}\big), \tag{4.14}$$

where P_{out} is the probability of received SINR, γ_s, being less than a given threshold value γ_{th}. The signal-to-interference-plus-noise ratio (SINR) for any given link/branch is measured as follows:

$$\gamma_s(\tau) = \frac{p_{tx}\,|h_{s,d}(\tau)|^2}{\sum_{i=1}^{n}\big(p_{tx}\,|h_{int_i,d}(\tau)|^2\big) + |\nu(\tau)|^2}, \tag{4.15}$$

where $\gamma_s(\tau)$ is the measured SINR value of a signal s at time instant τ, p_{tx} is the transmit power, n is the number of interfering nodes, $|h_{s,d}|$ and $|h_{int_i,d}|$ are the average channel gains across the time instant of the signal-of-interest and the i^{th} interfering signal, respectively. $|\nu|$ represents the instantaneous noise level at the destination node. The received noise power is set at -100 dBm. The averaged

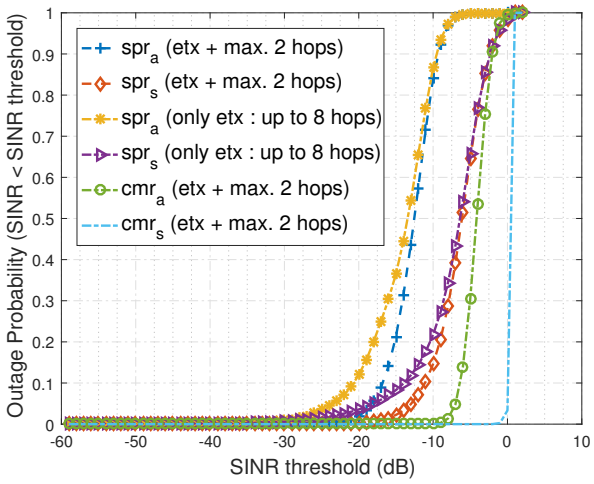

Figure 4.9: Average outage probability with respect to SINR thresholds for SPR and CMR (associated with CSMA/CA), with different routing metrics (e.g., only ETX, ETX + max. 2 hops) for 10 coexisting decentralised BANs; Subscript a and s refers to adaptive and static carrier sensing, respectively. Receiver sensitivity -100 dBm, transmit power 0 dBm

outage probability with respect to SINR thresholds found from SPR and CMR with adaptive and static (at -86 dBm) carrier sensing scheme applied over 10 coexisting BANs is shown in Fig. 4.9. It is demonstrated that the use of a static threshold (i.e., -86 dBm) in CSMA/CA improves the outage probability with respect to SINR as it constantly avoids a significant interference level, although resulting in a longer back-off period (Fig. 4.7) and throughput degradation (Fig. 4.8).

Packet Delivery Ratio (PDR)

The averaged packet delivery ratio (PDR) with respect to different receive sensitivities for the given scheme with adaptive CSMA/CA and TDMA approach is presented in Fig. 4.10. It is shown that adaptive CSMA/CA yields better performance than a higher duty cycle TDMA. With a packet delivery ratio of 90% (or packet error rate (PER) of 10%, as $PER = 1 - PDR$), the SPR with adaptive CSMA/CA provides 4 dB improvement over SPR with TDMA. It can also be seen that CMR gives more than 50% (up to 65%) performance improvement over SPR with adaptive CSMA/CA, at -88 dBm receive sensitivity. Additionally, the best-

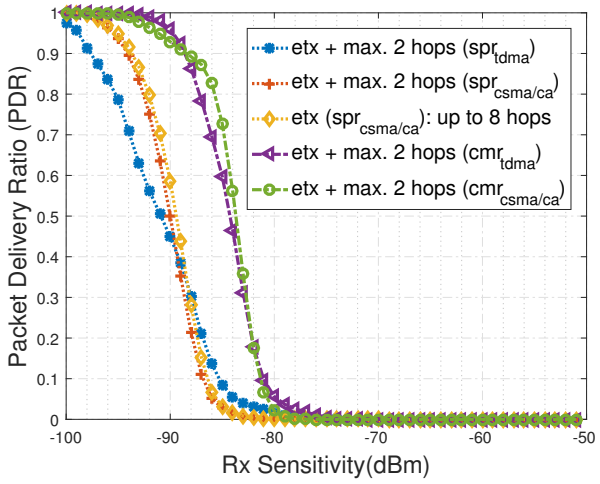

Figure 4.10: Average packet delivery ratio with respect to different receive sensitivities for SPR and CMR (associated with adaptive CSMA/CA and 8.3% duty cycle TDMA), with different routing metrics (e.g., only ETX, ETX + max. 2 hops) for 10 coexisting BANs; Transmit power 0 dBm

case (at -100 dBm receive sensitivity) PDR for SPR and CMR is almost 100% which is equivalent to a negligible PER (thus significantly surpassing the IEEE 802.15.6 BAN Standard requirement of PER being less than 10%).

Spectral Efficiency

The spectral efficiency (ζ) over BANs across which routing occurs is estimated as follows:

$$\zeta = \frac{\Theta \times n_c}{B}, \tag{4.16}$$

where n_c is the number of actively routed BAN channels and B is the bandwidth. The aggregated throughput can be defined as $(\Theta \times n_c)$, where the single channel throughput Θ can be measured as follows:

$$\Theta = \frac{P_{succ} \times \ell}{T}, \tag{4.17}$$

where P_{succ} is the number of successfully delivered packets over the total time T and ℓ is the length of the packet. The bandwidth and packet size can be found from Table 4.1, which are chosen in accordance with the IEEE 802.15.6 Standard

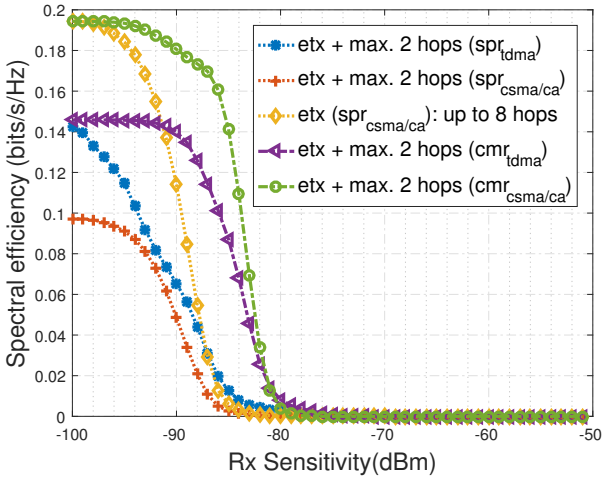

Figure 4.11: Average spectral efficiency for 10 coexisting BANs with respect to different receive sensitivities for SPR and CMR (associated with adaptive CSMA/CA and 8.3% duty cycle TDMA), with different routing metrics (e.g., only ETX, ETX + max. 2 hops), at transmit power 0 dBm

for narrowband communications [222]. The average spectral efficiency of the overall network with respect to different receive sensitivities for adaptive CSMA/CA and higher (8.3%) duty cycle TDMA are presented in Fig. 4.11. It can be seen that, adaptive CSMA/CA shows improvement over TDMA while contributing up to 6% performance improvement over higher duty cycle TDMA at best-case scenario (at -100 dBm receive sensitivity). Even though, the adaptive CSMA/CA with SPR (ETX + max. 2 hops) technique suffers from lower spectral efficiency because of the hop restriction, it shows improvement when performing SPR without any hop restriction due to the increased number of transmissions with longer paths.

4.4 Summary

In this chapter, we have analysed cross-layer methods — SPR and CMR (incorporating cooperative combining), validated using experimental measurements, to optimise radio communications and mitigate interference across many co-located wireless body area networks or BANs (forming a BBN), by utilising distinct features at the physical, MAC and network layers. Along with studying the performance of

low duty cycle TDMA, we have introduced a simplified adaptive cross-layer carrier sensing mechanism for CSMA/CA in case of routing information across a BBN. We have shown that the proposed CMR achieves up to 14 dB performance improvement with 8.3% TDMA duty cycle, and 10 dB improvement with 0.2% TDMA duty cycle over SPR, at 10% outage probability with respect to an acceptable SINR. Also, CMR provides up to 9 dB improvement over SPR with 90% packet delivery ratio. Moreover, CMR contributes to suitable BAN spectral efficiency of up to 0.15 bits/s/Hz at -95 dBm receive sensitivity.

On the other hand, adaptive CSMA/CA demonstrates more than 50% gain over static carrier sensing, in terms of throughput (successful packets/s) vs. packet arrival rate, as well as providing improved latency. We have also compared the performance of adaptive CSMA/CA with a high duty cycle TDMA by performing cross-layer optimised dynamic routing, SPR and CMR, validated by experimental measurements. It was shown that adaptive CSMA/CA yields better performance than TDMA while providing up to 4 dB, 20% and 6% improvement over higher (8.3%) duty cycle TDMA in terms of PDR, throughput and spectral efficiency, respectively. The demonstrated feasibility of our proposed methods motivate the practical deployment of many closely-located BANs at large-scale, in both highly-connected medical and non-medical applications. In the next chapter, we investigate and characterise the predictive behaviour of real-life body-centric channels, to be deployed for predictive optimisation of those channels with greater accuracy.

4.5 Related Publications

- **Samiya Shimly**, David B. Smith, and Samaneh Movassaghi: 'Cross-layer optimized routing with low duty cycle TDMA across multiple wireless body area networks', in *IEEE International Conference on Communications (ICC'*17*)*, May, 2017.

- **Samiya M. Shimly**, David B. Smith, and Samaneh Movassaghi: 'Cross-Layer Designs for Body-to-Body Networks: Adaptive CSMA/CA with Distributed Routing', in *IEEE International Conference on Communications (ICC'*18*)*, May, 2018.

Chapter 5

Predictive Characteristics of Real-life Body-centric Channels

5.1 Introduction

Wireless body-to-body networks (BBNs) are envisioned to be self-organising, smart, and mobile networks that create their own centralised/decentralised network connection without any external coordination to improve the end-to-end network connectivity in various circumstances. This type of autonomous decision making activity requires systematic prediction and modelling of the channel behaviour, which leads to the investigation of the 'wide-sense-stationarity' (Definition 5.1) and 'long-memory' (Definition 5.2) characteristics of the channel, which significantly affect the performance of predictive analysis and characterisation of the channel [146,157].

Definition 5.1. *(Wide-sense-stationarity or second-order stationarity) A process $X(t)$ is wide-sense-stationary if the first and second moments, e.g., mean, auto-covariance of $X(t)$ are independent of time t, such as,*

$$E[X(t)] = \mu_x(t_1) = \mu_x(t_1 + \omega), \quad for\ all\ \omega\ \epsilon\ t,$$

$$Cov[X(t_1), X(t_2)] = Cov[x(t1, t2)] = Cov[x(t1 + \omega, t2 + \omega)], \quad for\ all\ \omega\ \epsilon\ t,$$

where $\mu_x(t)$ is the mean of $X(t)$ and $Cov[X(t_1), X(t_2)] = E\big[\{X(t_1) - \mu_x(t)\}\{X(t_2) - \mu_x(t)\}\big]$ depends on ω where $\omega = t_2 - t_1$. In other words, the auto-covariance will

remain similar for a given lag duration ω, regardless of the position of ω over the channel.

Definition 5.2. *(Stationary long-memory process) A second-order stationary process X is long-range dependent or has long-memory property if the auto-correlation function decays very slowly (hyperbolic decay) such as*

$$\lim_{\omega \to \infty} r_{xx}(\omega) = 0, \tag{5.1}$$

and, is not summable [242]:

$$\sum_{\omega=0}^{\infty} r_{xx}(\omega) = \infty \tag{5.2}$$

As stated in [146], much analysis of wireless signals and time-series modelling assumes that time-varying channel gains are at least wide-sense-stationary (with uncorrelated scattering) whilst real-world radio channels often demonstrate 'quasi-stationary' behaviour [243]. Therefore, it is crucial to investigate the wide-sense-stationarity (WSS) of radio channels to exploit the WSS period/duration (Definition 5.3) for appropriate channel characterisation.

Definition 5.3. *(Wide-sense-stationary duration) The WSS duration/segment is the average duration over the channel for which the channel can be considered WSS (probability of satisfying the WSS assumption is greater than or equal to a given threshold). The WSS duration, $X(t)_\psi$ can be expressed as $X(t)_\psi = \gamma_{X(t)_\psi} \geq \theta$, where θ is the threshold ranges between 50% to 70%.*

As stated in [244], in a conventional sense, second order stationary (or WSS) random functions are considered to be short-range dependent or memoryless [245, 246]. However, it is not likely that a wide-sense-stationary channel is always memoryless, as is the case in a stationary long-memory process (Definition 5.2) where the channel samples possess long-term statistical dependence, known as long-range dependence (LRD) or long-memory – the term 'memory' indicates to what extent past information is related to future consequences. Analysis of these types of processes can produce spurious results if dealt with by standard memoryless models, e.g., Markov chains. Basically, body-centric channels are slowly-varying in nature due to human body dynamics and shadowing by body parts [226], which

indicates possible dependence or auto-correlation between samples. Therefore, it is important to evaluate long-range dependence (LRD) or long-memory property along with wide-sense-stationarity of body-centric channels to perform accurate modelling, characterisation and predictive analysis.

Wide-sense-stationarity together with long-range dependence have not been broadly investigated for wireless networks (and even more particularly for wireless body-centric networks). Some related work in terms of WSS and LRD characteristics of wireless channels have been listed in the literature review in Chapter 2. To the best of our knowledge, this work is the first detailed investigation of the WSS and LRD properties of body-centric channels (specifically body-to-body channels), based on the work in [99] (where the authors showed that, on-body channels are typically non-stationary). Here, we aim to answer the following important questions:

- *What is the expected range of WSS duration for 'everyday' wireless body-to-body channels?*
- *Do the WSS characteristics vary for B2B channels between different on-body sensor locations in different environments?*
- *Do wireless body-centric channels have long-memory?*
- *Are the WSS characteristics of body-centric channels associated with long-range dependence?*
- *What is the importance and benefit of the WSS duration for stationary long-range dependent body-centric channels?*
- *Is retaining long-memory sufficient to make reliable prediction for body-centric channels?*

Hence, in this work, we perform the same stationarity tests from [247] over different experimental datasets with different numbers of people/BANs, i.e., 3, 8, 10, 20 coexisting in different surroundings, e.g., cafe, pub, indoor/outdoor to examine the potential range of the WSS duration for B2B channels in 2.36 GHz narrowband. We also investigate the long-range dependence or long-memory of the channels in

association with the Hurst exponent [248] and the pattern of the decaying auto-correlation function (ACF). Our key findings from such estimation of WSS and LRD characteristics based on experimental measurements in 2.36 GHz narrowband are as follows:

- The expected range of WSS duration for body-to-body channels is 0.5 s to 9 s (approximately 5 s) with 95% confidence level and 0.5 s to 15 s (approximately 8 s) with 99% confidence level.
- The shadowing effect from different wearable sensor locations, body postures/movements and indoor/outdoor environments contributes to the varying WSS characteristics of narrowband body-to-body channels. For instance, in an experimental scenario with 8 co-located BANs, the left-hip-to-left-wrist link (shadow fading distribution: Burr type XII) can hold the WSS duration for up to 4 s, with 95% confidence level. On the other hand, the left-hip-to-left-hip link (shadow fading distribution: Rician) depicts almost non-stationary behaviour with several test statistics with 95% confidence level.
- In all circumstances, B2B channels show more stability over time than on-body channels with respect to satisfying the null hypothesis assumption of WSS (on-body channels show non-stationary characteristics in almost all cases).
- Body-centric channels have hyperbolic decay of their auto-correlation function, which can be inferred as the presence of long-range dependence or long-memory.
- Both on-body and B2B channels have higher value of their Hurst exponent (around 0.9) which is indicative of long-memory.
- There is no causal link between the WSS and LRD characteristics of body-centric channels. Both WSS and non-WSS channels can hold LRD characteristics.
- The WSS duration of B2B channels helps to estimate a period over which prediction can be reliably made from received channel samples with long-range dependence.

- Having only long-memory is not sufficient for performing predictive analysis, as unlike B2B channels, on-body channels depict non-stationary behaviour, which limits the efficiency of the predictability of those channels.

5.2 Experimental Scenarios

The general description of the experimental scenario for the experimental datasets used throughout the thesis is presented in Chapter 3. In this chapter, we analyse the WSS and LRD characteristics of body-centric channels with an extensive amount of channel measurements from different experimental datasets[1] consisting of various numbers of co-located mobile people/BANs, i.e., 8, 10, 20 co-located BANs. A brief description of those datasets is given below:

5.2.1 Dataset 1 (3 BANs wearing hubs/transceivers)

In this dataset, there were 8 coexisting BANs with three receivers/on-body sensors on Left–Wrist (LW), Right–upper–Arm (RA), and Left–Hip (LH), respectively. Amongst them, 3 BANs (or subjects) were wearing an extra on-body sensor (transceiver) on Right–Hip (RH). Hence, the result for a specific body-to-body (B2B) channel (i.e., RH–LW, RH–RA, RH–LH) is averaged over (3×7) links, except the RH–RH links among transceivers where the result is averaged over only (3×2) links. The sampling rate for each channel in this dataset is 66.7 Hz.

5.2.2 Dataset 2 (8 coexisting BANs)

In this dataset, each BAN/subject is wearing three on-body sensors: one transceiver on the Left–Hip (LH) and two receivers on the Left–Wrist (LW) and Right–upper–Arm (RA), respectively. The result for a specific body-to-body (B2B) channel is averaged over (8×7) links. The sampling rate for each channel in this dataset is 25 Hz.

[1]available in http://doi.org/10.4225/08/5947409d34552 [215]

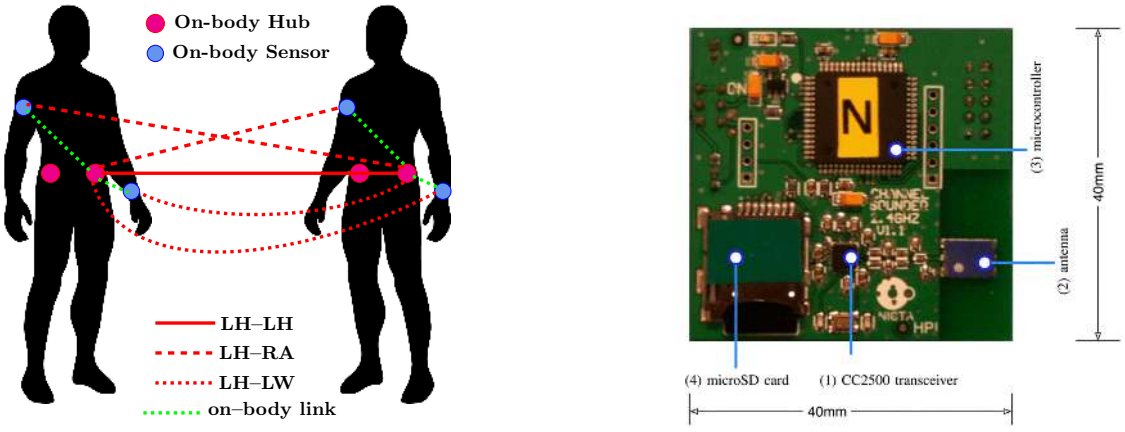

(a) (b)

Figure 5.1: (a) Different on-body sensor locations and example of body-centric links (on-body, body-to-body) with two co-located BANs; (b) The radio-frequency testbed with major components highlighted. Battery (disconnected) is on reverse side

5.2.3 Dataset 3 (10 coexisting BANs)

In this dataset, each BAN/subject is wearing three on-body sensors: one transceiver on the Left–Hip (LH) and two receivers on the Left–Wrist (LW) and Right–upper–Arm (RA), respectively. The result for a specific body-to-body (B2B) channel is averaged over (10×9) links. The sampling rate for each channel in this dataset is 20 Hz.

5.2.4 Dataset 4 (20 coexisting BANs)

Here, each BAN wore one transmitter/on-body sensor on Right–Hip (RH). The sampling rate for each channel in this dataset is 10 Hz. Although, there were 20 coexisting BANs, all the B2B links were not used to estimate the results. In fact the result is averaged over around 160 links for the body-to-body (RH–RH) channel.

5.3 Test of Significance for WSS

To investigate the wide-sense-stationarity (WSS) of the B2B channels, we use the 'frequentist' approach along with the null hypothesis significance testing (NHST)

Table 5.1: The body-to-body channels with different sensor locations. '×' indicates the B2B channels correspond to datasets with different number of coexisting BANs

Dataset No.	coexisting BANs	Sampling Rate (per link)	Body-to-body links with different sensor locations						
			LH–LH	LH–RA	LH–LW	RH–RH	RH–LW	RH–RA	RH–LH
1	8 BANs (3 transmitting)	66.7 Hz				×	×	×	×
2	8 BANs	25 Hz	×	×	×				
3	10 BANs	20 Hz	×	×	×				
4	20 BANs	10 Hz				×			

[249] from different test statistics (i.e., difference between mean, variance, and distribution properties). Wide-sense-stationarity requires that the first and second moments (i.e., mean, variance, auto-covariance) of a time varying stochastic process $X(t)$ do not vary with respect to time t (Definition 5.1). In this chapter, WSS is tested over a wide range of window lengths (L) from 100 ms to 100 s, $L = [100, 200, 300, ..., 100000]$ ms. Here, we follow the process from [99], where the whole channel is divided into m consecutive non-overlapping intervals of length ℓ (where $\ell = L/2$) to perform $(m-1)$ independent pairwise comparisons across two consecutive intervals. Hence, for each window length L, i.e., $(L = 2\ell)$, there will be $(m-1)$ pairwise independent null hypothesis tests. An illustration of the pairwise comparison is provided in Fig. 5.2. We consider a lower bound for the amount of samples in an interval, i.e., 30 samples according to [250] to minimise the probability of Type-I and Type-II errors. We estimate the average probability of stationarity for a window length of L over $(m-1)$ tests with NHST, which provides the percentage of the channel being stationary as a function of L, disregarding the position of L over the channel. We consider:

H_0: *L retains WSS (null hypothesis).*
H_1: *L does not retain WSS (alternative hypothesis).*

Then,

$$p_L = \mathbb{P}\big\{T_L > T_{L_{obs}} \big| H_0\big\}, \tag{5.3}$$

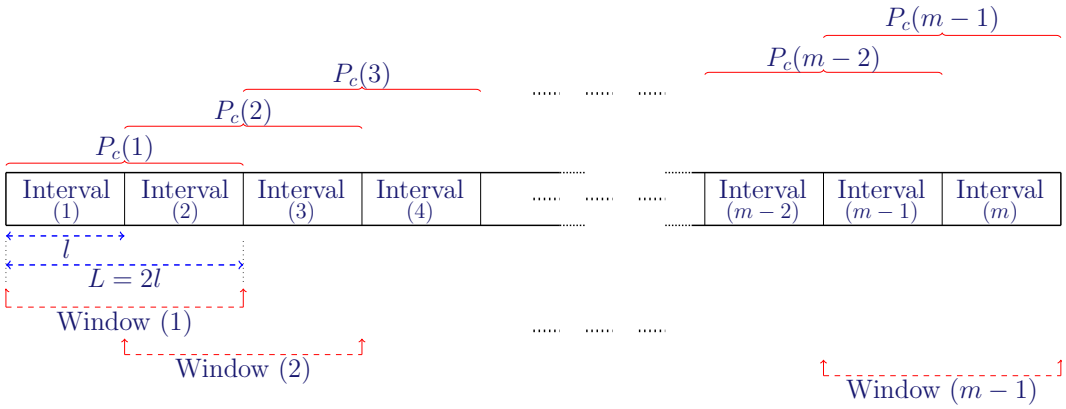

Figure 5.2: $(m-1)$ pairwise comparison (P_c) across two consecutive intervals (ℓ)

where p_L (often called p-value) is a measure of evidence (i.e., strong evidence/weak evidence) against the null hypothesis[2,3]. This implies the observation of a more extreme test statistic (T_L) than the one actually observed $(T_{L_{obs}})$, given that the null hypothesis is true (observing a significant difference due to random sampling error while there was none or negligible difference).

$$\textit{if } p_L \geq \alpha, \quad H_0 \textit{ is not rejected},$$

$$\textit{if } p_L < \alpha, \quad H_0 \textit{ is rejected in favour of } H_1,$$

where α is the significance level/threshold for measuring the significance of the test outcome (based on p_L). For instance, a $p_L \geq 0.05$ indicates weak evidence against the null hypothesis as there is 5% or more risk of concluding that a difference exists when there is no actual difference, therefore the null hypothesis is not rejected. We examine different statistical significance levels (α) with $\alpha \ \epsilon \ \{0.01, 0.05\}$, which corresponds to a confidence level $(c\ell)$ of $c\ell \ \epsilon \ \{0.99, 0.95\}$, as $c\ell = (1-\alpha)$. For example, $\alpha = 0.05$ implies that while there is 5% probability of incorrectly rejecting the null hypothesis, there is 95% probability that the confidence interval contains

[2]A measure of deviation from the actual outcome of the stationarity tests when the null hypothesis is true. A higher value of p_L implies weak evidence against the null hypothesis and a lower value implies strong evidence against the null hypothesis.

[3]The p-value is often interpreted as the probability of incorrectly rejecting the null hypothesis, which is a misconception (as described in [251]) resulted from the mixing of two approaches (i.e., Fishers p-value approach and Neyman-Pearsons alpha level) in the widely used NHST.

the null hypothesis value, i.e., 0 for difference, 1 for ratio [252].

The average probability of stationarity (γ_L) for a window length L over the entire period can be calculated as follows:

$$\gamma_L = \frac{\sum_{i=1}^{m-1} W_i}{m-1}, \qquad W_i = \begin{cases} 1, & \widetilde{p_L}^i \geq \alpha \\ 0, & \widetilde{p_L}^i < \alpha, \end{cases} \tag{5.4}$$

which indicates the percentage of pairwise comparisons (for a window length L) that satisfy the null hypothesis assumption over the whole period (from $m-1$ pairwise comparisons). A given L with a higher value of γ_L, e.g., greater than or equal to 70% can be considered as WSS, as it fails to reject the null hypothesis for the majority of the cases. That also complies with the definition of WSS (second property of Definition 5.1), which is to have the WSS characteristics valid for L over the channel regardless of its position. When calculating the average ${p_L}^i$ for the i^{th} pairwise comparison (i^{th} window) over multiple similar links from different subjects, we choose the median (typical) value ($\widetilde{p_L}^i$) to obtain a more robust estimation, as the median is not affected by outliers.

Here, we apply one-way ANOVA [253], Brown-Forsythe (B–F) [254] and Kolmogorov-Smirnov (K–S) [255] tests to evaluate the mean, variance, and distribution consistency of the body-centric channels. ANOVA relies on the assumption of the normality and homogeneity of the variances of the underlying distribution. In general, the B2B channels are not normally distributed (they typically possess a skewed distribution). Fortunately, ANOVA is fairly robust to moderate deviations from normality [256], specially with a large number of observations. Additionally, it is not very sensitive against the homoscedasticity (homogeneity of the variances) assumption with balanced data (when the sets/intervals are the same size and have similar distribution) [257]. Alternatively, a non-parametric version of the ANOVA (Kruskal-Wallis (K–W) test [258]) can be used, which does not depend on the normality assumption. By comparing the results of the K–W test and ANOVA test, negligible difference was observed. Hence, the classical one-way ANOVA analysis results are provided here.

The B–F test is a modified version of the Levene's test [259] (estimation of the

deviation from the mean), which does not rely on the normality assumption, and therefore provides good robustness against many types of non-normal data while retaining good statistical power [260, 261]. Also, non-parametric tests are more useful when investigating physical phenomena, e.g., radio propagation, as unlike parametric tests they make no assumptions regarding the probability distributions of the sampled process [146]. The advantage of the K–S test (which tests whether the test samples come from the same distribution) is that the distribution of the test statistic does not depend on the underlying CDF (cumulative distribution function) being tested. The p-values for the test statistics are calculated using the asymptotic p-value calculation [262] with an approximation to the true distribution of the observed samples in each interval.

The description and estimation of the test statistics for these statistical hypothesis tests is provided in appendix A. We also investigated the variation in short-time power spectral coefficients [150] (appendix A) of the B2B channels in windowed data segments over time with dataset 3 in [247], where we estimated the variance of the multi-taper power spectral density (PSD) of specific data segments (e.g., 5s, 10s) over the whole channel. We found that for these data segments with most of the B2B channels, the power spectral variation is negligible, which satisfies the WSS assumption.

5.4 Experimental outcome of WSS investigation

In this section, we demonstrate the results obtained from the hypothesis tests with different experimental datasets (described in Section III and Table 5.1). We also provide some justifications of our findings based on the experimental results. The average probability of stationarity (found from ANOVA, B–F, and K–S hypothesis tests) with respect to different window lengths for dataset $1-4$ (Table 5.1) is shown in Figs. 5.3 to 5.6, respectively. The probability of stationarity for a B2B link with a given sensor-location pair is estimated from $(m-1)$ median p-values, calculated from $(m-1)$ pairwise comparisons of multiple similar links between identical source and destination nodes.

5.4.1 Results of Dataset 1

For dataset 1, the minimum window length to be considered for precisely assessing an assumption of WSS is 1 s (interval length of 0.5 s with around 30 samples). According to the hypothesis tests (Fig. 5.3), the Right-hip-to-Left-Hip (RH-LH) links satisfies the WSS assumption (in 70% of cases) for longer window lengths of up to 3 s and 5 s with 95% and 99% confidence levels, respectively. However, the other B2B links, e.g., RH–RA, RH–RH, RH–LW hold a WSS assumption for lower window lengths ranging from 1 s to 3 s (can be more than that with respect to homogeneity of variance (Fig. 5.3b). It can also be seen from Fig. 5.3c that the on-body channels do not satisfy the WSS assumption even for the minimum required window length (1 s), except for the on-body links between Right-Hip-to-Left-Hip.

5.4.2 Results of Dataset 2

For dataset 2, the minimum window length to be considered for precisely assessing an assumption of WSS is 2.4 s (interval length of 1.2 s with around 30 samples). It can be seen from the test results in Fig. 5.4 that the Left-Hip-to-Left-Wrist (LH-LW) links show better probability (around 70%) of satisfying the null hypothesis for a window length of up to 4 s and 8 s with confidence levels of 95% and 99%, correspondingly. However, the other two B2B links hardly satisfy the WSS assumption for the minimum required window length of 2.4 s in most cases. In Fig. 5.4c, the on-body channels also exhibit non-stationary behaviour.

5.4.3 Results of Dataset 3

For dataset 3, the minimum window length to be considered for precisely assessing an assumption of WSS is 3 s (interval length of 1.5 s with around 30 samples). The results of hypothesis tests are shown in Fig. 5.5, where the LH–LH links (hub-to-hub channels) show better probability of stationarity than the other B2B channels. This channel can hold reasonable stationarity (in 70% to 80% of cases) with window lengths of up to 9 s and (more than) 10 s with 95% and 99% confidence levels, respectively. The LH–RA links also satisfy the WSS assumption in 70% of cases over the channel for up to 5 s and 9 s window lengths (with 95% and 99%

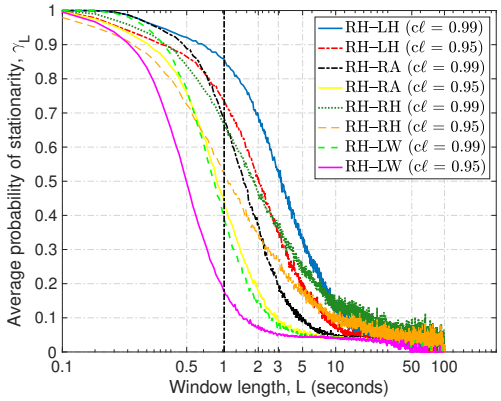

(a) ANOVA

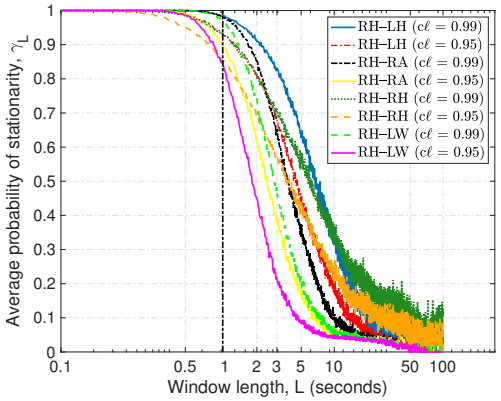

(b) B–F

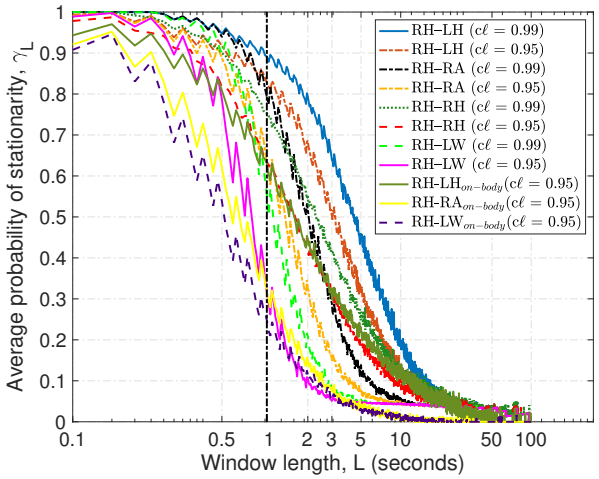

(c) K–S

Figure 5.3: Average probability of stationarity with (a) ANOVA, (b) B–F, and (c) K–S hypothesis tests for different body-to-body links of dataset 1, i.e., R. Hip to L. Hip (RH–LH), R. Hip to R. upper Arm (RH–RA), R. hip to R. hip (RH–RH), R. Hip to L. Wrist (RH–LW). The results for each link are averaged over (3×7) links except RH–RH link (averaged over (3×7) links). The minimum required window length to precisely investigate WSS is 1 s (indicated by black dotted vertical line).

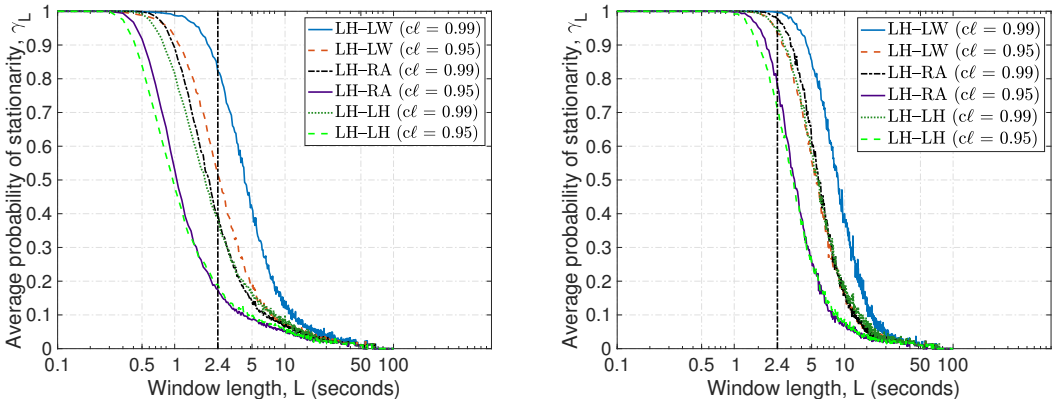

(a) ANOVA (b) B–F

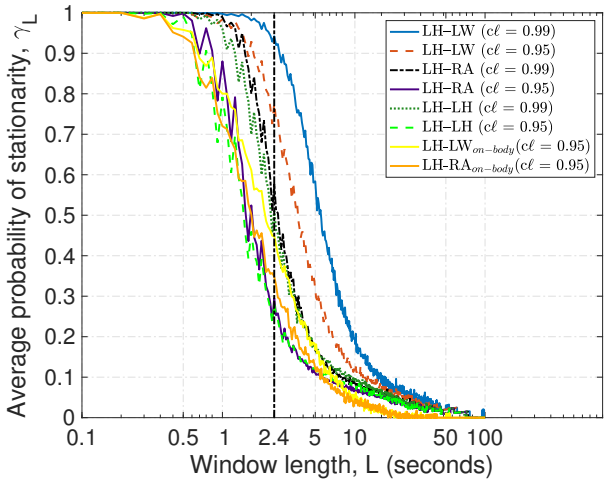

(c) K–S

Figure 5.4: Average probability of stationarity with (a) ANOVA, (b) B–F, and (c) K–S hypothesis tests for different body-to-body links of dataset 2, i.e., L. Hip to L. Wrist (LH–LW), L. Hip to R. upper Arm (LH–RA), L. hip to L. hip (LH–LH). The results for each link are averaged over (8×7) links from 8 subjects. The minimum required window length to precisely investigate WSS is 2.4 s (indicated by black dotted vertical line).

confidence levels, respectively). With 95% confidence level, the on-body channels show non-stationary characteristics in this scenario (Fig. 5.5c).

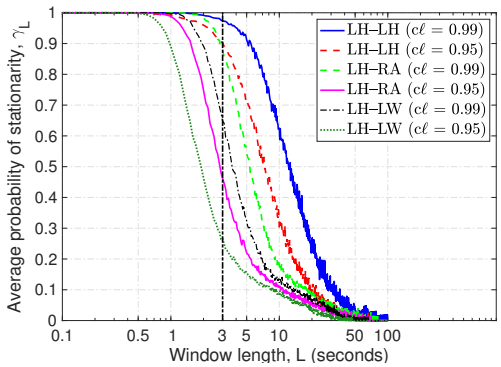

(a) ANOVA

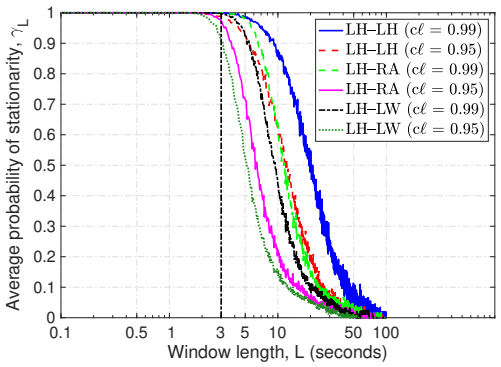

(b) B–F

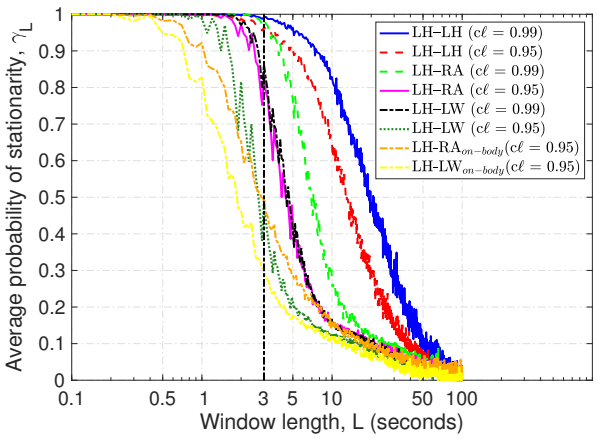

(c) K–S

Figure 5.5: Average probability of stationarity with (a) ANOVA, (b) B–F, and (c) K–S hypothesis tests for different body-to-body links of dataset 3, i.e., L. hip to L. hip (LH–LH), L. Hip to R. upper Arm (LH–RA), L. Hip to L. Wrist (LH–LW). The results for each link are averaged over (10×9) links from 10 subjects. The minimum required window length to precisely investigate WSS is 3 s (indicated by black dotted vertical line).

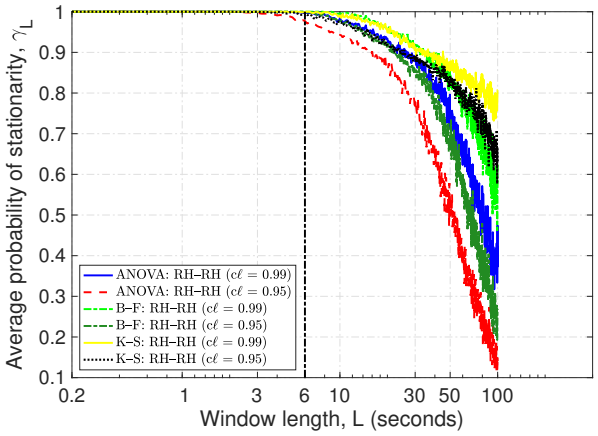

Figure 5.6: Average probability of stationarity with different hypothesis tests, i.e., ANOVA, B–F, K–S for body-to-body links of dataset 4, i.e., Right-Hip-to-Right-Hip (RH–RH). The results for each link are averaged over 160 links from 20 subjects. The minimum required window length to precisely investigate WSS is 6 s (indicated by black dotted vertical line).

5.4.4 Results of Dataset 4

For dataset 4, the minimum window length to be considered for precisely assessing an assumption of WSS is 6 s (interval length of 3 s with around 30 samples). From Fig. 5.6, it can be seen that the body-to-body links (RH–RH) show acceptable probability (70% to 80%) of being stationary with different hypothesis tests over very large window lengths ranging from 35 s to 85 s (more than 400 samples), with 95% confidence level.

The acceptable amount of WSS duration from different stationarity tests for various sensor location pairs (with different datasets) are presented in Table 5.2. We have also shown the test results for best-case and worst-case stationarity with single B2B links, for different channels in dataset 3 with K–S and B–F hypothesis tests in Fig. 5.7. It can be seen that the best-case LH–LH and LH–RA links are showing higher amount of stationarity, e.g., around 80% probability of satisfying the null hypothesis assumption for a window length of 50 s (with K–S test). And, the best-case LH–LW link is showing better stationarity than the averaged outcome (Fig. 5). On the other hand, in the worst-case scenario, the B2B links are not satisfying the null hypothesis for the minimum required window length with K–S test and

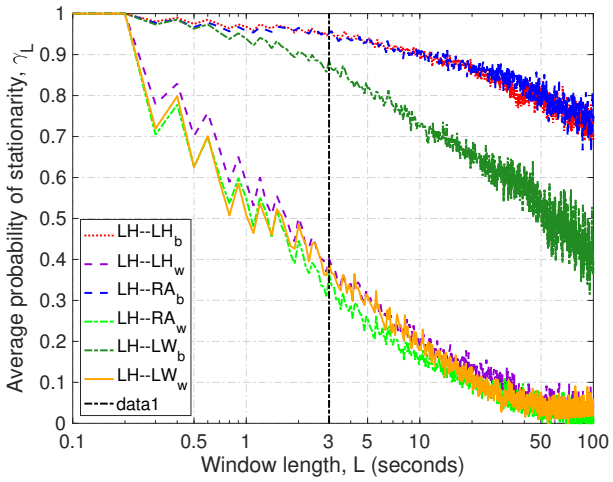

(a) K–S

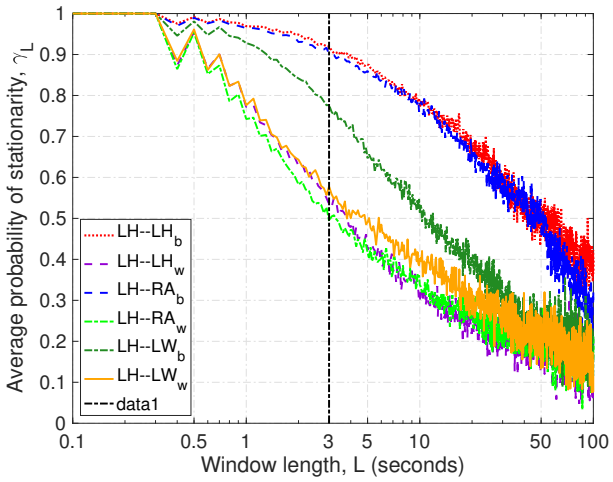

(b) B–F

Figure 5.7: (a) K–S and (b) B–F hypothesis test results for the probability of stationarity (with $c\ell = 0.95$) across different body-to-body links, i.e., left-hip-to-left-hip (LH-LH), left-hip-to-right-upper-arm (LH-RA), left-hip-to-left-wrist (LH-LW). Subscript 'b' and 'w' imply the best and worst case, respectively.

are hardly satisfying the null hypothesis (with around 50% probability) with B–F test. It can also be seen from Fig. 5.7 that in the case of longer window lengths the B2B channels have lower probability of satisfying the B–F test (homogeneity of variance) than the K–S test (consistency of distribution).

Table 5.2: The WSS duration (in second) with 70% probability of stationarity for various sensor location pairs of B2B links with different stationarity tests and confidence levels (i.e., 95%, 99%); 'N/A' implies to the case where the B2B channel does not satisfy the WSS assumption for minimum required window length

Dataset No.	Body-to-body Link	with 95% Confidence Level			with 99% Confidence Level		
		ANOVA	B–F	K–S	ANOVA	B–F	K–S
1	RH–LH	1 s	3 s	2 s	2 s	5 s	3 s
	RH–RA	0.5 s	2 s	1 s	1 s	3 s	2 s
	RH–RH	0.5 s	2 s	1 s	1 s	3 s	2 s
	RH–LW	N/A	1 s	0.5 s	0.5 s	2 s	1 s
2	LH–LW	2.4 s	4 s	3 s	3 s	8 s	4 s
	LH–RA	N/A	2.4 s	N/A	N/A	5 s	2.4 s
	LH–LH	N/A	2.4 s	N/A	N/A	5 s	2.4 s
3	LH–LH	5 s	9 s	9 s	9 s	15 s	13 s
	LH–RA	N/A	5 s	4 s	4 s	9 s	6 s
	LH–LW	N/A	4 s	N/A	3 s	7 s	4 s
4	RH–RH	35 s	50 s	85 s	60 s	75 s	> 100 s

Claim 5.1. *Let $\psi[X(a,b)_\sigma]$ be the WSS duration/segment of a body-to-body channel X between on-body sensor locations from a to b with shadowing effect σ. Then*

$$\psi[X(a,b)_\sigma] \;=\; {L_w}^{cl}\;, \qquad \begin{cases} {L_w}^{cl} \,\epsilon\, \mathbb{R} : 0.5s \leq {L_w}^{cl} \leq 9s, & \textit{for } cl = 95\%. \\ {L_w}^{cl} \,\epsilon\, \mathbb{R} : 0.5s \leq {L_w}^{cl} \leq 15s, & \textit{for } cl = 99\%. \end{cases}$$

Proof. The range of the WSS duration for body-to-body channels can be justified by using Chebyshev's interval found from Chebyshev's theorem [263]. According to this theorem, at least 75% of the data must lie within 2 standard deviations from the mean and 89% of the data must lie within 3 standard deviations from the mean, which can be generalised as

$$P\big\{\mathbb{E}(X) - k\sigma \leq X \leq \mathbb{E}(X) + k\sigma\big\} \geq \big(1 - \frac{1}{k^2}\big), \quad k > 1,$$

where X is the set of observations. We apply Chebyshev's theorem over all the WSS duration (based on different stationarity tests) for various B2B channels (listed in Table 5.2). We exclude the values found from dataset 4 where the WSS durations

are exceptionally high, which is assumed to be the consequence of temporal aliasing due to lower sampling rate for a bigger number of co-located BANs (20 subjects), wearing only a single transmitter.

We find that for 95% confidence level, 90% of the WSS duration fall between Chebyshev's interval of $[0\ s, 8\ s]$ (with ± 2 standard deviations from the mean, i.e., 3 s with 95% confidence level) and 100% values fall between Chebyshev's interval of $[0\ s, 10\ s]$ (with ± 3 standard deviations from the mean). Also, for 99% confidence level, 92% of the values fall between Chebyshev's interval of $[0\ s, 12\ s]$ (with ± 2 standard deviations from the mean, e.g., 5 s with 99% confidence level) and 100% of values fall between Chebyshev's interval of $[0\ s, 26\ s]$ (with ± 3 standard deviations from the mean). By considering the lower and upper limits of the WSS duration from Table 5.2, the WSS duration of B2B channels ranges from 0.5 s to 9 s with 95% confidence level, which can go up to 15 s with 99% confidence level. □

Remark 5.1. *To obtain a typical measure of the WSS duration, we can approximate the results from dataset* 2 *and* 3 *where the people/BANs have similar sensor location set-ups. From the more general K–S hypothesis test (Appendix A), the approximate amount for the WSS duration is around* 5 *s with* 95% *or* 99% *confidence level. Also, from B–F hypothesis test which is another powerful non-parametric test that calculates the F statistic resulting from an one-way ANOVA on the absolute deviations from the median (Appendix A), the approximate WSS duration are* 5 *s (with* 95% *confidence level) and* 8 *s (with* 99% *confidence level).*

Claim 5.2. *$\psi[X(a,b)_\sigma]$ depends on (a,b) and σ, where (a,b) is a given sensor-location pair and σ is the shadowing effect from the surrounding body-movements and body-parts for a given amount of co-located BANs, and the particular indoor/outdoor environment.*

Proof. It is observable from the above results and the summary in Table 5.2 that the WSS duration (Definition 5.3) is not similar for B2B channels between different sensor location pairs in a given scenario or environment. Furthermore, it is not likely that the B2B channels between the same sensor location pairs in different scenarios/environments will satisfy the WSS assumption for a similar time period.

For instance, the LH–LH link in dataset 3 (Fig. 5.5c) shows 90% probability of stationarity for a window length of 5 s, whereas the LH–LW link (Fig. 5.5c) depicts

non-stationary behaviour for the same window length with only 20% chance of satisfying the WSS assumption. Furthermore, the maximum amount of WSS period varies for different B2B channels with the same dataset (Table 5.2). Therefore, the WSS duration varies for B2B channels between different sensor location pairs depending on the shadowing characteristics (shown in Table 5.4 in Section VII).

Additionally, the LH–LH link is considered to be the most stationary in the dataset with 10 BANs (dataset 3, Fig. 5.5) in a pub environment, whereas the same link is the least stationary (hardly satisfies the WSS assumption with minimum required window length) in the dataset with 8 BANs (dataset 2, Fig. 5.4) in a cafe environment. On the other hand, the left-hip-to-left-wrist (LH–LW) link is the least stationary in dataset 3, but the most stationary in dataset 2. Hence, it can be inferred that the similar $\psi[X(a,b)_\sigma]$ will not be held for channels between the same sensor locations, e.g., (a,b) for all σ, and $\psi[X(a,b)_\sigma]$ will vary depending on the sensor-location pair (a,b) and the corresponding σ of the channel. □

Remark 5.2. *As a consequence, to make the most out of the WSS assumption of B2B channels, it is recommended that the wide-sense-stationarity should be tested for B2B channels before applying that WSS amount/segment for modelling or forecasting the channel behaviour, as the WSS assumption and WSS duration can vary for different B2B channels (with different sensor location pairs and shadowing effect caused from different surroundings).*

Observation 5.1. *The probability of satisfying the WSS assumption for body-centric channels gradually decreases with increasing window length.*

Discussion. It can be seen from the results of the stationarity tests that the probability of stationarity reduces significantly (becomes non-stationary) with larger window lengths. The body-centric channels used in this chapter are collected from a measurement of around one hour (although the results are averaged over many channels between similar sensor locations of the coexisting BANs), which leads to an open question – if the decrease in stationarity can be an artefact of larger windows (hence a lower number of windows) and sampling rate. However, the results in this chapter do not truly depend on the number of windows used for the stationarity tests. For instance, in dataset $1-3$, a similar number of windows are tested for window lengths of 9.5 s, 10 s, and 10.5 s, respectively. It can also be seen from

the results of the stationarity tests, e.g., K–S hypothesis test that the channels in dataset 1 and 2 have very lower probability of stationarity for the given window lengths, whereas some of the channels in dataset 3 have higher probability of stationarity for these specific window lengths. It is possible that the sensor locations and shadowing effects from the co-located people and environment (as mentioned above) contribute more to the varying probability of stationarity than any other factors. Also, as discussed later (observations 5.2 and 5.3) in the following section, the auto-correlation between samples of the body-centric channels analysed here, does not significantly affect whether those channels are stationary. □

5.5 Long-Range Dependence or 'Long-memory'

Long-range dependence (LRD) or Long-memory is a very important characteristic for effective modelling and characterisation of the wireless channel behaviour in predictive analysis. It is the level of statistical dependence between two points in a time series. The 'memory' refers to how profoundly the past can impact the future or, in other words, how useful is the past data to predict the future consequences. If a channel possesses long-range-dependence, more realisations of past channels have to be used to predict future channel instants with greater accuracy. We investigate the LRD characteristics of body-to-body and on-body channels from different datasets based on two different factors: the decaying pattern of the auto-correlation function (ACF) and the Hurst exponent. We discuss the results from dataset 3 in the following subsections (all the other datasets produced similar outcome).

5.5.1 Decaying pattern of auto-correlation function

A rough analysis of the dependence is to compare the decaying pattern of the auto-correlation function (ACF) of the channel with an exponential decay. For a short-memory or memoryless process, the dependence between two points in a time series decreases rapidly with an increase in time difference, hence the ACF has an exponential decay (faster decay) or goes down to 0 after a certain time lag. On the other hand, if the channel possesses long-memory, the ACF decays more slowly

(power-like decay) than an exponential decay.

We analyse the average ACF of different on-body/B2B channels where we fit the single term exponential and power series models (EQs. (5.5) and (5.6), respectively) to the ACF decay, which uses the trust-region algorithm with a non-linear least-squares method.

$$f(x) = a \times \exp^{bx}, \tag{5.5}$$

$$f(x) = a \times x^{b}, \tag{5.6}$$

where a and b are the coefficients with 95% confidence bounds.

The power and exponential fit to the measured averaged ACF for different B2B and on-body channels from Dataset 3 (with 10 co-located BANs) are shown in Figs. 5.8 and 5.9, respectively. To determine the optimum result, the models are fitted to the ACF decay to a moderate correlation coefficient of 0.5 (below which the auto-correlation between samples is generally considered to be weak). We measure the goodness-of-fit with the sum of squared errors of prediction (SSE) statistic [264] (EQ. (5.7)), which is the sum of the squares of deviations predicted from actual empirical values of data. It is a measure of the discrepancy between the data and an estimation model. A value closer to 0 indicates that the model has a smaller random error component, and that the fit will be more useful for prediction.

$$SSE = \sum_{i=1}^{n} (y_i - y_i')^2, \tag{5.7}$$

where n is the number of observations, y_i is the i^{th} value of the variable to be predicted and y_i' is the predicted value of y_i.

It can be seen from Figs. 5.8 and 5.9 that both the on-body and B2B channels show a power-like decay for the auto-correlation function (SSE closer to 0), which implies that these channels can possess long-range dependence. The values of the coefficients and SSE for different fits with different B2B/on-body channels are listed in Table 5.3. We also found power-like decay for ACFs in both best-case and worst-case links (in terms of coherence time).

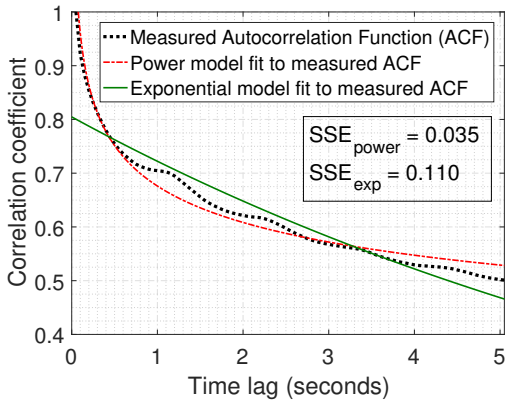

(a) ACF (LH–LH)

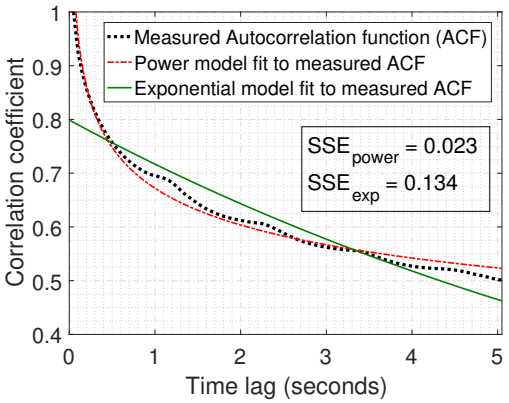

(b) ACF (LH–RA)

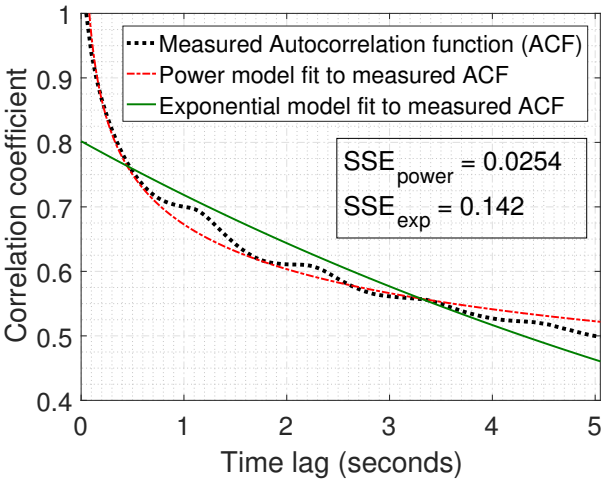

(c) ACF (LH–LW)

Figure 5.8: Power fit and exponential fit to averaged auto-correlation decay of different body-to-body channels, i.e., LH–LH, LH–RA, LH–LW from Dataset 3 (10 co-located BANs); SSE implies to the sum squared error of the fits. A SSE value closer to 0 indicates that the model has a smaller random error component, and that the fit will be more useful for prediction.

Table 5.3: Fitting parameters with SSE values for power and exponential fits to the ACF decay of different B2B and on-body channels with 10 co-located BANs

on-body/B2B channels	Power Model Fit			Exponential Model Fit		
	a	b	SSE	a	b	SSE
LH–LH (B2B)	1.067	-0.152	0.035	0.805	-0.00541	0.11
LH–RA (B2B)	1.069	-0.155	0.023	0.799	-0.00541	0.134
LH–LW (B2B)	1.077	-0.157	0.0254	0.802	-0.00549	0.142
LH–RA (on-body)	1.035	-0.165	0.0103	0.814	-0.0091	0.085
LH–LW (on-body)	1.125	-0.137	0.124	0.789	-0.00217	0.198

5.5.2 Hurst exponent

A more systematic approach to analyse the dependence of the channels is estimating the Hurst exponent, which is also referred to as the index of dependence and indicates the extent or strength of the auto-correlation between the samples. The Hurst exponent is a useful statistical method to analyse channel characteristics without making assumptions about stationarity (opposed to the stationarity assumption made in the null hypothesis analysis). The value of the Hurst exponent (h_E) ranges between 0 and 1. If $h_E = 0.5$, then there is no correlation/dependence between the points of the channel. While if ($0.5 < h_E < 1$), then the channel characteristics are persistent, e.g., an increment/decrement is followed by another increment/decrement and that characteristic tends to last for a long time into the future. And, if ($0 < h_E < 0.5$), then the channel characteristics are anti-persistent, e.g., an increment is followed by a decrement in the future and vice-versa – resulting in significant fluctuation. In summary, as h_E shifts away from 0.5 (in either direction), it indicates stronger correlation between the samples along with the persistency of the correlation, e.g., persistent/anti-persistent, hence the channel becomes more predictable.

For measuring the Hurst exponent, we follow the rescaled range (R/S) analysis method described in [248,265]. First, we calculate the dependence of the rescaled range on the time span τ over the whole channel N, where $\tau \epsilon [N, N/2, N/4, ..., N/2^k]$; k is a positive value. We then calculate the averaged rescaled range $R(\tau)/S(\tau)$ for each τ from all the partial time span with length τ_n over the whole channel. The estimation method is given below:

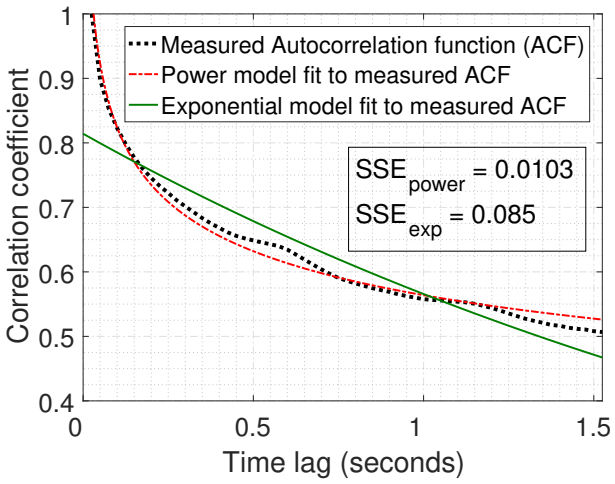

(a) ACF (LH–$\text{RA}_{\text{on-body}}$)

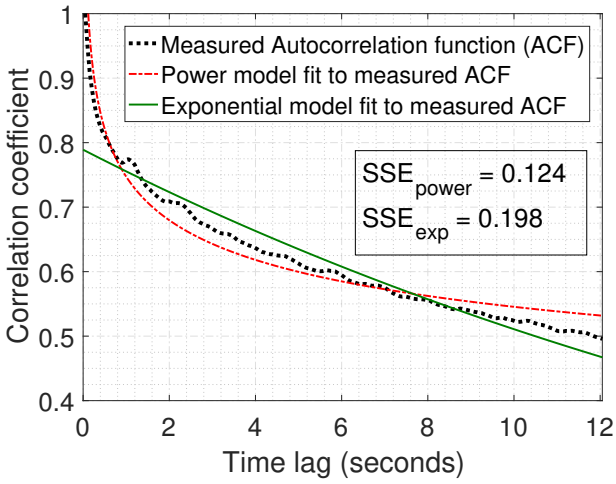

(b) ACF (LH–$\text{LW}_{\text{on-body}}$)

Figure 5.9: Power fit and exponential fit to averaged auto-correlation decay of different on-body channels, i.e., LH–RA, LH–LW from Dataset 3 (10 co-located BANs); SSE is the sum squared error of the fits

Let $X(\tau)$ be a part of the signal with a specific time span τ. The rescaled range of each part as $X(\tau)$ with length τ_n over the whole channel is calculated as follows,

$$\frac{R(\tau)}{S(\tau)} = \frac{max[Z(\tau)] - min[Z(\tau)]}{\sqrt{\frac{1}{\tau_n}\sum_{i=1}^{\tau_n}\left(X_i(\tau) - X_m(\tau)\right)^2}}, \tag{5.8}$$

where $S(\tau)$ is the standard deviation and $R(\tau)$ is the range estimated from the bounds of the cumulative deviate series $Z(\tau)$, which is calculated as follows,

$$Z_t(\tau) = \sum_{i=1}^{t} Y_i(\tau), \quad t = 1, 2, ..., \tau_n, \tag{5.9}$$

where

$$Y(\tau) = X_j(\tau) - X_m(\tau), \quad j = 1, 2, ..., \tau_n, \tag{5.10}$$

is the mean-adjusted series, and

$$X_m(\tau) = \frac{1}{\tau_n} \sum_{i=1}^{\tau_n} X_i(\tau), \tag{5.11}$$

is the mean of $X(\tau)$.

The Hurst exponent H is estimated by fitting the power law $E[R(\tau)/S(\tau)] = \tau_n^H$ to the data, which can be found from the slope of a log-log plot of the R/S statistics (by plotting $\log[R(\tau)/S(\tau)]$ as a function of $\log\tau$).

We average the $E[R(\tau)/S(\tau)]$ value from different groups of similar B2B/on-body links and measure the approximate Hurst exponent for specific type of B2B/on-body links. The results from dataset 3 are shown in Fig. 5.10, where all of the links are demonstrating a higher value (around 0.9) of Hurst index which is indicative of having long-range dependence. Also, we estimate the Hurst exponent for some best-case and worst-case links (in terms of coherence time) where we found that even in worst-case (very small coherence time), the B2B channels have a Hurst exponent of around 0.75 (> 0.5), which can go up to 1 for best-case link.

Claim 5.3. *The body-centric channels can retain long-memory or long-range dependence.*

Proof. It is shown in the above results (Figs. 5.8 and 5.9) that both the body-to-body and on-body channels demonstrate a hyperbolic/power-like decay (rather than an exponential decay) for the auto-correlation functions. One of the major attributes of the power-law is its scale invariance. If we scale the argument x in

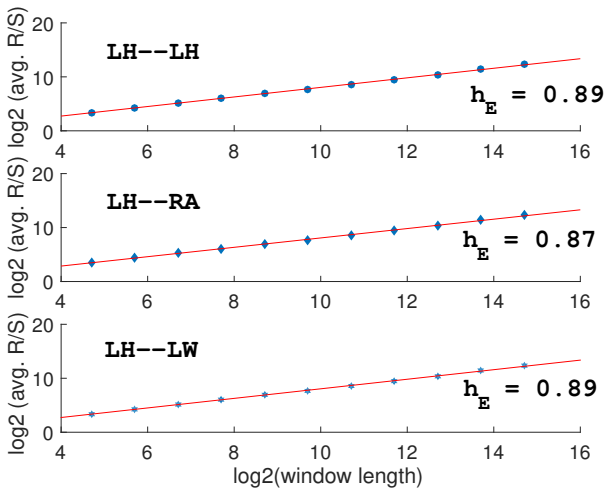

(a) Hurst Exponent (B2B)

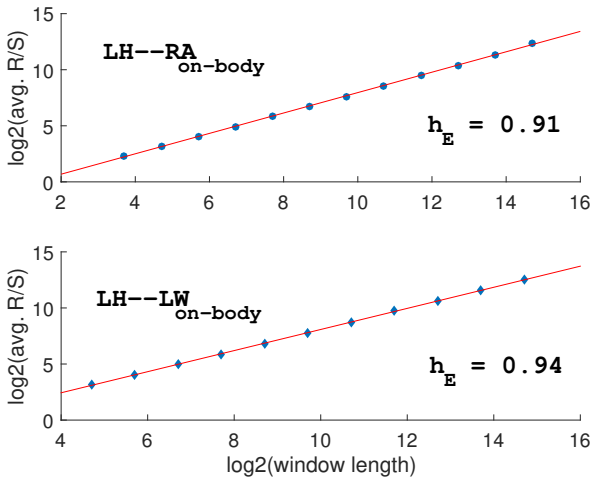

(b) Hurst Exponent (on-body)

Figure 5.10: Hurst regression from averaged R/S values for different B2B and on-body links, i.e., LH–LH, LH–RA, LH–LW from Dataset 3 (10 co-located BANs). Hurst exponent (h_E) is calculated from the slopes of the red lines. The higher value (around 0.9) of h_E is indicative of having long-range dependence.

EQ. (5.6) by a constant factor C, such as

$$f(Cx) = a(Cx)^b = C^b a x^b = C^b f(x) \propto f(x),$$

then it produces a simple multiplication or proportional scaling of the function

itself. That is, all $f(x)$ with a scaling exponent b are homogeneous of degree b, since each is generally a scaled version of the others. On the other hand, exponential decays are memoryless or dominate quick variation (proved in [266]).

Hence, slower (power-like) decay (or the scale homogeneity) of the ACFs is indicative of statistical dependence between the samples of the body-centric channels. Another major characteristic of LRD processes is that they have a Hurst exponent greater than 0.5, which is also the case for both of those channels – Hurst exponent is around 0.9 (Fig. 5.10). From these results it can be inferred that body-centric channels (B2B/on-body) incorporate long-memory or long-range dependence. □

Claim 5.4. *The wide-sense-stationarity and long-range dependence of the body-centric channels are not correlated.*

Proof. From Proposition 5.3, all types of body-centric channels (on-body/B2B) demonstrate long-range dependence. On the other hand, from the experimental results of Section V, it can be seen that B2B channels are more stationary than on-body channels (typically, on-body channels depict non-stationary behaviour [99]). Hence, it can directly be inferred that there is no mutual connection between stationarity and long-range dependence properties. Both stationary and non-stationary body-centric channels can have long memory or long-range dependence. This is further discussed in the following observation. □

Observation 5.2. *For a body-centric channel, the variation in correlation coefficient $r(\omega)$ of a time lag ω $[\omega \geq 0]$ does not significantly impact the stationarity characteristics of ω.*

Discussion. It can be seen from Figs. 5.5c and 5.8 (with Dataset 3) that even with a similar amount of auto-correlation, e.g., $r \geq 0.5$ for $\omega \leq 5$ s (Fig. 5.8), different B2B links, i.e., LH–LH, LH–RA, LH–LW can hold different amounts of stationarity (Fig. 5.5c). For instance, with the K–S hypothesis test (Fig. 5.5c) at 95% confidence level, LH–LH link exhibits more stationarity than the other two links (and can hold reasonable stationarity for around 10 s) whereas the LH–LW link depicts non-stationary behaviour. This can also be deduced for on-body channels (in Fig. 5.9), where they have very different amount of auto-correlation but both of them are considered as non-stationary (Fig. 5.5c).

From the above discussion, we can see that there is no relation between long-range dependence (which indicates significant auto-correlation between samples) and wide-sense-stationarity of the body-centric channels. □

Observation 5.3. *There is no effect of reduced auto-correlation on the stationarity outcome of body-centric channels.*

Discussion. The authors in [99] investigated the effects of reduced auto-correlation on the stationarity (possibility of Type-I Error) of on-body channels by down-sampling the signals. According to their analysis, reduced auto-correlation does not significantly improve the channel stationarity. This is also evident from Fig. 5.9 where the LH–RA (on-body) channel has much lower amount of auto-correlation ($r \geq 0.5$ for $\omega \leq 3$ s) than LH–LW (on-body) channel ($r \geq 0.5$ for $\omega \leq 12$ s), yet the stationarity is not improved accordingly (Fig. 5.5c) and, both of them are considered non-stationary in terms of minimum required amount of samples for the hypothesis tests.

Additionally, if there was a significant effect of reduced auto-correlation on the stationarity outcome of the B2B channels, the probability of stationarity of those links would have improved (even slightly) for the window length of more than 5 s ($r < 0.5$ for $\omega > 5$ s). On the contrary, it can be seen from Fig. 5.5 that the probability of stationarity gradually decreases (goes down to 0 at window length of ≥ 50 s) despite the reduced auto-correlation ($r < 0.5$) on the increased lag or window length. □

Observation 5.4. *$\psi(X_\lambda)$ can be utilised as pivotal points in predictive analysis of stationary LRD process X_λ, where $\psi(X_\lambda)$ is the WSS duration of X_λ.*

Discussion. As in X_λ, the past event can affect the future events, it is important to know how much information is adequate to predict the future. It is practically impossible according to the definition of LRD (Definition 5.2), where the sum of the correlation coefficients $r(\omega)$ does not converge as $\omega \to \infty$ (ACF decays very slowly). Although, LRD implies that the longer the observation, the better the prediction, it is not practically feasible to use indefinitely large observations due to time and resource constraints. Therefore, $\psi(X_\lambda)$ can be utilised to approximate the period over which the channel samples can be used for prediction of X_λ with

greater accuracy, where some past values can be used to predict the future values within $\psi(X_\lambda)$ and progress iteratively with possible overlapping. □

5.6 Modelling Body-to-Body Channels

The body-centric channels are generally dominated by body-shadowing resulted from slowly-varying dynamics of the surrounding body-parts and movements. Specifically, in the case of BAN coexistence (BBNs), the links between different bodies can experience significant shadowing from nearby users' bodies and obstacles, because of the continuous movement (postural/ambulatory) of the BAN entities and the power absorption (of up to 60 dB [96]) by the human body. It is discussed in [82, 227] that for body-centric channels, considering the shadowing as large-scale fading is inappropriate and estimating traditional distance-based path-loss measures in terms of line-of-sight/non-line-of-sight categorisation is misleading. However, small-scale fading occurs in body-centric channels due to the ambulatory and postural movement of the mobile BAN entities in a close proximity, which is also often dominated by shadowing [226]. As a result, many studies of body-centric channels have characterised the fading model of the received signal without decomposing into body-shadowing and small-scale components [82,197,218,226,267–269].

For on-body channels, many narrowband [195, 270] and ultra-wideband [271, 272] characterisation has been performed in literature where the popular fading models include lognormal [82], gamma [82], generalised gamma [82], Ricean [268], Nakagami-M [199], and Weibull [218] distributions. In [273], Cotton *et al.* showed that the $\kappa - \mu$ distribution demonstrates a good fit to the small-scale fading of narrowband B2B channels between two subjects in comparison to other models, e.g., Nakagami-m, lognormal, Rice, and Weibull. And, the authors in [274] argued that the ultra-wideband inter-body shadowing between two subjects can be best described with a lognormal model. In this chapter, we investigate the first-order and second-order statistics, e.g., shadow fading distributions, time-dependence for characterising the narrowband body-to-body channels collected from multiple co-located BANs. Here, we discuss the results from dataset 3 with 10 co-located subjects/BANs.

5.6.1 Fading Characteristics

The B2B channels are generally considered as fading channels due to the continuous movement and power absorption by the body-parts of different entities that significantly affects the propagation channels between T_x and R_x devices. We characterise the shadow fading (slow flat-fading dominated by shadowing from surrounding human body and body-parts) distributions for narrowband body-to-body channels of dataset 3 (with 10 co-located people) between different sensor location pairs, where the channel gains (magnitude values) for each type of channel (between specific sensor-location pairs) is averaged over 90 links with similar sensor-location pairs. As the channels are transmitting in a round-robin, each channel gain sample is averaged from 90 samples transmitted each 50 ms (this period is well-fitted within the coherence time of B2B channels, e.g., around 1 second [225]). The statistical modelling of different B2B channels from dataset 3 are presented in Fig. 5.11, and some of the best fits with maximum likelihood estimate (MLE) parameters [238] for those links are provided in Table 5.4.

It can be seen from Table 5.4 that the shadow fading characteristics of narrowband B2B links in general can be best described by Burr (Burr type XII) and Weibull distributions. The other distributions that are sometimes also applicable for B2B channels are the generalised extreme value (GEV), log-logistic, Rician, lognormal, and gamma. The three-parameter Burr type XII is a generalisation of the log-logistic distribution, hence it is also referred to as generalised log-logistic distribution [275]. The use of the log-logistic is often proposed as an alternative to the lognormal (with heavier tails). Thus, the Burr offers an even more flexible alternative to the lognormal with all of the advantages of the log-logistic (as the log-logistic distribution is a special case of the Burr) [241]. The probability density function (PDF) of the Burr distribution is as follows:

$$f(x \mid \alpha, c, k) = \frac{\alpha c}{k}\Big(\frac{x}{k}\Big)^{\alpha-1}\Big[1+\Big(\frac{x}{k}\Big)^{\alpha}\Big]^{-c-1}, \qquad x > 0, \tag{5.12}$$

where $\alpha(>0)$ is the scale parameter and $c(>0)$ and $k(>0)$ are the shape parameters of the Burr distribution. The density of the distribution is unimodal (having one clear peak) if $c > 1$ and L-shaped if $c \leq 1$. The Weibull distribution is also

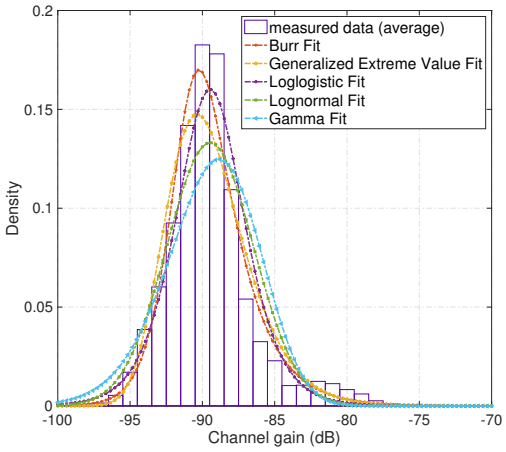

(a) LH–LH

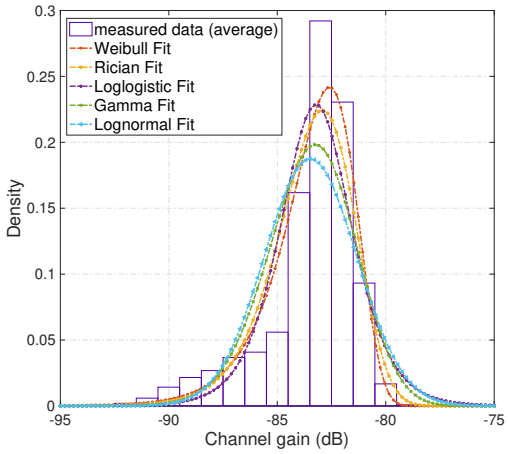

(b) LH–RA

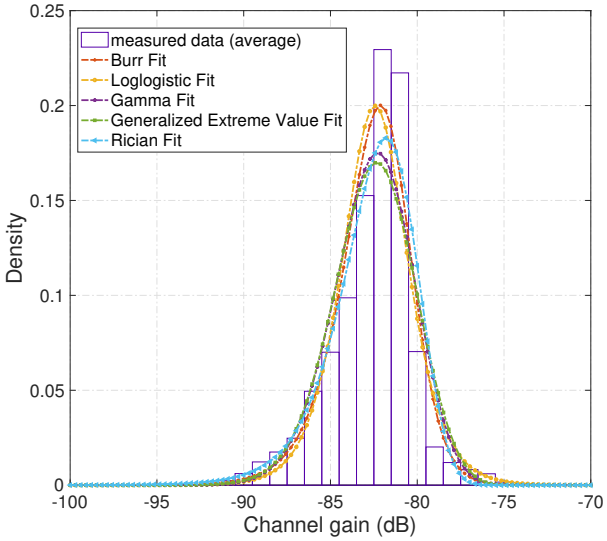

(c) LH–LW

Figure 5.11: Statistical model fits to probability distribution of measured averaged channel gains (amplitudes) for B2B links with different sensor-location pairs — i.e., (a) LH–LH, (b) LH–RA, (c) LH–LW — of dataset 3.

Table 5.4: Log-likelihood values (LLVs) and maximum likelihood estimate (MLE) parameters of different statistical fits to the probability distribution function (PDF) of B2B links with different sensor-location pairs of dataset 3; GEV implies to Generalised Extreme Value

B2B link	Statistical Fit	LLV	MLE Parameters
LH–LH (average of links)	Burr	534202	$\alpha = 0.0000281$, $c = 7.69$, $k = 0.497$
	GEV	533226	$k = 0.173$, $\sigma = 0.00000847$, $\mu = 0.0000293$
	log-logistic	532556	$\mu = -10.3$, $\sigma = 0.180$
	lognormal	529918	$\mu = -10.3$, $\sigma = 0.345$
	gamma	525754	$a = 7.50$, $b = 0.00000481$
LH–LH (best-case link)	log-logistic	597162	$\mu = -11.6$, $\sigma = 0.140$
LH–LH (worst-case link)	Weibull	407367	$\alpha = 0.000190$, $\beta = 1.19$
LH–RA (average of links)	Weibull	519970	$\alpha = 0.0000742$, $\beta = 5.71$
	Rician	518179	$s = 0.00006704$, $\sigma = 0.0000145$
	log-logistic	514610	$\mu = -9.58$, $\sigma = 0.126$
	gamma	514434	$a = 18.8$, $b = 0.00000366$
	lognormal	511745	$\mu = -9.61$, $\sigma = 0.245$
LH–RA (best-case link)	log-logistic	599759	$\mu = -11.6$, $\sigma = 0.134$
LH–RA (worst-case link)	Weibull	401522	$\alpha = 0.000227$, $\beta = 1.35$
LH–LW (average of links)	Burr	503749	$\alpha = 0.0000883$, $c = 5.86$, $k = 2.011$
	log-logistic	502719	$\mu = -9.49$, $\sigma = 0.144$
	gamma	502190	$a = 14.7$, $b = 0.00000523$
	GEV	501840	$k = -0.125$, $\sigma = 0.0000185$, $\mu = 0.0000685$
	Rician	501671	$s = 0.0000739$, $\sigma = 0.0000202$
LH–LW (best-case link)	log-logistic	586970	$\mu = -11.6$, $\sigma = 0.176$
LH–LW (worst-case link)	Burr	423835	$\alpha = 0.000126$, $c = 1.903$, $k = 1.34$

shown to be the most appropriate distribution for most cases in the pseudo-dynamic situations of body-centric channels [276]. The B2B channels can also be modelled

with the following Weibull probability density function:

$$f(x \mid \alpha, \beta) = \frac{\beta}{\alpha}\Big(\frac{x}{\alpha}\Big)^{\beta-1} \exp\left(-\Big(\frac{x}{\alpha}\Big)^{\beta}\right), \quad x > 0, \tag{5.13}$$

where α and β are the scale and shape parameters, respectively.

Generalised extreme value (GEV) [277] combines three simpler distributions, i.e., type I (Gumbel), type II (Frechet), and type III (Weibull), to allow a range of possible shapes that includes all three distributions. The PDF for GEV is:

$$f(x|k,\mu,\sigma) = \left(\frac{1}{\sigma}\right) \exp\left(-\big(1{+}k\frac{x-\mu}{\sigma}\big)^{-\frac{1}{k}}\right)\left(1{+}k\frac{x-\mu}{\sigma}\right)^{-1-\frac{1}{k}}; \quad \text{for } 1{+}k\frac{x-\mu}{\sigma} > 0, \tag{5.14}$$

where $(k \neq \emptyset)$, μ, and σ are the shape, location, and scale parameter, respectively.

And, the PDF for the log-logistic distribution [278] is:

$$f(x \mid \mu, \sigma) = \frac{1}{x\sigma}\frac{e^{z}}{(1+e^{z})^{2}}; \quad x \geq 0, \mu > 0, \sigma > 0, \tag{5.15}$$

where $z = \frac{\log(x)-\mu}{\sigma}$, and μ and σ are the mean and standard deviation of the logarithmic values, respectively.

We also provide the fading parameters for some best and worst links (in terms of wide-sense-stationarity) of different types of B2B channels in Table 5.4 where we show that in the best-case (with higher stationarity) the B2B links can be characterised with a log-logistic distribution, and in worst-case the best fits are Burr and Weibull distributions.

5.6.2 Time-dependence

We also characterise the coherence time (second-order statistics) of narrowband body-to-body channels between different sensor-location pairs of dataset 3. The median (typical) coherence time for different sensor-location pairs with respect to different correlation coefficients, i.e., $0.7, 0.5$ (of the ACF, calculated by equation 5.16 [279]) are presented in Table 5.5. Also, we provide some best and worst links (in terms of auto-correlation) coherence time for different B2B channels in the same

Table 5.5: Median (med.), best-case, and worst-case coherence time for different B2B channels (LH–LH, LH–RA, LH–LW) with 10 co-located BANs (dataset 3); for correlation coefficient, $r \geq 0.7$ and $r \geq 0.5$.

r	Different B2B channels								
	LH–LH (med.)	LH–LH (best)	LH–LH (worst)	LH–RA (med.)	LH–RA (best)	LH–RA (worst)	LH–LW (med.)	LH–LW (best)	LH–LW (worst)
$r \geq 0.7$	1.1 s	5 s	150 ms	900 ms	23.6 s	50 ms	700 ms	25.5 ms	150 ms
$r \geq 0.5$	5 s	18 s	3.6 s	4.7 s	86 s	150 ms	5 s	110 s	450 ms

table (Table 5.5).

$$r_k = \frac{\frac{1}{T}\sum_{t=1}^{T-k}(y_t - \overline{y})(y_{t+k} - \overline{y})}{c_0}, \tag{5.16}$$

where r_k is the auto-correlation for lag k, and c_0 is the sample variance of the time series.

5.7 Prospective Use-cases

Here, we state some of the possible applications from our experimental investigations of the WSS and LRD characteristics of body-centric channels.

5.7.1 Statistical characterisation

Due to the WSS property, appropriate statistical characterisation, e.g., first-order, second-order statistics of B2B channels can be performed (as provided in the previous section). For instance, the WSS duration of B2B channels have distribution consistency (according to the K–S hypothesis test), which can be investigated for different segments of the channel to get an approximation of the distribution fits and estimated parameters. Besides, the B2B channels can be modelled with predictive analysis based on the distribution properties and the coherence time by utilising long-range dependence characteristics. This is not the case for on-body channels as they exhibit an inconsistent distribution in almost all cases, over short or long time segments. Furthermore, due to the non-stationary behaviour, the second-order statistics will not be consistent over time for on-body channels.

5.7.2 Modelling long-range dependence

As stationary long-range dependent channels are considered to have long-memory, they can not be modelled by well-known stochastic Markov models which considers that the future state only depends on the state of the current sample, hence memoryless. Instead, a semi-Markov approach would be more efficient when modelling stationary long-memory process, e.g., B2B channels, also in some cases of on-body channels [97], as this approach does not follow the memoryless nature of the Markovian model but is Markovian at the specific jumps [280]. A Markov model with memory can also be used (an example prospective work) where the WSS windows can be divided into intervals consisting of multiple samples. The observations from one interval can then be used to estimate the channel condition of the next interval as they are assumed to maintain similar channel characteristics. The same procedure can be applied for following windows with/without overlapping (as according to Definition 5.1, the WSS segment is considered to be valid regardless its position over the channel) and so on. In that way, we hold on to the more recent (important) information and forget the unnecessary information, yet make a more accurate estimation for future samples based on the information from past samples.

In order to model the long-range dependent process (with locally stationary or non-stationarity characteristics), Granger and Joyeux introduced auto-regressive fractionally integrated moving average (ARFIMA) model in [281], which nests an ARMA (auto-regressive moving average) model by fractionally integrating a non-stationary process. In [282], the authors used a piece-wise ARFIMA process for modelling non-stationary channels with long-range dependence. A stochastic model based on WSSUS (wide-sense-stationary uncorrelated scattering) assumption [243] was proposed in [283], where the authors model non-stationary small-scale fading by modelling the change in delay and Doppler frequency of scatterers as a linear function of time.

5.7.3 Predictive control/decision-making

One of the major applications of WSS and LRD properties is in predictive analysis [284]. When a channel has statistical dependence or long-range dependence

between data points, it becomes more predictable as statistical inference can be made more accurately based on several past correlated data. Besides, to avoid complex estimation from a large amount of previous data, the WSS period/duration can be utilised to approximate pivotal points for using recent information to predict the near future channel characteristics with greater accuracy within the WSS duration. Also, learning algorithms can be applied for making intelligent decisions to control and optimise the performance of the body-to-body channels that hold WSS and LRD characteristics.

5.8 Summary

This chapter provided extensive analysis of the wide-sense-stationarity and long-range dependence characteristics of wireless body-centric channels (on-body/body-to-body) at 2.36 GHz narrowband with a number of experimental datasets captured over many hours, consisting of a different number of co-located BANs in different scenarios. We employed null hypothesis significance tests with different test statistics to get an approximation of the WSS duration with an acceptable range for B2B channels from different set-ups. We also investigated the effect of different on-body sensor locations and environments on the WSS properties of body-centric channels. Additionally, we estimated the Hurst parameter and the ACF decay of the body-centric channels to examine the presence of LRD characteristics in these channels.

It has been shown that almost all B2B channels can satisfy a WSS assumption for a certain period of time, ranging from 0.5 s to 15 s, depending on the on-body sensor locations and the shadowing effect caused by movement, body-posture and surroundings. On the other hand, as shown in prior works, most on-body channels do not exhibit WSS characteristics even for the minimum amount of samples required for the tests to be considered as valid. We also found that the ACFs of both on-body and B2B channels decay very slowly (hyperbolic decay) and the estimated Hurst exponent from the channels have higher values (approximately 0.9), which implies that both on-body and B2B channels have long-memory. However, due to its WSS characteristics, B2B channels can be predicted with more accuracy than on-body channels.

It has also been demonstrated that the statistical dependence between the data points of body-centric channels does not affect their WSS characteristics, which is, as evident from the outcomes of WSS tests of on-body and B2B channels, despite the fact that both of those channels has long-range dependence. Furthermore, the length of WSS of B2B channels can be utilised to avoid the complexity of using an unknown amount of information for predictive analysis with long-memory channels. We have also shown that the shadow fading of narrowband B2B channels can be best described by Burr type XII, log-logistic, and Weibull distributions, and the typical coherence time of narrowband B2B channels is around 1 second. We have also addressed how our findings might be applied for future channel modelling and prediction of body-centric channels. Our work can serve as a precise documentation of WSS and LRD characteristics to use in channel characterisation and prediction for real-life, low-power wireless body-centric networks taking small-scale and shadow fading into consideration. In the next chapter, we utilise the WSS and LRD characteristics to formulate a multi-objective MDP, for applying adaptive scheduling to jointly optimise throughput, latency, and energy consumption of body-to-body channels.

5.9 Related Publications

- **Samiya M. Shimly**, David B. Smith, and Samaneh Movassaghi: 'Wide-Sense-Stationarity of Everyday Wireless Channels for Body-to-Body Networks', in *IEEE International Conference on Communications (ICC'*18*)*, May, 2018.

- **Samiya M. Shimly**, David B. Smith, Samaneh Movassaghi, and Leif W. Hanlen: 'An Empirical Study of Stationarity and Long-Range Dependence of Wireless Body-centric Channels', under review, *ACM Transactions on Sensor Networks*, September, 2019.

Chapter 6

Multi-Objective Optimisation for Real-life BBNs

6.1 Introduction

In this chapter, we perform analytics for body-to-body (B2B) communications utilising the predictive characteristics determined in the previous chapter. Wireless body-to-body networks (BBNs) are resource-constrained networks that operate in dynamic environments where global coordination is not possible. Moreover, BBN channels experience interference and shadowing due to human-body movements, e.g., ambulatory and postural movements, obstruction by body-parts. Therefore, these networks need to be self-organised and perform dynamic optimisation for efficient resource utilisation. One of the widely used optimisation tools for such dynamic systems is a Markov decision process (MDP) [160] where different probability-based decisions are made at epochs, often to optimise a specific network objective. But there are situations when multiple, possibly conflicting, objectives need to be optimised for, as in [285, 286]. This is particularly the case for body-centric communications, due to their various resource constraints [2, 287]. In this chapter, we aim to address the following issue:

How to utilise the predictive characteristics of B2B channels for multi-objective optimisation over BBNs?

Therefore, we employ a multi-objective Markov decision process (MOMDP)

[288, 289] for adaptive scheduling to optimise the performance of BBNs in terms of different performance metrics. We also define and analyse a decision period or sojourn time for the Markov decision process used in this work, by utilising the predictive characteristics, i.e., wide-sense-stationarity (WSS) [247] and long-range dependence (LRD) [290] (described in Chapter 5) of B2B channels.

In multi-objective optimisation, the solution is often the most desired trade-off between multiple competing objectives [291]. Here, our goal is to achieve a Pareto optimal trade-off between increased throughput and decreased continuous latency that reduces energy consumption as much as possible. To define the conditions for the Pareto optimal state that will produce the most balanced outcome across all objectives, we examine different combinations of packet success rate and continuous latency with a brute-force approach. The domain used for the exhaustive search consists of a significantly large amount of real-life B2B links with extensive channel measurements. There are 270 links, each for a duration of approximately 45 minutes, containing a total of around 720 million samples (2664800 data points per link), collected from a reasonable number of colocated BANs performing 'everyday' mixed activities (e.g., walking, sitting, standing, turning, talking) in indoor/outdoor environments (e.g., building, office space, street, cafe/pub). Such extensive analysis provides a normalized outcome from many typical BBN scenarios. The same dataset is also used as training data for the offline learning and policy search of the MOMDP. For the adaptive scheduling with MOMDP here, the two most popular medium access techniques for body-centric networks – time division multiple access (TDMA) and carrier sense multiple access with collision avoidance (CSMA/CA) — are combined. As stated in Chapter 4, TDMA has maximum bandwidth utilisation and lower power consumption compared to CSMA/CA [240], whereas CSMA/CA provides higher throughput by continuously sensing the medium as opposed to TDMA with fixed waiting intervals. However, fixed interval TDMA has higher latency for very slowly-varying body-centric channels under severe channel attenuation, which can be reduced in CSMA/CA with an effective carrier sensing mechanism [292].

Therefore, *our aim is to adaptively exploit the advantages of both TDMA and CSMA/CA for jointly optimising the throughput, continuous latency, and energy consumption of B2B communications between any two BANs (direct link) in the*

presence of other coexisting (interfering) BANs, with multi-objective predictive decision-making utilising properties of body-to-body channels. We perform the decision-making employing real-life experimental measurements collected from closely-located mobile people with body-worn sensors. We compare our Pareto optimum outcome (from adaptively selecting between TDMA and CSMA/CA actions with different parameters) with the results of TDMA and CSMA/CA schemes applied separately. From experimental results across additional 168 tested narrowband B2B channels from a similar set-up as the training dataset, we find that

- The Pareto optimum outcome (f^*) can provide up to 3.4 times better throughput than TDMA (with a 10% duty cycle), but also can consume up to 3.2 times more energy (because of the increased active period) than TDMA (as TDMA schemes have fixed duty cycles). Then again, f^* produces an acceptable amount of continuous latency with respect to TDMA — a slightly (around 5%) higher amount of continuous latency than TDMA schemes for smaller intervals and similar amount of continuous latency as TDMA for longer intervals (≥ 4 s).

- CSMA/CA with -70 dBm carrier sense threshold (cs_{th}) consumes around 2.3 times more energy, and has much higher continuous latency, than the Pareto optimum f^*, although it provides almost twice as much throughput than the Pareto optimum (f^*). For instance, CSMA/CA with $cs_{th} = -70$ dBm has a continuous latency of greater than or equal to 250 ms for around 46% of the total time, whereas f^* produces the same amount of latency for less than 30% of the total time.

- The Pareto optimum outcome has the highest packet delivery ratio (PDR $> 80\%$), than all other actions.

- For the body-to-body channels with an increase in period of stationarity of the body-to-body channels, the performance of TDMA schemes degrades while the performance of CSMA/CA schemes improves, along with an improved trade-off between these two schemes for the Pareto optimum.

- It is also observed from the individual outcome of 168 channels tested separately that with the CSMA/CA schemes, the B2B channels are producing

either higher throughput with higher energy consumption, or lower throughput with higher continuous latency. On the other hand, TDMA schemes always provide lower throughput regardless of the amount of continuous latency, with fixed duty cycles. And the Pareto optimal solution provides a balanced trade-off between throughput, continuous latency, and energy consumption.

- The application of least square linear regression and goodness-of-fit sum squared error validate the consistency of the predictive MOMDP model.

6.2 System Model

A Markov decision process, as used here, follows the Markov property where it is assumed that the process is stationary or wide-sense-stationary (WSS), and the future state only depends on the current state and is independent of the past states. Generally, the decision epochs of MDP are discrete time variables, e.g., $1, 2, 3, ...$ with a constant holding/decision period, e.g., typically 1 data point, hence assuming no correlation between data points/samples. However, we have investigated the WSS property of B2B channels in [247] where we found that B2B channels typically hold the WSS characteristics (in around $70\% - 80\%$ of cases) for a certain period (i.e., 5 seconds), which is consistent over the whole time of operation. We also found in [247] that B2B channels are stationary long-memory processes that means, along with WSS, B2B channels can retain long-memory or long-range dependence (LRD) characteristics [290], which indicates significant auto-correlation between samples. Hence, for B2B channels, we formulate a discrete-time MDP with memory as follows:

$$P\{X_{t_{i+1}} = s' \mid X_{t_i} = s\}, \qquad t = [1, 2, ..., m],\ (s, s') \,\epsilon\, \mathbb{S} \tag{6.1}$$

where t is the decision interval that consists of m correlated samples, i is a non-negative integer ($i \,\epsilon\, \mathbb{N}$) that denotes the index of the decision interval, and $\mathbb{S}$ is the set of states. We choose the decision interval t based on the WSS duration of B2B channels. As we have found that the WSS duration remains consistent over time

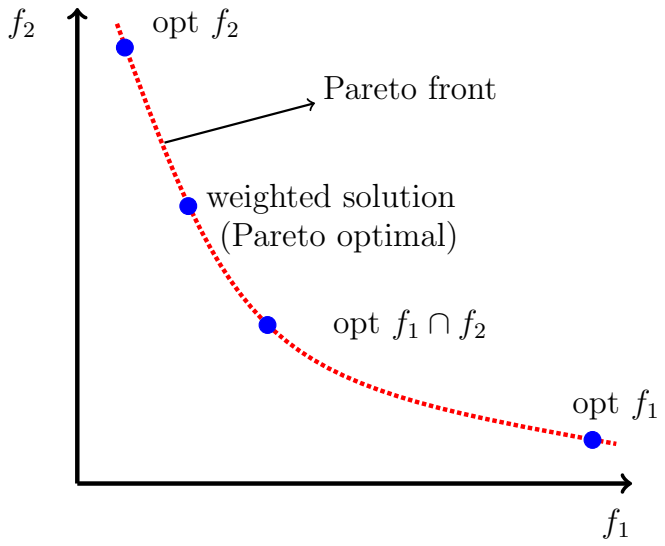

Figure 6.1: Pareto optimality between two objectives in a multi-objective function.

for B2B channels, we use half of the WSS duration as the decision period to satisfy the Markov property with memory, i.e., the future state in the decision period t_{i+1} depends only on the current state in the decision period t_i.

It should be noted that, in semi-Markov decision process (SMDPs) as an extension of MDPs, variable holding periods are permitted where the state conditions are measured over these holding periods [293]. Although, we use holding period or sojourn time between decision epochs, because of the fixed duration of that period here, a simple MDP formulation is more appropriate, where the decision period is considered as a whole entity with correlated samples. And, each entity depends on the past entity (not on the sequence of preceding entities) based on the duration for WSS, hence satisfying the generalised Markov property with memory (6.1). The formulation of the MDP and the experimental scenario are elaborated in the following subsections.

6.2.1 Formulation of the MDP

We formulate the problem of multi-objective optimisation for different performance metrics with adaptive scheduling as a finite state, finite horizon discrete-time Markov decision process (DTMDP) where the time between the decision epochs is

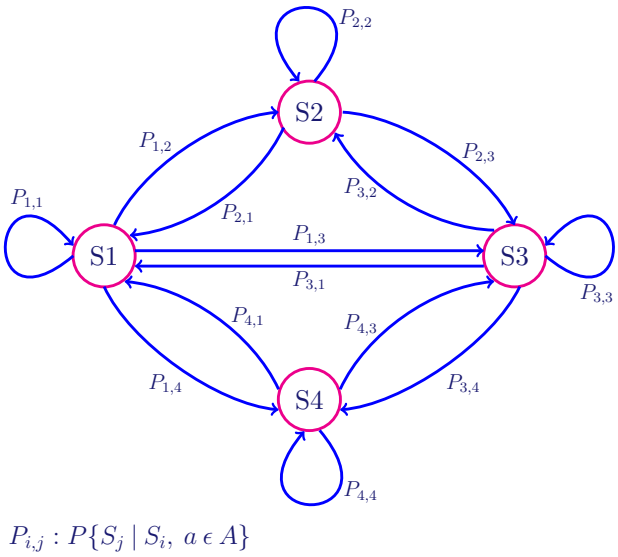

Figure 6.2: MDP transition probabilities from one state to another state with a given action $a \epsilon \mathbb{A}$.

fixed and consists of multiple samples. Technically, an MDP is a 4-tuple stochastic control problem: $M(\mathbb{S}, \mathbb{A}, \mathbb{T}, \mathbb{R})$ where $\mathbb{S}$ is the set of states in the system, $\mathbb{A}$ is the set of actions available, $\mathbb{T}$ is the state transition function defining the probability of going from one state ($s \epsilon \mathbb{S}$) to another state ($s' \epsilon \mathbb{S}$) by choosing action $a \epsilon \mathbb{A}$, and $\mathbb{R}$ is the reward function that is the reward for going to a certain state. The objective of an MDP is to calculate an optimal strategy or policy (π^*) that will maximise the end rewards. We formulate the multi-objective optimisation problem subject to a set of conditions for jointly optimising throughput, continuous latency, and energy consumption of B2B channels as follows:

$$\begin{aligned} & f^* = \mathbb{E}\big\{\omega_r \,|f_r - z_r^*|\big\}, \qquad r = (1,2,3) \\ & \text{subject to } c_p, \quad \{c_p : \ (p_s \geq 60\%, d < 125 \text{ ms}) \mid c_p \,\epsilon\, \mathbb{C}_{\mathbb{P}}\}, \end{aligned} \tag{6.2}$$

where f^* is the Pareto optimal solution that produces a vector for optimising different objectives r (here, the number of objectives is 3), ω is the weight depending on the specific objective, z^* is the solution if each objective is independently optimised, c_p is the condition for the Pareto optimal state, composed of packet success

rate (p_s) and continuous latency (d) of the channel, and $\mathbb{C}_{\mathbb{P}}$ is the set of conditions considered for the Pareto optimal state. The three objectives are:

$r = 1:$ maximise throughput

$r = 2:$ minimise continuous latency

$r = 3:$ minimise energy consumption.

It is important to define the conditions for the Pareto optimal state prior to applying the MDP, as there are multiple objectives that need to be jointly optimised for an acceptable outcome, which is not biased towards any particular objective. As mentioned earlier, the aim is to achieve a suitable trade-off between increased throughput and decreased continuous latency that also minimises the energy consumption, so we focus on the conditions of packet success rate (which indicates throughput) and continuous latency, to define the Pareto optimal state. We use different combinations of packet success rate and continuous latency to define the conditions in $\mathbb{C}_{\mathbb{P}}$, such that

$$\mathbb{C}_{\mathbb{P}} = \begin{cases} p_s \geq x', & x' \,\epsilon\, \{50\%, 60\%, 70\%, 80\%, 90\%\} \\ \quad \wedge & \\ d < y', & y' \,\epsilon\, \{125\text{ ms}, 250\text{ ms}\} \end{cases}$$

The amount of acceptable continuous latency is found from the guideline of the IEEE 802.15.6 BAN standard [29] for medical (less than 125 ms) and non-medical (less than 250 ms) applications[1]. The target is to reach a state that has higher packet success rate and lower continuous latency, with a moderate energy consumption. However, a higher packet success rate will produce higher throughput, which will also increase the active period and processing overhead resulting in increased energy consumption. Also, the decision-making pattern (choice of actions) of the MDP can get biased under certain conditions. Therefore, we choose the condition for the Pareto optimal state based on a brute-force approach[2] where we use all the combinations ($5 \times 2 = 10$ combinations) of the conditions in $\mathbb{C}_{\mathbb{P}}$ individually for the Pareto optimal state, to apply the MOMDP over a significant amount of B2B

[1]The IEEE 802.15.6 BAN standard guideline [29] can generally be applied for BBN, as the nodes/sensors in BBN are placed on different bodies in a close proximity.

[2]The combinations of the limited conditions for the two metrics provide a feasible search space for the brute-force approach.

links that are collected from many typical BBN scenarios. We found that with the given condition, c_p in (6.2), the multi-objective optimisation makes the most balanced use of different actions, as well as providing the highest packet delivery ratio[3] (greater than 80%), along with a suitable trade-off between throughput, continuous latency, and energy consumption. The concept of Pareto optimality is illustrated in Fig. 6.1 with a multi-objective function that has two objectives.

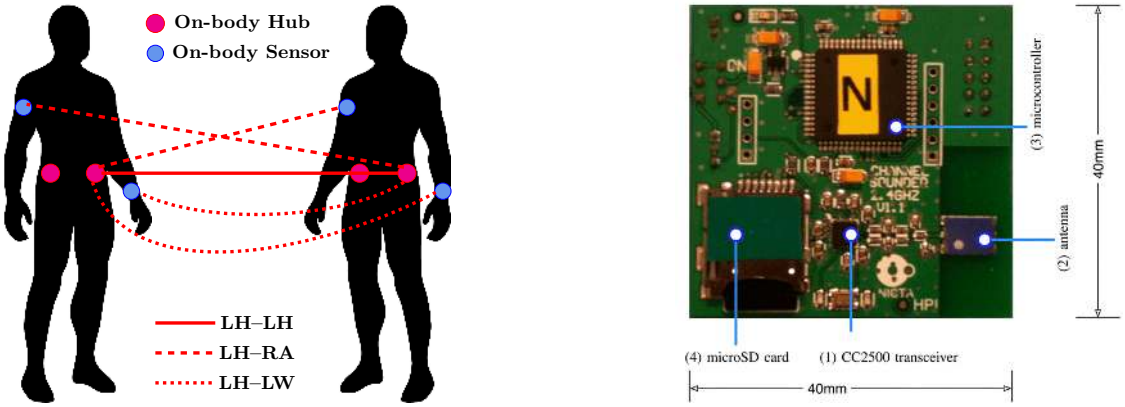

(a) (b)

Figure 6.3: (a) Different on-body sensor locations and example of body-to-body links with two co-located BANs; (b) The radio-frequency testbed with major components highlighted. Battery (disconnected) is on reverse side

States and decision epoch

Here, it is assumed that the state space $\mathbb{S}$ is finite where the state of a channel $\{s(c) \mid s \,\epsilon\, \mathbb{S},\, c \,\epsilon\, \mathbb{C}_{\mathbb{S}}\}$ is defined by a set of conditions $\mathbb{C}_{\mathbb{S}}$, jointly represented by two factors: packet success rate (p_s)

$$p_s : \; (p_s \geq 60\%) \vee (p_s < 60\%)$$

and continuous latency (d)

$$d : \; (d \geq 125 \text{ ms}) \vee (d < 125 \text{ ms})$$

[3]packet delivery ratio is equivalent to the packet success rate

Algorithm 5: Classification of state values in MDP

input : decision interval, t
output: classification of the channel state, $s(p_s, d)$ and state value of the decision interval, $V(S_t)$

if $p_s(t) \geq 60\%$ *&* $d(t) < 125\ ms$ **then**
  $s(p_s, d) \rightarrow 1$;
  [state 1 (Pareto optimal)]
else if $p_s(t) \geq 60\%$ *&* $d(t) \geq 125\ ms$ **then**
  $s(p_s, d) \rightarrow 2$;
  [state 2]
else if $p_s(t) < 60\%$ *&* $d(t) < 125\ ms$ **then**
  $s(p_s, d) \rightarrow 3$;
  [state 3]
else
  $s(p_s, d) \rightarrow 4$;
  [state 4]
end
$V(S_t) \leftarrow V(s(p_s, d))$;

The set of states, $\mathbb{S}$ of the MDP is formulated based on the Pareto optimal condition, where each state is labelled with a value from $\{1, 2, 3, 4\}$, as shown in Algorithm 5. We consider state 1 (in Algorithm 5) as the target state or Pareto optimal state, where the packet delivery ratio is greater than or equal to 60% and continuous latency is less than 125 ms. The objective is to always reach to the target state (i.e., state 1).

We divide the whole channel duration into small fixed-sized intervals/decision periods of 2.5 seconds based on the previously described acceptable WSS segments of around 5 seconds [247]. The state at a given decision interval is estimated from the samples over this 2.5 second period, and in each period there are multiple correlated samples, based on which a decision is made at the decision epoch. Thus, the future state over a decision interval of 2.5 s depends only on the current state over a decision interval of 2.5 s, satisfying the Markov property.

Actions/Decisions

The decision, implying action performed, at each epoch affects the transition probability of going to a good state or target state from the current state. Here, we use different scheduling schemes associated with time division multiple access (TDMA) and carrier sense multiple access with collision avoidance (CSMA/CA) as available actions at each decision epoch. TDMA with different low duty cycles (i.e., 10%, 5%, 1%) is implemented within a simple round-robin fashion among each hub of the BBN and the duty cycles are obtained by lowering the sampling rate of the channels to lessen the active period, hence reducing energy consumption. On the other hand, CSMA/CA is applied with suitable static carrier sense thresholds to increase throughput and decrease continuous latency in comparison to TDMA with its fixed waiting period. We use the maximum-interference-power-carrier-sensing (MPCS) for CSMA/CA proposed in [292] where the transmission is permitted only if the maximum interference power is less than an adaptive carrier sense threshold (cs_{th}) and the adaptive cs_{th} changes periodically after each decision period based on the channel condition of that decision period. Due to the complexity of keeping track of the changing cs_{th} when applying combined TDMA and CSMA/CA, we restrict to a choice of 3 values of cs_{th} (-70 dBm, -75 dBm, -78 dBm) that appear more frequently in the adaptive mechanism of [292]. The finite set of actions $\mathbb{A}$ are listed in Table 6.1.

Table 6.1: Set of Actions ($\mathbb{A}$)

Action	Description
1	TDMA with 10% duty cycle
2	TDMA with 5% duty cycle
3	TDMA with 1% duty cycle
4	CSMA/CA with $cs_{th} = -70$ dBm
5	CSMA/CA with $cs_{th} = -75$ dBm
6	CSMA/CA with $cs_{th} = -78$ dBm

State Transition Function

The state transition function $\mathbb{T}(s, a, s')$ defines the transition probability of going from state $s \,\epsilon\, \mathbb{S}$ to state $s' \,\epsilon\, \mathbb{S}$ with action $a \,\epsilon\, \mathbb{A}$ (shown in Fig. 6.2):

$$\mathbb{T}\big(s, a, s'\big) = P\big\{s'|s, a\big\}, \quad [(s, s') \,\epsilon\, \mathbb{S},\ a \,\epsilon\, \mathbb{A}].$$

Hence, for each action $a \,\epsilon\, \mathbb{A}$, there is an $[M \times M]$ transition probability matrix (here, with $M = 4$ states) such that

$$T^{a}_{s,s'} = P\big\{S_{t_{i+1}} = s' \mid S_{t_i} = s\big\}, \tag{6.3}$$

and,

$$\sum_{i=1}^{m} P\big\{s'_i|s, a\big\} = 1, \tag{6.4}$$

where S_t is the estimated state value of decision interval t (with multiple samples). We estimate the state transition function $\mathbb{T}(s, a, s')$: the expected probability of going from state s to state s' with a given action a, by pairwise estimation of continuous decision intervals after applying action a as

$$\frac{\sum\limits_{i=1}^{n-1} \mathbb{E}\{S_{t_{i+1}} = s' \mid S_{t_i} = s,\ a\}}{(n-1)}, \quad [(s, s') \,\epsilon\, \mathbb{S},\ a \,\epsilon\, \mathbb{A}], \tag{6.5}$$

where n is the number of decision intervals over the whole period of which the channel is active. We use 270 body-to-body links from the training set (from 10 closely located BANs) to estimate the transition function for each action.

Reward Function

The reward function $\mathbb{R}(s, a, s')$ evaluates the outcome when action a is chosen at state s:

$$\mathbb{R}\big(s, a, s'\big) = R\big\{s'|s, a\big\}, \quad [(s, s') \,\epsilon\, \mathbb{S},\ a \,\epsilon\, \mathbb{A}].$$

It defines the expected rewards/consequences for being in different states with respect to several conditions (as sown in Algorithm 5). For instance, the reward for

Algorithm 6: Optimal policy

input : transition probability ($\mathbb{T}$), set of states ($\mathbb{S}$), set of actions ($\mathbb{A}$)
output: optimal policy (π^*)

```
1 V(s) ← statevalue(s,T);
2 for all s ϵ 𝕊 do
3 |   for all a ϵ 𝔸 do
4 |   |   p_a ← P{V(s1) | V(s), a};
5 |   end
6 |   π(s) ← a : maximum(p_a);
7 end
8 π* ← π(s) for all s ϵ 𝕊;
```

being in state 1 is increased packet delivery ratio and reduced continuous latency, hence increased throughput. The expected sum of rewards is maximised by choosing an optimal action at each decision epoch. The overall expected reward (Pareto optimum) is then estimated across all decision intervals:

$$R^* = \sum_{i=1}^{n} \mathbb{E}[R_{t_i}] \tag{6.6}$$

Optimal Policy

The optimal policy (π^*) is the solution of an MDP which maps the state action pairs $\pi(s, a)$ and maximises the expected sum of rewards. At each decision epoch, the best action is chosen based on the estimated channel state ($s \,\epsilon\, \mathbb{S}$), which is considered to be the optimal action (π) for that state. We use the transition probability matrix to find the Pareto optimal action for each state — the action which gives the highest probability of going to the Pareto optimal state, i.e., state 1, from the current state, such that

$$\pi(s, a) = \max P\big\{V(s_1) \mid V(s), a\big\}, \quad s \,\epsilon\, \mathbb{S},\ a \,\epsilon\, \mathbb{A}. \tag{6.7}$$

The optimal actions for all the states in $\mathbb{S}$ then construct the optimal policy π^* (Algorithm 6). At each decision epoch, the best action is chosen from different TDMA and CSMA/CA schemes (actions 1 to 6 in $\mathbb{A}$), based on the estimated

Algorithm 7: Applying optimal policy

input : set of states ($\mathbb{S}$), set of actions ($\mathbb{A}$),
optimal policy (π^*)
output: Total expected reward

$t \rightarrow$ decision period/interval (contains multiple samples);
$n \rightarrow$ number of decision intervals;
$i \rightarrow$ index of decision interval;
$V(t_s) \leftarrow$ `statevalue(`s,t_1`)`;
for $i \leftarrow 2$ **to** n **do**
    $\pi \leftarrow$ `FindOptimalAction(`$\pi^*, V(t_s)$`)`;
    $Out_i \leftarrow$ `ApplyAction(`π, t_i`)`;
    $V(t_s) \leftarrow$ `statevalue(`s, Out_i`)`;
end
$Out \rightarrow \mathbb{E}\left[\sum_{i=1}^{n} R\{Out_i\}\big(V(Out_i), A\{t_i\}, V(Out_{i-1})\big)\middle|\pi^*\right]$;

channel state ($s \,\epsilon\, \mathbb{S}$) of the decision interval, which is considered to be the optimal action (π) for the next decision interval. As mentioned earlier, with the condition (c_p) chosen for the Pareto optimal state, the MOMDP makes the best use of different actions (adaptively chooses from both TDMA and CSMA/CA schemes). The optimal policy is used as a look-up table to choose the best action at the decision epochs, iteratively, over the whole channel duration for maximising the expected sum of rewards as:

$$\max_{\pi} \mathbb{E}\left[\sum_{i=1}^{n} R\{t_i\}\big[V(t_i), A\{t_i\}, V(t_{i-1})\big]\middle|\pi^*\right],$$

where t is the decision interval and n is the number of decision intervals over the whole period. The whole process is described with Algorithm 6 and 7. The result of applying the optimal policy is the optimised outcome or reward over the whole channel from adaptively combining different TDMA and CSMA/CA schemes. We use 168 B2B channels as a test set (with 8 closely located BANs) to obtain the average optimal outcome of the MDP.

6.2.2 Experimental Scenario

The open-access datasets [215][4] used (described in Chapter 3 and 5), consist of continuous extensive intra-BAN (on-body) and inter-BAN (body-to-body) channel gain data (estimated from measured RSSI values with 0 dBm transmit power), incorporating varying amount of movements for many tens of hours of measurements, captured from a range of measurement scenarios with various numbers of closely-located mobile people (wearing body-worn sensors/radios). The receive sensitivity is -100 dBm with a noise floor at (~ -101) dBm. The wearable radios (XBee/ZigBee devices) in each dataset were transmitting in a sequential order at 0 dBm power (along with -100 dBm receive sensitivity) with 5 ms separation between each other. Hence, each device is transmitting for 5 ms with a gap of $(n-1) \times 5$ ms where n is the number of transmitting devices. Each sample of the channel measurement was the average received signal strength indicator (RSSI) value over the 5 ms period. In this work, we perform linear interpolation between consecutive samples of the original measured channels, to be considered as channels with continuous samples for applying both TDMA and CSMA/CA schemes over the channels. The datasets employed in this analysis use 2.36 GHz narrowband. We use two different datasets with a similar setup for training and testing the predictive model:

Training dataset

In this dataset, 10 co-located mobile subjects were used with each subject wearing three on-body sensors: one transceiver on the Left–Hip (LH) and two receivers on the Left–Wrist (LW) and Right–upper–Arm (RA), respectively. The different body-to-body channels between these sensor locations are shown in Fig. 6.3a. As there are 10 people and each is transmitting to all others, there are $(10 \times 9) = 90$ links for each type B2B channels between a sensor location pair, i.e., LH–LH, LH–RA, LH–LW, hence a total of 270 B2B links, each for a duration of approximately 45 minutes that are employed for training the predictive model. As mentioned above, here the original measured channels are estimated with linear interpolation over the sampling period (transmission period + waiting period). For instance,

[4]available in http://doi.org/10.4225/08/5947409d34552

with a sampling rate of 20 Hz and 5 ms transmission time, the original channels had 1 sample in each 50 ms period for a given link. With the interpolated samples, we consider a transmission time of 1 ms (including transmission time of data packet $\approx$ 0.6 ms, control packet $\approx$ 0.2 ms and extra bits) for each sample. As a result, instead of 1 sample, there are now 50 samples in each 50 ms period, hence more than 2.5 million ($\sim$ 2664800) samples per link, which gives a total of around 720 million samples over the training dataset. The interpolated channels are reasonably similar as the actual channel measurement of 50 ms falls well within the coherence time of body-to-body channels (around 1 s [292]), which are also in general slow flat-fading channels. When applying TDMA, we then resample the interpolated channels with different sampling rates to achieve the expected duty cycles for TDMA.

Testing dataset

In this dataset, 8 co-located mobile subjects are used with the same set up in the training dataset. With 8 people, there are $(8 \times 7) = 56$ links for each type of B2B channel, i.e., LH–LH, LH–RA, LH–LW, hence a total of 168 B2B links, each for a duration of nearly 42 minutes, over which the predictive model is applied and tested. The original sampling rate and transmission time are 25 Hz and 5 ms, respectively, which results in 1 sample per 40 ms period. Similar as the training channels, the original testing channels are linearly interpolated with a transmission time of 1 ms, hence instead of 1 sample, there will be now 40 samples per 40 ms period, hence around 2.5 million ($\sim$ 2505160) samples per link, resulting in more than 420 million samples over the testing dataset.

6.3 Experimental Outcome and Analysis

In this section, we analyse the outcome of applying the MOMDP over body-to-body channels in terms of different objectives associated with throughput, continuous latency, and the active fraction over the whole period (which gives an estimate of the energy consumption). The results are averaged from a total of 168 experimental channel measurements used for testing the predictive model. In previous work, we performed the analysis of the predictive characteristics (WSS [247] and LRD [290])

Table 6.2: Performance Analysis Parameters

Parameter	**Value**
Carrier Frequency	2.36 GHz
Data rate	486 kbps
Transmission time (T_{trans})	1 ms
Transmit power (p_{tx})	0 dBm
Decision period/interval (t)	2.5 s
WSS duration	5 s
Measurement period (per link) for training data	$\sim$ 45 minutes
Measurement period (per link) for testing data	$\sim$ 42 minutes
Samples (per link) for training data	$\sim$ 2664800
Samples (per link) for testing data	$\sim$ 2505160

of B2B channels with different datasets and different sensor location pairs where we found that these characteristics are variable depending on on-body sensor positions, which also contribute to the shadowing effect across the B2B channels.

Hence, in this work, we also analyse the performance of the MOMDP over B2B channels with specific sensor location pairs, i.e., LH–LH, LH–RA, and LH–LW, where the transition probabilities for each of those pairs are estimated over 90 channels (between the same sensor location pairs) and the results are averaged over 56 channels (also between the same sensor location pairs). We compare the Pareto optimum outcome (f^*) that combines both TDMA and CSMA/CA in terms of the three objectives — maximising throughput, and minimising continuous latency and energy consumption — with the outcomes of different individual actions ($a \epsilon \mathbb{A}$). Additionally, we demonstrate the distribution of the outcome of the adaptive scheduling (combined TDMA and CSMA/CA), compared to individual actions, for all the 168 tested channels plotted individually in a scatter plot. Furthermore, we perform regression fit and sum squared error analysis to evaluate the efficiency of the MDP model for different actions. The experimental results are provided in the following subsections and the parameters used in this analysis are given in Table 6.2.

6.3.1 Throughput and Packet Delivery Ratio

The first of the three objectives of the predictive optimisation performed in this chapter is to optimise throughput. We estimate the throughput (in successful kilobits/second) with the following equation:

$$Throughput = \frac{P_{succ} \times \frac{P_{size}}{1000}}{\Delta}, \tag{6.8}$$

where P_{succ} is the successful data packets or samples, P_{size} is the sample size (in bits), and Δ is the total time (in second). We also estimate the packet delivery ratio (PDR), which is the ratio of the number of successfully delivered packets and the number of transmitted packets. The averaged results from 168 channels (including all the different sensor locations) are shown in Fig. 6.4 (for throughput) and Fig. 6.5 (for PDR). It is shown that the throughput with the Pareto optimal outcome (f^*) is 125 kbps, which is 3.4 times better than the throughput of a TDMA with 10% duty cycle ($a1$: 37 kbps) and 31 times better than a very lower (1%) duty cycle TDMA ($a3$: 4 kbps). CSMA/CA with $cs_{th} = -70$ dBm ($a4$) provides the highest amount of throughput (245 kbps), which is twice as the throughput of f^*, due to the higher active period of CSMA/CA (shown later in this section).

Importantly, it can be seen from Fig. 6.5 that the Pareto optimal solution (f^*) provides the highest packet delivery ratio (PDR), of more than 80%, which is higher than any other individual action ($a \, \epsilon \, \mathbb{A}$). It can also be seen that despite having very low throughput, TDMA schemes ($a1 - a3$) provide better PDR than CSMA/CA schemes ($a3 - a4$). The main reason behind this difference is the lower number of packet transmissions by low duty cycle TDMA, which results in a lower number of packet failures with respect to the number of transmitted packets. On the other hand, because of the higher active period, CSMA/CA transmits more packets, increasing the packet failure rate. Importantly, f^* provides a good balance between TDMA and CSMA/CA schemes by producing an acceptable throughput, as well as providing the highest PDR.

In case of different B2B channels (with different sensor location pairs), it can be seen from Fig. 6.6 that the B2B channel from left-hip-to-left-wrist (LH–LW) provides a better outcome (Fig. 6.6c) than other B2B channels (i.e., LH–LH, LH–

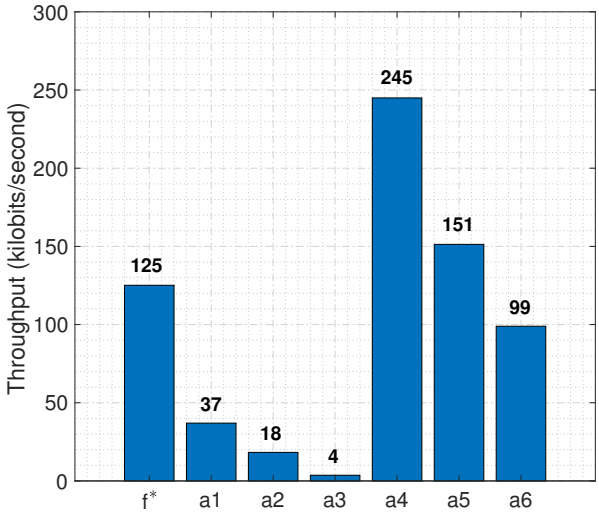

Figure 6.4: Average throughput from 168 tested channels over the whole period for the Pareto optimum (f^*) of the MOMDP and individual actions ($a \, \epsilon \, A$).

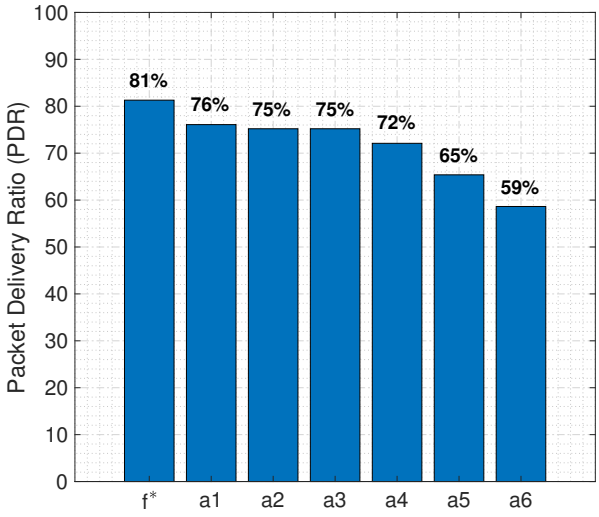

Figure 6.5: Average PDR from 168 tested channels over the whole period for the Pareto optimum (f^*) of the MOMDP and individual actions ($a \, \epsilon \, A$).

RA). This channel demonstrates an optimal throughput of 132 kbps which is 4.4 times better than action 1 ($a1$). The throughput of action 4 ($a4$) in Fig. 6.6 is

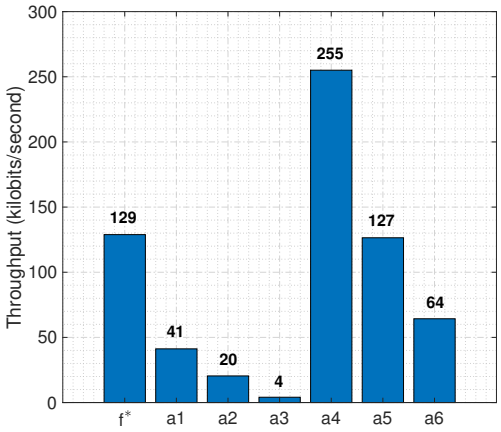

(a) LH–LH

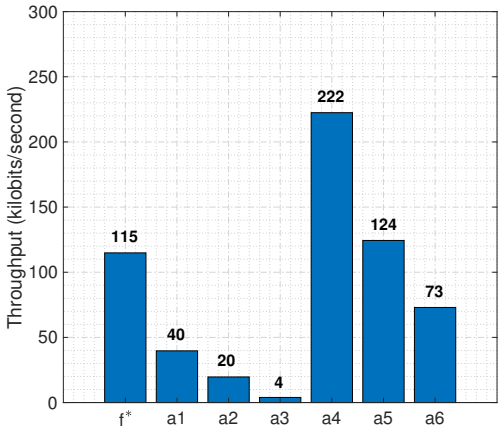

(b) LH–RA

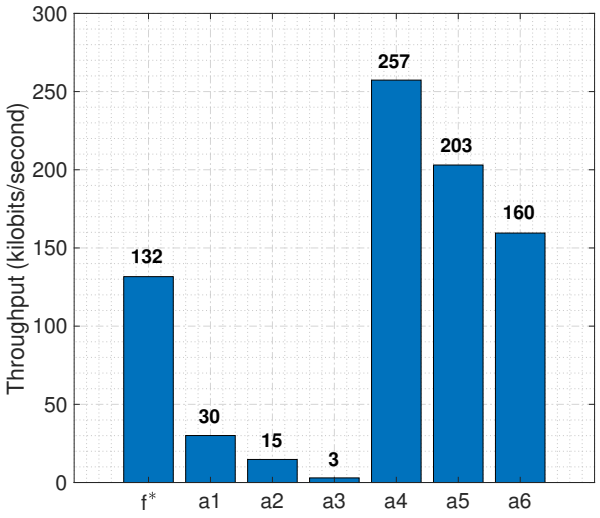

(c) LH–LW

Figure 6.6: Average throughput for different B2B channels (i.e., (a) LH–LH, (b) LH–RA, (c) LH–LW) estimated over 56 channels for each sensor location pair, for the Pareto optimum (f^*) and for individual actions ($a \, \epsilon \, A$).

almost double that of f^*, similar to the result in Fig. 6.4. We also found that the Pareto optimum outperforms all other individual actions for PDR. For instance, f^* with LH–LH links provides a PDR of 87%, which is very close to the IEEE 802.15.6 standard guideline (PDR $\geq$ 90%) [222] for packet delivery ratio of BANs.

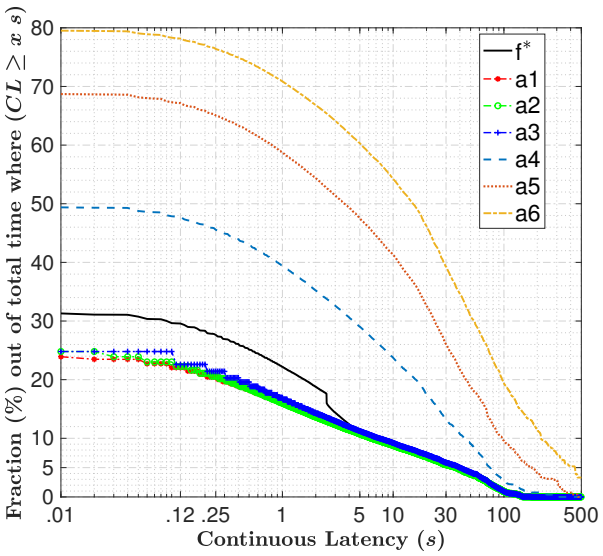

Figure 6.7: Fraction out of the total measured time for continuous latency $\geq$ x s (x axis values) for the Pareto optimum (f^*) and individual actions ($a \, \epsilon \, \mathbb{A}$) over the 168 tested channels.

6.3.2 Continuous Latency

The second of three objectives, continuous latency refers to the uninterrupted delay duration when the channel is in outage, or not transmitting, due to waiting or a back-off period. This is a very important performance measure for body-centric channels as these channels are often used for medical applications. Fig. 6.7 demonstrates the fraction or portion (on average) out of the total measured time with a continuous latency greater than or equal to x second (x-axis value) for the testing channels. It can be seen from Fig. 6.7 that CSMA/CA schemes experience larger continuous latency than TDMA schemes (due to the back-off mechanism in case of significant channel attenuation). For instance, with action 6 (CSMA/CA with $cs_{th} = -78$ dBm), the B2B channels encounter continuous delay greater than or equal to 125 ms for 78% of the overall period (on average), which reduces to 47% with action 4 (CSMA/CA with a $cs_{th} = -70$ dBm). On the other hand, TDMA schemes (action $1-3$) produce continuous delay greater then or equal to 125 ms for 22% to 23% of the whole period of the channels (on average). The Pareto optimal outcome (f^*) provides continuous delay greater than or equal to 125 ms for 29% of

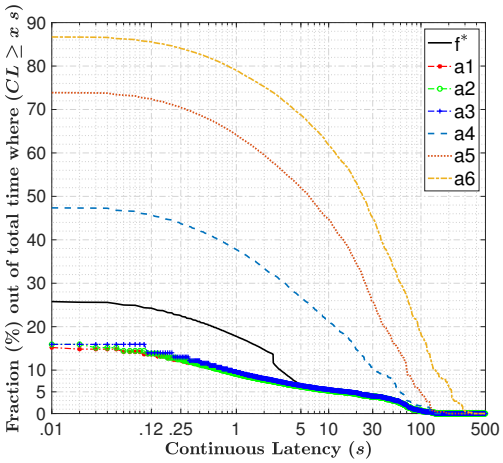

(a) LH–LH

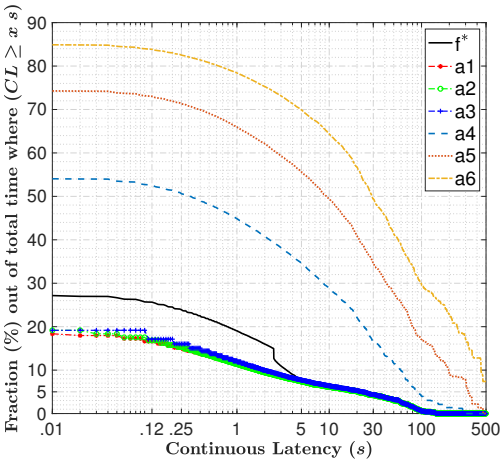

(b) LH–RA

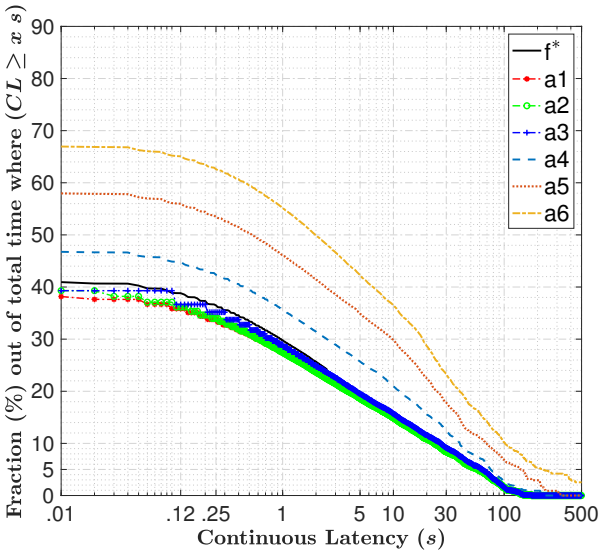

(c) LH–LW

Figure 6.8: Fraction out of the total measured time for continuous latency $\geq$ x s (x axis values) for different B2B channels, (a) LH–LH, (b) LH–RA, (c) LH–LW, for the Pareto optimum (f^*) and individual actions ($a \, \epsilon \, \mathbb{A}$) .

the overall period (on average), hence providing suitable trade-off between TDMA and CSMA/CA with reduced latency from CSMA/CA along with greater throughput than TDMA, as already shown. Additionally, the portion of longer continuous delay for f^* is similar to TDMA schemes — at less than 10%, for periods greater

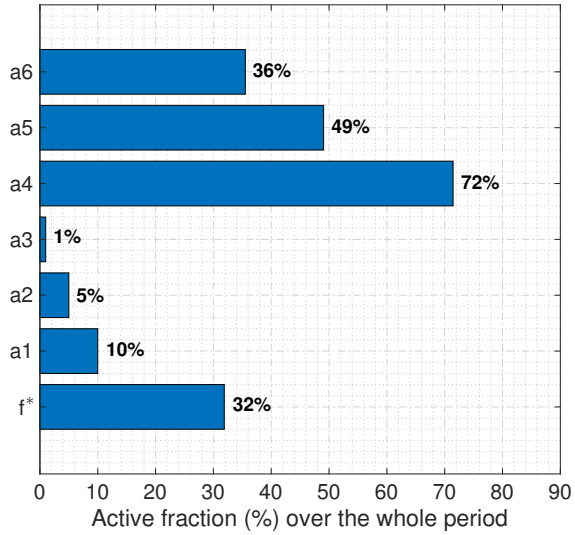

Figure 6.9: Active fraction (%) from all (168) tested channels over the whole period for the Pareto optimum (f^*) and individual actions ($a \, \epsilon \, \mathbb{A}$).

than 4 seconds.

We also investigate the continuous latency for different types of B2B channels between different sensor location pairs (shown in Fig. 6.8). It is shown that for LH–LH and LH–RA links, f^* produces greater continuous delay than TDMA (actions $1-3$) but the amount is lower than those produced with CSMA/CA schemes (actions $4-6$). In case of LH–LW links (Fig. 6.8c), the amount of continuous delay increases for TDMA schemes along with f^* (compared to other links) while the overall continuous latency decreases for the CSMA/CA schemes, yet is still higher than f^* and the TDMA schemes.

6.3.3 Active Fraction and Energy Consumption

The active fraction over a channel is the ratio of the active period (when the node is active and transmitting) to the total measured period of the channel:

$$\alpha = \left(\frac{P_{trans} \times T_{trans}}{\Delta}\right) \times 100, \tag{6.9}$$

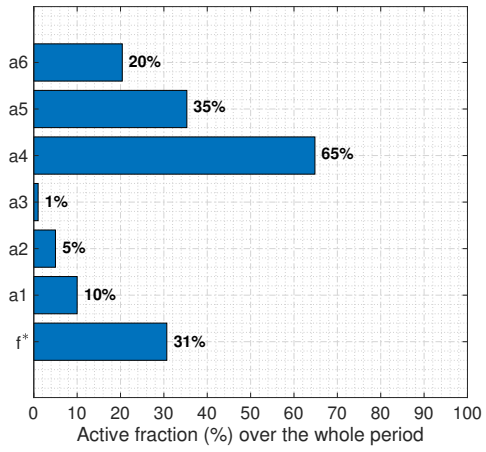

(a) LH–LH

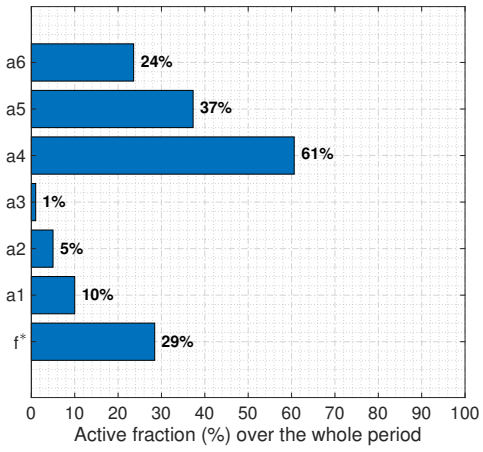

(b) LH–RA

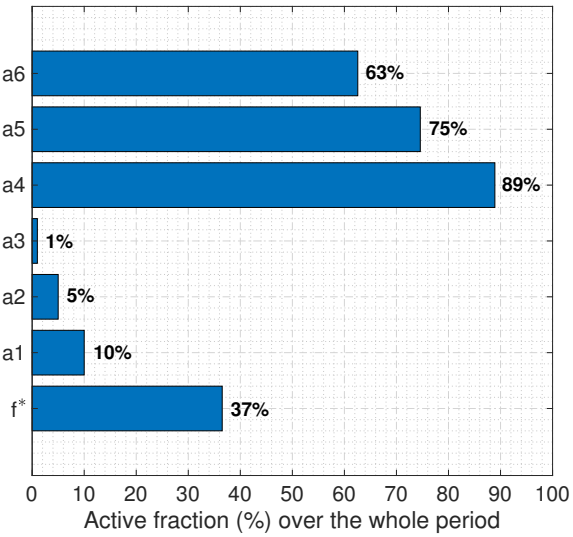

(c) LH–LW

Figure 6.10: Active fraction (%) for different B2B channels (i.e., (a) LH–LH, (b) LH–RA, (c) LH–LW) over the whole period for the Pareto optimum (f^*) and individual actions ($a \, \epsilon \, \mathbb{A}$) over 56 channels (for each sensor location pair).

where P_{trans} is the number of transmitted packets/samples and T_{trans} is the transmission time. The active fraction is directly proportional to energy consumption, as an increase in active fraction causes an increase in energy consumption. The active fractions over the whole period (on average) for B2B channels with different

actions are shown in Fig. 6.9.

It is shown that with the Pareto optimum (f^*), the channels remain active for 32% (on average) of the total time without any fixed duty cycle, which is around 22% higher than TDMA with 10% duty cycle ($a1$), hence consuming approximately 3.2 times more energy than $a1$ (but also providing much greater throughput than TDMA schemes: Fig. 6.4). On the other hand, action 4 (CSMA/CA with $cs_{th} = -70$ dBm) that has the highest throughput (Fig. 6.4), also has the highest active fraction (around 72%) which consumes 2.3 times more energy than f^*, along with producing higher continuous latency than f^*, as shown in Fig. 6.7.

The active fraction over different B2B links (between different sensor location pairs) is shown in Fig. 6.10. It can be seen that LH–LW links are active for a slightly greater percentage of time with f^*, 3.7 times more active period than TDMA with 10% duty cycle, compared to other links (LH–LH, LH–RA), that results in more energy consumption but also provides greater throughput with respect to other links (Fig. 6.6). Importantly, with LH–LW links, the active fraction with CSMA/CA schemes are increased, which contributes to the slightly higher active period (Fig. 6.10) and continuous latency (Fig. 6.8) of LH–LW links.

6.3.4 Spatial Distribution of Multivariate Outcomes

The averaged Pareto optimum for multi-objective optimisation along with the averaged outcome for individual actions, over all the tested channels is plotted in Fig. 6.11a, with respect to three criteria — throughput, percentage of continuous latency that is greater than 125 ms, and energy consumption. In the same figure (Fig. 6.11b,) all the Pareto optima and the outcomes of individual actions for all of the 168 tested channels are plotted individually with a scatter plot, to show the spatial distribution of these multivariate outcomes. It can be seen from Fig. 6.11b that with CSMA/CA schemes, most of the outcomes are either producing higher throughput with higher energy consumption, or lower throughput with higher percentage of larger continuous latency (i.e., greater than 125 ms). There are also some regions where the CSMA/CA schemes are producing less throughput with very high percentage of larger continuous latency and energy consumption. On the other hand, TDMA schemes are always producing less throughput (irrespective of

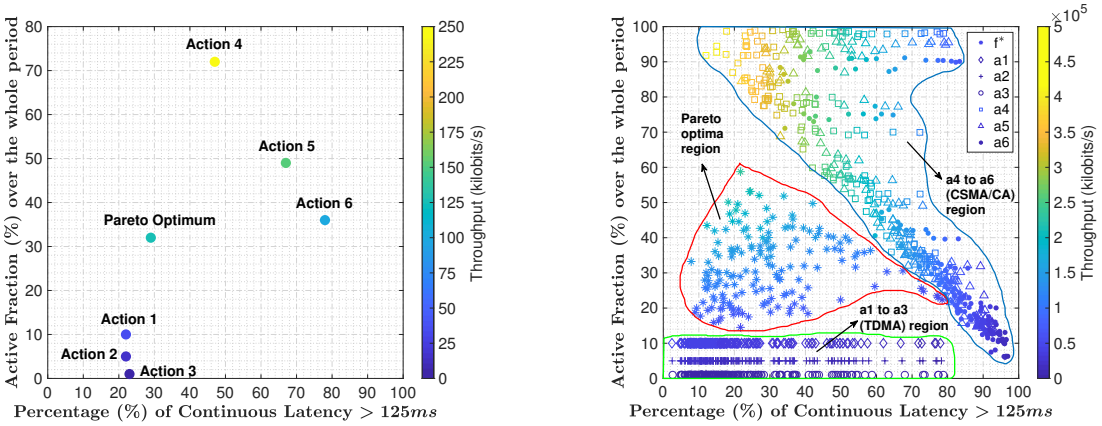

(a) (b)

Figure 6.11: (a) Average outcome of the MOMDP with respect to all three objectives; (b) Spatial distribution of the outcome of the MOMDP with respect to all three objectives. The x-axis shows the percentage of continuous latency > 125 ms over the total operating period.

the amount of larger continuous latency, which is significant in some cases) with fixed duty cycles. It can be clearly seen from Fig. 6.11 that the Pareto optima are providing a balance between the TDMA and CSMA/CA schemes, hence producing a desirable trade-off between throughput, continuous latency, and energy consumption of the B2B channels.

6.3.5 Evaluating the MOMDP

To evaluate and validate the multi-objective Markov decision process (MOMDP), we regress observed vs. predicted values from different actions and compare the slopes of different regression lines against the reference line (with a slope of 1). A simple least square linear regression method [294] is used to find the regression lines for different actions. This is demonstrated in Fig. 6.12a, where we plot the observed transition probabilities (from training channels) against the predicted transition probabilities (from testing channels) for different actions of the action set $\mathbb{A}$. For a hypothetically ideal predictive model, the slope of the regression of observed vs. predicted values will be 1, hence we compare the slope (a) of the regression lines with different actions against a 45 degree angled reference line with

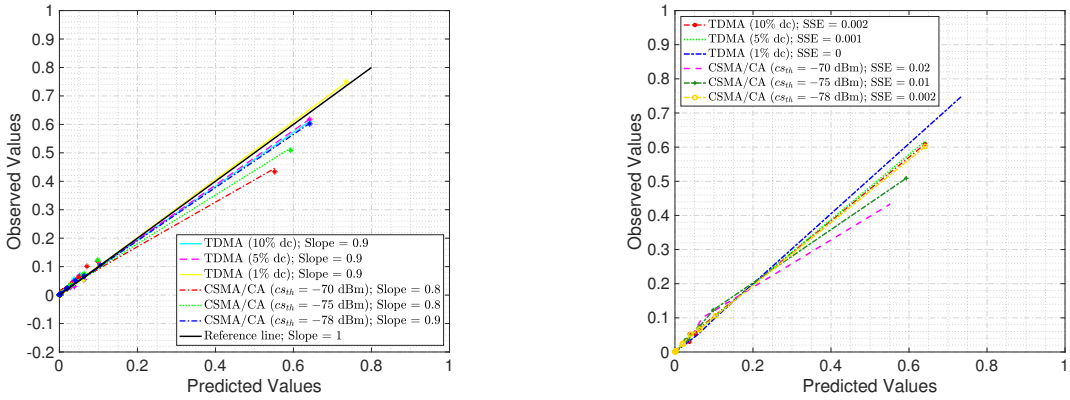

(a) (b)

Figure 6.12: (a) Linear regression fit and (b) sum squared error (SSE) of the MOMDP for different actions ($a \in \mathbb{A}$).

slope 1. From Fig. 6.12a, it can be seen that all of the regression lines have a slope greater than 0.7 and closer to 1, which indicates the consistency of the MOMDP model.

We also measure the goodness-of-fit with the sum squared error (SSE) statistic [264], which is the sum of the squares of deviations predicted from actual empirical values of data. It is a measure of the discrepancy between the data and an estimation model. A value closer to 0 indicates that the model has a smaller random error component, and that the fit will be more useful for prediction. The SSE values for the prediction with different actions are shown in Fig. 6.12b, where it can be seen that the predictions have smaller SSE values ranges from 0 to 0.02, which validates the MOMDP predictive analysis.

6.4 Discussion

In this section we make some general key observations following from analysis, leading to a brief discussion of extending this work.

Comment 6.1. *The predictive characteristics, i.e., WSS durations, of B2B channels affect the outcome of different actions, such as TDMA and CSMA/CA scheduling applied over those channels, which further affects the outcome of the MOMDP.*

Discussion. From the results of the MOMDP, it can be seen that, the performance of the multi-objective optimisation differs for B2B channels with different sensor location pairs (Figs. 6.6, 6.8, and 6.10). As mentioned in Section IV, from an extensive analysis of the predictive properties of B2B channels we previously found that the WSS duration varies for different sensor location pairs and respective shadowing between sensor locations of two bodies. For example, with the dataset of 8 coexisting BANs (used for testing the predictive model in this chapter), the LH–LW links remained wide-sense stationary for a longer period than other links (i.e., LH–LH, LH–RA), due to the variation in their fading characteristics. Interestingly, it can be seen from the above experimental results that the increased amount of stationarity has an adverse effect on TDMA with fixed duty cycles as opposed to CSMA/CA, which shows significant performance improvement with increased WSS duration.

Thus, in Fig. 6.6, it can be seen that the throughput is increased for actions 4 to 6 (CSMA/CA), whereas the throughput is decreased for actions 1 to 3 (TDMA) for LH–LW links (Fig. 6.6c), compared to the other B2B links. Because of the fixed active and waiting period of TDMA, greater signal attenuation across a stationary channel will continue for a longer period, and hence will produce less throughput, which can be improved with the carrier sensing and back-off mechanism of CSMA/CA, where the transmission occurs based on suitable channel conditions. Such variation is even more noticeable with the continuous latency of the LH–LW links (Fig. 6.8c) where the average continuous latency is increased for actions 1 to 3 (TDMA) because of the fixed duty cycle, whereas it is significantly reduced for actions 4 to 6 (CSMA/CA), compared to other links (Fig. 6.8).

As the Pareto optimum (f^*) combines different actions with TDMA and CSMA/CA, the outcome f^* is also affected by an increase in stationarity, e.g., the increase in continuous latency of the LH–LW links (Fig. 6.8) for f^*. However, LH–LW links (with better stationarity) provide comparatively better balance between TDMA and CSMA/CA than other B2B links. For instance, LH–LW links provide the highest throughput, 4.4 times better than TDMA (with a duty cycle of 10%), considerably lower active fraction and hence, lower energy consumption, by a factor of 2.4 than CSMA/CA (with $cs_{th} = -70$ dBm), along with producing similar continuous latency to TDMA and less continuous latency than CSMA/CA. Thus, overall

it can be inferred that the predictive characteristics (along with the shadow fading characteristics) of body-to-body channels have a significant effect on the outcome of the MOMDP. □

Comment 6.2. *Multiple Pareto optima can be derived from multi-objective optimisation to generate a Pareto set (Pareto frontier).*

Discussion. In this work, a single Pareto optimum is derived based on the conditions used for state classifications. For instance, the target of the MDP is to reach to a state with increased packet delivery ratio ($\geq 60\%$) and reduced continuous latency (< 125 ms). It can be seen from the averaged outcomes discussed above that this condition jointly optimises multiple objectives by providing greater throughput than TDMA with acceptable continuous latency (considering the longer periods of latency), and less energy consumption and continuous latency than CSMA/CA. As this is a Pareto optimum, no other solution can dominate this outcome, such as, to reduce the energy consumption, the active period of the channels need to be reduced, and as a result throughput will be decreased. Also, decreasing the active period will increase the waiting period, which will increase the continuous latency of the channel. Therefore, multiple Pareto optima can be derived for the problem in (6.2) to produce a Pareto set or Pareto frontier, which is subject to the given conditions. A Pareto frontier is the set of all parameterisations that are Pareto optimal, which can be obtained by aggregating all the different conditions for classifying the states, to improve or optimise different objectives of (6.2). This can be formulated as follows:

$$\rho_{f^*(\mathbb{C}_\mathbb{S})} = \left\{c' : (c'' > c', c'' \neq c') = \emptyset\right\}, \quad (c', c'') \, \epsilon \, \mathbb{C}_\mathbb{S}. \tag{6.10}$$

Exploring the Pareto frontier is useful for approximating the amount of trade-off for achieving different Pareto optima of the multi-objective function.

A constrained MDP (CMDP) could also be developed for the multi-objective optimisation for maximising particular objectives, according to specific applications, with constraints on others. For instance, only throughput can be optimised, i.e., maximised, by employing some deterioration boundary for continuous latency and energy consumption. Moreover, the conditions used here for defining the states,

i.e., packet delivery ratio and continuous latency, could be used as constraints together with some additional constraints on throughput or active fraction, as an alternate implementation of the multi-objective optimisation. □

6.5 Summary

We have developed and empirically analysed the feasibility of a multi-objective Markov decision process (MOMDP) to perform adaptive scheduling over real-life narrowband wireless body-to-body (B2B) channels. The MDP was formulated based on the predictive properties, wide-sense-stationarity and long-range dependence of body-centric channels. We defined the conditions for the Pareto optimal state for the MDP with a brute-force search by employing an extensive amount of real-life experimental B2B channels, which were also used to estimate the transition probability and optimal policy of the MOMDP. From the application of the MOMDP that adaptively chooses between different scheduling schemes, i.e., TDMA and CSMA/CA with different parameters, over a significant number of experimental channels, we obtained a Pareto optimum that dominates other Pareto optima according to multiple key criteria. We showed that the Pareto optimum (f^*) provides a desired trade-off between different conflicting objectives. Such as, f^* can provide better throughput than TDMA, up to 3.4 times that of TDMA with 10% duty cycle, along with increased energy consumption, approximately 3.2 times greater than TDMA. Furthermore, f^* produced slightly (around 5%) higher amount of continuous latency than TDMA for smaller intervals and similar amount of continuous latency (as TDMA) for longer intervals, e.g., $\geq$ 4 s. On the other hand, f^* produced less throughput than CSMA/CA, almost one half with a carrier sense threshold of -70 dBm, but also consumed considerably less energy and had much lower continuous latency than CSMA/CA. Additionally, f^* had the highest packet delivery ratio (more than 80%) compared to the individual actions ($a \, \epsilon \, \mathbb{A}$).

In addition to that, we validated the consistency of the MOMDP model, by performing linear regression and sum squared error analysis over the large-scale experimental data. It was also observed that the outcomes of the individual actions of the MOMDP depends on the WSS characteristics of body-centric channels — for B2B channels with an increase in stationarity the performance of TDMA actions

deteriorate while the performance of CSMA/CA actions improve, with the Pareto optimum providing a better balance between CSMA/CA and TDMA. A Pareto set or Pareto frontier can be developed with all Pareto optima subject to the state defining conditions used in this chapter. It is also alternately possible to optimise a specific objective with constraints on others for maximising the output according to a particular BBN application. Some other possible future directions include, application of Semi-Markov decision processes (SMDPs), neural networks and reinforcement learning with multi-objective optimisation, to compare with the MOMDP described in this chapter.

6.6 Related Publications

- **Samiya M. Shimly** and David B. Smith: 'Multi-Objective Markov Decision Process for Adaptive Scheduling in Wireless Body-to-Body Networks', under review in *IEEE Internet of Things Journal*, March, 2019.

Chapter 7

Conclusion and Future Work

In this chapter, we conclude the thesis by precisely describing some fundamental key points of the contributions made in this thesis, along with providing some future research directions that can be evolved from this study.

7.1 Conclusion

This thesis aimed to address the issues of reliable, efficient and optimised communications among closely located BANs (people with body-worn sensors), in order to extend the connectivity of distributed body-centric networks, i.e., BBNs (body-to-body networks) by utilising body-to-body (B2B) communications. Importantly, the proposed solutions of this thesis were validated with extensive real-life experimental narrowband channel measurements collected from a reasonable number of co-located BANs/subjects in different empirical scenarios, which provides a generalised performance evaluation of practical BBN framework. Existing research, along with research gaps related to optimisation of the body-centric communications (studied here) have been discussed, following the description of the general communications architecture, technology standards, and challenges associated with BAN coexistence. As discussed body-centric channels experience shadowing by human body and body-parts, e.g., during postural and ambulatory movements in close proximity, which degrades the reliability of those channels. Sometimes this shadowing lasts for a longer period, e.g., with a simple postural change when the subject

has less mobility — during sleep, mobility impairment; and dense coexistence in a close vicinity. In such cases, a cooperative path through nearby body-worn sensors (whether on the same body or a different body) can contribute to improve the reliability of the communications between the source and destination, as was demonstrated here. Additionally, due to the resource constraints of these networks, efficient optimisation, of the type in this thesis of the body-centric communications is required for practical implementation of such networks.

Therefore, at first, we investigated the performance of cooperative receive diversity (with two-hop communications) for on-body and off-body channels of various sleeping subjects, with two different cooperative combining techniques, i.e., selection combining and switch-and-examine combining. It was demonstrated that two-hop cooperative communications can substantially improve the reliability of direct link communication, in case of body-centric channels incorporating significant shadowing (i.e., channels with subject sleeping). Then, we proposed two cross-layer optimised dynamic routing techniques — shortest path routing (SPR) and cooperative multi-path routing (CMR) that incorporates 3-branch selection combining, to improve and optimise the reliability and efficiency of routing information across BBN. The physical layer channel state information was directly sent to the network layer to choose the best route according to the channel condition, in a periodic basis (based on coherence time). The proposed CMR (with multiple paths) reduces retransmissions and increases throughput compared to SPR (with single path), by the use of alternate cooperative paths. Furthermore, CMR reduces end-to-end delay and energy consumption compared to SPR and other state-of-the-art WSN routing protocols (i.e., ORPL, LOADng).

We also analysed the performance of SPR and CMR with interference mitigation, associated with different MAC layer schemes, i.e., low duty cycle TDMA (time division multiple access) and novel adaptive CSMA/CA (carrier sense multiple access with collision avoidance), by performing PHY-MAC-Network cross-layer optimisation. It was shown by empirical analysis that even with a lower duty cycle (0.2%) TDMA, CMR improves the outage probability and packet delivery ratio compared to SPR. For CSMA/CA, we proposed a novel adaptive cross-layer carrier sensing mechanism that adjusts the carrier sense threshold (i.e., receive signal strength indicator) periodically based on the slowly-varying channel condition with

an adequate periodic time-stamping for routing updates, which then was applied over SPR and CMR techniques. In comparison to static carrier sensing, the proposed adaptive mechanism produced negligible continuous delay of longer intervals and, provided increased throughput (successful packets/s) and packet arrival rate (as well as compared to a TDMA with higher duty cycle of 8.3%).

Subsequently, we characterised the predictive behaviour of body-centric channels to explore the feasibility of prediction-based optimisation over such channels, in order to build self-organised BBNs, capable of autonomous decision-making. Therefore, we investigated the wide-sense-stationarity (WSS) and long-range dependence (LRD) characteristics of body-centric channels that are essential for predictive analysis. We demonstrated that unlike on-body channels (which are considered as non-stationary), a WSS assumption can be held for body-to-body channels for a range of window lengths between 0.5 s and 15 s (typically $5-8$ s) depending on the on-body sensor locations and the shadowing effect of the corresponding B2B channel. We also found that both on-body and body-to-body channels can retain LRD or long-memory characteristics. Along with the LRD property, the WSS duration of B2B channels can be utilised to estimate the period over which reliable prediction can be made from multiple samples with greater accuracy. Thus, we developed a multi-objective Markov decision process (MOMDP) that utilised WSS and LRD of body-centric channels, to apply adaptive scheduling that combines both TDMA and CSMA/CA schemes. The multi-objective optimisation performed in this thesis jointly optimises three separate metrics: throughput, continuous latency, and energy consumption of body-to-body (B2B) communications. A Pareto optimal solution was devised from the MOMDP that provided a desirable trade-off between the three objectives of maximising throughput, and minimising continuous latency and energy consumption. It was also observed that WSS characteristics of body-centric channels have a significant effect on the outcome of such analytics.

The proposed solutions, validated with experimental analysis in this thesis are very beneficial for deploying real-life body-centric networks with distributed large-scale systems, associated with self-organised, reliable, and optimised communications. Importantly, the work in this thesis leads to more potential methods that can also improve reliability and efficiency of body-centric communications, as discussed in the following section.

7.2 Future Work

This thesis successfully addressed reliability and optimised connectivity of body-centric communications across many closely located body area networks, with real-life experimental analysis. Potential future research work that could be performed in extension of our study includes:

- For the cooperative multi-path routing (CMR) proposed in this thesis, we employed two different paths with a maximum of two hops (route-hops), following from the percentage of hop counts estimated from a specific number of co-located BANs, i.e., 10 BANs. For practically deploying this technique at a larger scale, routing paths with more than two hops may be required, which can be further analysed with a larger number of co-located BANs/subjects, to investigate the hop count limit and efficiency of multi-path routing for such networks.

- To further optimise delay and energy consumption of the proposed CMR, opportunistic relaying and routing could be applied. For example, instead of performing 3-branch selection combining at each route-hop, cooperative combining could be performed only when necessary, such as when the direct link is not available. The branch with the best relay could also be selected as a cooperative link (opportunistic relaying) among the available cooperative relayed links.

- With the two tiered architecture described in this thesis for body-centric networks (i.e., BBN at upper tier, BAN at lower tier), different frequency bands and technology standards could be applied in different tiers, so as to improve scalability and efficiency of such networks.

- The predictive characteristics of body-centric channels described in this thesis were based on some specific real-life scenarios and activities for a number of closely located subjects. Therefore, further investigation into WSS and LRD could be carried out for more densely populated networks in a range of scenarios with subjects very closely located, as well as being more dispersed, based on capturing more empirical data. Additionally, as stated earlier, the

majority of body-centric networks analysis assumes that the radio channel is wide-sense stationary, but this is often not the case. Thus, further predictive analytics design could be performed in light of the deployment scenario in body-centric networks, and operation, with respect to appropriate LRD and WSS properties.

- Multi-objective optimisation could alternatively be implemented with reinforcement learning, or other machine learning techniques, to compare with the MDP framework proposed in this thesis. Also, constrained MDP could also be applied to maximise one objective by putting constraints on others according to the particular application.

- Wireless body-centric networks are very much susceptible to security attacks and intrusions, as mentioned in chapter 2. For body-to-body communications, this problem is crucial as the data passes through different user's sensor devices. Therefore, it is very important to ensure legitimate access to the stored and transmitted information along with secured communications for such networks, which has not been adequately addressed so far. To improve the acceptance and usability of BBNs, data encryption algorithm and context-aware access control mechanism could be developed and integrated with the data dissemination protocols of coexisting BANs.

Appendix A

Hypothesis Tests

ANOVA Test

The ANOVA (Analysis of Variance) test is used for analysing the variation (as the name implies) or difference between the means of two or more sets of observations. We use the parametric one-way ANOVA test statistic ($T_{L_{anova}}$) which is the ratio of the mean square variance between the intervals to the mean square variance within each interval [253].

$$T_{L_{anova}} = \frac{\overline{S}_{between}}{\overline{S}_{within}}, \tag{A.1}$$

where

$$\overline{S}_{between} = \frac{\sum_{i=1}^{m_t} n_i(\overline{X}_i - \overline{X})^2}{m_t - 1}, \tag{A.2}$$

and

$$\overline{S}_{within} = \frac{\sum_{i=1}^{m_t} \sum_{j=1}^{n_i} (\overline{X}_{ij} - \overline{X}_i)^2}{N - m_t}, \tag{A.3}$$

where m_t is the number of intervals over which the hypothesis is being tested (here, $m_t = 2$), X_{ij} is the jth element of the ith interval, n_i is the number of observations in ith interval and N is the total number of observations across m_t intervals. $\overline{X}_i$ is the mean of i^{th} interval and $\overline{X}$ is the mean over m_t intervals $\left(\overline{X} = \frac{1}{N}\sum_{i=1}^{N} X_i\right)$.

Brown–Forsythe Test

To investigate the homogeneity of the variances over the window lengths, hence further testing the homoscedasticity assumption made for ANOVA, we use the

non-parametric Brown–Forsythe (B–F) test [254], which calculates the F statistic resulting from an one-way ANOVA on the absolute deviations from the median.

$$T_{L_{BF}} = \frac{\frac{\sum_{i=1}^{m_t} n_i(\bar{d}_i - \bar{d})^2}{m_t - 1}}{\frac{\sum_{i=1}^{m_t}\sum_{j=1}^{n_i}(\bar{d}_{ij} - \bar{d}_i)^2}{N - m_t}}, \tag{A.4}$$

where $d = \left|X_{ij} - \widetilde{X_i}\right|$ and $\widetilde{X_i}$ is the median of the i^{th} interval.

For Levene's test [259], $d = \left|X_{ij} - \overline{X_i}\right|$ where $\overline{X_i}$ is the mean of the i^{th} interval.

Kolmogorov–Smirnov Test

We use the non-parametric two-sided Kolmogorov-Smirnov (K-S) two-sample test [255] to examine whether the samples of two consecutive intervals come from the same distribution. This test is sensitive to any difference in median, dispersion, and skewness between two distributions, as it estimates the maximum absolute difference between the two empirical distributions as follows,

$$T_{L_{KS}} = sup_{(x)}\left|F_y(x) - F_z(x)\right|, \qquad x = x_1, ..., x_{n+l}, \tag{A.5}$$

where $T_{L_{KS}}$ is the K-S test statistic and, $y = X(t_1), ..., X(t_n)$ and $z = X(t_{1+l}), ..., X(t_{n+l})$ are two consecutive intervals of $X(t)$, where t_n is the element at time instance t.

Power Spectral Variation

$$\widehat{S_k}^{\xi}(f) = \left| \sum_{t=1}^{L} g_k(t) X_\xi(t) e^{-i2\pi ft/L} \right|^2 \qquad \xi = [1, 2, ..., M], \tag{A.6}$$

where $\widehat{S_k}^{\xi}(f)$ is the k^{th} eigenspectrum found from the absolute square of the Short Time Fourier Transform (STFT) of window length L and $g_k(t)$ is the k^{th} rectangular window/taper from the discrete prolate spheroidal (Slepian) sequences of length L. M is the number of windows over the whole channel ($M = N_c/L$ where N_c is the

length of the whole channel).

$$\widehat{S}_{\xi}(f) = \frac{1}{K}\sum_{k=0}^{K-1}\widehat{S_k}^{\xi}(f), \tag{A.7}$$

where K is the total number of the discrete prolate spheroidal sequences and $\widehat{S}_{\xi}(f)$ is the multi-taper PSD estimation, which is the average of the K modified periodograms.

$$\widehat{S}(f) = \frac{1}{M}\sum_{\xi=1}^{M}\widehat{S}_{\xi}(f), \tag{A.8}$$

where $\widehat{S}(f)$ is the average of PSD for M windows over the whole channel and the variance of PSD with window length L over the whole channel is

$$\vartheta_L = \frac{1}{M}\sum_{\xi=1}^{M}\left(\widehat{S}_{\xi}(f) - \widehat{S}(f)\right)^2 \tag{A.9}$$

The power spectral variation (V_L) with window length L over the whole channel is measured as follows,

$$V_L = \frac{1}{LM}\sum_{t=1}^{L}\sum_{\xi=1}^{M}\left(\widehat{S}_{\xi}(f) - \widehat{S}(f)\right)^2 \tag{A.10}$$

The amount of V_L would be 0 when the channel is stationary over the window length L [150].

Bibliography

[1] Riccardo Cavallari, Flavia Martelli, Ramona Rosini, Chiara Buratti, and Roberto Verdone, "A survey on wireless body area networks: Technologies and design challenges," *IEEE Communications Surveys & Tutorials*, vol. 16, no. 3, pp. 1635–1657, 2014.

[2] Samaneh Movassaghi, Mehran Abolhasan, Justin Lipman, David Smith, and Abbas Jamalipour, "Wireless body area networks: A survey," *IEEE Communications Surveys & Tutorials*, vol. 16, no. 3, pp. 1658–1686, 2014.

[3] Huasong Cao, Victor Leung, Cupid Chow, and Henry Chan, "Enabling technologies for wireless body area networks: A survey and outlook," *IEEE Communications Magazine*, vol. 47, no. 12, 2009.

[4] Statista, "Facts and statistics on wearable technology," `https://www.statista.com/topics/1556/wearable-technology/`, 2019.

[5] Peter S Hall and Yang Hao, "Antennas and propagation for body centric communications," in *First European Conference on Antennas and Propagation, France*. IEEE, 2006, pp. 1–7.

[6] Jean Sebanstien-Bedo Orange, Ana Garcia Armada, Barry Evans, Alex Galis, and Holger Karl, "White paper for research beyond 5G," *Accessed*, vol. 23, pp. 2016, 2015.

[7] Qammer H Abbasi, Masood Ur Rehman, Khalid Qaraqe, and Akram Alomainy, *Advances in body-centric wireless communication: Applications and state-of-the-art*, Institution of Engineering and Technology, 2016.

[8] Benoît Latré, Bart Braem, Ingrid Moerman, Chris Blondia, and Piet Demeester, "A survey on wireless body area networks," *WIRELESS NETWORKS*, vol. 17, no. 1, pp. 1–18, 2011.

[9] Mark S Humayun, James D Weiland, Gildo Y Fujii, Robert Greenberg, Richard Williamson, Jim Little, Brian Mech, Valerie Cimmarusti, Gretchen Van Boemel, Gislin Dagnelie, et al., "Visual perception in a blind subject with a chronic microelectronic retinal prosthesis," *Vision research*, vol. 43, no. 24, pp. 2573–2581, 2003.

[10] James D Weiland, Wentai Liu, and Mark S Humayun, "Retinal prosthesis," *Annu. Rev. Biomed. Eng.*, vol. 7, pp. 361–401, 2005.

[11] Kyung Sup Kwak, Sana Ullah, and Niamat Ullah, "An overview of IEEE 802.15.6 standard," in *3rd International Symposium on Applied Sciences in Biomedical and Communication Technologies (ISABEL), Rome, Italy.* IEEE, Nov, 2010, pp. 1–6.

[12] IEEE Standards Association et al., "Ieee standard for local and metropolitan area networkspart 15.6: Wireless body area networks," *IEEE Standard for Information Technology, IEEE*, vol. 802, no. 6, pp. 1–271, 2012.

[13] Carles Gomez, Joaquim Oller, and Josep Paradells, "Overview and evaluation of Bluetooth low energy: An emerging low-power wireless technology," *Sensors*, vol. 12, no. 9, pp. 11734–11753, 2012.

[14] Matti Hämäläinen, Tuomas Paso, Lorenzo Mucchi, Marc Girod-Genet, John Farserotu, Hirokazu Tanaka, Woon Hau Chin, and Lina Nachabe Ismail, "ETSI TC Smartban: Overview of the wireless body area network standard," in *Medical Information and Communication Technology (ISMICT), 2015 9th International Symposium on.* IEEE, 2015, pp. 1–5.

[15] LAN/MAN Standards Committee et al., "Part 15.4: wireless medium access control (MAC) and physical layer (PHY) specifications for low-rate wireless personal area networks (lr-wpans)," *IEEE Computer Society*, 2003.

[16] Ian F Akyildiz, Weilian Su, Yogesh Sankarasubramaniam, and Erdal Cayirci, "Wireless sensor networks: a survey," *Computer networks*, vol. 38, no. 4, pp. 393–422, 2002.

[17] Jaap C Haartsen, "The Bluetooth radio system," *IEEE personal communications*, vol. 7, no. 1, pp. 28–36, 2000.

[18] Brian P Crow, Indra Widjaja, Jeong Geun Kim, and Prescott T Sakai, "IEEE 802.11 wireless local area networks," *IEEE Communications magazine*, vol. 35, no. 9, pp. 116–126, 1997.

[19] Nandakishore Kushalnagar, Gabriel Montenegro, and Christian Schumacher, "IPv6 over low-power wireless personal area networks (6LoWPANs): overview, assumptions, problem statement, and goals," Tech. Rep., Internet Engineering Task Force (IETF), 2007.

[20] Robert T Collins, Alan J Lipton, Takeo Kanade, Hironobu Fujiyoshi, David Duggins, Yanghai Tsin, David Tolliver, Nobuyoshi Enomoto, Osamu Hasegawa, Peter Burt, et al., "A system for video surveillance and monitoring," *VSAM final report*, pp. 1–68, 2000.

[21] Amitabha Ghosh, Nitin Mangalvedhe, Rapeepat Ratasuk, Bishwarup Mondal, Mark Cudak, Eugene Visotsky, Timothy A Thomas, Jeffrey G Andrews, Ping Xia, Han Shin Jo, et al., "Heterogeneous cellular networks: From theory to practice," *IEEE communications magazine*, vol. 50, no. 6, pp. 54–64, 2012.

[22] Samiya Shimly, David B Smith, and Samaneh Movassaghi, "Cross-layer optimized routing with low duty cycle TDMA across multiple wireless body area networks," in *IEEE International Conference on Communications (ICC), France*, May, 2017, pp. 1–6.

[23] Simon L Cotton and William G Scanlon, "Channel characterization for single- and multiple-antenna wearable systems used for indoor body-to-body communications," *IEEE Transactions on Antennas and Propagation*, vol. 57, no. 4, pp. 980–990, 2009.

[24] Dhafer Ben Arbia, Muhammad Mahtab Alam, Rabah Attia, and Elyes Ben Hamida, "Data dissemination strategies for emerging wireless body-to-body networks based internet of humans," in *11th International Conference on Wireless and Mobile Computing, Networking and Communications (WiMob)*. IEEE, 2015, pp. 1–8.

[25] Dorothy Monekosso, Francisco Florez-Revuelta, and Paolo Remagnino, "Ambient assisted living [guest editors' introduction]," *IEEE Intelligent Systems*, vol. 30, no. 4, pp. 2–6, 2015.

[26] Jacek Lewandowski, Hisbel E Arochena, Raouf NG Naguib, and Kuo-Ming Chao, "A portable framework design to support user context aware augmented reality applications," in *Third International Conference on Games and Virtual Worlds for Serious Applications*. IEEE, 2011, pp. 144–147.

[27] Ryan Aylward and Joseph A Paradiso, "Sensemble: a wireless, compact, multi-user sensor system for interactive dance," in *Proceedings of the 2006 conference on New interfaces for musical expression*. IRCAMCentre Pompidou, 2006, pp. 134–139.

[28] Sanghyun Seo, Hakjeon Bang, and Hunjoo Lee, "Coloring-based scheduling for interactive game application with wireless body area networks," *The Journal of Supercomputing*, vol. 72, no. 1, pp. 185–195, 2016.

[29] B Zhen, M Patel, S Lee, E Won, and A Astrin, "Tg6 technical requirements document (trd) id: 802.15-08-0644," in *IEEE submission*, 2008.

[30] MirHojjat Seyedi, Behailu Kibret, Daniel TH Lai, and Michael Faulkner, "A survey on intrabody communications for body area network applications," *IEEE Transactions on Biomedical Engineering*, vol. 60, no. 8, pp. 2067–2079, 2013.

[31] Qiong Wang, Takeyoshi Tayamachi, Ippei Kimura, and Jianqing Wang, "An on-body channel model for UWB body area communications for various postures," *IEEE Transactions on Antennas and Propagation*, vol. 57, no. 4, pp. 991–998, 2009.

[32] J Agud Ruiz, Jiang Xu, and Shigeru Shimamoto, "Propagation characteristics of intra-body communications for body area networks," in *CCNC 2006. 2006 3rd IEEE Consumer Communications and Networking Conference, 2006.* IEEE, 2006, vol. 1, pp. 509–513.

[33] Nidhi Bhargav, Simon L Cotton, and David B Smith, "An experimental-based analysis of inter-BAN co-channel interference using the $\kappa - \mu$ fading model," *IEEE Transactions on Antennas and Propagation*, vol. 65, no. 2, pp. 983–988, 2017.

[34] Simon L Cotton, William G Scanlon, and Peter S Hall, "A simulated study of co-channel inter-BAN interference at 2.45 GHz and 60 GHz," in *The 3rd European Wireless Technology Conference*. IEEE, 2010, pp. 61–64.

[35] Zahoor Khan, Nauman Aslam, Shyamala Sivakumar, and William Phillips, "Energy-aware peering routing protocol for indoor hospital body area network communication," *Procedia Computer Science*, vol. 10, pp. 188–196, 2012.

[36] Zahoor A Khan, Shyamala Sivakumar, William Phillips, and Nauman Aslam, "A new patient monitoring framework and energy-aware peering routing protocol (EPR) for body area network communication," *Journal of Ambient Intelligence and Humanized Computing*, vol. 5, no. 3, pp. 409–423, 2014.

[37] Matthew Keally, Gang Zhou, Guoliang Xing, Jianxin Wu, and Andrew Pyles, "PBN: towards practical activity recognition using smartphone-based body sensor networks," in *Proceedings of the 9th ACM Conference on Embedded Networked Sensor Systems*. ACM, 2011, pp. 246–259.

[38] Won-Jae Yi, Weidi Jia, and Jafar Saniie, "Mobile sensor data collector using android smartphone," in *2012 IEEE 55th International Midwest Symposium on Circuits and Systems (MWSCAS)*. IEEE, 2012, pp. 956–959.

[39] John W Peifer, Andrew Hopper, Michael Burrow, Barry Sudduth, Samir Panchal, Andy Quay, W Edward Price, and John R Searle, "Telemedicine system using voice video and data encapsulation and de-encapsulation for

communicating medical information between central monitoring stations and remote patient monitoring stations," Nov. 16 1999, US Patent 5,987,519.

[40] Brian Rosenfeld and Michael Breslow, "Telecommunications network for remote patient monitoring," Aug. 14 2007, US Patent 7,256,708.

[41] Adam Darkins, Patricia Ryan, Rita Kobb, Linda Foster, Ellen Edmonson, Bonnie Wakefield, and Anne E Lancaster, "Care coordination/home telehealth: the systematic implementation of health informatics, home telehealth, and disease management to support the care of veteran patients with chronic conditions," *Telemedicine and e-Health*, vol. 14, no. 10, pp. 1118–1126, 2008.

[42] David Malan, Thaddeus Fulford-Jones, Matt Welsh, and Steve Moulton, "CodeBlue: An ad hoc sensor network infrastructure for emergency medical care," in *International workshop on wearable and implantable body sensor networks*. Boston, MA;, 2004, vol. 5.

[43] Tia Gao, Christopher Pesto, Leo Selavo, Yin Chen, JeongGil Ko, JongHyun Lim, Andreas Terzis, Andrew Watt, James Jeng, Bor-rong Chen, et al., "Wireless medical sensor networks in emergency response: Implementation and pilot results," in *2008 IEEE Conference on Technologies for Homeland Security*. IEEE, 2008, pp. 187–192.

[44] Sushruta Mishra and Hiren Thakkar, "Features of WSN and data aggregation techniques in WSN: A survey," *Int. J. Eng. Innov. Technol.(IJEIT)*, vol. 1, no. 4, pp. 264–273, 2012.

[45] Celal Ceken, "An energy efficient and delay sensitive centralized MAC protocol for wireless sensor networks," *Computer Standards & Interfaces*, vol. 30, no. 1-2, pp. 20–31, 2008.

[46] BeomSeok Kim and Jinsung Cho, "A novel priority-based channel access algorithm for contention-based MAC protocol in WBANs," in *Proceedings of the 6th International Conference on Ubiquitous Information Management and Communication*. ACM, 2012, p. 1.

[47] Ernesto Ibarra, Angelos Antonopoulos, Elli Kartsakli, and Christos Verikoukis, "HEH-BMAC: Hybrid polling MAC protocol for WBANs operated by human energy harvesting," *Telecommunication systems*, vol. 58, no. 2, pp. 111–124, 2015.

[48] Marc Bechler, H-J Hof, Daniel Kraft, Frank Pahlke, and Lars Wolf, "A cluster-based security architecture for ad hoc networks," in *IEEE INFOCOM 2004*. IEEE, 2004, vol. 4, pp. 2393–2403.

[49] Jaime Lloret, Miguel Garcia, Diana Bri, and Juan Diaz, "A cluster-based architecture to structure the topology of parallel wireless sensor networks," *Sensors*, vol. 9, no. 12, pp. 10513–10544, 2009.

[50] Mohamed Lehsaini, Herve Guyennet, and Mohammed Feham, "A novel cluster-based self-organization algorithm for wireless sensor networks," in *2008 International Symposium on Collaborative Technologies and Systems*. IEEE, 2008, pp. 19–26.

[51] Mohamed Lehsaini, Hervé Guyennet, and Mohammed Feham, "CES: Cluster-based energy-efficient scheme for mobile wireless sensor networks," in *Wireless Sensor and Actor Networks II*, pp. 13–24. Springer, 2008.

[52] Pin Nie and Bo Li, "A cluster-based data aggregation architecture in WSN for structural health monitoring," in *2011 7th International Wireless Communications and Mobile Computing Conference*. IEEE, 2011, pp. 546–552.

[53] S Suganya, "A cluster-based approach for collaborative target tracking in wireless sensor networks," in *2008 First International Conference on Emerging Trends in Engineering and Technology*. IEEE, 2008, pp. 276–281.

[54] Changhong Wang, Qiang Wang, and Shunzhong Shi, "A distributed wireless body area network for medical supervision," in *2012 IEEE International Instrumentation and Measurement Technology Conference Proceedings*. IEEE, 2012, pp. 2612–2616.

[55] Rajesh B Amin, Donald V Hanley, Glenn C Morrow, and John Allahyari, "Architecture for an IP centric distributed network," Mar. 30 2004, US Patent 6,714,987.

[56] Maulin Patel and Jianfeng Wang, "Applications, challenges, and prospective in emerging body area networking technologies," *IEEE Wireless communications*, vol. 17, no. 1, pp. 80–88, 2010.

[57] Jan-Hinrich Hauer, Vlado Handziski, and Adam Wolisz, "Experimental study of the impact of WLAN interference on IEEE 802.15.4 body area networks," in *European Conference on Wireless Sensor Networks*. Springer, 2009, pp. 17–32.

[58] Rahul C Shah, Lama Nachman, and Chieh-yih Wan, "On the performance of Bluetooth and IEEE 802.15.4 radios in a body area network," in *Proceedings of the ICST 3rd international conference on Body area networks*. ICST (Institute for Computer Sciences, Social-Informatics and , 2008, p. 25.

[59] Alan Chi Wai Wong, Mark Dawkins, Gabriele Devita, Nikolaos Kasparidis, Andreas Katsiamis, Oliver King, Franco Lauria, Johannes Schiff, and Alison J Burdett, "A 1V 5mA multimode IEEE 802.15.6/Bluetooth low-energy WBAN transceiver for biotelemetry applications," *IEEE Journal of Solid-State Circuits*, vol. 48, no. 1, pp. 186–198, 2013.

[60] Yao-Hong Liu, Xiongchuan Huang, Maja Vidojkovic, Ao Ba, Pieter Harpe, Guido Dolmans, and Harmke de Groot, "A 1.9nJ/b 2.4 GHz multistandard (Bluetooth low energy/Zigbee/IEEE 802.15.6) transceiver for personal/body-area networks," in *2013 IEEE International Solid-State Circuits Conference Digest of Technical Papers*. IEEE, 2013, pp. 446–447.

[61] H. Li, Y. Schwoerer, J. Yoon, J. Farserotu, W. Yang, K. Sayrafian, D. Miniutti, and D. Lewis, "IEEE 802.15.6 regulation subcommittee report," Tech. Rep., Institute of Electrical and Electronics Engineers (IEEE), May, 2010.

[62] Dan Budin, Alexander Herman, and Colin Lanzl, "Wireless local area network communications system," Jan. 4 1994, US Patent 5,276,703.

[63] Domenico Porcino and Walter Hirt, "Ultra-wideband radio technology: potential and challenges ahead," *IEEE communications magazine*, vol. 41, no. 7, pp. 66–74, 2003.

[64] O Fagbohun, "Comparative studies on 3G, 4G and 5G wireless technology," *IOSR Journal of Electronics and Communication Engineering*, vol. 9, no. 3, pp. 88–94, 2014.

[65] Lou Frenzel, "Whats the difference between Bluetooth low energy and ANT," *electronic, design, Web resource*, 2012.

[66] ACW Wong, D McDonagh, O Omeni, C Nunn, M Hernandez-Silveira, and AJ Burdett, "Sensium: An ultra-low-power wireless body sensor network platform: Design & application challenges," in *2009 Annual International Conference of the IEEE Engineering in Medicine and Biology Society*. IEEE, 2009, pp. 6576–6579.

[67] Zarlink Semiconductor, "ZL70101 medical implantable RF transceiver data sheet," 2007.

[68] Paul Darbee, "INSTEON: the details," *Smarthome Technology*, pp. 1–64, 2005.

[69] Miya Knight, "How safe is Z-Wave?[wireless standards]," *Computing and Control Engineering*, vol. 17, no. 6, pp. 18–23, 2006.

[70] Min Chen, Sergio Gonzalez, Athanasios Vasilakos, Huasong Cao, and Victor C Leung, "Body area networks: A survey," *Mobile networks and applications*, vol. 16, no. 2, pp. 171–193, 2011.

[71] Raluca Maria Aileni, George Suciu, Cristina Mihaela Balaceanu, Cristian Beceanu, Petrache Ana Lavinia, Carmen-Violeta Nadrag, Sever Pasca, Carlos Alberto Valderrama Sakuyama, and Alexandru Vulpe, "Body area network (BAN) for healthcare by wireless mesh network (WMN)," in *Body Area Network Challenges and Solutions*, pp. 1–17. Springer, 2019.

[72] Ana Koren and Dina Šimunić, "Modelling an energy-efficient Zigbee (IEEE 802.15.4) body area network in IoT-based smart homes," in *41st International Convention on Information and Communication Technology, Electronics and Microelectronics (MIPRO)*. IEEE, 2018, pp. 0356–0360.

[73] Cheolhee Park and Theordore S Rappaport, "Short-range wireless communications for next-generation networks: UWB, 60 GHz millimeter-wave WPAN, and ZigBee," *IEEE Wireless Communications*, vol. 14, no. 4, pp. 70–78, 2007.

[74] Lin Shizhuang, Jingyu Liu, and Yanjun Fang, "ZigBee based wireless sensor networks and its applications in industrial," in *IEEE international conference on automation and logistics*. IEEE, 2007, pp. 1979–1983.

[75] David Culler and Samita Chakrabarti, "6LoWPAN: Incorporating ieee 802.15.4 into the IP architecture," *White paper*, 2009.

[76] Stanislav Safaric and Kresimir Malaric, "ZigBee wireless standard," in *Proceedings ELMAR 2006*. IEEE, 2006, pp. 259–262.

[77] Sajdl Ondrej, Bradac Zdenek, Fiedler Petr, and Hyncica Ondrej, "ZigBee technology and device design," in *International Conference on Networking, International Conference on Systems and International Conference on Mobile Communications and Learning Technologies (ICNICONSMCL'06)*. IEEE, 2006, pp. 129–129.

[78] Axel Sikora and Voicu F Groza, "Coexistence of IEEE 802.15.4 with other systems in the 2.4 ghz-ISM-band," in *2005 IEEE Instrumentationand Measurement Technology Conference Proceedings*. IEEE, 2005, vol. 3, pp. 1786–1791.

[79] Khusvinder Gill, Shuang-Hua Yang, Fang Yao, and Xin Lu, "A ZigBee-based home automation system," *IEEE Transactions on consumer Electronics*, vol. 55, no. 2, pp. 422–430, 2009.

[80] David Egan, "The emergence of ZigBee in building automation and industrial controls," *Computing and Control Engineering*, vol. 16, no. 2, pp. 14–19, 2005.

[81] Ahmad Salehi Shahraki, Muhammed Mahbubur Razzaque, Inmaculada Tomeo-Reyes, and Nasir Hussain, "IEEE 802.15.6 standard in wireless body area networks from a healthcare point of view," in *22nd Asia-Pacific Conference on Communications (APCC)*. IEEE, 2016, pp. 523–528.

[82] David B Smith, Dino Miniutti, Tharaka A Lamahewa, and Leif W Hanlen, "Propagation models for body-area networks: A survey and new outlook," *IEEE Antennas and Propagation Magazine*, vol. 55, no. 5, pp. 97–117, 2013.

[83] D Smith, D Miniutti, L Hanlen, A Zhang, D Lewis, D Rodda, and B Gilbert, "Power delay profiles for dynamic narrowband body area network channels id: 15-09-0187-01-0006," *IEEE submission*, 2009.

[84] Heinrich Luecken, Thomas Zasowski, Christoph Steiner, Florian Troesch, and Armin Wittneben, "Location-aware adaptation and precoding for low complexity IR-UWB receivers," in *Ultra-Wideband, 2008. ICUWB 2008. IEEE International Conference on*. IEEE, 2008, vol. 3, pp. 31–34.

[85] Patricia McDermott-Wells, "Bluetooth scatternet models," *IEEE potentials*, vol. 23, no. 5, pp. 36–39, 2004.

[86] Rohit Kapoor, Manthos Kazantzidis, Mario Gerla, and Per Johansson, "Multimedia support over Bluetooth piconets," in *Proceedings of the first workshop on Wireless mobile internet*. ACM, 2001, pp. 50–55.

[87] Joseph Decuir, "Introducing Bluetooth Smart: Part ii: Applications and updates.," *IEEE Consumer Electronics Magazine*, vol. 3, no. 2, pp. 25–29, 2014.

[88] Alf Helge Omre and Steven Keeping, "Bluetooth low energy: wireless connectivity for medical monitoring," *Journal of diabetes science and technology*, vol. 4, no. 2, pp. 457–463, 2010.

[89] Emmanouil Georgakakis, Stefanos A Nikolidakis, Dimitrios D Vergados, and Christos Douligeris, "An analysis of Bluetooth, ZigBee and Bluetooth low energy and their use in WBANs," in *International Conference on Wireless Mobile Communication and Healthcare*. Springer, 2010, pp. 168–175.

[90] Balasundaram Subbusundaram and Priyadarshan Jawaharlal, "System implementation of pushing data to handheld devices via Bluetooth high speed specification, version 3.0+ HS," in *2010 6th International Conference on Wireless Communications Networking and Mobile Computing (WiCOM)*. IEEE, 2010, pp. 1–4.

[91] David C Wyld, "RuBee: applying low-frequency technology for retail and medical uses," *Management Research News*, vol. 31, no. 7, pp. 549–554, 2008.

[92] Roy Want, "An introduction to RFID technology," *IEEE pervasive computing*, , no. 1, pp. 25–33, 2006.

[93] Thomas James Barber, *BodyLAN–a low-power communications system*, Ph.D. thesis, Massachusetts Institute of Technology, 1996.

[94] Muneer Bani Yassein, Wail Mardini, and Ashwaq Khalil, "Smart homes automation using Z-wave protocol," in *2016 International Conference on Engineering & MIS (ICEMIS)*. IEEE, 2016, pp. 1–6.

[95] Christopher M Talbot, Michael A Temple, Timothy J Carbino, and J Addison Betances, "Detecting rogue attacks on commercial wireless Insteon home automation systems," *Computers & Security*, vol. 74, pp. 296–307, 2018.

[96] Leif W Hanlen, Dino Miniutti, David Rodda, and Ben Gilbert, "Interference in body area networks: Distance does not dominate," in *IEEE 20th International Symposium on Personal, Indoor and Mobile Radio Communications (PIMRC)*. IEEE, 2009, pp. 281–285.

[97] Vasanta G Chaganti, Leif W Hanlen, and Tharaka A Lamahewa, "Semi-Markov modeling for body area networks," in *IEEE International Conference on Communications (ICC)*. IEEE, 2011, pp. 1–5.

[98] Raffaele DErrico and Laurent Ouvry, "A statistical model for on-body dynamic channels," *International journal of wireless information networks*, vol. 17, no. 3-4, pp. 92–104, 2010.

[99] Vasanta Chaganti, Leif Hanlen, and David Smith, "Are narrowband wireless on-body networks wide-sense stationary?," *IEEE Transactions on Wireless Communications*, vol. 13, no. 5, pp. 2432–2442, 2014.

[100] Samaneh Movassaghi, Mehran Abolhasan, and Justin Lipman, "A review of routing protocols in wireless body area networks," *Journal of Networks*, vol. 8, no. 3, pp. 559–575, 2013.

[101] Mehran Abolhasan, Tadeusz Wysocki, and Eryk Dutkiewicz, "A review of routing protocols for mobile ad hoc networks," *Ad hoc networks*, vol. 2, no. 1, pp. 1–22, 2004.

[102] Kemal Akkaya and Mohamed Younis, "A survey on routing protocols for wireless sensor networks," *Ad hoc networks*, vol. 3, no. 3, pp. 325–349, 2005.

[103] Maryam Asgari, Mehdi Sayemir, and Mohammad Shahverdy, "Overview of routing algorithms in WBAN," *Advances in Computer Science: an International Journal*, vol. 4, no. 4, pp. 14–20, 2015.

[104] Samaneh Movassaghi, Akbar Majidi, Abbas Jamalipour, David Smith, and Mehran Abolhasan, "Enabling interference-aware and energy-efficient coexistence of multiple wireless body area networks with unknown dynamics," *IEEE Access*, vol. 4, pp. 2935–2951, 2016.

[105] S Cheng and C Huang, "Network merging: Design strategies of an ultra low power and high reliability MAC," *IEEE submission, Doc. ID. IEEE*, pp. 802–15, 2009.

[106] MA Ameen, Ahsanun Nessa, and Kyung Sup Kwak, "QoS issues with focus on wireless body area networks," in *2008 Third International Conference on Convergence and Hybrid Information Technology*. IEEE, 2008, vol. 1, pp. 801–807.

[107] Bogdan Antonescu and Stefano Basagni, "Wireless body area networks: challenges, trends and emerging technologies," in *Proceedings of the 8th international conference on body area networks*. ICST (Institute for Computer

Sciences, Social-Informatics and Telecommunications Engineering), 2013, pp. 1–7.

[108] BI Statista, "Wearable device sales revenue worldwide from 2016 to 2022 (in billion US dollars)," *Statista Inc.: New York, NY, USA*, 2017.

[109] V Yussuff and R Sanderson, "The world market for wireless charging in wearable technology," *IHS: Englewood, CO, USA*, 2014.

[110] Ming Li, Wenjing Lou, and Kui Ren, "Data security and privacy in wireless body area networks," *IEEE Wireless communications*, vol. 17, no. 1, pp. 51–58, 2010.

[111] Samaher Al-Janabi, Ibrahim Al-Shourbaji, Mohammad Shojafar, and Shahaboddin Shamshirband, "Survey of main challenges (security and privacy) in wireless body area networks for healthcare applications," *Egyptian Informatics Journal*, vol. 18, no. 2, pp. 113–122, 2017.

[112] Samee U Khan, Albert Y Zomaya, and Assad Abbas, *Handbook of Large-Scale Distributed Computing in Smart Healthcare*, Springer, 2017.

[113] Moshaddique Al Ameen, Jingwei Liu, and Kyungsup Kwak, "Security and privacy issues in wireless sensor networks for healthcare applications," *Journal of medical systems*, vol. 36, no. 1, pp. 93–101, 2012.

[114] Yifan Chen, Jianqi Teo, Joshua Chong Yue Lai, Erry Gunawan, Kay Soon Low, Cheong Boon Soh, and Predrag B Rapajic, "Cooperative communications in ultra-wideband wireless body area networks: Channel modeling and system diversity analysis," *IEEE Journal on Selected Areas in Communications*, vol. 27, no. 1, pp. 5–16, 2009.

[115] Xigang Huang, Hangguan Shan, and Xuemin Shen, "On energy efficiency of cooperative communications in wireless body area network," in *Wireless Communications and Networking Conference (WCNC), 2011 IEEE*. IEEE, 2011, pp. 1097–1101.

[116] KS Deepak and Anchare V Babu, "Improving energy efficiency of incremental relay based cooperative communications in wireless body area networks," *International Journal of Communication Systems*, vol. 28, no. 1, pp. 91–111, 2015.

[117] Gabriel E Arrobo and Richard D Gitlin, "Improving the reliability of wireless body area networks," in *Engineering in Medicine and Biology Society, EMBC, 2011 Annual International Conference of the IEEE*. IEEE, 2011, pp. 2192–2195.

[118] Sheeraz Ahmed, Nadeem Javaid, Sidrah Yousaf, Ashfaq Ahmad, Muhammad Moid Sandhu, Muhammad Imran, Zahoor Ali Khan, and N Alrajeh, "Co-LAEEBA: Cooperative link aware and energy efficient protocol for wireless body area networks," *Computers in Human Behavior*, vol. 51, pp. 1205–1215, 2015.

[119] Gabriel E Arrobo and Richard D Gitlin, "New approaches to reliable wireless body area networks," in *Microwaves, Communications, Antennas and Electronics Systems (COMCAS), 2011 IEEE International Conference on*. IEEE, 2011, pp. 1–6.

[120] Jie Dong and David Smith, "Cooperative body-area-communications: Enhancing coexistence without coordination between networks," in *Personal Indoor and Mobile Radio Communications (PIMRC), 2012 IEEE 23rd International Symposium on*. IEEE, 2012, pp. 2269–2274.

[121] J. Dong and D. Smith, "Opportunistic relaying in wireless body area networks: Coexistence performance," in *IEEE International Conference on Communications (ICC), Hungary*, Jun, 2013, pp. 5613–5618.

[122] Jie Dong and David Smith, "Joint relay selection and transmit power control for wireless body area networks coexistence," in *Communications (ICC), 2014 IEEE International Conference on*. IEEE, 2014, pp. 5676–5681.

[123] Lusheng Wang, Claire Goursaud, Navid Nikaein, Laura Cottatellucci, and Jean-Marie Gorce, "Cooperative scheduling for coexisting body area net-

works," *IEEE Transactions on Wireless Communications*, vol. 12, no. 1, pp. 123–133, 2013.

[124] Thomas Watteyne, Isabelle Augé-Blum, Mischa Dohler, and Dominique Barthel, "AnyBody: a self-organization protocol for body area networks," in *Proceedings of the ICST 2nd international conference on Body area networks*. ICST (Institute for Computer Sciences, Social-Informatics and Telecommunications Engineering), 2007, p. 6.

[125] Jack Culpepper, Lan Dung, and Melody Moh, "Hybrid indirect transmissions (HIT) for data gathering in wireless micro sensor networks with biomedical applications," in *Proceedings of the IEEE 18th Annual Workshop on Computer Communications, Dana Point, CA, USA*, Oct, 2003, pp. 124–133.

[126] Bart Braem, Benoit Latre, Ingrid Moerman, Chris Blondia, and Piet Demeester, "The wireless autonomous spanning tree protocol for multihop wireless body area networks," in *IEEE 3rd Annual International Conference on Mobile and Ubiquitous Systems: Networking & Services*. IEEE, 2006, pp. 1–8.

[127] Bart Braem, Benoît Latré, Chris Blondia, Ingrid Moerman, and Piet Demeester, "Improving reliability in multi-hop body sensor networks," in *IEEE 2nd International Conference on Sensor Technologies and Applications, SENSORCOMM'08*. IEEE, 2008, pp. 342–347.

[128] Antonio G Ruzzelli, Raja Jurdak, Gregory MP O'Hare, and Peter Van Der Stok, "Energy-efficient multi-hop medical sensor networking," in *Proceedings of the 1st ACM SIGMOBILE international workshop on Systems and networking support for healthcare and assisted living environments*. ACM, 2007, pp. 37–42.

[129] Anirban Bag and Mostafa A Bassiouni, "Biocomm–a cross-layer medium access control (MAC) and routing protocol co-design for biomedical sensor networks," *International Journal of Parallel, Emergent and Distributed Systems*, vol. 24, no. 1, pp. 85–103, 2009.

[130] Kumar R. Sharavanan P.T. and Sridharan D., "A comparative study of cross layer protocols in WBAN," *Australian journal of basic and applied sciences*, vol. 9, no. 16, pp. 294–300, May, 2015.

[131] Begonya Otal, Luis Alonso, and Christos Verikoukis, "Highly reliable energy-saving MAC for wireless body sensor networks in healthcare systems," *IEEE Journal on Selected Areas in Communications*, vol. 27, no. 4, pp. 553–565, Jun, 2009.

[132] Garth V Crosby, Tirthankar Ghosh, Renita Murimi, and Craig A Chin, "Wireless body area networks for healthcare: a survey," *International Journal of Ad Hoc, Sensor & Ubiquitous Computing*, vol. 3, no. 3, pp. 1, Jun, 2012.

[133] Umer Fiaz Abbasi, Azlan Awang, and Nor Hisham Hamid, "A cross-layer opportunistic MAC/routing protocol to improve reliability in WBAN," in *IEEE Asia-Pacific Conference on Communications (APCC), Pattaya, Thailand*, Oct, 2014, pp. 36–41.

[134] Xufei Mao, Shaojie Tang, Xiahua Xu, Xiang-Yang Li, and Huadong Ma, "Energy-efficient opportunistic routing in wireless sensor networks," *IEEE Transactions on Parallel and Distributed Systems*, vol. 22, no. 11, pp. 1934–1942, 2011.

[135] Hsueh-Wen Tseng, Ruei-Yu Wu, and Yi-Zhang Wu, "An efficient cross-layer reliable retransmission scheme for the human body shadowing in IEEE 802.15.6-based wireless body area networks," *IEEE Sensors Journal*, vol. 16, no. 9, pp. 3282 – 3292, Mar, 2016.

[136] Tim Winter, "RPL: IPv6 routing protocol for low-power and lossy networks," Tech. Rep., Internet Engineering Task Force (IETF), 2012.

[137] Omprakash Gnawali, Rodrigo Fonseca, Kyle Jamieson, David Moss, and Philip Levis, "Collection tree protocol," in *Proceedings of the 7th ACM conference on embedded networked sensor systems*. ACM, 2009, pp. 1–14.

[138] Simon Duquennoy, Olaf Landsiedel, and Thiemo Voigt, "Let the tree bloom: Scalable opportunistic routing with ORPL," in *Proceedings of the 11th ACM Conference on Embedded Networked Sensor Systems*. ACM, 2013, p. 2.

[139] Thomas Clausen, Jiazi Yi, and Axel Colin De Verdiere, "LOADng: Towards AODV version 2," in *IEEE Vehicular Technology Conference (VTC Fall)*. IEEE, 2012, pp. 1–5.

[140] Charles Perkins, Elizabeth Belding-Royer, and Samir Das, "Ad hoc on-demand distance vector (AODV) routing," Tech. Rep., Internet Engineering Task Force (IETF), 2003.

[141] Jiazi Yi, Thomas Clausen, and Antonin Bas, "Smart route request for on-demand route discovery in constrained environments," in *IEEE International Conference on Wireless Information Technology and Systems (ICWITS)*. IEEE, 2012, pp. 1–4.

[142] Antonin Bas, Jiazi Yi, and Thomas Clausen, "Expanding ring search for route discovery in LOADng routing protocol," in *Proceedings of The 1st International Workshop on Smart Technologies for Energy, Information and Communication*, 2012.

[143] Lichuan Liu, Zhigang Wang, and MengChu Zhou, "Cooperative multipath routing and relay based on noncoherent detection in wireless sensor networks," in *IEEE International Conference on Automation Science and Engineering (CASE), Arlington, VA*. IEEE, Aug, 2008, pp. 128–132.

[144] Steven Kay, "A new nonstationarity detector," *IEEE Transactions on Signal Processing*, vol. 56, no. 4, pp. 1440–1451, 2008.

[145] Gregory C Reinsel, *Elements of multivariate time series analysis*, Springer Science & Business Media, 2003.

[146] Tricia J Willink, "Wide-sense stationarity of mobile MIMO radio channels," *IEEE Transactions on Vehicular Technology*, vol. 57, no. 2, pp. 704–714, 2008.

[147] Laura Bernadó, Thomas Zemen, Fredrik Tufvesson, Andreas F Molisch, and Christoph F Mecklenbräuker, "The (in-) validity of the WSSUS assumption in vehicular radio channels," in *23rd IEEE International Symposium on Personal Indoor and Mobile Radio Communications (PIMRC), Sydney, Australia*, 2012, pp. 1757–1762.

[148] Robert JC Bultitude, "Estimating frequency correlation functions from propagation measurements on fading radio channels: a critical review," *IEEE Journal on Selected Areas in Communications*, vol. 20, no. 6, pp. 1133–1143, 2002.

[149] Dmitry Umansky and Matthias Patzold, "Stationarity test for wireless communication channels," in *IEEE Global Telecommunications Conference (GLOBECOM), Hawaii, USA*, 2009, pp. 1–6.

[150] Prabahan Basu, Daniel Rudoy, and Patrick J Wolfe, "A nonparametric test for stationarity based on local Fourier analysis," in *IEEE International Conference on Acoustics, Speech and Signal Processing (ICASSP), Taipei, Taiwan*, 2009, pp. 3005–3008.

[151] Harold Edwin Hurst, "Long term storage capacity of reservoirs," *ASCE Transactions*, vol. 116, no. 776, pp. 770–808, 1951.

[152] Benoit B Mandelbrot and James R Wallis, "Robustness of the rescaled range R/S in the measurement of noncyclic long run statistical dependence," *Water Resources Research*, vol. 5, no. 5, pp. 967–988, 1969.

[153] Will E Leland, Murad S Taqqu, Walter Willinger, and Daniel V Wilson, "On the self-similar nature of ethernet traffic (extended version)," *IEEE/ACM Transactions on networking*, vol. 2, no. 1, pp. 1–15, 1994.

[154] Qiong Li and David L Mills, "On the long-range dependence of packet round-trip delays in internet," in *IEEE International Conference on Communications (ICC), Atlanta, USA*, 1998, pp. 1185–1191.

[155] Carlos Oliveira, Jaime Bae Kim, and Tatsuya Suda, "Long-range dependence in IEEE 802.11b wireless LAN traffic: an empirical study," in *IEEE 18th*

Annual Workshop on Computer Communications (CCW), CA, USA, 2003, pp. 17–23.

[156] Qilian Liang, "Ad hoc wireless network traffic-self-similarity and forecasting," *IEEE Communications Letters*, vol. 6, no. 7, pp. 297–299, 2002.

[157] Muhammad Usman Ilyas and Hayder Radha, "Long range dependence of IEEE 802.15.4 wireless channels," in *IEEE International Conference on Communications (ICC), Beijing, China*, 2008, pp. 4261–4265.

[158] AG Spilling, AR Nix, MA Beach, and TJ Harrold, "Self-organisation in future mobile communications," *Electronics & Communication Engineering Journal*, vol. 12, no. 3, pp. 133–147, 2000.

[159] Xue Wang, Junjie Ma, Sheng Wang, and Daowei Bi, "Distributed energy optimization for target tracking in wireless sensor networks," *IEEE Transactions on Mobile Computing*, vol. 9, no. 1, pp. 73–86, 2010.

[160] R Bellmann, "Dynamic programming princeton university press," *Princeton, NJ*, 1957.

[161] Martin L Puterman, *Markov decision processes: discrete stochastic dynamic programming*, John Wiley & Sons, 2014.

[162] Mohammad Abu Alsheikh, Dinh Thai Hoang, Dusit Niyato, Hwee-Pink Tan, and Shaowei Lin, "Markov decision processes with applications in wireless sensor networks: A survey," *IEEE Communications Surveys & Tutorials*, vol. 17, no. 3, pp. 1239–1267, 2015.

[163] Zhichu Lin and Mihaela van der Schaar, "Autonomic and distributed joint routing and power control for delay-sensitive applications in multi-hop wireless networks," *IEEE Transactions on Wireless Communications*, vol. 10, no. 1, pp. 102–113, 2011.

[164] Jie Hao, Zheng Yao, Kui Huang, Baoxian Zhang, and Cheng Li, "An energy-efficient routing protocol with controllable expected delay in duty-cycled wireless sensor networks," in *Communications (ICC), 2013 IEEE International Conference on*. IEEE, 2013, pp. 6215–6219.

[165] Bharat Shrestha, Ekram Hossain, and Kae Won Choi, "Distributed and centralized hybrid CSMA/CA-TDMA schemes for single-hop wireless networks," *IEEE Transactions on Wireless Communications*, vol. 13, no. 7, pp. 4050–4065, 2014.

[166] Charles Pandana and KJ Ray Liu, "Near-optimal reinforcement learning framework for energy-aware sensor communications," *IEEE Journal on Selected Areas in Communications*, vol. 23, no. 4, pp. 788–797, 2005.

[167] Abdellatif Kobbane, M-A Koulali, Hamidou Tembine, Mohammed El Koutbi, and Jalel Ben-Othman, "Dynamic power control with energy constraint for multimedia wireless sensor networks," in *Communications (ICC), 2012 IEEE International Conference on*. IEEE, 2012, pp. 518–522.

[168] Huijiang Li, Neeraj Jaggi, and Biplab Sikdar, "Relay scheduling for cooperative communications in sensor networks with energy harvesting," *IEEE Transactions on Wireless Communications*, vol. 10, no. 9, pp. 2918–2928, 2011.

[169] Kolar Purushothama Naveen and Anurag Kumar, "Relay selection for geographical forwarding in sleep-wake cycling wireless sensor networks," *IEEE Transactions on Mobile Computing*, vol. 12, no. 3, pp. 475–488, 2013.

[170] Nicolo Michelusi, Kostas Stamatiou, and Michele Zorzi, "Transmission policies for energy harvesting sensors with time-correlated energy supply," *IEEE Transactions on Communications*, vol. 61, no. 7, pp. 2988–3001, 2013.

[171] Mojtaba Nourian, Alex S Leong, and Subhrakanti Dey, "Optimal energy allocation for Kalman filtering over packet dropping links with imperfect acknowledgments and energy harvesting constraints," *IEEE Transactions on Automatic Control*, vol. 59, no. 8, pp. 2128–2143, 2014.

[172] Eitan Altman, "Applications of Markov decision processes in communication networks," in *Handbook of Markov decision processes*, pp. 489–536. Springer, 2002.

[173] Soumen Moulik, Sudip Misra, Chandan Chakraborty, and Mohammad S Obaidat, "Prioritized payload tuning mechanism for wireless body area network-based healthcare systems," in *Global Communications Conference (GLOBECOM), 2014 IEEE*. IEEE, 2014, pp. 2393–2398.

[174] Yuriy Tselishchev, Lavy Libman, and Athanassios Boulis, "Energy-efficient retransmission strategies under variable TDMA scheduling in body area networks," in *Local Computer Networks (LCN), 2011 IEEE 36th Conference on*. IEEE, 2011, pp. 374–381.

[175] Daphney-Stavroula Zois, Marco Levorato, and Urbashi Mitra, "Energy-efficient, heterogeneous sensor selection for physical activity detection in wireless body area networks," *IEEE Transactions on signal processing*, vol. 61, no. 7, pp. 1581–1594, 2013.

[176] Andson Balieiro, Peterson Yoshioka, Kelvin Dias, Dave Cavalcanti, and Carlos Cordeiro, "A multi-objective genetic optimization for spectrum sensing in cognitive radio," *Expert Systems with Applications*, vol. 41, no. 8, pp. 3640–3650, 2014.

[177] Zesong Fei, Bin Li, Shaoshi Yang, Chengwen Xing, Hongbin Chen, and Lajos Hanzo, "A survey of multi-objective optimization in wireless sensor networks: Metrics, algorithms, and open problems," *IEEE Communications Surveys & Tutorials*, vol. 19, no. 1, pp. 550–586, 2017.

[178] Eitan Altman, *Constrained Markov decision processes*, vol. 7, CRC Press, 1999.

[179] Kun Zheng, Husheng Li, Robert C Qiu, and Shuping Gong, "Multi-objective reinforcement learning based routing in cognitive radio networks: Walking in a random maze," in *Computing, Networking and Communications (ICNC), 2012 International Conference on*. IEEE, 2012, pp. 359–363.

[180] Yingqi Yin, Fengye Hu, Ling Cen, Yu Du, and Lu Wang, "Balancing long lifetime and satisfying fairness in WBAN using a constrained Markov decision process," *International Journal of Antennas and Propagation*, vol. 2015, 2015.

[181] Samaneh Movassaghi, Mehran Abolhasan, and David Smith, "Cooperative scheduling with graph coloring for interference mitigation in wireless body area networks," in *2014 IEEE wireless communications and networking conference (WCNC)*. IEEE, 2014, pp. 1691–1696.

[182] Daniele Domenicali, Luca De Nardis, and Maria-Gabriella Di Benedetto, "UWB body area network coexistence by interference mitigation," in *2009 IEEE international conference on ultra-wideband*. IEEE, 2009, pp. 713–717.

[183] Marwa Salayma, Ahmed Al-Dubai, Imed Romdhani, and Youssef Nasser, "Wireless body area network (WBAN): a survey on reliability, fault tolerance, and technologies coexistence," *ACM Computing Surveys (CSUR)*, vol. 50, no. 1, pp. 3, 2017.

[184] Mrinmoy Barua, Md Shamsul Alam, Xiaohui Liang, and Xuemin Shen, "Secure and quality of service assurance scheduling scheme for WBAN with application to ehealth," in *2011 IEEE Wireless Communications and Networking Conference*. IEEE, 2011, pp. 1102–1106.

[185] Ruixia Liu, Yinglong Wang, Minglei Shu, and Shangbin Wu, "Throughput assurance of wireless body area networks coexistence based on stochastic geometry," *PloS one*, vol. 12, no. 1, pp. e0171123, 2017.

[186] Sean F Heaney, William G Scanlon, Emi Garcia-Palacios, Simon L Cotton, and Adrian McKernan, "Characterization of inter-body interference in context aware body area networking (CABAN)," in *2011 IEEE GLOBECOM Workshops (GC Wkshps)*. IEEE, 2011, pp. 586–590.

[187] Elyes Ben Hamida, Muhammad Mahtab Alam, Mickael Maman, Benoît Denis, and Raffaele D'Errico, "Wearable body-to-body networks for critical and rescue operationsthe CROW2 project," in *2014 IEEE 25th Annual International Symposium on Personal, Indoor, and Mobile Radio Communication (PIMRC)*. IEEE, 2014, pp. 2145–2149.

[188] Simon L Cotton, Raffaele D'Errico, and Claude Oestges, "A review of radio channel models for body centric communications," *Radio Science*, vol. 49, no. 6, pp. 371–388, 2014.

[189] Mickael Maman, Francesco Mani, Benoît Denis, and Raffaele D'Errico, "Evaluation of multiple coexisting body area networks based on realistic on-body and body-to-body channel models," in *2016 10th International Symposium on Medical Information and Communication Technology (ISMICT)*. IEEE, 2016, pp. 1–5.

[190] M Maman and L Ouvry, "BATMAC: An adaptive TDMA MAC for body area networks performed with a space-time dependent channel model," in *2011 5th International Symposium on Medical Information and Communication Technology*. IEEE, 2011, pp. 1–5.

[191] Kenichi Takizawa, Takahiro Aoyagi, and Ryuji Kohno, "Channel modeling and performance evaluation on UWB-based wireless body area networks," in *2009 IEEE International Conference on Communications*. IEEE, 2009, pp. 1–5.

[192] Paul Ferrand, Mickael Maman, Claire Goursaud, Jean-Marie Gorce, and Laurent Ouvry, "Performance evaluation of direct and cooperative transmissions in body area networks," *Annals of Telecommunications-annales des télécommunications*, vol. 66, no. 3-4, pp. 213–228, 2011.

[193] David B Smith, Dino Miniutti, Leif W Hanlen, et al., "Characterization of the body-area propagation channel for monitoring a subject sleeping," *IEEE Transactions on antennas and propagation*, vol. 59, no. 11, pp. 4388–4392, 2011.

[194] Raffaele D'Errico and Laurent Ouvry, "Time-variant BAN channel characterization," in *2009 IEEE 20th International Symposium on Personal, Indoor and Mobile Radio Communications*. IEEE, 2009, pp. 3000–3004.

[195] David Smith, Leif Hanlen, Jian Zhang, Dino Miniutti, David Rodda, and Ben Gilbert, "Characterization of the dynamic narrowband on-body to off-body area channel," in *IEEE International Conference on Communications (ICC)*. IEEE, 2009, pp. 1–6.

[196] Andrew Fort, Claude Desset, Julien Ryckaert, Philippe De Doncker, Leo Van Biesen, and Piet Wambacq, "Characterization of the ultra wideband

body area propagation channel," in *2005 IEEE International Conference on Ultra-Wideband*. IEEE, 2005, pp. 6–pp.

[197] Simon L Cotton and William G Scanlon, "Characterization and modeling of the indoor radio channel at 868 mhz for a mobile bodyworn wireless personal area network," *IEEE Antennas and Wireless Propagation Letters*, vol. 6, pp. 51–55, 2007.

[198] Kenichi Takizawa, Takahiro Aoyagi, Jun-ichi Takada, Norihiko Katayama, Kamya Yekeh, Yazdandoost Takehiko, and Kobayashi Ryuji Kohno, "Channel models for wireless body area networks," in *2008 30th Annual International Conference of the IEEE Engineering in Medicine and Biology Society*. IEEE, 2008, pp. 1549–1552.

[199] Simon L Cotton and William G Scanlon, "An experimental investigation into the influence of user state and environment on fading characteristics in wireless body area networks at 2.45 ghz," *IEEE Transactions on Wireless Communications*, vol. 8, no. 1, pp. 6–12, 2009.

[200] Simon L Cotton, "A statistical model for shadowed body-centric communications channels: Theory and validation," *IEEE Transactions on Antennas and Propagation*, vol. 62, no. 3, pp. 1416–1424, 2014.

[201] Andreas F Molisch, Jeffrey R Foerster, and Marcus Pendergrass, "Channel models for ultrawideband personal area networks," *IEEE wireless communications*, vol. 10, no. 6, pp. 14–21, 2003.

[202] John D Day and Hubert Zimmermann, "The OSI reference model," *Proceedings of the IEEE*, vol. 71, no. 12, pp. 1334–1340, 1983.

[203] Begonya Otal, Luis Alonso, and Christos Verikoukis, "Novel QoS scheduling and energy-saving MAC protocol for body sensor networks optimization," in *Proceedings of the ICST 3rd international conference on Body area networks*. ICST (Institute for Computer Sciences, Social-Informatics and , 2008, p. 27.

[204] Laurie Hughes, Xinheng Wang, and Tao Chen, "A review of protocol implementations and energy efficient cross-layer design for wireless body area networks," *Sensors*, vol. 12, no. 11, pp. 14730–14773, 2012.

[205] Hangguan Shan, Ho Ting Cheng, and Weihua Zhuang, "Cross-layer cooperative MAC protocol in distributed wireless networks," *IEEE Transactions on Wireless Communications*, vol. 10, no. 8, pp. 2603–2615, 2011.

[206] Laaziz Lahlou, Amira Meharouech, Jocelyne Elias, and Ahmed Mehaoua, "MAC-Network cross-layer energy optimization model for wireless body area networks," in *2015 International Conference on Protocol Engineering (ICPE) and International Conference on New Technologies of Distributed Systems (NTDS)*. IEEE, 2015, pp. 1–5.

[207] Hadda Ben Elhadj, Jocelyne Elias, Lamia Chaari, and Lotfi Kamoun, "A priority based cross layer routing protocol for healthcare applications," *Ad Hoc Networks*, vol. 42, pp. 1–18, 2016.

[208] Gregory G Raleigh and VK Jones, "Multivariate modulation and coding for wireless communication," *IEEE Journal on Selected Areas in Communications*, vol. 17, no. 5, pp. 851–866, 1999.

[209] Walter R Braun and Ulrich Dersch, "A physical mobile radio channel model," *IEEE transactions on Vehicular Technology*, vol. 40, no. 2, pp. 472–482, 1991.

[210] Xiliang Zhong and Cheng-Zhong Xu, "Energy-efficient wireless packet scheduling with quality of service control," *IEEE Transactions on Mobile Computing*, vol. 6, no. 10, pp. 1158–1170, 2007.

[211] Baris Atakan and Ozgur B Akan, "Immune system based distributed node and rate selection in wireless sensor networks," in *2006 1st Bio-Inspired Models of Network, Information and Computing Systems*. IEEE, 2006, pp. 1–8.

[212] Özgür B Akan et al., "Immune system-based energy efficient and reliable communication in wireless sensor networks," in *Advances in Biologically Inspired Information Systems*, pp. 187–207. Springer, 2007.

[213] Köksal Gündoğdu and Ali Çalhan, "An implementation of wireless body area networks for improving priority data transmission delay," *Journal of medical systems*, vol. 40, no. 3, pp. 75, 2016.

[214] Mari Carmen Domingo, "Packet size optimization for improving the energy efficiency in body sensor networks," *ETRI Journal*, vol. 33, no. 3, pp. 299–309, 2011.

[215] D Smith, L Hanlen, D Rodda, B Gilbert, J Dong, and V Chaganti, "Body area network radio channel measurement set," 2012.

[216] Vasanta Chaganti, Leif Hanlen, and David Smith, "Non-stationarity of body area networks for sleep monitoring," *Electronics Letters*, vol. 49, no. 15, pp. 927–929, 2013.

[217] Leif Hanlen, Vasanta Chaganti, Barry Gilbert, David Rodda, Tharaka Lamahewa, and David Smith, "Open-source testbed for body area networks: 200 sample/sec, 12 hrs continuous measurement," in *IEEE 21st International Symposium on Personal, Indoor and Mobile Radio Communications Workshops (PIMRC Workshops), Turkey*, Sep, 2010, pp. 66–71.

[218] DB Smith, J Zhang, LW Hanlen, Dino Miniutti, David Rodda, and Ben Gilbert, "Temporal correlation of dynamic on-body area radio channel," *Electronics Letters*, vol. 45, no. 24, pp. 1212–1213, 2009.

[219] David B Smith, "Cooperative switched combining for wireless body area networks," in *23rd International Symposium on Personal Indoor and Mobile Radio Communications (PIMRC), Sydney, Australia*. IEEE, Sep, 2012, pp. 2275–2280.

[220] B Zhen, "Body area network (BAN) technical requirements," *15-08-0037-03-0006-ieee-802-15-6-technical-requirements-document-v-5-0. doc*, 2008.

[221] Daniel Lewis, "802.15.6 call for applications-response summary," *15-08-0407-00-0006-tg6-applications-summary. doc*, 2008.

[222] IEEE 802.15 Task Group 6, "IEEE standard for local and metropolitan area networks-part 15.6: Wireless body area networks (WBANs)," *IEEE Standard for Information Technology*, vol. 802, no. 6, pp. 1–271, 2012.

[223] P Buonadonna and Gilman Tolle, "MultihopLQI," 2004.

[224] Vineet Srivastava and Mehul Motani, "Cross-layer design: a survey and the road ahead," *IEEE Communications Magazine*, vol. 43, no. 12, pp. 112–119, 2005.

[225] Samiya M Shimly, David B Smith, and Samaneh Movassaghi, "Cross-layer designs for body-to-body networks: Adaptive CSMA/CA with distributed routing," in *IEEE International Conference on Communications (ICC), USA*, May, 2018, pp. 1–6.

[226] David B Smith and Leif W Hanlen, "Channel modeling for wireless body area networks," in *Ultra-Low-Power Short-Range Radios*, pp. 25–55. Springer, 2015.

[227] LW Hanlen, Dino Miniutti, David Smith, David Rodda, and Ben Gilbert, "Co-channel interference in body area networks with indoor measurements at 2.4 ghz: Distance-to-interferer is a poor estimate of received interference power," *International Journal of Wireless Information Networks*, vol. 17, no. 3-4, pp. 113–125, 2010.

[228] David Smith, Leif Hanlen, Dino Miniutti, Jian Zhang, David Rodda, and Ben Gilbert, "Statistical characterization of the dynamic narrowband body area channel," in *IEEE 1st International Symposium on Applied Sciences on Biomedical and Communication Technologies, ISABEL'08.* IEEE, 2008, pp. 1–5.

[229] David B Smith, Leif W Hanlen, Jian Andrew Zhang, Dino Miniutti, David Rodda, and Ben Gilbert, "First-and second-order statistical characterizations of the dynamic body area propagation channel of various bandwidths," *annals of telecommunications-annales des télécommunications*, vol. 66, no. 3-4, pp. 187–203, 2011.

[230] Zheng Wang and Jon Crowcroft, "Analysis of shortest-path routing algorithms in a dynamic network environment," *ACM SIGCOMM Computer Communication Review*, vol. 22, no. 2, pp. 63–71, Apr, 1992.

[231] Marija Z Malnar and Nataša J Nesković, "Comparison of ETX and HOP count metrics using Glomosim simulator," in *9th International Conference on Telecommunication in Modern Satellite, Cable, and Broadcasting Services, TELSIKS'09, Nis, Serbia*. IEEE, Oct, 2009, pp. 85–88.

[232] Athanassios Boulis, David Smith, Dino Miniutti, Lavy Libman, and Yuriy Tselishchev, "Challenges in body area networks for healthcare: The MAC," *IEEE Communications Magazine*, vol. 50, no. 5, 2012.

[233] Olaf Landsiedel, Euhanna Ghadimi, Simon Duquennoy, and Mikael Johansson, "Low power, low delay: opportunistic routing meets duty cycling," in *Proceedings of the 11th international conference on Information Processing in Sensor Networks*. ACM, 2012, pp. 185–196.

[234] Philip Levis, Eric Brewer, David Culler, David Gay, Samuel Madden, Neil Patel, Joe Polastre, Scott Shenker, Robert Szewczyk, and Alec Woo, "The emergence of a networking primitive in wireless sensor networks," *Communications of the ACM*, vol. 51, no. 7, pp. 99–106, 2008.

[235] Philip Levis, Neil Patel, David Culler, and Scott Shenker, "Trickle: A self-regulating algorithm for code propagation and maintenance in wireless sensor networks," in *Proc. of the 1st USENIX/ACM Symp. on Networked Systems Design and Implementation*, 2004.

[236] T Clausen, J Yi, and U Herberg, "Experiences with RPL: IPv6 routing protocol for low power and lossy networks," in *Proceedings of the 83rd IETF Plenary Meeting, Paris, France*, 2012, pp. 25–30.

[237] Mališa Vučinić, Bernard Tourancheau, and Andrzej Duda, "Performance comparison of the RPL and LOADng routing protocols in a home automation scenario," in *IEEE Wireless Communications and Networking Conference (WCNC)*. IEEE, 2013, pp. 1974–1979.

[238] In Jae Myung, "Tutorial on maximum likelihood estimation," *Journal of mathematical Psychology*, vol. 47, no. 1, pp. 90–100, 2003.

[239] Hákon Gudbjartsson and Samuel Patz, "The Rician distribution of noisy MRI data," *Magnetic resonance in medicine*, vol. 34, no. 6, pp. 910–914, 1995.

[240] Luis Filipe, Florentino Fdez-Riverola, Nuno Costa, and António Pereira, "Wireless body area networks for healthcare applications: Protocol stack review," *International Journal of Distributed Sensor Networks*, vol. 501, pp. 213705, 2015.

[241] William J Zimmer, J Bert Keats, and FK Wang, "The Burr XII distribution in reliability analysis," *Journal of Quality Technology*, vol. 30, no. 4, pp. 386, 1998.

[242] Jan Beran, *Statistics for long-memory processes*, vol. 61, CRC press, 1994.

[243] Philip Bello, "Characterization of randomly time-variant linear channels," *IEEE transactions on Communications Systems*, vol. 11, no. 4, pp. 360–393, 1963.

[244] Ming Li and Jia-Yue Li, "On the predictability of long-range dependent series," *Mathematical Problems in Engineering*, vol. 2010, no. 397454, pp. 1–9, 2010.

[245] Norbert Wiener, *Extrapolation, interpolation, and smoothing of stationary time series: with engineering applications*, MIT press Cambridge, 1949.

[246] A N Kolmogorov, W L Doyle, and Ivan Selin, *Interpolation and extrapolation of stationary random sequences*, Rand Corporation, 1962.

[247] Samiya M Shimly, David B Smith, and Samaneh Movassaghi, "Wide-sense-stationarity of everyday wireless channels for body-to-body networks," in *IEEE International Conference on Communications (ICC), USA*, May, 2018, pp. 1–6.

[248] Bo Qian Khaled Rasheed and B Qian, "Hurst exponent and financial market predictability," in *IASTED conference on Financial Engineering and Applications (FEA 2004)*, 2004, pp. 203–209.

[249] Raymond S Nickerson, "Null hypothesis significance testing: a review of an old and continuing controversy.," *Psychological methods*, vol. 5, no. 2, pp. 241, 2000.

[250] DS Wilks, "Resampling hypothesis tests for autocorrelated fields," *Journal of Climate*, vol. 10, no. 1, pp. 65–82, 1997.

[251] Raymond Hubbard and María Jesús Bayarri, "Confusion over measures of evidence (p's) versus errors (α's) in classical statistical testing," *The American Statistician*, vol. 57, no. 3, pp. 171–178, 2003.

[252] Sze Huey Tan and Say Beng Tan, "The correct interpretation of confidence intervals," *Proceedings of Singapore Healthcare*, vol. 19, no. 3, pp. 276–278, 2010.

[253] Henry Scheffe, *The analysis of variance*, vol. 72, John Wiley & Sons, 1999.

[254] Morton B Brown and Alan B Forsythe, "Robust tests for the equality of variances," *Journal of the American Statistical Association*, vol. 69, no. 346, pp. 364–367, 1974.

[255] Jean Dickinson Gibbons and Subhabrata Chakraborti, "Nonparametric statistical inference," in *International encyclopedia of statistical science*, pp. 977–979. Springer, 2011.

[256] Lisa M Lix, Joanne C Keselman, and HJ Keselman, "Consequences of assumption violations revisited: A quantitative review of alternatives to the one-way analysis of variance F test," *Review of educational research*, vol. 66, no. 4, pp. 579–619, 1996.

[257] Prophet Statguide, "Do your data violate one-way ANOVA assumptions," *National Center for Research Resources*, 1997.

[258] Wayne W Daniel, "Kruskal-Wallis one-way analysis of variance by ranks," *Applied Nonparametric Statistics*, pp. 226–234, 1990.

[259] Howard Levene, "Robust tests for equality of variances," *Contributions to probability and statistics*, vol. 1, pp. 278–292, 1960.

[260] Brian B Schultz, "Levene's test for relative variation," *Systematic Zoology*, vol. 34, no. 4, pp. 449–456, 1985.

[261] Marie-Anne Félix and Michalis Barkoulas, "Pervasive robustness in biological systems," *Nature Reviews. Genetics*, vol. 16, no. 8, pp. 483, 2015.

[262] Michael A Stephens, "Use of the Kolmogorov-Smirnov, cramér-von mises and related statistics without extensive tables," *Journal of the Royal Statistical Society. Series B (Methodological)*, vol. 32, no. 1, pp. 115–122, 1970.

[263] N Costa Pereira, "A short proof of Chebyshev's theorem," *The American Mathematical Monthly*, vol. 92, no. 7, pp. 494–495, 1985.

[264] Richard William Farebrother, *Fitting Linear Relationships: A History of the Calculus of Observations 1750-1900*, Springer Science & Business Media, 1999.

[265] J Feder, *Fractals*, Plenum Press, New York, 1988.

[266] Rossitza Dodunekova, "Characterization of the geometric and exponential random variables," *Communications in Statistics-Theory and Methods*, vol. 33, no. 8, pp. 1755–1765, 2004.

[267] Vasanta G Chaganti, David B Smith, and Leif W Hanlen, "Second-order statistics for many-link body area networks," *IEEE Antennas and Wireless Propagation Letters*, vol. 9, pp. 322–325, 2010.

[268] Andrew Fort, C Desset, P Wambacq, and LV Biesen, "Indoor body-area channel model for narrowband communications," *IET microwaves, antennas & propagation*, vol. 1, no. 6, pp. 1197–1203, 2007.

[269] Minseok Kim and Jun-ichi Takada, "Statistical model for 4.5-ghz narrowband on-body propagation channel with specific actions," *IEEE antennas and wireless propagation letters*, vol. 8, pp. 1250–1254, 2009.

[270] William G Scanlon and Simon L Cotton, "Understanding on-body fading channels at 2.45 ghz using measurements based on user state and environment," in *Antennas and Propagation Conference, 2008. LAPC 2008. Loughborough*. IEEE, 2008, pp. 10–13.

[271] Andreas F Molisch, Dajana Cassioli, Chia-Chin Chong, Shahriar Emami, Andrew Fort, Balakrishnan Kannan, Johan Karedal, Juergen Kunisch, Hans Gregory Schantz, Kazimierz Siwiak, et al., "A comprehensive standardized model for ultrawideband propagation channels," *IEEE Transactions on Antennas and Propagation*, vol. 54, no. 11, pp. 3151–3166, 2006.

[272] Andrew Fort, Julien Ryckaert, Claude Desset, Philippe De Doncker, Piet Wambacq, and Leo Van Biesen, "Ultra-wideband channel model for communication around the human body," *IEEE Journal on Selected Areas in Communications*, vol. 24, no. 4, pp. 927–933, 2006.

[273] Simon L Cotton, William G Scanlon, and Jim Guy, "The κ-μ distribution applied to the analysis of fading in body to body communication channels for fire and rescue personnel," *IEEE Antennas and Wireless Propagation Letters*, vol. 7, no. 1, pp. 66–69, 2008.

[274] Yu Wang, Ivan B Bonev, Jesper Ø Nielsen, IstvÁn Z Kovacs, and Gert F Pedersen, "Characterization of the indoor multiantenna body-to-body radio channel," *IEEE Transactions on Antennas and Propagation*, vol. 57, no. 4, pp. 972–979, 2009.

[275] Pandu R Tadikamalla, "A look at the Burr and related distributions," *International Statistical Review/Revue Internationale de Statistique*, vol. 48, no. 3, pp. 337–344, 1980.

[276] Attaphongse Taparugssanagorn, Carlos Pomalaza-Ráez, Raffaello Tesi, Matti Hämäläinen, and Jari Iinatti, "Effect of body motion and the type of antenna on the measured UWB channel characteristics in medical applications

of wireless body area networks," in *IEEE International Conference on Ultra-Wideband (ICUWB), Vancouver, BC*, Sep, 2009, pp. 332–336.

[277] Jonathan Richard Morley Hosking, James R Wallis, and Eric F Wood, "Estimation of the generalized extreme-value distribution by the method of probability-weighted moments," *Technometrics*, vol. 27, no. 3, pp. 251–261, 1985.

[278] Ramesh C Gupta, Olcay Akman, and Sergey Lvin, "A study of log-logistic model in survival analysis," *Biometrical Journal: Journal of Mathematical Methods in Biosciences*, vol. 41, no. 4, pp. 431–443, 1999.

[279] George EP Box, Gwilym M Jenkins, Gregory C Reinsel, and Greta M Ljung, *Time series analysis: forecasting and control*, John Wiley & Sons, 2015.

[280] Predrag R Jelenković and Ana Radovanović, "Least-recently-used caching with dependent requests," *Theoretical computer science*, vol. 326, no. 1-3, pp. 293–327, 2004.

[281] Clive WJ Granger and Roselyne Joyeux, "An introduction to long-memory time series models and fractional differencing," *Journal of time series analysis*, vol. 1, no. 1, pp. 15–29, 1980.

[282] Li Song and Pascal Bondon, "A procedure for modeling non-stationary signals with long range dependence," *IFAC Proceedings Volumes*, vol. 44, no. 1, pp. 4440–4445, 2011.

[283] Snjezana Gligorevic, "Stochastic modeling of non-stationary channels," in *IEEE 7th European Conference on Antennas and Propagation (EuCAP), Gothenburg, Sweden*, 2013, pp. 1677–1681.

[284] Matthias Grossglauser and J-C Bolot, "On the relevance of long-range dependence in network traffic," *IEEE/ACM transactions on networking*, vol. 7, no. 5, pp. 629–640, 1999.

[285] M Zeleny and JL Cochrane, *Multiple criteria decision making*, McGraw-Hill New York, 1982.

[286] Diederik M Roijers, Shimon Whiteson, and Frans A Oliehoek, "Computing convex coverage sets for multi-objective coordination graphs," in *International Conference on Algorithmic DecisionTheory*. Springer, 2013, pp. 309–323.

[287] Mark A Hanson, Harry C Powell Jr, Adam T Barth, Kyle Ringgenberg, Benton H Calhoun, James H Aylor, and John Lach, "Body area sensor networks: Challenges and opportunities," *Computer*, vol. 42, no. 1, pp. 58–65, 2009.

[288] Diederik M Roijers, Peter Vamplew, Shimon Whiteson, and Richard Dazeley, "A survey of multi-objective sequential decision-making," *Journal of Artificial Intelligence Research*, vol. 48, pp. 67–113, 2013.

[289] Krishnendu Chatterjee, Rupak Majumdar, and Thomas A Henzinger, "Markov decision processes with multiple objectives," in *Annual Symposium on Theoretical Aspects of Computer Science*. Springer, 2006, pp. 325–336.

[290] Samiya M. Shimly and David B. Smith, "Towards smart wireless body-centric networks," in *IEEE International Conference on Communications (ICC) N2Women-WICE Workshop, Kansas, USA. available on arxiv*. May, 2018, pp. 1–2, IEEE.

[291] Carlos A Coello Coello, Gregorio Toscano Pulido, and M Salazar Lechuga, "Handling multiple objectives with particle swarm optimization," *IEEE Transactions on evolutionary computation*, vol. 8, no. 3, pp. 256–279, 2004.

[292] Samiya M Shimly, David B Smith, and Samaneh Movassaghi, "Cross-layer designs for body-to-body networks: Adaptive CSMA/CA with distributed routing," in *IEEE International Conference on Communications (ICC), USA*, May, 2018, pp. 1–6.

[293] Melike Baykal-Gürsoy and K Gürsoy, "Semi-Markov decision processes," *Wiley Encyclopedia of Operations Research and Management Sciences*, 2010.

[294] Peter Whittle, *Prediction and regulation by linear least-square methods*, English Universities Press London, 1963.